Herbert Jaeger

Machine Learning (WMAI010-05.2020-2021.1B)

Lecture Notes

V 1.7, Nov 17, 2021

Master Program in Artificial Intelligence
Rijksuniversiteit Groningen, Bernoulli Institute

Contents

A note on mathematical background that is required. Neural networks process "training data" and these data typically originally come in the format of Excel files (yes! empirical scientists who actually generate those valuable "raw data" often use Excel!), which are just *matrices* if seen with the eye of a machine learner. Furthermore, neural networks are shaped by connecting neurons with weighted "synaptic links", and these weights are again naturally sorted in matrices. And the main operation that a neural network actually does is formalized by a matrix-vector multiplication. So it's matrices and vectors all over the place, no escape possible. You will need at least a basic, robust understanding of linear algebra to survive or even enjoy this course. We will arrange a linear algebra crash refresher early in the course. A good free online resource is the book "Mathematics for Machine Learning" (Deisenroth, Faisal, and Ong 2019).

Furthermore, to a lesser degree, also some familiarity with statistics and probability is needed. You find a summary of the must-knows in the appendix of these lecture notes, and again a tutorial exposition in Deisenroth, Faisal, and Ong 2019.

Finally, a little (not much) calculus is needed to top it off. If you are familiar with the notion of partial derivatives, that should do it. In case of doubt - again it's all (and more) in Deisenroth, Faisal, and Ong 2019.

1 Introduction

1.1 Human Versus Machine Learning

Humans learn. Animals learn. Societies learn. Machines learn. It looks like "learning" were a universal phenomenon and all we had to do is to develop a solid scientific theory of "learning", turn that into algorithms and then let "learning" happen on computers. Wrong wrong wrong. Human learning is very different from animal learning (and amoebas learn different things in different ways than chimpanzees), societal learning is quite another thing as human or animal learning, and machine learning is as different from any of the former as cars are from horses.

Human learning is incredibly scintillating and elusive. It is as complex and impossible to understand as you are yourself — look into a mirror and think of *all* the things you can *do*, all of your body motions from tying your shoes to playing the guitar; thoughts you can think from "aaagrhhh!" to "I think therefore I am"; achievements personal, social, academic; *all* the things you can remember including your first kiss and what you did 20 seconds ago (you started reading this paragraph, in case you forgot); your plans for tomorrow and the next 40 years; well, just *everything* about you — and almost everything of that wild collection is the result of a fabulous mixing learning of some kind with other miracles and wonders of life. To fully understand human learning, a scientist would have to integrate *at least* the following fields and phenomena:

body, brain, sensor & motor architecture · physiology and neurophysiology · body growth · brain development · motion control from eye gaze stabilization to dance choreography · exploration, curiosity, play · creativity · social interaction · drill and exercise and rote learning · reward and punishment, pleasure and pain · the universe, the earth, the atmosphere, water, food, caves · evolution · dreaming · remembering · forgetting · aging · other people, living · other people, long dead · machines, tools, buildings, toys · words and sentences · concepts and meanings · letters and books and schools · traditions ...

Recent spectacular advances in machine learning may have nurtured the impression that machines come already somewhat close. Specifically, neural networks with many cascaded internal processing stages (so-called *deep* networks) have been trained to solve problems that were considered close to impossible only a few years back. A showcase example (one that got me hooked) is automated image caption (technical report: Kiros, Salakhutdinov, and Zemel 2014). At `http://www.cs.toronto.edu/~nitish/nips2014demo` you can find stunning examples of caption phrases that have been automatically generated by a neural network based system which was given photographic images as input. Figure 1 shows some screenshots. This is a demo from 2014. Since deep learning is evolv-

ing incredibly fast, it's already rather outdated today and current image caption generators come much closer to perfection. But back in 2014 this was a revelation. Other fascinating examples of deep learning are face recognition (Parkhi, Vedaldi, and Zisserman 2015), online text translation (Bahdanau, Cho, and Bengio 2015), inferring a Turing machine (almost) from input-output examples (Graves et al 2016), or playing the game of Go at and beyond the level of human grand-masters (Silver et al. 2016). I listed these examples when I wrote the first edition of these lecture notes and I am too lazy to update this list every year (though I should), — instead this year (2021) I just point out the current best deep learning system, a text generation system called GPT-3 (read more about it on Wikipedia and in this instructively critical blog).

So, apparently machine learning algorithms come close to human performance in several tasks or even surpass humans, and these performance achievements have been *learnt* by the algorithms, — thus, machines today can learn like humans??!? The answer is NO. ML researchers (the *really good* ones, not the average TensorFlow user) are highly aware of this. Outside ML however, naive spectators (from the popular press, politics, or other sciences) often conclude that since learning machines can perform similar feats as humans, they also learn like humans. It takes some effort to argue why this is not so (read Edelman 2015 for a refutation from the perspective of cognitive psychology). I cannot embark on this fascinating discussion at this point. Very roughly speaking, it's the same story again as with chess-playing algorithms: the best chess programs win against the best human chess players, but not by fair means — chess programs are *based on larger amounts of data* (recorded chess matches) than humans can memorize, and chess programs can do *vastly more computational operations per second* than a human can do. Brute force wins over human brains at some point when there is enough data and processing bandwidth. Progress has accelerated in the last years because increasingly large training datasets have become available and fast enough computing systems have become cheap enough.

This is not to say that powerful "deep learning" just means large datasets and fast machines. These conditions are necessary but not sufficient. In addition, also numerous algorithmical refinements and theoretical insights in the area of statistical modeling had to be developed. Some of these algorithmical/theoretical concepts will be presented in this course.

Take-home message: The astonishing learning achievements of today's ML are based on statistical modeling techniques, raw processing power and a lot of a researcher's personal experience and trial-and-error optimization. It's technology and maths, not neurobiology or psychology. Dismiss any romantic ideas about ML that you may have had. ML is data technology stuff for sober engineers. But you are allowed to become very excited about that stuff, and that stuff can move mountains.

Tags

- bicyclers
- riders
- bikers
- equestrians
- bicyclists

Nearest Caption in the Training Dataset

a couple of people on four horses walking the streets .

Generated Captions

- a couple of men and horses on a street .
- some people are riding horses on a street .
- a group of people walking on horseback on a street .
- a couple of people with horses walk down the street .
- a group of people riding horses down a street .

Tags

- docks
- pontoon
- dockside
- boats
- pontoons

Nearest Caption in the Training Dataset

a group of people on a bridge beside a boat .

Generated Captions

- several people are on a dock in the water .
- a group of people are on a boat in the distance .
- some people on a boat in the harbor .
- a group of people are on the dock on a large boat .
- some people are on a bridge over a boat .

Tags

- ledges
- ledge
- flagstone
- porches
- casters

Nearest Caption in the Training Dataset

three men are sawing a tree into sections .

Generated Captions

- the two men are trying to use a tree .
- two men sitting in front of a wood tree .
- four men are working on a concrete structure .
- two men are working on wood .
- a man and a child in a wooden park are sitting on a farm .

Figure 1: Three screenshots from the image caption demo at `http://www.cs.toronto.edu/~nitish/nips2014demo`. A "deep learning" system was trained on some tens of thousands of photos showing everyday scenes. Each photo in the training set came with a few short captions provided by humans. From these training data, the system learnt to generate tags and captions for new photos. The tags and captions on the left were produced by the trained system upon input of the photos at the right.

1.2 The two super challenges of ML - from an eagle's eye

In this section I want to explain, on an introductory, pre-mathematical level, that large parts of ML can be understood as the art of estimating probability distributions from data. And that this art faces a double super challenge: the unimaginably *complex geometry* of real-world data distributions, and the extreme *scarcity of information* provided by real-world data. I hope that after reading this section you will be convinced that machine learning is impossible. Since however GPT-3 exists, where is the trick? ... A nice cliff hanger, you see — I want to make you read on.

1.2.1 The superchallenge of complex geometry

In order to highlight the data geometry challenge, I will use the demo task highlighted in Figure 1 as an example. Let us follow the sacred tradition of ML and first introduce an acronym that is not understandable to outsiders: TICS = the Toronto Image Caption System.

The TICS dataset and learning task and demo implementation come from one of the three labs that have pioneered the field which is now known as *Deep Learning* (DL, our next acronym), namely Geoffrey Hinton's Lab at the University of Toronto. (The other two widely acclaimed DL pioneers are Yoshua Bengio, University of Montréal, and Yann LeCun, Courant Institute of Mathematics, New York; Hinton, Bengio and LeCun received the 2018 Turing award – the Nobel prize in computer science). The TICS demo is a beautiful case to illustrate some fundamentals of machine learning.

After training, TICS, at first sight, implements a *function*: test image in, caption (and tags) out. If one looks closer, the output however is not just a single caption phrase, but a list of several captions ("generated captions" in Figure 1) rank-ordered by probability: captions that TICS thinks are more probable are placed higher in the list. Indeed TICS computes a relative probability value for each suggested caption. This probability value is not shown in the screenshots.

Let us look at this in a little more detail.

TICS captions are based on a finite vocabulary of English words. For simplicity let us assume that the length of captions that TICS generates is always 10 words. The neural networks that purr under the hood of TICS cannot process "words" – the only data type that they can handle is real-valued vectors. One of the innovations which boosted DL is a method to represent words by vectors such that *semantic similarity* of words is captured by *metric closeness* of vectors: the vector representing the word "house" lies close to the vector for "building" but far away from the vector for "mouse". A landmark paper where you can learn more about this technique is Mikolov et al. 2013, an accessible tutorial is Minnaar 2015. A typical size for such semantic word vectors is a dimension of a few 100's – let's say, TICS uses 300-dimensional word vectors (am too lazy to check out the exact dimension that was used). Thus, a caption can be represented by a sequence of

ten 300-dimensional vectors, which boils down to a single 3000-dimensional vector, that is, a point $c \in \mathbb{R}^{3000}$.

Similarly, an input picture sized 600×800 pixels with 3 color channels is represented to TICS as a vector u of dimension $3 \times 600 \times 800 = 1,440,000$.

Now TICS generates, upon a presentation of an input picture vector u, a list of what it believes to be the five most probable captions for this input. That is, TICS must have an idea of the probability ratios of different caption candidates. Formally, if C denotes the random variable (RV) that returns captions c, and if U denotes the RV which produces sample input pictures u, TICS must compute ratios of conditional probabilities of the form $P(C = c_i|U = u)/P(C = c_j|U = u)$. In the semantic word vector space, these ratios become ratios of the values of probability density functions (pdf) over the caption vector space $\mathbb{R}^{3000}$. For every input image u, TICS *must* have some representation of the 3000-dimensional pdf describing the probabilities of caption candidates for image u.

Now follow me on a little excursion into geometric imagination.

Consider some specific vector $c \in \mathbb{R}^{3000}$ which represents a plausible 10-word caption for image u, that is, the pdf value $p(c)$ is relatively large. What happens to the pdf value if we move away from c by taking a little step $\delta \in \mathbb{R}^{3000}$ of length, say, $\|\delta\| = 0.1$, that is, how does $p(c + \delta)$ compare to $p(c)$? This depends on the direction in which δ points. In a few directions, $p(c + \delta)$ will be about as large as $p(c)$. This happens when δ points toward another caption vector c' which has one word replaced by another word that is semantically close. For example, consider the caption *"A group of people on a bridge beside a boat"*. The last 300 elements in the 3000-dimensional vector c coding this caption stand for the word *boat*. Replacing this caption by *"a group of people on a bridge beside a ship"* gives another codevector $c' \in \mathbb{R}^{3000}$ which is the same as c except in the last 300 components, which have been replaced by the semantic word vector for *ship*. Then, if δ points from c toward c' (that is, δ is a fraction of $c' - c$), $p(c + \delta)$ will not differ from $p(c)$ in a major way.

If you think a little about it, you will come to the conclusion that such δ which leave $p(c+\delta)$ roughly at the same level are always connected with replacing words by semantically related words. Other change directions δ^* will either make no semantical sense or destroy the grammatical structure connected with c. The pdf value $p(c + \delta^*)$ will drop dramatically compared to $p(c)$ in those cases.

Now, in a 10-word caption, how many replacements of some word with a related one exist? Some words will be grammatical function words (*"a"*, *"'of"* etc.) which admit only a small number of replacements, or none at all. The words that carry semantic meaning (*"'group"*, *"people"* etc.) typically allow for a few sense-making replacements. Let us be generous and assume that a word in a 10-word caption, on avaerage, can be replaced by 5 alternative words such that after the replacement, the new caption still is a reasonable description of the input image.

This means that around c there will be $5 \cdot 10 = 50$ directions in which the relatively large value of $p(c)$ stays large. Assuming these 50 directions are given

by linearly independent δ vectors, we find that around c there is a 50-dimensional affine linear subspace S of $\mathbb{R}^{3000}$ in which we can find high p values in the vicinity of c, while in the 2950 directions orthogonal to S, the value of p will drop fast if one moves away from c.

Ok., this was a long journey to a single geometric finding: locally around some point c where the pdf is relatively large, the pdf will stay relatively large only a small fraction of the directions - these directions span a low-dimensional hyperplane around c. If you move a little further away from c on this low-dimensional "sheets", following the lead of high pdf values, you will find that this high-probability surface will take you on a curved path - these high-probability sheets in $\mathbb{R}^{3000}$ are not flat but curved.

The mathematical abstraction of such relatively high-probability, low-dimensional, curved sheets embedded in $\mathbb{R}^{3000}$ is the concept of a *manifold*. Machine learning professionals often speak of the "data manifold" in a general way, in order to indicate that the geometry of high-probability areas of real-world pdfs consists of "thin" (low-dimensional), curved sheet-like domains curled into the embedding data space. It is good for ML students to know the clean mathematical definition of a manifold. Although the geometry of real-world pdfs will be less clean than this mathematical concept, it provides a useful set of intuitions, and advanced research in DL algorithms frequently starts off from considering manifold models.

So, here is brief intro to the mathematical concept of a manifold. Consider an n-dimensional real vector space $\mathbb{R}^n$ (for the TICS output space of caption encodings this would be $n = 3000$). Let $m \leq n$ be a positive integer not larger than n. An m-dimensional manifold $\mathcal{M}$ is a subset of $\mathbb{R}^n$ which locally can be smoothly mapped to $\mathbb{R}^m$, that is, at each point of $\mathcal{M}$ one can smoothly map a neighborhood of that point to a neighborhood of the origin in the m-dimensional Euclidean coordinate system (Figure 2**A**).

1-dimensional manifolds are just lines embedded in some higher-dimensional $\mathbb{R}^n$ (Figure 2**B**), 2-dimensional manifolds are surfaces, etc. Manifolds can be wildly curved, knotted (as in Figure 2**C**), or fragmented (as in Figure 2**B**). Humans cannot visually imagine manifolds of dimension greater than 2.

The "data manifold" of a real-world data source is not a uniquely or even well-defined thing. For instance, returning to the TICS example, the dimension of the manifold around a caption c would depend on an arbitrary threshold fixed by the researcher – a direction δ would / would not lead out of the manifold if the pdf decreases in that direction faster than this threshold. Also (again using the caption scenario) around some good captions c the number of "good" local change directions will differ from the number around another, equally good, but differently structured caption c'. For these and other reasons, claiming that data distributions are shaped like manifolds is a strongly simplifying abstraction.

Despite the fact that this abstraction does not completely capture the geometric-statistical complexity of real-world data points, the geometric intuitions behind the manifold concept have led to substantial insight into the (mal-)functioning of

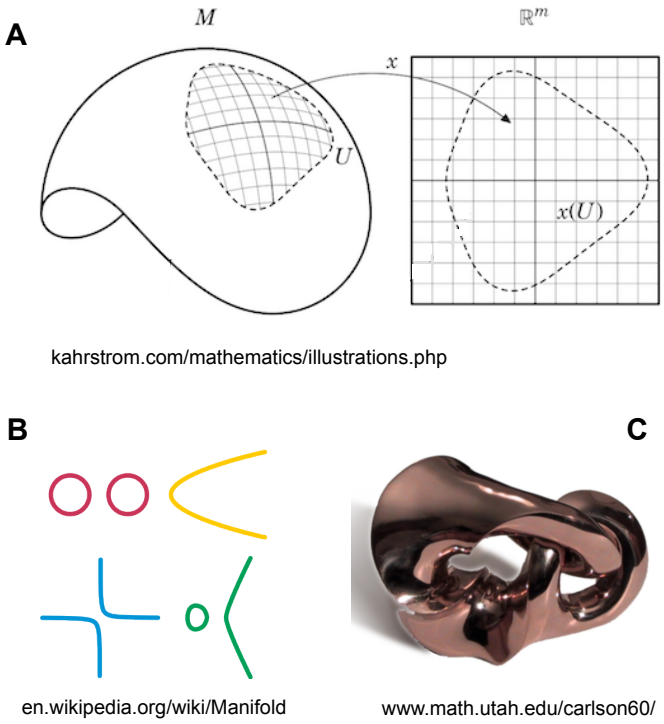

Figure 2: **A** An m-dimensional manifold can be locally "charted" by a bijective mapping to a neighborhood of the origin in $\mathbb{R}^m$. Example shows a curved manifold of dimension $m = 2$ embedded in $\mathbb{R}^3$. **B** Some examples of 1-dimensional manifolds embedded in $\mathbb{R}^2$ (each color corresponds to one manifold — manifolds need not be connected). **C** A more wildly curved 2-dimensional manifold in $\mathbb{R}^3$ (the manifold is the surface of this strange body).

machine learning methods. *Adversarial attacks* on deep networks is a good example of the usefulness of the data manifold concept. Take a look at Figure 3 – taken from a much-cited paper (I. J. Goodfellow, Shlens, and Szegedy 2014, 9000 cites on Google Scholar) which explores the phenomenon of adversarial attacks. The left panel shows a photo of a panda (one would think). It is given as input to a deep network that had been trained to classify images. The network correctly classifies it as "panda", with a "confidence" of 58%. The middle panel shows a noise pattern. If a very small multiple (factor 0.007) of this noise pattern is added to the panda picture, one gets the picture shown in the right panel. For the human eye there is no change. However, the neural network now classifies it as "gibbon" with a dead-sure confidence level of 99%.

What has happened here? Well, this is a manifold story. Let's say that the panda image is sized 600 × 600 pixels (I didn't check) with three color channels. Thus, mathematically, such images are points in $\mathbb{R}^{1080000}$. When the neural network was trained, it was presented with a large number of example images, that is, a point cloud in $\mathbb{R}^{1080000}$. The outcome of the learning algorithm is an esti-

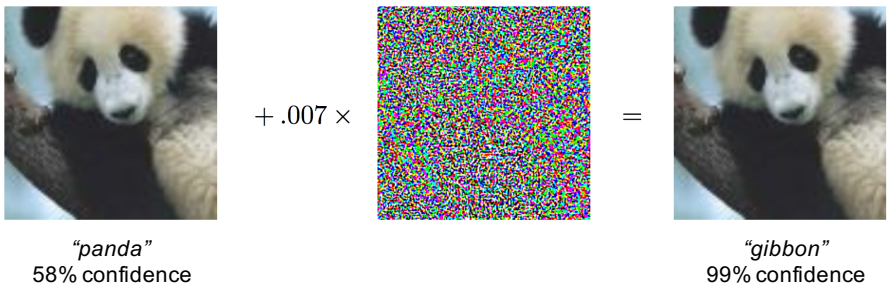

Figure 3: Manifold magic: Turning a panda into a gibbon. For explanation see text. Picture taken from I. J. Goodfellow, Shlens, and Szegedy 2014

mate (up to an undetermined scaling factor) of a pdf in $\mathbb{R}^{1080000}$. Geometrically speaking, this pdf is highly concentrated along a low-dimensional manifold, call it $\mathcal{M}$. The dimension of this manifold is given by the number of neurons in the most narrow layer of the neural network, say $m = 1000$ (this would be a standard order of magnitude in such deep networks; I didn't check). Thus, the original panda picture corresponds to a point u on a 1000-dimensional manifold which is curled into a 1,080,000-dimensional embedding space. In terms of dimensions, the manifold uses only about one out of thousand dimensions! Now, add that noise image (call it δ) to u, getting the rightmost panel picture as $u + \delta$. If δ is prepared in a way that it points in a direction orthogonal to $\mathcal{M}$, the value of the pdf will shrink dramatically. The network, when presented with input $u + \delta$, will "think" that it has never seen anything like this $u + \delta$ image, and will return a random classification – "gibbon" in this case.

Adversarial examples are today widely used in a number of different ways to improve the quality of deep learning applications. Check out Section 7.13 in the bible of deep learning (I. Goodfellow, Bengio, and Courville 2016) for a primer.

Back to our TICS example. As the first stage in their neural processing pipeline the designers of this learning system set up a layered neural network whose input layer (the "retina" of the network) had 1,440,000 neurons (one neuron per color pixel), and whose output layer had 4096 neurons. This means that the 1,440,000 dimensional raw input image vectors were projected on a manifold that had only 4096 dimensions. The right "folding" of this manifold was effected by the neural network training.

Takehome summary: real-world data distributions are typically concentrated in exceedingly thin (low-dimensional), badly curled-up sheets in the embedding (high-dimensional) data space $\mathbb{R}^n$. Machine learning models, such as the TICS system, must contain some kind of model of this distribution. Such models will also typically feature a concentration of probability mass in very thin, curled sheets. A *universal challenge for virtually all machine learning methods* is to develop modeling techniques that can represent such complex, manifold-like distribution geometries, and "learn" to align the model distribution with the data distribution.

Gray haired man in black suit and yellow tie working in a financial environment.
A graying man in a suit is perplexed at a business meeting.
A businessman in a yellow tie gives a frustrated look.
A man in a yellow tie is rubbing the back of his neck.
A man with a yellow tie looks concerned.

A butcher cutting an animal to sell.
A green-shirted man with a butcher's apron uses a knife to carve out the hanging carcass of a cow.
A man at work, butchering a cow.
A man in a green t-shirt and long tan apron hacks apart the carcass of a cow while another man hoses away the blood.
Two men work in a butcher shop; one cuts the meat from a butchered cow, while the other hoses the floor.

Figure 4: Two images and their annotations from the training dataset. Taken from Young et al. 2014.

A frequently found keyword that points to this bundle of ideas and challenges is "data manifold".

1.2.2 The superchallenge of lack of information

I continue to use the TICS system to illustrate this second challenge. What follows will again require an effort in geometrical thinking, but that's the nature of vector data and the information contained in them.

The data used for training TICS contained about 30,000 photos taken from Flickr, each of which was annotated by humans with 5 captions. Figure 4 shows two examples. Each photo was sized 600×800 pixels, with three color channels, making a total of 1,440,000 numbers as we have already stated. We will consider the intensity values as normalized to the range $[0, 1]$, which makes each photo a vector in the unit hypercube $[0, 1]^{1,440,000}$. Assuming as before that captions can be coded as 3000-dimensional vectors, which we will also take as normalized to a numeric range of $[0, 1]$, a photo-caption pair makes a vector in $[0, 1]^{1,440,000+3,000} = [0, 1]^{1,443,000}$. In order to simplify the following discussion we assume that each training image came with a single caption only. Thus, the training data consisted in 30,000 points in the 1,443,000-dimensional unit hypercube.

It is impossible for humans to visualize, imagine or even hallucinate the wild ways of how points can be spatially distributed in a 1,443,000-dimensional vector space. In Figure 5 I attempt a visualization of the TICS data scenario in a 3-dimensional projection of this 1,443,000-dimensional space – three dimensions being the largest spatial dimension that our brains can handle. The rendering in Figure 5 corresponds to a dataset where each "photo" is made of merely two grayscale pixels. Each such "photo" is thus a point in the square $[0, 1]^2$ (light blue area in the figure, spanned by the two pixel intensities x_1, x_2). Each caption is coded by a single number $y \in [0, 1]$. We furthermore simplify the situation by assuming that the training dataset contains only two photos u_1, u_2. The caption coding vector of a photo is here reduced to a single number, plotted above the photo's coordinates on the y-axis (blue crosses). The two blue crosses in the figure

thus represent the information contained in the training data.

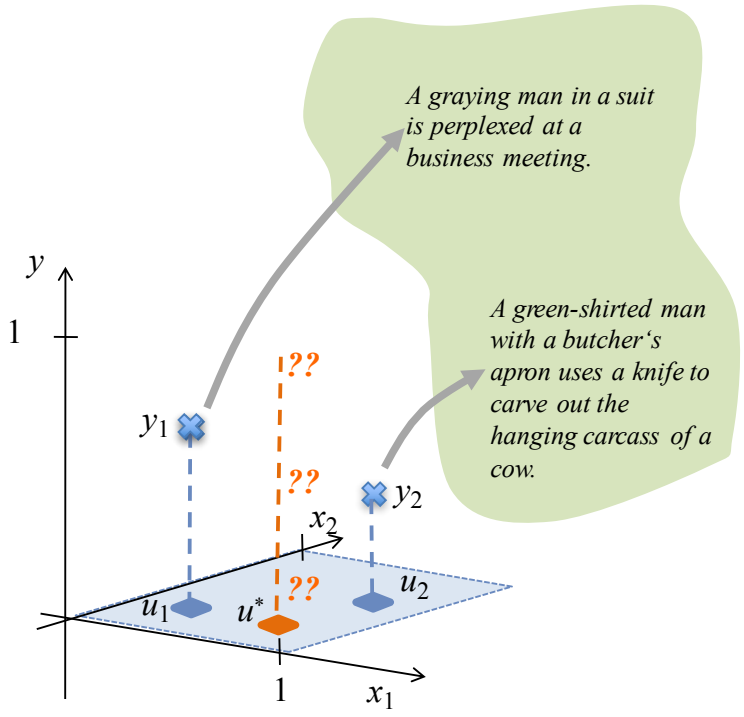

Figure 5: Training data for TICS (highly simplified). The photo dataspace (light blue square spanned by pixel intensities x_1, x_2) is here reduced to 2 dimensions, and the caption dataspace to a single one only (y-axis). The training dataset is assumed to contain two photos only (blue diamonds u_1, u_2), each with one caption (blue crosses with y-values y_1, y_2). A test image u^* (orange diamond) must be associated by TICS, after it has been trained, with suitable caption which lies somewhere in the y-direction above u^* (dashed orange ??-line).

Now consider a new test image u^* (orange diamond in the figure). The TICS system must determine a suitable caption for u^*, that is, an appropriate value y^* – a point somewhere on the orange broken ??-line in the figure.

But all that TICS knows about captions is contained the two training data points (blue crosses). If you think about it, there seems to be *no way* for TICS to infer from these two points where y^* should lie. *Any* placement along the ??-line is logically possible!

In order to determine a caption position along the ??-line, TICS *must* add some optimization criterion to the scenario. For instance, one could require one of the following conditions:

1. Make y^* that point on the ??-line which has the smallest total distance to all the training points.

2. One might wish to grant closer-by training images a bigger impact on the caption determination than further-away training images. Thus, if $d(u_i, u^*)$ denotes the distance between training image u_i and test image u^*, set y^* to the weighted mean of the training captions y_i, where the weights are inversely proportional to the distance of the respective images:

$$y^* = \frac{1}{\sum_i d(u_i, u^*)^{-a}} \sum_i d(u_i, u^*)^{-a} y_i.$$

   The parameter a modulates how the impact of further-away images decays with distance.

3. Place a spherical 3-dimensional Gaussian with variance σ^2 around every blue cross. Determine $p(y^*)$ to be that point on the ??-line where the sum of these Gaussians is maximal.

4. Consider all smoothly curved line segments L in the 3-dimensional data cube in Figure 5 which connect the blue crosses and cut through the ??-line. For any such L, consider the integral $\gamma(L)$ of absolute curvature along L. Find that curved line segment L_{opt} which minimizes $\gamma(L)$. Then declare the crossing of this L_{opt} with the ??-line to be y^*. – Like in the second proposal above, one would also want to emphasize the impact of close-by images, which would lead to a weighted curvature integral.

I collect some observations from this list:

- All of these optimization criteria make some intuitive sense, but they would lead to different results. The generated captions will differ depending on which criterion is chosen.

- The criteria rest on quite different intuitions. It is unclear which one would be better than another one, and on what grounds one would compare their relative merits. A note in passing: finding comparison criteria to assess relative merits of different statistical estimation procedures is a task that constitutes an entire, important branch of statistics. For an introduction you might take a look at my lecture notes on "Principles of statistical modeling", Section 19.3.1 "Comparing statistical procedures" (`https://www.ai.rug.nl/minds/uploads/LN_PSM.pdf`).

- Criteria 2 and 3 require the choice of design parameters (a, σ^2). The other criteria could be upgraded to include reasonable design parameters too. It is absolutely typical for machine learning algorithms to have such *hyperparameters* which need to be set by the experimenter. The effects of these hyperparameters can be very strong, determining whether the final solution is brilliant or useless.

- Casting an optimization criterion into a working algorithmic procedure may be challenging. For criteria 1, 2 and 3 in the list, this would be relatively easy. Turning criterion 4 into an algorithm looks fearsome.

- Each of the criteria leads to implicit constraints on the geometric shape of learnable data manifolds.

Some methods in ML are cleanly derived from optimization criteria, with mathematical theory backing up the design of algorithms. An example of such well-understood methods are *decision trees* which will be presented first in our course. Other branches employ learning algorithms that are so complex that one loses control over what is actually optimized, and one has only little insight in the geometrical and statistical properties of the models that are delivered by these methods. This is particularly true for deep learning methods.

There is something like an irreducible arbitrariness of choosing an optimization condition, or, if one gives up on fully understanding what is happening, an arbitrariness in the design of complex learning algorithms. This turns machine learning into a quite personal preference thing, even into an art.

To put this all in a nutshell: the available training data do not include the information of how the information contained in them should be "optimally" extracted, or *what* kind of information should be extracted. This could be called a *lack of epistemic information* (my private terminology; epistemology is the branch of philosophy that is concerned with the question by which methods of reasoning humans get acquire knowledge, and with the question what "knowledge" is in the first place - check out `https://en.wikipedia.org/wiki/Epistemology` if you are interested in these deep, ancient, unsolved questions).

The discussion of lacking epistemic information is hardly pursued in today's ML, although there have been periods in the last decades when fierce debates on such issues have been led.

But there is also another lack of information which *is* a standard theme in today's ML textbooks. This issue is called the *curse of dimensionality*. I will highlight this curse with our TICS demo again.

In mathematical terminology, after training our super-simplified 3-dimensional TICS system from Figure 5 is able to compute a function $f : [0,1]^2 \to [0,1]$ which computes a caption $f(u^*)$ for every input test image $u^* \in [0,1]^2$. The only information TICS has at learning time is contained in the training data points (blue crosses in our figure).

Looking at Figure 5, estimating a function $f : [0,1]^2 \to [0,1]$ from just the information contained in the two blue crosses is clearly a dramatically underdetermined task. You may argue that the version of the TICS learning task which I gave in Figure 5 has been simplified to an unfair degree, and that the real TICS system had not just 2, but 30,000 training images to learn on.

But, in fact, for the full-size TICS the situation is even much, *much* worse than what appears in Figure 5:

- In the caricature demo there were 2 training images scattered in a 2-dimensional (pixel intensity) space. That is, as many data points as dimensions. In contrast, in TICS there are 30,000 images scattered in a 1,440,000-dimensional pixel intensity space: that is, about 50 times more dimensions than data points! How should it be possible at all to estimate a function from $[0,1]^{1440000}$ to $[0,1]^{3000}$ when one has so much fewer training points than dimensions!?

- There is another fact about high-dimensional spaces which aggravates the situation. In the n-dimensional unit hypercube, the greatest possible distance between two points is equal to the longest diagonal in this hypercube, $\sqrt{n}$, which amounts to 1200 in the TICS image space. This growth of length of the main diagonal with dimension n carries over to a growth of average distances between random points in n-dimensional hypercubes. In simple terms, the higher the dimension, the wider will training data points lie apart from each other.

The two conditions together – fewer data points than dimensions, and large distances between the points – make it appear impossible to estimate a function on $[0,1]^{1440000}$ from just those 30,000 points.

This is the dreaded "curse of dimensionality".

In plain English, the curse of dimensionality says that in high-dimensional data spaces, the available training data points will be spread exceedingly thinly in the embedding data space, and they will lie far away from each other. Metaphorically speaking, training data points are a few flickering stars in a vast and awfully empty universe. But, most learning tasks require one to fill the empty spaces with information.

1.3 Looking at Human Intelligence, Again

An adult human has encoded in his/her brain a very useful, amazingly accurate and detailed model of that human's outer world, which allows the human to almost immediately create a "situation model" of his/her current physical and social environment, based on the current, ever-new sensor input. This situation model is a condensed, meaningful representation of the current environment. This is analog to the TICS scenario (after training), where the new input is a test image and the situation model corresponds to a distribution over captions.

After what we have seen above, how is it possible for a human brain to learn a meaningful and reliable representation of the world (that is, a manifold in brain state space) at all?

In fact, we do not know. But neuroscientists, psychologists and cognitive scientists have come up with a number of ideas.

An adult human has had a childhood and youth's time to learn most of his/her world model. The "training data" are the sensory impressions collected in, say, the first 25 years of the human's life. Thinking of a sensory impression as a vector,

it is hard to say what is the dimension of this vector. A lower bound could be found in the number of sensory neural fibers reaching the brain. The optical nerve has about 1,000,000 fibres. Having two of them, plus all sorts of other sensory fibers reaching the brain (from the nose, ears, body), let us boldly declare that the dimension of sensor inputs to the brain is 3 million. Now, the learning process for a human differs from TICS learning in that sensory input arrives in a continuous stream, not in isolated training images. In order to make the two scenarios comparable, assume furthermore that a human organizes the continuous input stream into "snapshots" at a rate of 1 snapshot "picture" of the current sensory input per second (cognitive psychologists will tell us that the rate is likely less). In the course of 25 years, with 12 wake hours per day, this makes about 25 $\times$ 360 $\times$ 12 $\times$ 3600 $\approx$ 390 million "training snapshot images". This gives a ratio of number of training points over data dimension of 390 million / 3 million = 130, which looks so much better than the ratio of 30,000 / 1,443,000 $\approx$ 0.02 in TICS's case.

But even the ratio of 130 data points per dimension is still hopeless, and the curse of dimensionality strikes just as well. Why?

For simplicity we again assume that the 3-million dimensional sensor image vectors are normalized to a range of [0, 1], making a sensor impression a point in $[0,1]^{3000000}$. Statisticians, machine learners, and many cognitive scientists would tell us that the "world model" of a human can be considered to be a probability distribution over the sensory image space $[0,1]^{3000000}$. This is a hypercube with $2^{3000000}$ corners. In order to estimate a probability distribution over an n-dimensional hypercube, a statistician would demand to have many more datapoints than the cube has corners (to see why, think about estimating a probability distribution over the one-dimensional unit hypercube [0, 1] from data points on that interval, then extrapolate to higher dimensions). That is, a brain equipped with ordinary statistical methods would demand to have many more than $2^{3000000}$ training data points to distil a world model from that collection of experiences. But there are only 390 million such datapoints collected in 25 years. The ratio 390 million / $2^{3000000}$ is about $2^{-2999972}$. That is, a human would have to have a youth lifetime of about $25 \times 2^{2999972} \approx 2^{2999977}$ years in order to learn a statistically defendable world model.

Still, the human brain (and the human around it, with the world around the human around that brain) somehow can do it in 25 years. Cognitive scientists believe that the key to this magic lies in the evolutionary history of man. Through millions of years of incremental, evolutionary brain structure optimization, starting from worm brains or earlier, the human brain is *pre-structured* in exactly such ways that it comes with a built-in-by-birth data manifold geometry which reduces the 3 million-dimensional raw sensor data format to a *much* lower-dimensional manifold surface. Then, 390 million data points may be enough to cover this manifold densely enough for meaningful distribution estimates.

The question which built-in experience pre-shapings a human brings to the

table at birth time has a long tradition in philosophy and psychology. A recent line of work that brings this tradition to bear on machine learning is in the research of Joshua Tenenbaum – check out, for instance, Tenenbaum, Griffiths, and Kemp 2006 if you are interested.

1.4 A Remark on "Modeling"

Machine learning in its modern form aims at modeling real-world systems, just like what the natural sciences aim for. But the motivation is different.

Physicists, chemists, biologists et al. want to *understand* reality through their models. Their models should tell the truth – in suitable abstraction – about reality; the models should be *veridical* (from Latin, "saying the truth"). The inner workings of a model should reflect the inner workings of reality. For instance, a detailed chemical model of a reaction which changes a substance A into a substance B should give an account of the kinetic and quantum-mechanical substeps that actually take place in this reaction. Newton's laws of motion explain the dance of planets by formulas made of variables which should correspond to physically real quantities – like gravitational forces, masses or velocities. Models whose inner mechanisms or mathematical variables are intended to capture real mechanisms and real quantities are called *analytical* models.

Machine learners, in contrast, are application oriented. They want *useful* models. ML models of pieces of reality must *function* well in their respective application context. The inner workings of an ML model need not mirror the inner workings of the modeled system. Machine learning models are thus almost always *blackbox* models (a possible exception being Bayesian networks, will be treated in Session 9 of this course). A blackbox model of some real-world system just captures the externally observable input-output behavior of the modeled system, but it may use any internal mathematical or algorithmical tricks that its designer can think of. Neural networks are a striking example. A neural network trained for predicting the next day's stock index will be made of hundreds or even millions of interacting variables ("neuron activations") which have no corresponding counterpart in the reality of stock markets.

Figure 6 sketches how blackbox models work. They are derived ("learnt", "estimated") from data emitted by the source system, and they should generate synthetic data that "fit" (have a similar distribution as) the real-world data. And that's it. The structure of the blackbox model need not agree in any way with the structure of the source system – in Figure 6, this is a robot, while the model is a neural network whose structure has no correspondence whatsoever in the robot design.

Analytical and blackbox models have complementary merits:

- Setting up the structure of an analytical model requires from the modeler to have insight into the concerned laws of nature – an expert's business. A

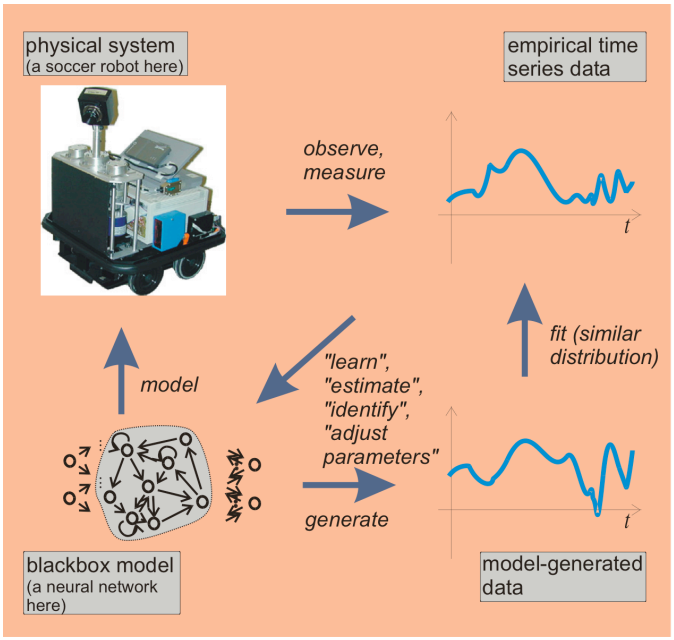

Figure 6: How blackbox models work. For explanation see text.

blackbox model can be successfully created by a village idiot with access to TensorFlow.

- A blackbox model requires training data. There are cases where such data are not available in sufficient quantity. Then analytical modeling is the only way to go.

- As a rule, analytical models are much more compact than blackbox models. Compare $E = m\,c^2$ with the TICS system, which consists of several modules, some of which are neural networks with hundreds of thousands of variables.

- When the target system that one wants to model is very complex, there is typically no chance for an analytical model. Example: an analytical model of how humans describe images in captions would have to include accounts of the human brain and the cultural conditions of language use. No way. Only blackbox models can be used here.

- The great – really very great – advantage of analytical models is that they generalize to all situations within their scope. The laws of gravitation can be applied to falling apples as well as to the majestic whirling of galaxies. If a blackbox model would have been trained by Newton on data collected from the sun and planets motions, this model would be exclusively applicable to our planetary system, not to apples and not to galaxies.

An interesting and very relevant modeling task is to model the earth's atmosphere for weather forecasting. This modeling problem has been intensely worked

on for many decades, and an interesting mix of analytical and blackbox methods marks the state of the art. If there is time and interest I will expand on this in the tutorial session.

I conclude this section with a tale from my professional life which nicely illustrates the difference between analytical and blackbox modeling. I was once called to consult a company in the chemical industry. They wanted a machine learning solution for the following problem. In one of their factories they had built a production line whose output was a certain artificial resin. Imagine a large hall full of vessels, heaters, pumps and valves and tubes. The production process of that resin was prone to a particularly nasty possible failure: if the process would not be controlled correctly, some intermediate products might solidify. The concerned vessels, tubes and valves would be blocked and could not be cleared – necessitating to disassemble the facility and replace the congested parts with new ones. Very expensive! The chemical engineers had heard of the magic of neural networks and wanted one of these, which should give them early warnings if the production process was in danger of drifting into the danger zone. I told them that this was (maybe) possible if they could provide training data. What training data, please? Well, in order to predict failure, a neural network needs examples of this failure. So, could the engineers please run the facility through a reasonably large number of solidification accidents, a few hundreds maybe for good statistics? Obviously, that was that. Only analytical modeling would do here. A good analytical model would be able to predict any kind of imminent solidification situtions. But that wasn't an option either because the entire production process was too complex for an accurate enough analytical model. Now put yourself into the skin of the responsible chief engineer. What should he/she do to prevent the dreaded solidification to happen, ever? Another nice discussion item for our tutorial session.

1.5 The Machine Learning Landscape

ML as a field which perceives itself as a field under this name is relatively young, say, about 40 years (similar research was called "pattern recognition" earlier). It is interdisciplinary and has historical and methodological connections to neuroscience, cognitive science, linguistics, mathematical statistics, AI, signal processing and control; it uses mathematical methods from statistics (of course), information theory, signal processing and control, dynamical systems theory, mathematical logic and numerical mathematics; and it has a very wide span of application types. This diversity in traditions, methods and applications makes it difficult to study "Machine Learning". Any given textbook, even if it is very thick, will reflect the author's individual view and knowledge of the field and will be partially blind to other perspectives. This is quite different from other areas in computer science, say for example formal languages / theory of computation / computational complexity where a widely shared repertoire of standard themes and methods cleanly define the field.

I have a brother, Manfred Jaeger, who is a machine learning professor at Aalborg university (`http://people.cs.aau.dk/~jaeger/`). We naturally often talk with each other, but never about ML because I wouldn't understand what he is doing and vice versa. We have never met at scientific conferences because we attend different ones, and we publish in different journals.

The leading metaphors of ML have changed over the few decades of the field's existence. The main shift, as I see it, was from "cognitive modeling" to "statistical modeling". In the 1970-1980s, a main research motif/metaphor in ML (which was hardly named like that then) was to mimic human learning on computers, which connected ML to AI, cognitive science and neuroscience. While these connections persist to the day, the mainstream self-perception of the field today is to view it very soberly as the craft of estimating complex probability distributions with efficient algorithms and powerful computers.

My personal map of the ML landscapte divides it into four main segments with distinct academic communities, research goals and methods:

Segment 1: Theoretical ML. Here one asks what are the fundamental possibilities and limitations of inferring knowledge from observation data. This is the most abstract and "pure maths" strand of ML. There are cross-connections to the theory of computational complexity. Practical applicability of results and efficient algorithms are secondary. Check out `https://en.wikipedia.org/wiki/Computational_learning_theory` and `https://en.wikipedia.org/wiki/Statistical_learning_theory` for an impression of this line of research.

Segment 2: Symbolic-logic learning, data mining. Here the goal is to infer symbolic knowledge from data, to extract logical rules from data, to infer facts about the real world expressed in fragments of first-order logic or other logic formalisms, often enriched with probabilistic information. Neural networks are rarely used. A main motif is that these resulting models be human-understandable and directly useful for human end-users. Key terms are "knowledge discovery", "data mining", or "automated knowledge base construction". This is the area of my brother's research. Check out `https://en.wikipedia.org/wiki/Data_mining` or `https://en.wikipedia.org/wiki/Inductive_logic_programming` or Suchanek et al. 2013 for getting the flavor. This is an application-driven field, with applications e.g. in bioinformatics, drug discovery, web mining, document analysis, decision support systems.

A beautiful case study is the PaleoDeepDive project described in Peters et al. 2014. This large-scale project aimed at making paleontological knowledge easily searchable and more realiable. Palaeontology is the science of extinct animal species. Its "raw data" are fossil bones. It is obviously difficult to reliably classify a handfuly of freshly excavated bones as belonging

to a particular species – first, because one usually doesn't dig out a complete skeleton, and second because extinct species are not known in the first place. The field is plagued by misclassifications and terminological uncertainties – often a newly found set of bones is believed to belong to a newly discovered species, for which a new name is created, although in reality other fossil findings already named differently belong to the same species. In the PaleoDeepDive project, the web was crawled to retrieve virtually all scientific pdf documents relating to paleontology – including documents that had been published in pre-digital times and were just image scans. Using optical character recognition and image analysis methods at the front end, these documents were made machine readable, including information contained in tables and images. Then, unsupervised, logic-based methods were used to identify suspects for double naming of the same species, and also the opposite: single names for distinct species – an important contribution to purge the evolutionary tree of the animal kingdom.

Segment 3: Signal and pattern modeling. This is the most diverse sector in my private partition of ML and it is difficult to characterize globally. The basic attitude here is one of quantitative-numerical blackbox modeling. Our TICS demo would go here. The raw data are mostly numerical (like physical measurement timeseries, audio signals, images and video). When they are symbolic (texts in particular), one of the first processing steps typically encodes symbols to some numerical vector format. Neural networks are widely used and there are some connections to computational neuroscience. The general goal is to distil from raw data a numerical representation (often implicit) of the data distribution which lends itself to efficient application purposes, like pattern classification, time series prediction, motor control to name a few. Human-user interpretability of the distribution representation is not easy to attain, but has lately become an important subject of research. Like Segment 2, this field is decidedly application-driven. Under the catchword "deep learning" a subfield of this area has recently received a lot of attention.

Segment 4: Agent modeling and reinforcement learning. The overarching goal here is to model entire intelligent agents — humans, animals, robots, software agents — that behave purposefully in complex dynamical environments. Besides learning, themes like motor control, sensor processing, decision making, motivation, knowledge representation, communication are investigated. An important kind of learning that is relevant for agents is *reinforcement learning* — that is, an agent is optimizing its action-decision-making in a lifetime history based on reward and punishment signals. The outcome of research often is *agent architectures*: complex, multi-module "box-and-wiring diagrams" for autonomous intelligent systems. This is likely the most interdisciplinary corner of ML, with strong connections to cogni-

tive science, the cognitive neurosciences, AI, robotics, artificial life, ethology, and philosophy.

It is hard to judge how "big" these four segments are in mutual comparison. Surely Segment 1 receives much less funding and is pursued by substantially fewer researchers than segments 2 and 3. In this material sense, segments 2 and 3 are both "big". Segment 4 is bigger than Segment 1 but smaller than 2 or 3. My own research lies in 3 and 4. In this course I focus on the third segment — you should be aware that you only get a partial glimpse of ML.

A common subdivision of ML, partly orthogonal to my private 4-section partition, is based on three fundamental kinds of learning tasks:

Supervised learning. Training data are "labelled pairs" (x_n, y_n), where x is some kind of "input" and y is some kind of "target output" or "desired / correct output". TICS is a typical example, where the x_n are images and the y_n are captions. The learning objective is to obtain a mechanism which, when fed with new test inputs x_{test}, returns outputs y_{test} that generalize in a meaningful way from the training sample. The underlying mathematical task is to estimate the conditional distributions $P_{Y \mid X}$ from the training sample (check the end of Appendix B for a brief explanation of this notation). The learnt input-output mechanism is "good" to the extent that upon input x_{test} it generates outputs that are distributed according to the true conditional distribution $P(Y = y \mid X = x_{\text{test}})$, just as we have seen in the TICS demo. Typical and important special cases of supervised learning are *pattern classification* (the y are correct class labels for the input patterns x) or *timeseries prediction* (the y are correct continuations of initial timeseries x). Segment 3 from my private segmentation of ML is the typical stage for supervised learning.

Unsupervised learning. Training data are just data points x_n. The task is to discover some kind of "structure" (regularities, symmetries, redundancies...) in the data distribution which can be used to create a compressed representation of the data. Unsupervised learning can become very challenging when data points are high-dimensional and/or when the distribution has a complex shape. Unsupervised learning is often used for *dimension reduction*. The result of an unsupervised learning process is a dimension-reducing, *encoding* function e which takes high-dimensional data points x as inputs and returns low-dimensional encodings $e(x)$. This encoding should preserve most of the information contained in the original inputs x. That is, there should also exist a *decoding* function d which takes encodings $e(x)$ as inputs and transforms them back to the high-dimensional format of x. The overall loss in the encoding-decoding process should be small, that is, one wishes to obtain $x \approx d(e(x))$. A discovery of underlying rules and regularities is the typical goal for data mining applications, hence unsupervised learning is the

main mode for Segment 2 from my private dissection of ML. Unsupervised methods are often used for data preprocessing in other ML scenarios, because most ML techniques suffer from curse of dimensionality effects and work better with dimension-reduced input data.

Reinforcement learning. The set-up for reinforcement learning (RL) is quite distinct from the above two. It is always related to an agent that can choose between different *actions* which in turn change the *state* of the environment the agent is in, and furthermore the agent may or may not receive *rewards* in certain environment states. RL thus involves at least the following three types of random variables:

- action random variables A,
- world state random variables S,
- reward random variables R.

In most cases the agent is modeled as a stochastic process: a temporal *sequence* of actions $A_1, A_2, \ldots$ leads to a sequence of world states $S_1, S_2, \ldots$, which are associated with rewards $R_1, R_2, \ldots$. The objective of RL is to learn a strategy (called *policy* in RL) for choosing actions that maximize the reward accumulated over time. Mathematically, a policy is a conditional distribution of the kind

$$P(A_n = a_n \,|,\, S_1 = s_1, \ldots, S_{n-1} = s_{n-1}; A_1 = a_1, \ldots, A_{n-1} = a_{n-1}),$$

that is, the next action is chosen on the basis of the "lifetime experience" of previous actions and the resulting world states. RL is naturally connected to my Segment 4. Furthermore there are strong ties to neuroscience, because neuroscientists have reason to believe that individual neurons in a brain can adapt their functioning on the basis of neural or hormonal reward signals. Last but not least, RL has intimate mathematical connections to a classical subfield of control engineering called *optimal control*, where the (engineering) objective is to steer some system in a way that some long-term objective is optimized. An advanced textbook example is to steer an interplanetary missile from earth to some other planet such that fuel consumption is minimized. Actions here are navigation maneuvres, the (negative) reward is fuel consumption, the world state is the missile's position and velocity in interplanetary space.

The distinction between supervised and unsupervised learning is not clear-cut. Training tasks that are globally supervised (like TICS) may benefit from, or plainly require, unsupervised learning subroutines for transforming raw data into meaningfully compressed formats (like we saw in TICS). Conversely, globally unsupervised training mechanisms may contain supervised subroutines where intermediate "targets" y are introduced by the learning system. Furthermore, today's

advanced ML applications often make use of *semi-supervised* training schemes. In such approaches, the original task is supervised: learn some input-output model from labelled data (x_n, y_n). This learning task may strongly benefit from including additional unlabelled input training points $\tilde{x}_m$, helping to distil a more detailed model of the input distribution P_X than would be possible on the basis of only the labelled x_n data. Again, TICS is an example: the data engineers who trained TICS used 70K un-captioned images in addition to the 30K captioned images to identify that 4096-dimensional manifold more accurately.

Also, reinforcement learning is not independent of supervised and unsupervised learning. A good RL scheme often involves supervised or unsupervised learning subroutines. For instance, an agent trying to find a good policy will benefit from data compression (= unsupervised learning) when the world states are high-dimensional; and an agent will be more capable of choosing good actions if it possesses an input-output model (= supervised learning) of the environment — inputs are actions, outputs are next states.

2 Decision trees and random forests

This section describes a class of machine learning models which is classical and simple and intuitive and useful. Decision trees and random forests are not super "fashionable" in these deep learning times, but practicians in data analysis use them on a daily basis. The main inventions in this field have been made around 1980-2000. In this chapter I rely heavily on the decision tree chapters in the classical ML textbooks of Mitchell 1997 and Duda, Hart, and Stork 2001, and for the random forest part my source is the landmark paper by Breiman 2001 which, as per today (Nov 15, 2021), has been cited 81000 times (Google Scholar). Good stuff to know, apparently.

Note: In this chapter of the lecture notes I will largely adhere to the notation used in Breiman 2001 in order to make it easier for you to read that key paper if you want to dig deeper. If in your professional future you want to use decision tree methods, you will invariably use them in random forests, and in order to understand what you are actually doing, you will have to read Breiman 2001 (like hundreds of thousands before you). Unfortunately, the notation used by Breiman is inconsistent, which makes the mathematical part of that paper hard to understand. My hunch is that most readers skipped the two mathy sections and read only the experimental sections with the concrete helpful hints for algorithm design and gorgeous results. Inconsistent or even plainly incorrect mathematical notation (and mathematical thinking) happens a lot in "engineering applied math" papers and makes it difficult to really understand what the author wants to say (see my ramblings in my lecture notes on "Principles of Statistical Modeling", Chapter 14, "A note on what you find in textbooks", online at `https://www.ai.rug.nl/minds/uploads/LN_PSM.pdf`). Therefore I will not use Breiman's notation 1-1, but modify it a little to make it mathematically more consistent.

2.1 A toy decision tree

Figure 7 shows a simple decision tree. It can be used to *classify* fruit. If you have a fruit in your hands that you don't know by name, then you can use this decision tree to find out what fruit you have there, in an obvious way:

- Start at the root node of the tree. The root node is labeled with a property that fruit have (`color?` is the root property used in the figure).
- Underneath the root node you find child nodes, one for each of the three possible color attributes *green*, *yellow*, *red*. Decide which color your fruit has and proceed to that child node. Let us assume that your fruit was yellow. Then you are now at the child node labelled `shape?`.
- Continue this game of moving downwards in the tree according to the direction decisions taken at each node according to the attributes of the fruit in

your hand. If you reach a leaf node of this tree, it will be labeled with the type of your fruit. If your fruit is yellow, round and small, it's a lemon!

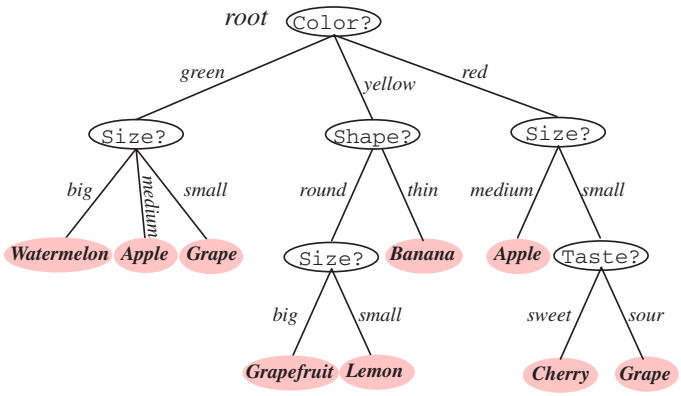

Figure 7: A simple decision tree. Taken from Duda, Hart, and Stork 2001.

A decision tree is not unique. You could, for instance, create another tree whose root node queries the `size?` property, and which would lead to exactly the same ultimate decisions as the tree shown in the figure (exercise!).

If each internal (= non-leaf) node in a decision tree has exactly two child nodes, one speaks of a binary decision tree. These are particularly pleasant for mathematical analysis and algorithm design. Every decision tree can be transformed into an equivalent binary decision tree with an obvious procedure. Figure 8 shows the binary tree obtained from the fruit tree of Figure 7.

This is obviously a toy example. But decision trees can become really large and useful. A classical example are the botanic field guide books used by biologists to classify plants (Figure 9). I am a hobby botanist and own three such decision trees. Together they weigh about 1.5 kg and I have been using them ever since I was eighteen or so.

In the basic versions of decision tree learning, they are learnt from data which are given as class-labeled attribute vectors. For instance, training data for our fruit tree might look like this:

nr.	**Color**	**Size**	**Taste**	**Weight**	**Shape**	**Class**
1	green	big	sweet	heavy	round	Watermelon
2	green	?	?	heavy	round	Watermelon
3	red	small	sweet	light	round	Cherry
4	red	small	sweet	light	round	Apple
...	...	...	...	...	...	...
3000	red	big	?	medium	round	Apple

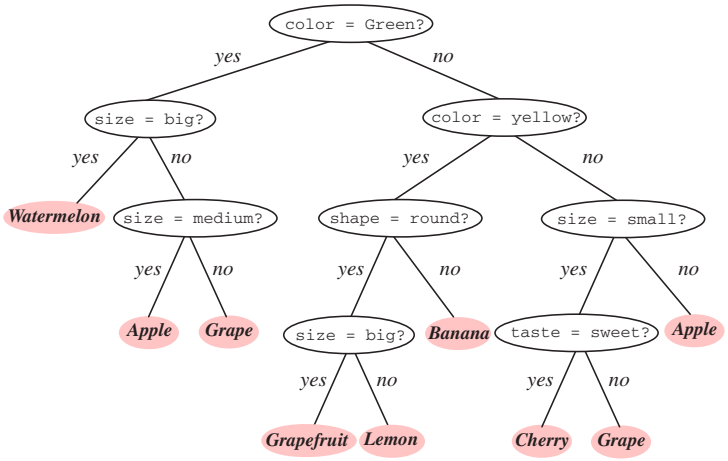

Figure 8: A binary version of the decision tree shown in Figure 7. Taken from Duda, Hart, and Stork 2001.

Here we get a first inkling that decision tree learning might not be as trivial as the final result in Figure 7 makes it appear. The above fruit training data table has missing values (marked by "?"); not all properties from the training data are used in the decision tree (property "Weight" is ignored); some examples of the same class have different attribute vectors (first two rows give different characterizations of watermelons); some identical attribute vectors have different classes (rows 3 and 4). In summary: real-world training data will be partly redundant, partly inconsistent and will be containing errors and gaps. All of this points in the same direction: statistical analyses will be needed to learn decision trees.

2.2 Formalizing "training data"

Before we describe decision tree learning, I want to squeeze in a little rehearsal of mathematical concepts and their notation.

In my notation in this chapter I will be leaning on Breiman's notation as far as possible. Breiman's notation is unfortunately incomplete and inconsistent. Here I use a complete, correct notation, adhering to the standards of mathematical probability theory. I am aware that many participants of this course will be unfamiliar with probability theory and its formal notation standards. Because machine learning ultimately rests on probability theory, I strongly recommend that at some point you learn to master the basics of probability theory (for instance, from my lecture notes for the legacy course "Principles of Statistical Modeling", online: `https://www.ai.rug.nl/minds/uploads/LN_PSM.pdf`). Only if you understand probability you can get a full grasp on machine learning. But it is clear that many students will not have the time or inclination to learn about probability theory. Therefore I will try to introduce notation and concepts in two ways throughout

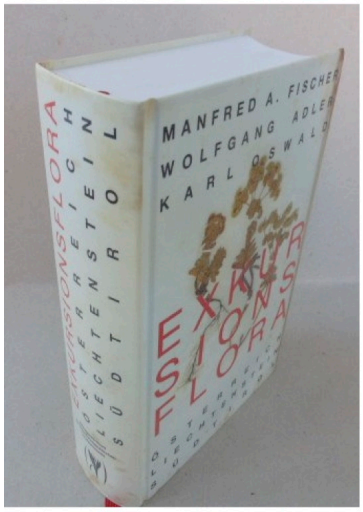

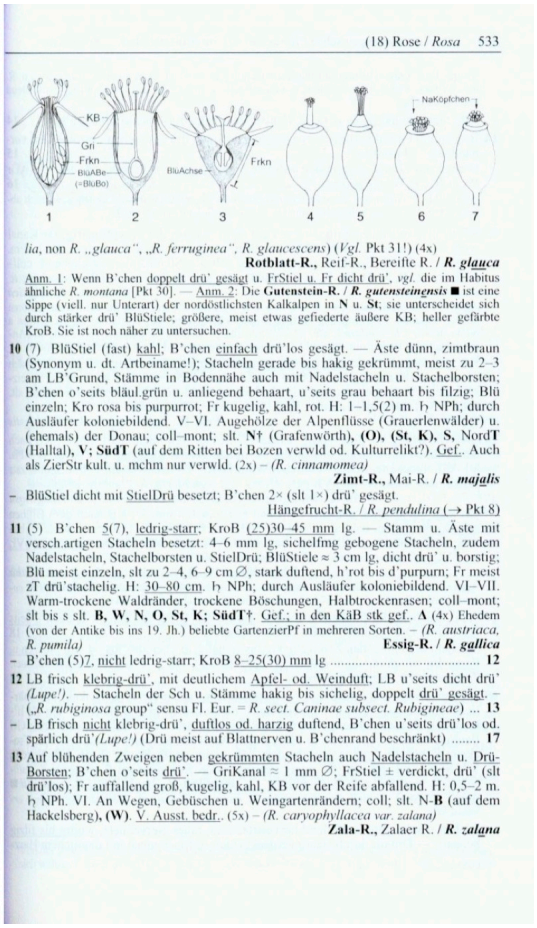

Figure 9: Another decision tree. The right image shows a page from this botany field guide. What you see on this page is, in fact, a small section of a large binary classification tree. Image source: iberlibro.com, booklooker.de.

this course: in a rigorous "true math" version, and in an intuitive "makes some sense" version.

I called the fruit attribute data table above a *sample*. Samples are mathematical objects of key importance in statistics and machine learning (where they are also called "training data"). Samples are always connected with *random variables* (RVs). Here is how.

First, the intuitive version. As an empirical fruit scientist, you would obtain a "random draw" to get the training data table in a very concrete way: you would go to the fruit market, collect 3000 fruit "at random", observe and note down their color, size, taste, weight and shape attributes in an Excel table, and for each of the 3000 fruit you also ask the fruit vendor for the name of the fruit to get an almost but not quite surely correct class label which you also note down in the last column of the table.

The mathematical representation of observing and noting down the attributes

of the i-th fruit that you have picked (where $i = 1, \ldots, 3000$) is $X_i(\omega)$. X_i is the random variable which is the mathematical model of the observation procedure – X_i could be described as the procedure "pick a random fruit and observe and report the attribute vector". The ω in $X_i(\omega)$ is the occasion when you actually executed the procedure X_i – say, ω stands for the concrete data collection event when you went to the Vismarkt in Groningen last Tuesday and visited the fruit stands. If the entire procedure of collecting 3000 fruit specimen is executed on another occasion – for instance, a week earlier, or by your friend on the same day – this would be mathematically represented by another ω. For instance, $X_i(\omega)$ might be the attribute vector that you observed for the i-th fruit last Tuesday, $X_i(\omega')$ would be the attribute vector that you observed for the i-th fruit one week earlier, $X_i(\omega'')$ would be the attribute vector that your friend observed for the i-th last Tuesday when he did the whole thing in parallel with you, etc. In mathematical terminology, these "observation occasions" ω are called *elementary events*.

Similarly, $Y_i(\omega)$ is the fruit class name that you were told by the vendor when you did the data sampling last Tuesday; $Y_i(\omega')$ would be the ith fruit name you were told when you did the whole exercise a week earlier already, etc.

The three thousand pairs $(X_i(\omega), Y_i(\omega))$ correspond to the rows in the data table. I will call each of these $(X_i(\omega), Y_i(\omega))$ a *data point*. To get the entire table as a single mathematical object – namely, the sample – one combines these single fruit data points by a product operation, obtaining $(\mathbf{X}(\omega), \mathbf{Y}(\omega))$, where $\mathbf{X} = \bigotimes_{i=1,\ldots,N} X_i$ and $\mathbf{Y} = \bigotimes_{i=1,\ldots,N} Y_i$.

And here is the rigorous probability theory account of the $(\mathbf{X}(\omega), \mathbf{Y}(\omega))$ notation. As always in probability theory and statistics, we have an underlying *probability space* $(\Omega, \mathfrak{A}, P)$. In this structure, Ω is the set of all possible *elementary events* $\omega \in \Omega$. $\mathfrak{A}$ is a subset structure imposed on the set Ω called a *σ-field*, and P is a *probability measure* on $(\Omega, \mathfrak{A})$. The random variable $\mathbf{X}$ is a function which returns *samples*, that is collections of N training data points. We assume that all samples which could be drawn have N data points; this assumption is a matter of convenience and simplifies the ensuing notation and mathematical analysis a lot. – It is a good exercise to formalize the structure of a sample in more detail. A single data point consists of an attribute vector $\mathbf{x}$ and a class label y. In formal notation, we have m properties $Q_1, \ldots, Q_m$, and property Q_j has a set A_j of possible attribute values. Thus, $\mathbf{x} \in A_1 \times \ldots \times A_m$. We denote the set of possible class labels by C. A data point $(X_i(\omega), Y_i(\omega))$ is thus an element of the set $(A_1 \times \ldots \times A_m \times C)$. See Appendix A for the mathematical notation used in creating product data structures. We denote the *sample space* of any random variable Z by S_Z. The sample space for X_i is thus $S_{X_i} = A_1 \times \ldots \times A_m$ and for Y_i it is $S_{Y_i} = C$. Because $S_{X_i} = S_{X_j}, S_{Y_i} = S_{Y_j}$ for all $1 \leq i, j \leq N$, for simplicity we also write S_X for $A_1 \times \ldots \times A_m$ and S_Y for C.

The entire training data table is an element of the sample space $S_{\mathbf{X}\otimes\mathbf{Y}}$ of the product RV $\mathbf{X}\otimes\mathbf{Y} = (\bigotimes_{i=1,\ldots,N} X_i)\otimes(\bigotimes_{i=1,\ldots,N} Y_i)$. Just to exercise formalization

skills: do you see that

$$S_{\mathbf{X}} \times S_{\mathbf{Y}} = (A_1 \times \ldots \times A_m)^N \times C^N = (A_1 \times \ldots \times A_m \times C)^N = S_{\mathbf{X} \otimes \mathbf{Y}}?$$

To round off our rehearsal of elementary concepts and notation, I repeat the basic connections between random variables, probability spaces and sample spaces: a random variable Z always comes with an underlying probability space $(\Omega, \mathfrak{A}, P)$ and a sample space S_Z. The RV is a *function* $Z : \Omega \to S_Z$, and induces a *probability distribution* on S_Z. This distribution is denoted by P_Z.

I torture you with these exercises in notation like a Russian piano teacher will torture his students with technical finger-exercising *études*. It is technical and mechanical and the suffering student may not happily appreciate the necessity of it all, – and yet this torture is a precondition for becoming a virtuoso. The music of machine learning is played in tunes of probability, no escape.

I am aware that, if you did not know these probability concepts before, this condensed rehearsal cannot possibly be understandable. Probability theory is one of the most difficult to learn sectors of mathematics and it takes weeks of digesting and exercising to embrace the concepts of probability spaces, random variables and sample spaces (not to speak of σ-fields). I will give a condensed probability basics tutorial in the tutorial sessions accompanying this course if there is a demand. Besides that I want to recommend my lecture notes "Principles of Statistical Modeling" which I mentioned before. They come from a graduate course whose purpose was to give a slow, detailed, understandable, yet fully correct introduction to the concepts of probability theory and statistics.

2.3 Learning decision trees: setting the stage

After this rough terrain excursion into probability notation we can start to discuss decision tree learning.

Despite the innocent looks of decision trees, no universally "optimal" method is known how to learn them from training data. But it is known what are the basic options for designing a decision tree learning algorithm. There are a few key decisions the algorithm designer has to make in order to assemble a learning algorithm for decision trees, and standard algorithmic building blocks for each of the design decisions are known. We will now present these design options in turn.

Two things must be given before a learning algorithm can be assembled and learning can start: (A) the training data, and (B) an optimization criterion. While (A) is obvious, (B) deserves a few words of explanation.

We observe that decision tree learning is a case of supervised learning. The training data is a collection of labeled samples $(\mathbf{x}_i, y_i)_{i=1,\ldots,N} = (X_i(\omega), Y_i(\omega))_{i=1,\ldots,N}$, where $\mathbf{x}_i \in A_1 \times \ldots A_m = S_X$ is an attribute vector and $y_i \in C = S_Y$ is a class label. A decision tree represents a function $h : S_X \to S_Y$ in an obvious way: using the sequential decision procedure outlined in Section 2.1, a vector of observed attributes leads you from the root node to some leaf, and that leaf gives a class label.

In statistics, such functions $h : S_X \to S_Y$ are generally called *decision functions* (also in other supervised learning settings that do not involve decision trees), a term that I will also sometimes use.

Decision tree learning is an instance of the general case of supervised learning: the training data are labeled pairs $(\mathbf{x}_i, y_i)_{i=1,\ldots,N}$, with $\mathbf{x}_i \in S_X, y_i \in S_Y$, and the learning aims at finding a decision function $h : S_X \to S_Y$ which is "optimal" in some sense.

In what sense can such a function $h : S_X \to S_Y$ (in this section: such a decision tree) be "optimal"? How can one quantify the "goodness" of functions of the type $h : S_X \to S_Y$?

This is a very non-trivial question as we will learn to appreciate as the course goes on. For supervised learning tasks, the key to optimizing a learning procedure is to declare a *loss function* at the very outset of a learning project. A loss function is a function

$$L : S_Y \times S_Y \to \mathbb{R}^{\geq 0}, \tag{1}$$

which assigns a nonnegative real number to a pair of class labels. The loss function is used to compare the classification $h(\mathbf{x})$, returned by a decision function h on input $\mathbf{x}$, with the correct value. After having learnt a decision function h from a training sample $S_{\mathbf{X}} \times S_{\mathbf{Y}}$, one can quantify the performance of h averaged over the training data, obtaining a quantity R^{emp} that is called the *empirical risk*:

$$R^{\mathsf{emp}}(h) = \frac{1}{N} \sum_{i=1,\ldots,N} L(h(\mathbf{x}_i), y_i). \tag{2}$$

Most supervised machine learning procedures are built around some optimization procedure which searches for decision functions which minimize the empirical risk, that is, which try to give a small average loss on the training data.

I emphasize that minimizing the empirical loss (or in another common wording, minimizing the "training error") by a clever learning algorithm will usually not lead to a very useful decision function. This is due to the problem of *overfitting*. "Overfitting" means, intuitively speaking, that if the learning algorithm tries everything to be good (= small loss) on the training data, it will attempt to minimize the loss individually for each training data point. This means, in some way, to learn the training data "by heart" – encode an exact memory of the training data points in the learnt decision function h. This is not a good idea because later "test" data points will be different, and the decision function obtained by "rote learning" will not know how to *generalize* to the new data points. The ultimate goal of supervised machine learning is not to minimize the empirical loss (that is, to have small loss on the training data), but to minimize the loss on future "test" data which were not available for training. Thus, the central optimization criterion for supervised learning methods is to find decision functions h which have a small *risk*

$$R(h) = E[L(h(X), Y)], \tag{3}$$

where E is the *statistical expectation* operator (see Appendix D). That is, a good decision function h should incur a small expected loss – it should have small "testing error". At a later point in this course we will analyse the problem of avoiding overfitting in more detail. For now it is enough to be aware that overfitting is a very serious threat, and that in order to avoid it one should not allow the models h to dress themselves too closely around the training data points.

For a classification task with a finite number of class labels, like in our fruit example, a natural loss function is one that simply counts misclassifications:

$$L^{\mathsf{count}}(h(\mathbf{x}), y) = \begin{cases} 0, & \text{if } h(\mathbf{x}) = y \\ 1, & \text{if } h(\mathbf{x}) \neq y \end{cases} \tag{4}$$

This *counting loss* is often a natural choice, but in many situations it is not appropriate. Consider, for instance, medical diagnostic decision making. Assume you visit a doctor with some vague complaints. Now compare two scenarios.

- Scenario 1: after doing his diagnostics the doctor says, "sorry to tell you but you have cancer and you should think about making your will" – and this is a wrong diagnosis; in fact you are quite healthy.
- Scenario 2: after doing his diagnostics the doctor says, "good news, old boy: there's nothing wrong with you except you ate too much yesterday" – and this is a wrong diagnosis; in fact you have intestinal cancer.

These two errors are called the "false positive" and the "false negative" decisions. A simple counting loss would optimize medical decision making such that the average number of any sort of error is minimized, regardless whether it is a false negative or a false positive. But in medicine, false negatives should be avoided as much as possible because their consequences can be lethal, whereas false positives will only cause a passing anxiety and inconvenience. Accordingly, a loss function used to optimize medical decision making should put a higher penality (= larger L values) on false negatives than on false positives.

Generally, and specifically so in *operations research* and *decision support systems*, loss functions can become very involved, including a careful balancing of conflicting ethical, financial or other factors. However, we will not consider complex loss functions here and stick to the simple counting loss. This loss is the one that guided the design of the classical decision tree learning algorithms. And now, finally, we have set the stage for actually discussing learning algorithms for decision trees!

2.4 Learning decision trees: the core algorithm

Ok., let us go concrete. We are given training data $(\mathbf{x}_i, y_i)_{i=1,\ldots,N}$ (in real life often an Excel table), and – opting for the counting loss – we want to find an

optimal (more realistically: a rather good) decision tree h^{opt} which will minimize misclassifications on new "test" data.

In order to distil this h^{opt} from the training data, we need to set up a *learning algorithm* which, on input $(\mathbf{x}_i, y_i)_{i=1,\ldots,N}$, outputs h^{opt}.

All known learning algorithms for decision trees incrementally build h^{opt} from the root node downwards. The first thing a decision tree learning algorithm (DTLA) must do is therefore to decide which property is queried first, making it the root node.

To understand the following procedures, notice that a decision tree iteratively splits the training dataset in increasingly smaller, disjoint subsets. The root node can be associated with the entire training dataset – call it D. If the root node ν_{root} queries the property Q_j and this property has k_j attributes $a^j_1, \ldots, a^j_{k_j}$, there will be k child nodes $\nu_1, \ldots, \nu_{k_j}$ where node ν_l will be covering all training datapoints that have attribute a^j_l; and so forth down the tree. In detail: if $\nu_{l_1 l_2 \cdots l_r}$ is a tree node at level r (counting from the root), and this node is associated with the subset $D_{l_1 l_2 \cdots l_r}$ of the training data, and this node queries property Q_u which has attributes $a^u_1, \ldots, a^u_{k_u}$, then the child node $\nu_{l_1 l_2 \cdots l_r l_s}$ will be that subset of $D_{l_1 l_2 \cdots l_r}$ which contains those training data points that have attribute a^u_s of property Q_u.

The classical solution to this problem of selecting a property Q for the root node is to choose that property which leads to a "maximally informative" split of the training dataset in the first child node level. Intuitively, the data point subsets associated with the child nodes should be as "pure" as possible with respect to the classes $c \in C$.

In the best of all cases, if there are q different classes (that is, $|C| = q$), there would be a property $Q_{\mathsf{supermagic}}$ with q attributes which already uniquely identify classes, such that each first-level child node is already associated with a "pure" set of training examples all from the same class – say, the first child node covers only apples, the second only bananas, etc.

This will usually not be possible, among other reasons because normally there is no property with exactly as many attributes as there are classes. Thus, "purity" of data point sets associated with child nodes needs to be measured in a way that tolerates class mixtures in each node. The measure that is traditionally invoked in this situation comes from information theory. It is the *entropy* of the class distribution within a child node. If D_l is the set of training points associated with a child node ν_l, and n^l_i is the number of data points in D_l that are from class i (where $i = 1, \ldots, q$), and the total size of D_l is n^l, then the entropy S_l of the "class mixture" in D_l is given by

$$S_l = -\sum_{i=1,\ldots,q} \frac{n^l_i}{n^l} \log_2 \left(\frac{n^l_i}{n^l} \right). \tag{5}$$

If in this sum a term $\frac{n^l_i}{n^l}$ happens to be zero, by convention the product $\frac{n^l_i}{n^l} \log_2 \left(\frac{n^l_i}{n^l} \right)$ is set to zero, too. I quickly rehearse two properties of entropy which

are relevant here:

- Entropies are always nonnegative.
- The more "mixed" the set D_l, the higher the entropy S_l. In one extreme case, D_l is 100% clean, that is, it contains only data points of a single class. Then $S_l = 0$. The other extreme is the greatest possible degree of mixing, which occurs when there is an equal number of data points from each class in D_l. Then S_l attains its maximal possible value of $-q\,(1/q)\,\log_2(1/q) = \log q$.

When S_l is zero, the set D_l is "pure" — it contains examples of only one class. The larger S_l, the less pure D_l. This has led to the terminology to call the entropy measure S_l an *impurity* measure.

The entropy of the root node is

$$S_{\mathsf{root}} = -\sum_{i=1,\ldots,q} \frac{n_i^{\mathsf{root}}}{N} \log_2 \left(\frac{n_i^{\mathsf{root}}}{N} \right),$$

where n_i^{root} is the number of examples of class i in the total training data set D and N is the number of training data points. Following the terminology of Duda, Hart, and Stork 2001, I will denote the impurity measure of the root by $i_{\mathsf{entropy}}(\nu_{\mathsf{root}}) := S_{\mathsf{root}}$.

More generally, if ν is child node of the root, and this node is associated with the training data point set D_ν, and $|D_\nu| = n$, and the q classes are represented in D_ν by subsets of size $n_1, \ldots, n_q$, the entropy impurity of ν is given by

$$i_{\mathsf{entropy}}(\nu) = -\sum_{i=1,\ldots,q} \frac{n_i}{n} \log_2 \left(\frac{n_i}{n} \right). \tag{6}$$

If the root node ν_{root} queries the property Q_j and this property has k attributes, then the mixing of classes averaged over all child nodes $\nu_1, \ldots, \nu_k$ is given by

$$\sum_{l=1,\ldots,k} \frac{|D_l|}{N}\, i_{\mathsf{entropy}}(\nu_l),$$

where D_l is the point set associated with ν_l.

Subtracting this average class mixing found in the child nodes from the class mixing in the root, one obtains the *information gain* achieved by opting for property Q_j for the root node:

$$\Delta i_{\mathsf{entropy}}(\nu_{\mathsf{root}}, Q_j) = i_{\mathsf{entropy}}(\nu_{\mathsf{root}}) - \sum_{l=1,\ldots,k} \frac{|D_l|}{N}\, i_{\mathsf{entropy}}(\nu_l). \tag{7}$$

It can be shown that this quantity is always nonnegative. It is maximal when all child nodes have pure data point sets associated with them.

For any other node ν labeled with property Q, where Q has k attributes, and the size of the set associated with ν is n and the sizes of the sets associated with the k child nodes $\nu_1, \ldots, \nu_k$ are $n_1, \ldots, n_k$, the information gain for node ν is

$$\Delta i_{\mathsf{entropy}}(\nu, Q) = i_{\mathsf{entropy}}(\nu) - \sum_{l=1,\ldots,k} \frac{n_l}{n}\, i_{\mathsf{entropy}}(\nu_l). \tag{8}$$

The procedure to choose a property for the root node is to compute the information gain for all properties and select the one which maximizes the information gain.

This procedure of choosing that query property which leads to the greatest information gain is repeated tree-downwards as the tree is grown by the DTLA. A node is not further expanded and thus becomes a leaf node if (i) either the training dataset associated with this node is 100% pure (contains only examples from a single class), or if (ii) one has reached the level q, that is, all available properties have been queried on the path from the root to that node. In case (i) the leaf is labeled with the unique class of its associated data point set. In case (ii) it is labeled with the class that has the largest number of representatives in the associated data point set.

Information gain is the most popular and historically first criterion used for determining the query property of a node. But other criteria are used too. I mention three.

The first is a normalized version of the information gain. The motivation is that the information gain criterion (8) favours properties that have more attributes over properties with fewer attributes. This requires a little explanation. Generally speaking, properties with many attributes statistically tend to lead to purer data point sets in the children nodes than properties with only few attributes. To see this, compare the extreme cases of a property with only a single attribute, which will lead to a zero information gain, with the extreme case of a property that has many more attributes than there are data points in the training dataset, which will (statistically) lead to many children node data point sets which contain only a single example, that is, they are 100% pure. A split of the data point set D_ν into a large number of very small subsets is undesirable because it is a door-opener for overfitting. This preference for properties with more attributes can be compensated if the information gain is normalized by the entropy of the data set splitting, leading to the *information gain ratio* criterion, which here is given for the root node:

$$\Delta_{\mathsf{ratio}}\, i_{\mathsf{entropy}} = \frac{\Delta i_{\mathsf{entropy}}(\nu_{\mathsf{root}}, Q_j)}{-\sum_{l=1,\ldots,k} \frac{|D_l|}{N} \log_2 \frac{|D_l|}{N}}. \tag{9}$$

The second alternative that I mention measures the impurity of a node by its *Gini impurity*, which for a node ν associated with set D_ν, where $|D_\nu| = n$ and the subsets of points in D_ν of classes $1, \ldots, q$ have sizes $n_1, \ldots, n_q$, is

$$i_{\mathsf{Gini}}(\nu) = \sum_{1 \le i,j \le q; i \ne j} \frac{n_i}{n}\, \frac{n_j}{n} = 1 - \sum_{1 \le i \le q} \left(\frac{n_i}{n}\right)^2,$$

which is the error rate when a category decision for a randomly picked point in D_ν is made randomly according to the class distribution within D_ν.

The third alternative is called the *misclassification impurity* in Duda, Hart, and Stork 2001 and is given by

$$i_{\mathsf{misclass}}(\nu) = 1 - \max\{\frac{n_l}{n} \,|\, l = 1, \ldots, q\}.$$

This impurity measure is the minimum (taken over all classes c) probability that a point from D_ν which is of class c is misclassified if the classification is randomly done according to the class distribution in D_ν.

Like the entropy impurity, the Gini and misclassification impurities are non-negative and equal to zero if and only if the set D_ν is 100% pure. Like it was done with the entropy impurity, these other impurity measures can be used to choose a property for a node ν through the gain formula (8), plugging in the respective impurity measure for i_{entropy}.

This concludes the presentation of the core DTLA. It is a *greedy* procedure which incrementally constructs the tree, starting from its root, by always choosing that property for the node currently being constructed which maximizes the information gain (7) or one of the alternative impurity measures.

You will notice some unfortunate facts:

- An optimization scheme which works by iteratively applying *local* greedy optimization steps will generally not yield a *globally* optimal solution.
- We started from claiming that our goal is to learn a tree which minimizes the count loss (or any other loss we might opt for). However, none of the impurity measures and the associated local gain optimization is connected in a mathematically transparent way with that loss. In fact, no computationally tractable method for learning an empirical-loss-minimal tree exists: the problem is NP-complete (Hyafil and Rivest 1976).
- It is not clear which of the impurity measures is best for the goal of minimizing the empirical loss.

In summary, we have here a *heuristic* learning algorithm (actually, a family of algorithms, depending on the choice of impurity measure) which is based on intuition and the factual experience that it works reasonably well in practice. Only heuristic algorithms are possible due to the NP-completeness of the underlying optimization problem.

2.5 Dealing with overfitting

If a decision tree is learnt according to the core algorithm, there is the danger that it overfits. This means that it performs well on the training data – that is, it has small empirical loss – which boils down to a condition where all leaf nodes are

rather pure. A zero empirical loss is easily attained if the number of properties and attributes is large. Then it will be the case that every training example has a unique combination of attributes, which leads to 100% pure leaf nodes, and every leaf having only a small set of training examples associated with it, maybe singleton sets. Then one has zero misclassifications of the training examples. But, intuitively speaking, the tree has just memorized the training set. If there is some "noise" in the attributes of data points, new examples (not in the training set) will likely have attribute combinations that lead the learnt decision tree on wrong tracks.

We will learn to analyze and fight overfitting later in the course. At this point I only point out that if a learnt tree T overfits, one can typically obtain from it another tree T' which overfits less, by *pruning* T. Pruning a tree means to select some internal nodes and delete all of their children. This makes intuitive sense: the deeper one goes down in a tree learnt by the core algorithm, the more does the branch reflect "individual" attribute combinations found in the training data.

To make this point particularly clear, consider a case where there are many properties, but only one of them carries information relevant for classification, while all others are purely random. For instance, for a classification of patients into the two classes "healthy" and "has_cancer", the binary property "has_increased_ leukocyte_count" carries classification relevant information, while the binary property "given_name_starts_with_A" is entirely unconnected to the clinical status. If there are enough such irrelevant properties to uniquely identify each patient in the training sample, the core algorithm will (i) most likely find that the relevant property "has_increased_leukocyte_count" leads to the greatest information gain at the root and thus use it for the root decision, and (ii) subsequently generate tree branches that lead to 100% pure leaf nodes. Zero training error and poor generalization to new patients results. The best tree here would be the one that only expands the root node once, exploiting the only relevant property.

With this insight in mind, there are two strategies to end up with trees that are not too deep.

The first strategy is *early stopping*. One does not carry the core algorithm to its end but at each node which one has created, one decides whether a further expansion would lead to overfitting. A number of statistical criteria are known to decide when it is time to stop expanding the tree; or one can use cross-validation (explained in later chapters in these lecture notes). We do not discuss this further here – the textbook by Duda explains a few of these statistical criteria. A problem with early stopping is that it suffers from the *horizon effect*: if one stops early at some node, a more fully expanded tree might exploit further properties that are, in fact, relevant for classification refinement underneath the stopped node.

The second strategy is *pruning*. The tree is first fully built with the core algorithm, then it is incrementally shortened by cutting away end sections of branches. An advantage of pruning over early stopping is that it avoids the horizon effect. Duda says (I am not a decision tree expert and can't judge) that pruning

should be preferred over early stopping "in small problems" (whatever "small" means).

2.6 Variants and refinements

The landscape of decision tree learning is much richer than what we can explore in a single lecture. Two important topics which I omit (treated briefly in Duda's book):

Missing values. Real-world datasets will typically have missing values, that is, not all training or test examples will have attribute values filled in for all properties. Missing values require adjustments both in training (an adapted version of impurity measures which accounts for missing values) and in testing (if a test example leads to a node with property Q and the example misses the required attribute for Q, the normal classification procedure would abort). The Duda book dedicates a subsection to recovery algorithms.

Numerical properties. Many real-world properties, like for instance "velocity" or "weight", have a continuous numerical range for attribute values. This requires a split of the continuous value range into a finite number (often two) of discrete bins which then serve as discrete attributes. For instance, the range of a "body_weight" property might be split into two ranges "<50kg" and "≥50kg", leading to a new property with only two attributes. These ranges can be further split into finer-grained subproperties which would be queried downstream in the tree, for instance querying for "<45kg" vs. "45kg≤50kg underneath the "<50kg" node. Heuristics must be used to determine splitting boundaries which lead to well-performing (correct and cheap = not too many nodes) trees. Again – consult Duda.

All in all, there is a large number of design decisions to be made when setting up a decision tree learning algorithm, and a whole universe of design criteria and algorithmic sub-procedures is available in the literature. Some combinations of such design decisions have led to final algorithms which have become branded with names and are widely used. Two algorithms which are invariably cited (and which are available in professional toolboxes) are the ID3 algorithm and its more complex and higher-performant successor, the C4.5 algorithm. They had been introduced by the decision tree pioneer Ross Quinlan in 1986 and 1993, respectively. The Duda book gives brief descriptions of these canonical algorithms.

2.7 Random forests

Decision tree learning is a subtle affair. If one designs a DTLA by choosing a specific combination of the many design options, the tree that one gets from a training dataset D will be influenced by that choice of options. It will not

be "the optimal" tree which one might obtain by some other choice of options. Furthermore, if one uses pruning or early stopping to fight overfitting, one will likely end up with trees that, while not overfitting, are underfitting – that is, they do not exploit all the information that is in the training data. In summary, whatever one does, one is likely to obtain a decision tree that is significantly sub-optimal.

This is a common situation in machine learning. There are only very few machine learning techniques where one has full mathematical control over getting the best possible model from a given training dataset, and decision tree learning is not among them. Fortunately, there is also a common escape strategy for minimizing the quality deficit inherent in most learning designs: *ensemble methods*. The idea is to train a whole collection (called "ensemble") of models (here: trees), each of which is likely suboptimal (jargon: each model is obtained from a "weak learner"), but if their results on a test example are diligently combined, the merged result is much better than what one gets from each of the models in the ensemble. It's the idea of crowd intelligence.

"Ensemble methods" is an umbrella term for a wide range of techniques. They differ, obviously, in the kind of the individual models, like for instance decision trees vs. neural networks. Second, they vary in the methods of how one generates diversity in the ensemble. Ensemble methods work well only to the extent that the individual models in the ensemble probe different aspects in the training data – they should look at the data from different angles, so to speak. Thirdly, ensemble methods differ in the way how the results of the individual models are combined. A general theory for setting up an ensemble learning scheme is not available – we are again thrown back to heuristics. The Wikipedia articles on "Ensemble learning" and "Ensemble averaging (machine learning)" give a condensed overview.

Obviously, ensemble methods can only be used when the computational cost of training a single model is rather low. This is the case for decision tree learning. Because training an individual tree will likely not give a competitive result, but is cheap, it is common practice to train not a single decision tree but an entire ensemble – which in the case of tree learning is called a *random forest*. In fact, random forests can yield competitive results (for instance, compared to neural networks) at moderate cost, and are therefore often used in practical applications.

The definite reference on random forests is Breiman 2001. The paper has two parts. In the first part, Breiman gives a mathematical analysis of why combining decision trees does not lead to overfitting, and derives an instructive upper bound on the generalization error (= risk, see Section 2.3). These results were in synchrony with mainstream theory work in other areas of machine learning at the time and made this paper *the* theory anchor for random forests. However, I personally find the math notation used by Breiman opaque and hard to penetrate, and I am not sure how many readers could understand it. The second, larger part of this paper describes several variants and extensions of random forest algorithms, discusses their properties and benchmarks some of them against the leading clas-

sification learning algorithms of the time, with favourable outcomes. This part is an easy read and the presented algorithms are not difficult to implement. My hunch is that it is the second rather than the first part which led to the immense impact of this paper.

Here I give a summary of the paper, in reverse order, starting with the practical algorithm recommended by Breiman. After that I give an account of the most conspicuous theoretic results in transparent standard probability notation.

In ensemble learning one must construct many *different* models in an automated fashion. One way to achieve this is to employ a *stochastic* learning algorithm. A stochastic learning algorithm can be seen as a learning algorithm which takes two arguments. The first argument is the training data D, the same as in ordinary, non-stochastic learning algorithms. The second argument is a random vector, denoted by Θ in Breiman's paper, which is set to different random values in each run of the algorithm. Θ can be seen as a vector of control parameters in the algorithm; different random settings of these control parameters lead to different outcomes of the learning algorithm although the training data are always the same, namely D.

Breiman proposes two ways in order to make the tree learning stochastic:

Bagging. In each run of the learning algorithm, the training dataset is *resampled with replacement*. That is, from D one creates a new training dataset D' of the same size as D by randomly copying elements from D into D'. This is a general approach for ensemble learning, called *bagging*. The Wikipedia article on "Bootstrap aggregating" gives an easy introduction if you are interested in learning more.

Random feature selection is the term used by Breiman for a randomization technique where, at each node whose query property has to be chosen during tree growing, a small subset of all still unqueried properties is randomly drawn as candidates for the query property of this node. The winning property among them is determined by the information gain criterion.

Combining these two randomness-producing mechanisms with a number of other design decisions not mentioned here, Breiman obtains a stochastic learning algorithm which, with ensembles of size 100, outperformed other methods that were state-of-the-art at that time.

The random vector Θ, which is needed for a concise specification and a mathematical analysis of the resulting stochastic tree learning algorithm, is some essentially arbitrary encoding of the random choices made for bagging and random feature selection.

The main theoretical result in Breiman's paper is his Theorem 2.3:

$$PE^* \leq \bar{\varrho}\,(1 - s^2)/s^2.$$

This theorem certainly added much to the impact of the paper, because it gives an intuitive guidance for the proper design of random forests, and also because it

connected random decision tree forests to other machine learning methods which were being mathematically explored at the time when the paper appeared. I will now try to give a purely intuitive explanation, and then conclude this section with a clean-math explanation of this theorem.

- The quantity PE^*, called *generalization error* by Breiman, is the probability that a random forest (in the limit of its size going to infinity) makes wrong decisions. Obviously one wants this probability to be as small as possible.

- The quantity $\bar{\varrho}$ is a certain statistical correlation measure which measures how similar, on average across the tree population in a forest, the various trees will arrive at different classifications on test data points. This measure is maximal if all trees always yield the same classification results, and it is minimal if, roughly speaking, their classification results are statistically independent.

- The quantity s, which satisfies $0 \leq s \leq 1$, called by Breiman the *strength* of the stochastic tree learning algorithm, measures a certain "discerning power" of the average tree in a forest, that is, how large is the probability gap between an average tree making the right decision and the probability for the tree to make a wrong decision. s ranges in $[0, 1]$ and if the strength is equal to the maximal value of 1, then all trees in the forest always make correct decisions on all test data points. If it is zero, then the trees make more incorrect decisions than correct ones on average across the forest and test data points.

Note that the factor $(1 - s^2)/s^2$ ranges between zero and infinity and is monotonously increasing with decreasing s. It is zero with maximal strength $s = 1$, and it is infinite if the strength is zero.

The theorem gives an upper bound on the generalization error observed in (asymptotically infinitely large) random forests. The main message is that this bound is a product of a factor $\bar{\varrho}$ which is smaller when the different trees in a forest vary more in their response to test inputs, with a factor $(1-s^2)/s^2$ which is smaller when the trees in the forest place a larger probability gap between correct and the second most common decision across the forest. The suggestive message of all of this is that in designing a stochastic decision tree learning algorithm one should

- aim at maximizing the response variability across the forest, while

- attempting to ensure that trees mostly come out with correct decisions.

If one succeeds to generate trees that always give correct decisions, one has maximal strength $s = 1$ and the generalization error is obviously zero. This will usually be impossible. Instead, the stochastic tree learning algorithm will produce trees that have a residual error probability, that is, $s < 1$. Then the first factor

implies that one should aim at a stochastic tree generation mechanism which (while fixing the strength) show great variability in their response behavior.

The remainder of this section is only for those of you who are familiar with probability theory, and this material will not be required in the final exam. I will give a mathematically transparent account of Breiman's Theorem 2.3. This boils down to an exercise in clean mathematical formalism. We start by formulating the ensemble learning scenario in rigorous probability terms. There are two underlying probability spaces involved, one for generating data points, and the other for generating the random vectors Θ. I will denote these two spaces by $(\Omega, \mathfrak{A}, P)$ and $(\Omega^*, \mathfrak{A}^*, P^*)$ respectively, with the second one used for generating Θ. The elements of Ω, Ω^* will be denoted by ω, ω^*, respectively.

Let X be the RV which generates attribute vectors,

$$X : \Omega \to A_1 \times \ldots \times A_m,$$

and Y the RV which generates class labels,

$$Y : \Omega \to C.$$

The random parameter vectors Θ can be vectors of any type, numerical or categorical, depending on the way that one chooses to parametrize the learning algorithm. Let T dennote the space from which Θ's can be picked. For a forest of K trees one needs K random vectors Θ_j, where $j = 1, \ldots, K$. Let

$$Z_j : \Omega^* \to T$$

be the RV which generates the j-th parameter vector, that is, $Z_j(\omega^*) = \Theta_j$. The RVs Z_j $(j = 1, \ldots, K)$ are independent and identically distributed (iid).

In the remainder of this section, we fix some training dataset D. Let $h(\cdot, \Theta)$ denote the tree that is obtained by running the stochastic tree learning algorithm with parameter vector Θ. This tree is a function which outputs a class decision if the input is an attribute vector, that is,

$$h(\mathbf{x}, \Theta) \in C.$$

When Θ is fixed, we can view h as a function of the RV X, thus

$$h(X, \Theta) : \Omega \to C$$

is a random variable.

Now the stage is prepared to re-state Breiman's central result (Theorem 2.3) in a transparent notation.

Breiman starts by introducing a function mr, called *margin function for a random forest*,

$$\begin{aligned} mr : (A_1 \times \ldots \times A_m) \times C &\to \mathbb{R} \\ (\mathbf{x}, y) &\mapsto P^*(h(\mathbf{x}, Z) = y) - \max_{\tilde{y} \neq y} \{P^*(h(\mathbf{x}, Z) = \tilde{y})\}, \end{aligned}$$

where Z is a random variable distributed like the Z_j.

If you think about it you will see that $mr(\mathbf{x}, y) > 0$ if and only if a very large forest (in the limit of its size going to infinity) will classify the data point $(\mathbf{x}, y)$ correctly, and $mr(\mathbf{x}, y) < 0$ if the forest will come to a wrong collective decision.

On the basis of this margin function, Breiman defines the *generalization error* PE^* by

$$PE^* = P(mr(X, Y) < 0).$$

The expectation of mr over data examples is

$$s = E[mr(X, Y)].$$

s is a measure to what extent, averaged over data point examples, the correct answer probability (over all possible decision trees) is larger than the highest probability of deciding for any other answer. Breiman calls s the *strength* of the parametrized stochastic learning algorithm. The stronger the stochastic learning algorithm, the greater the probability margin between correct and wrong classifications on average over data point examples.

Breiman furthermore introduces a *raw margin function* rmg_Θ, which is a function of X and Y parametrized by Θ, through

$$rmg_\Theta(\omega) = \begin{cases} 1, & \text{if } h(X(\omega), \Theta) = Y(\omega), \\ -1, & \text{if } h(X(\omega), \Theta) \text{ gives the maximally probable among the} \\ & \text{wrong answers in an asymptotically infinitely large forest,} \\ 0, & \text{else.} \end{cases} \tag{10}$$

Define $\varrho(\Theta, \Theta')$ to be the correlation (= covariance normalized by division with standard deviations) between rmg_Θ and $rmg_{\Theta'}$. For given Θ, Θ', this is a number in $[-1, 1]$. Seen as a function of Θ, Θ', $\varrho(\Theta, \Theta')$ maps each pair Θ, Θ' into $[-1, 1]$, which gives a RV which we denote with the same symbol ϱ for convenience,

$$\varrho(Z, Z') : \Omega^* \to [-1, 1],$$

where Z, Z' are two independent RVs with the same distribution as the Z_j.

Let

$$\bar{\varrho} = E[\varrho(Z, Z')]$$

be the expected value of $\varrho(Z, Z')$. It measures to what extent, in average across random choices for Θ, Θ', the resulting two trees $h(\cdot, \Theta)$ and $h(\cdot, \Theta')$ have both the same correct or wrong decision averaged over data examples.

And here is, finally, Breiman's Theorem 2.3:

$$PE^* \leq \bar{\varrho}\,(1 - s^2)/s^2, \tag{11}$$

whose intuitive message I discussed earlier.

3 Elementary supervised temporal learning

In this section I give an introduction to a set of temporal data modeling methods which combine simplicity with broad practical usefulness: learning temporal tasks by training a linear regression map that transforms input signal windows to output data. In many scenarios, this simple technique is all one needs. It can be programmed and executed in a few minutes (really!) and you should run this technique as a first baseline whenever you start a serious learning task that involves time series data.

This section deals with *numerical* timeseries where the data format for each time point is a real-valued scalar or vector. This includes the majority of all learning tasks that arise in the natural sciences, in engineering, robotics, speech and in image processing.

Methods for dealing with *symbolic* timeseries (in particular texts, but also discrete action sequences of intelligent agents / robots, DNA sequences and more) can be obtained by encoding symbols into numerical vectors and then apply numerical methods. Often however one uses methods that operate on symbol sequences directly (all kinds of discrete-state dynamical systems, deterministic or stochastic, like finite automata, Markov chains, hidden Markov models, dynamical Bayesian networks, and more). I will not consider such methods in this section.

My secret educational agenda in this section is that this will force you to rehearse linear regression - which is such a basic, simple yet widely useful method that everybody should have a totally 100% absolute unshakeable secure firm hold on it.

3.1 Recap: linear regression

Remark on notation: throughout these lecture notes, vectors are column vectors unless otherwise noted. I use $'$ to denote vector or matrix transpose.

I start with a generic rehearsal of linear regression, independent of temporal learning tasks.

The linear regression task is specified as follows:

Given: a collection $(\mathbf{x}_i, y_i)_{i=1,\ldots,N}$ of N training data points, where $\mathbf{x}_i \in \mathbb{R}^n$ and $y_i \in \mathbb{R}$.

Wanted: a linear map from $\mathbb{R}^n$ to $\mathbb{R}$, represented by a *regression weight vector* $\mathbf{w}$ (a row vector of size n), which solves the minimization problem

$$\mathbf{w} = \operatorname*{argmin}_{\mathbf{w}^*} \sum_{i=1}^{N} (\mathbf{w}^* \, \mathbf{x}_i - y_i)^2. \tag{12}$$

In machine learning terminology, this is a supervised learning task, because the training data points include "teacher" outputs y_i. Note that the abstract

data format $(\mathbf{x}_i, y_i)_{i=1,\ldots,N}$ is the same as for decision trees, but here the data are numerical and there they were symbolic.

By a small modification, one can make linear regression much more versatile. Note that any weight vector $\mathbf{w}^*$ in (12) will map the zero vector $\mathbf{0} \in \mathbb{R}^n$ on zero. This is often not what one wants to happen. If one enriches (12) by also training a *bias* $b \in \mathbb{R}$, via

$$(\mathbf{w}, b) = \operatorname*{argmin}_{\mathbf{w}^*, b^*} \sum_{i=1}^{N} (\mathbf{w}^* \mathbf{x}_i + b^* - y_i)^2,$$

one obtains an *affine* linear function (linear plus offset). The common way to set up lineare regression such that affine linear solutions become possible is to pad the original input vectors $\mathbf{x}_i$ with a last component of constant size 1, that is, in (12) one uses $n+1$-dimensional vectors $[\mathbf{x}; 1]$ (using Matlab notation for the vertical concatentation of vectors). Then a solution of (12) on the basis of the padded input vectors will be a regression weight vector $[\mathbf{w}, b] \in \mathbb{R}^{n+1}$, with the last component b giving the offset.

We now derive a solution formula for the minimization problem (12). Most textbooks start from the observation that the objective function $\sum_{i=1}^{N} (\mathbf{w}\mathbf{x}_i - y_i)^2$ is a quadratic function in the weights $\mathbf{w}$ and then one uses calculus to find the minimum of this quadratic function by setting its partial derivatives to zero. I will present another derivation which does not need calculus and better reveals the underlying geometry of the problem.

Let $\mathbf{x}_i = (x_i^1, \ldots, x_i^n)'$ be the ith input vector. The key to understand linear regression is to realize that the N values $x_1^j, \ldots, x_N^j$ of the j-the component in these vectors ($j = 1, \ldots, n$) can be regarded as an N-dimensional vector $\varphi_j = (x_1^j, \ldots, x_N^j)' \in \mathbb{R}^N$. Similarly, the N target values $y_1, \ldots, y_N$ can be combined into an N-dimensional vector y. Figure 10 **Top** shows a case where there are $N = 10$ input vectors of dimension $n = 4$.

Using these N-dimensional vectors as a point of departure, geometric insight gives us a nice clue how $\mathbf{w}$ should be computed. To admit a visualization, we consider a case where we have only $N = 3$ input vectors which each have $n = 2$ components. This gives two $N = 3$ dimensional vectors φ_1, φ_2 (Figure 10 **Bottom**). The target values y_1, y_2, y_3 are combined in a 3-dimensional vector y.

Notice that in machine learning, one should best have more input vectors than the input vectors have components, that is, $N > m$. In fact, a very coarse rule of thumb – with many exceptions – says that one should aim at $N > 10\,n$ (if this is not warranted, use unsupervised dimension reduction methods to reduce n). We will thus assume that we have fewer vectors φ_j than training data points. The vectors φ_j thus span an n-dimensional subspace in $\mathbb{R}^N$ (greenish shaded area in Figure 10 **Bottom**).

Notice (easy exercise, do it!) that the minimization problem (12) is equivalent

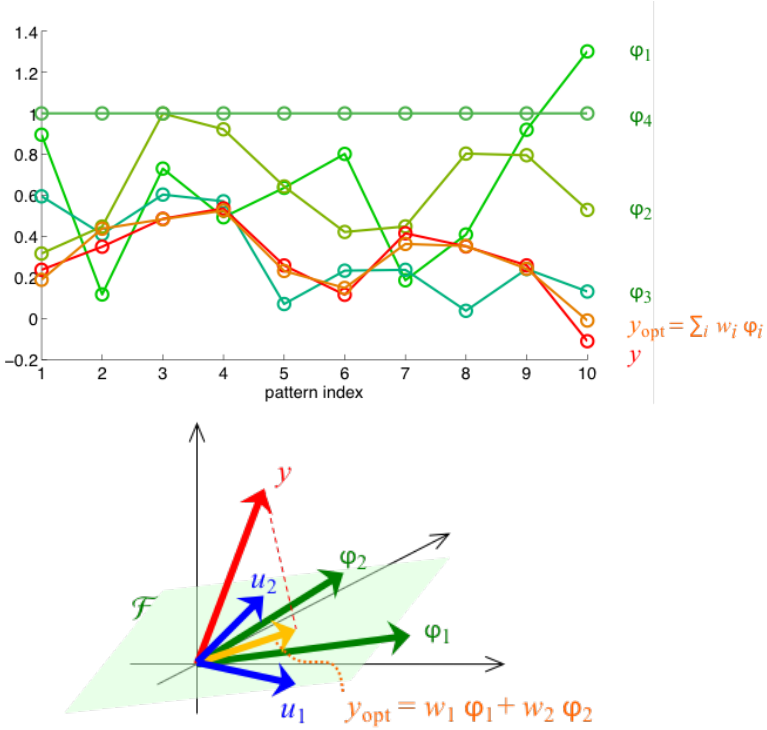

Figure 10: Two visualizations of linear regression. **Top.** This visualization shows a case where there are $N = 10$ input vectors $\mathbf{x}_i$, each one having $n = 4$ vector components $x_i^1, \ldots, x_i^4$ (green circles). The fourth component is a constant-1 bias. The ten values $x_1^j, \ldots, x_{10}^j$) of the j-th component (where $j = 1, \ldots, 4$) form a 10-dimensional (row) vector φ_j, indicated by a connecting line. Similarly, the ten target values y_i give a 10-dimensional vector y (shown in red). The linear combination $y_{\text{opt}} = \mathbf{w}[\varphi_1; \varphi_2; \varphi_3; \varphi_4]$ which gives the best approximation to y in the least mean square error sense is shown in orange. **Bottom.** The diagram shows a case where there the input vector dimension is $n = 2$ and there are $N = 3$ input vectors $\mathbf{x}_1, \mathbf{x}_2, \mathbf{x}_3$ in the training set. The three values x_1^1, x_2^1, x_3^1 of the first component give a three dimensional vector φ_1, and the three values of the second component give φ_2 (green). These two vectors span a 2-dimensional subspace $\mathcal{F}$ in $\mathbb{R}^N = \mathbb{R}^3$, shown in green shading. The three target values y_1, y_2, y_3 similarly make for a vector y (red). The linear combination $y_{\text{opt}} = w_1 \varphi_1 + w_2 \varphi_2$ which has the smallest distance to y is given by the projection of y on this plane $\mathcal{F}$ (orange). The vectors u_1, u_2 shown in blue is a pair of orthonormal basis vectors which span the same subspace $\mathcal{F}$

to

$$\mathbf{w} = \underset{\mathbf{w}^*}{\operatorname{argmin}} \|(\sum_{j=1}^{n} w_j^* \varphi_j) - y\|^2, \tag{13}$$

where $\mathbf{w}^* = (w_1^*, \ldots, w_n^*)$. We take another look at Figure 10 **Bottom**. Equation 13 tells us that we have to find the linear combination $\sum_{j=1}^{n} w_j \varphi_j$ which comes closest to y. Any linear combination $\sum_{j=1}^{n} w_j^* \varphi_j$ is a vector which lies in the linear subspace $\mathcal{F}$ spanned by $\varphi_1, \ldots, \varphi_n$ (shaded area in the figure). The linear combination which is closest to y apparently is the projection of y on that subspace. This is the essence of linear regression!

All that remains is to compute which linear combination of $\varphi_1, \ldots, \varphi_n$ is equal to the projection of y on $\mathcal{F}$. Let us call this projection y_{opt}. We may assume that the vectors $\varphi_1, \ldots, \varphi_n$ are linearly independent. If they would be linearly dependent, we could drop as many from them as is needed to reach a linearly independent set.

The rest is mechanical linear algebra.

Let $X = (\varphi_1, \ldots, \varphi_n)'$ be the $n \times N$ sized matrix whose rows are formed by the φ_j' (and whose colums are the $\mathbf{x}_i$). Then $X'X$ is a positive semi-definite matrix of size $N \times N$ with a singular value decomposition $X'X = U_N \Sigma_N U_N'$. Since the rank of X is $n < N$, only the first n singular values in Σ_N are nonzero. Let $U = (u_1, \ldots, u_n)$ be the $N \times n$ matrix made from the first n columns in U_N, and let Σ be the $n \times n$ diagonal matrix containing the n nonzero singular values of Σ_N on its diagonal. Then

$$X'X = U \Sigma U'. \tag{14}$$

This is sometimes called the *compact* SVD. Notice that the columns u_j of U form an orthonormal basis of $\mathcal{F}$ (blue arrows in Figure 10 **Bottom**).

Using the coordinate system given by $u_1, \ldots, u_n$, we can rewrite each φ_j as

$$\varphi_j = \sum_{l=1}^{n} (u_l' \varphi_j)\, u_l = UU'\varphi_j. \tag{15}$$

Similarly, the projection y_{opt} of y on $\mathcal{F}$ is

$$y_{\text{opt}} = \sum_{l=1}^{n} (u_l' y)\, u_l = UU'y, \tag{16}$$

But also $y_{\text{opt}} = X'\mathbf{w}'$. From (15) we get $X' = UU'X'$, which in combination with (16) turns $y_{\text{opt}} = X'\mathbf{w}'$ into

$$UU'y = UU'X'\mathbf{w}'.$$

A weight vector $\mathbf{w}$ solves this equation if it solves

$$U'y = U'X'\mathbf{w}'. \tag{17}$$

It remains to find a weight vector $\mathbf{w}$ which satisfies (17). I claim that $\mathbf{w}' = (X\,X')^{-1}\,X\,y$ does the trick, that is, $U'\,y = U'X'\,(X\,X')^{-1}\,X\,y$ holds.

To see this, first observe that XX' is nonsingular, thus $(XX')^{-1}$ is defined. Furthermore, observe that $U'y$ and $U'X'\,(XX')^{-1}\,X\,y$ are n-dimensional vectors, and that the $N \times n$ matrix $U\Sigma$ has rank n. Therefore,

$$U'\,y = U'X'\,(XX')^{-1}\,X\,y \iff U\Sigma U'\,y = U\Sigma U'X'\,(XX')^{-1}\,X\,y. \tag{18}$$

Replacing $U\Sigma U'$ by $X'\,X$ (compare Equation 14) turns the right equation in (18) into $X'\,X\,y = X'\,X\,X'\,(XX')^{-1}\,X\,y$, which is obviously true. Therefore, $\mathbf{w}' = (XX')^{-1}\,X\,y$ solves our optimization problem (13).

We summarize our findings:

Data. A set $(\mathbf{x}_i, y_i)_{i=1,\ldots,N}$ of n-dimensional input vectors $\mathbf{x}_i$ and scalar targets y_i.

Wanted. An n-dimensional row weight vector $\mathbf{w}$ which solves the linear regression objective from Equation 12.

Step 1. Sort the input vectors as columns into an $n \times N$ matrix X and the targets into an N-dimensional vector y.

Step 2. Compute the (transpose of the) result by

$$\mathbf{w}' = (XX')^{-1}\,X\,y. \tag{19}$$

Some further remarks:

- What we have derived here generalizes easily to cases where the data are of the form $(\mathbf{x}_i, \mathbf{y}_i)_{i=1,\ldots,N}$ where $\mathbf{x}_i \in \mathbb{R}^n, \mathbf{y}_i \in \mathbb{R}^k$. That is, the output data are vectors, not scalars. The objective is to find a $k \times n$ regression weight matrix W which solves

$$W = \operatorname*{argmin}_{W^*} \sum_{i=1}^{N} \|W^*\,\mathbf{x}_i - \mathbf{y}_i\|^2. \tag{20}$$

  The solution is given by

$$W' = (XX')^{-1}\,X\,Y,$$

  where Y is the $N \times k$ matrix that contains the $\mathbf{y}_i'$ in its rows.

- For an $a \times b$ sized matrix A, where $a \geq b$ and A has rank b, the matrix $A^+ := (A'A)^{-1}\,A'$ is called the (left) *pseudo-inverse* of A. It satisfies $A^+\,A = I_{b\times b}$. It is often also written as $A^\dagger$.

- Computing the inversion $(XX')^{-1}$ may suffer from numerical instability when XX' is close to singular. Remark: this happens more often than you would think - in fact, XX' matrices obtained from real-world, high-dimensional data are *often* ill-conditioned (= close to singular). You should always feel uneasy when your program code contains a matrix inverse! A quick fix is to always add a small multiple of the $n \times n$ identity matrix before inverting, that is, replace (19) by

$$\mathbf{w}'_{\text{opt}} = (XX' + \alpha^2 I_{n\times n})^{-1} X\, y. \tag{21}$$

  This is called *ridge regression*. We will see later in this course that ridge regression not only helps to circumvent numerical issues, but also offers a solution to the problem of overfitting.

- A note on terminology. Here we have described *linear* regression. The word "regression" is used in much more general scenarios. The general setting goes like this:

  Given: Training data $(\mathbf{x}_i, \mathbf{y}_i)_{i=1,\ldots,N}$, where $\mathbf{x}_i \in \mathbb{R}^n, \mathbf{y}_i \in \mathbb{R}^k$.

  Also given: a *search space* H containing candidate functions $h : \mathbb{R}^n \to \mathbb{R}^k$.

  Also given: a loss function $L : \mathbb{R}^k \times \mathbb{R}^k \to \mathbb{R}^{\geq 0}$.

  Wanted: A solution to the optimization problem

$$h_{\text{opt}} = \operatorname*{argmin}_{h\in\mathcal{H}} \sum_{i=1}^{N} L(h(\mathbf{x}_i), \mathbf{y}_i)$$

  In the case of linear regression, the search space $\mathcal{H}$ consists of all linear functions from $\mathbb{R}^n$ to $\mathbb{R}^k$, that is, it consists of all $k \times n$ matrices. The loss function is the *quadratic loss* which you see in (20). When one speaks of linear regression, the use of the quadratic loss is implied.

  Search spaces $\mathcal{H}$ can be arbitrarily large and rich in modeling options – for instance, $\mathcal{H}$ might be the space of all deep neural networks of a given structure and size.

  Classification tasks look similar to regression tasks at first sight: training data there have the format $(\mathbf{x}_i, c_i)_{i=1,\ldots,N}$. The difference is that that the target values c_i are not numerical but symbolic — they are class labels.

3.2 Temporal learning tasks

There are a number of standard learning tasks which are defined on the basis of timeseries data. Those tasks involve training data consisting of

an input signal $(\mathbf{u}(t))_{t\in\mathcal{T}}$, where $\mathcal{T}$ is an *ordered* set of time points and for every $t \in \mathcal{T}$, $\mathbf{u}(t) \in \mathbb{R}^k$;

a "teacher" output signal $(\mathbf{y}(t))_{t\in\mathcal{T}}$, where $\mathbf{y}(t) \in \mathbb{R}^m$.

For simplicity we will only consider discrete time with equidistant unit timesteps, that is $\mathcal{T} = \mathbb{N}$ (unbounded time) or $\mathcal{T} = \{0, 1, \ldots, T\}$ (finite time).

The learning task consists in training a system which operates in time and, if it is fed with the input signal $\mathbf{u}(t)$, produces an output signal $\hat{\mathbf{y}}(t)$ which approximates the teacher signal $\mathbf{y}(t)$ (in the sense of minimizing a loss $L(\hat{\mathbf{y}}(t) - \mathbf{y}(t))$ in time average over the training data). A few examples for illustration:

- Input signal: an ECG (electro cardiogram) signal; desired output: a signal which is constant zero as long as the ECG is normal, and jumps to 1 if there are irregularities in the ECG.
- Input signal: room temperature measurements from a thermometer. Output: value 0 as long as room temperature input signal is above certain threshold, value 1 if it is below the threshold (this is the input-output behavior of a thermostat, albeit a badly designed one - why?).
- Input signal: a noisy radio signal with lots of statics and echos. Desired output signal: the input signal in a version which has been de-noised and where echos have been cancelled.
- Input signal: a speech signal in English. Desired output: a speech signal in Dutch.

These are quite different sorts tasks. There are many names in use for quick references to temporal tasks. The ECG monitoring task would be called a *temporal classification* or *fault monitoring* task; the 0-1 switching of the badly designed thermostat is too simplistic to have a respectable name; radio engineers would speak of *de-noising* and *equalizing*, and speech translation is too uniquely complex to have a name besides "online speech translation". Input-output signal transformation tasks are as many and as diverse as there are wonders under the sun.

In many cases, one may assume that the current output data point $\mathbf{y}(t)$ only depends on inputs up to that time point, that is, on the input history $\ldots, \mathbf{u}(t-2), \mathbf{u}(t-1), \mathbf{u}(t)$. Specifically, $\mathbf{y}(t)$ does *not* depend on future inputs. Input-output systems where the output does not depend on future inputs are called *causal* systems in the signal processing world.

A causal system can be said to have *memory* if the current output $\mathbf{y}(t)$ is not fully determined by the current input $\mathbf{u}(t)$, but is influenced by earlier inputs as well. I must leave the meaning of "influenced by" vague at this point; we will make it precise in a later section when we investigate stochastic processes in more detail. All examples except the (poorly designed) thermostat example have memory.

Often, the output $\mathbf{y}(t)$ is influenced by long-ago input only to a negligeable extent, and it can be explained very well from only the input history extending back to a certain limited duration. All examples in the list above except the English

translation one have such limited relevant memory spans. In causal systems with bounded memory span, the current output $\mathbf{y}(t)$ thus depends on an input *window* $\mathbf{u}(t-d+1), \mathbf{u}(t-d+2), \ldots, \mathbf{u}(t-1), \mathbf{u}(t)$ of d steps duration. Figure 11 (top) gives an impression.

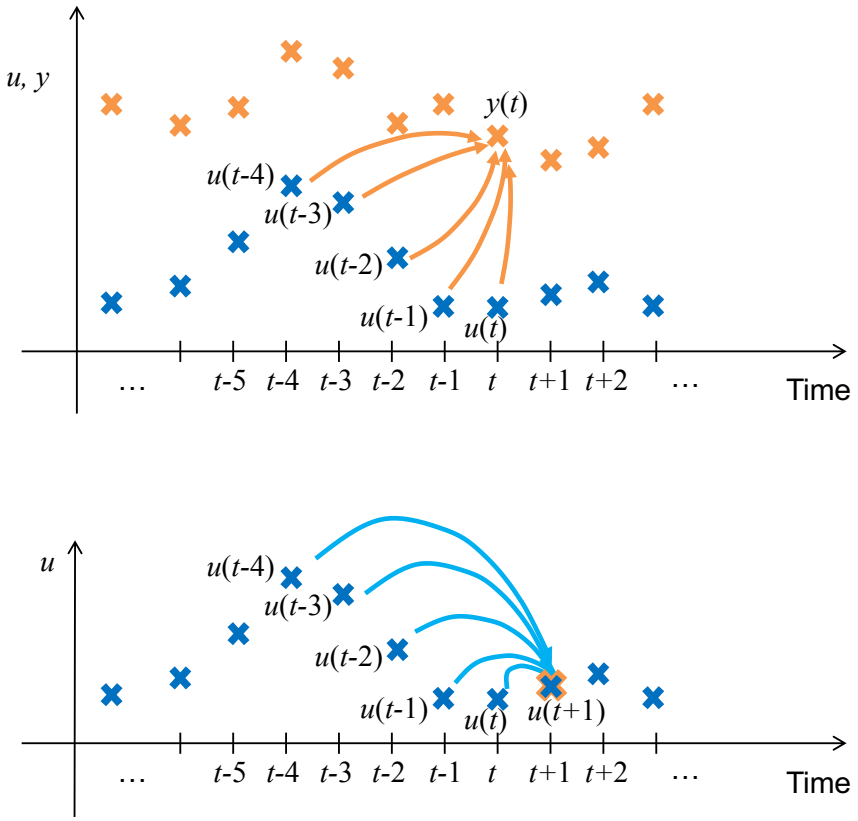

Figure 11: The principle of temporal system learning by window-based regression. The case of scalar input and output signals is shown. **Top:** an input signal $u(t)$ (blue crosses) is transformed to an output signal $y(t)$ (orange). **Bottom:** The special case of timeseries prediction (single step prediction). The window size in both diagrams is $d = 5$.

In this situation, learning an input-output system is a regression learning task. One has to find a regression function f of the kind

$$f : (\mathbb{R}^k)^d \to \mathbb{R}^m$$

which minimizes a chosen loss function on average over the training data time points.

The most convenient option is to go for the quadratic loss, which turns the fearsome input-output timeseries learning task into a case of linear regression.

Note that while in Section 3.1 I assumed that the input data points for linear regression were scalar, they are now k-dimensional vectors in general. This is not

a problem; all one has to do is to flatten the collection of d k-dimensional input vectors which lie in a window into a single $d \cdot k$ dimensional vector, and then apply (20) as before.

Linear regression is often surprisingly accurate, especially when one uses large windows and a careful regularization (to be discussed later in this course) through ridge regression. When confronted with a new supervised temporal learning task, the first thing one should do as a seasoned pro is to run it through the machinery of window-based linear regression. This takes a few minutes programming and gives, at least, a baseline for more sophisticated methods.

But, linear regression only can give linear regression functions. This is not good enough if the dynamical input-output system behavior has significant nonlinear components. Then one must find a nonlinear regression function f.

If that occurs, one can take resort to a simple method which yields nonlinear regression functions while not renouncing the conveniences of the basic linear regression learning formula (19). I discuss this for the case of scalar inputs $u(t) \in \mathbb{R}$. The trick is to add fixed nonlinear transforms to the collection of input arguments $u(t-d+1), u(t-d+2), \ldots, u(t)$. A common choice is to add polynomials. To make notation easier, let us rename $u(t-d+1), u(t-d+2), \ldots, u(t)$ to $u_1, u_2, \ldots, u_d$. If one adds all polynomials of degree 2, one obtains a collection of $d + d(d+1)/2$ input components for the regression, namely

$$\{u_1, u_2, \ldots, u_d\} \cup \{u_i u_j \mid 1 \leq i \leq j \leq d\}.$$

If one wants "even more nonlinearity", one can venture to add higher-order polynomials. The idea to approximate nonlinear regression functions by linear combinations of polynomial terms is a classical technique in signal processing, where it is treated under the name of *Volterra expansion* or *Volterra series*. Very general classes of nonlinear regression functions can be approximated to arbitrary degrees of precision with Volterra expansions.

Adding increasingly higher-order terms to a Volterra expansion obviously leads to a combinatorial explosion. Thus one will have to call upon some pruning scheme to use only those polynomial terms which lead to an increase of accuracy. There is a substantial literature in signal processing dealing with pruning strategies for Volterra series (google "Volterra pruning"). I personally would never try to use polynomials of degree higher than 2. If that doesn't give satisfactory results, I would switch to other modeling techniques, using neural networks for instance.

3.3 Time series prediction tasks

Looking into the future can make you rich, or wise, or satisfy your curiosity – these motivations are deeply rooted in human nature and thus it is no wonder that time series prediction is an important kind of task for machine learning.

Time series prediction tasks come in many variants and I will not attempt to draw the large picture but restrict this treatment to timeseries with integer timesteps and vector-valued observations, as in the previous subsections.

Re-using terminology and notation, the input signal in the training data is, as before, $(\mathbf{u}(t))_{t\in\mathcal{T}}$. If one wants to predict this sequence of observations h timesteps ahead (h is called *prediction horizon*), the desired output $\mathbf{y}(t)$ is just the input, shifted by h timesteps:

$$(\mathbf{y}(t))_{t\in\mathcal{T}} = (\mathbf{u}(t+h))_{t\in\mathcal{T}}.$$

A little technical glitch is that due to the timeshift h, the last h data points in the input signal $(\mathbf{u}(t))_{t\in\mathcal{T}}$ cannot be used as training data because their h-step future would lie beyond the maximal time T.

Framed as an $\mathbf{u}(t)$–to–$\mathbf{y}(t)$ input-output signal transformation task, all methods that can be applied for the latter can be used for timeseries prediction too. Specifically, simple window-based linear regression (as in Figure 11 bottom) is again a highly recommendable first choice for getting a baseline predictor whenever you face a new timeseries prediction problem with numerical timeseries.

3.4 State-based vs. signal-based timeseries modeling

So far, I have described some ways how one can use input observations to compute output signals. If one starts thinking about it, it seems that in some cases this should be impossible.

Many temporal learning tasks concern the input-output modeling of a physical *dynamical system*. The output signal is not (somehow magically) directly transformed from the input signal, but by a complex transformation which resides in the internal mechanisms of the physical system that sits "in the middle" between input and output signals. Just two examples:

- A radio reporter commenting a soccer game. Output: the reporter's speech signal. Input: what the reporter sees on the soccer field. Dynamical system in the middel: the reporter, especially his brain and vocal tract. – Two different reporters would comment the game differently, even if they see it from the same reporters' stand. Much of the specific information in the reporter's radio speech is not explainable by the raw soccer visual input, but arises from the reporter's specific knowledge and emotional condition. – Fun fact: attempting to developing machine learning methods for the automated commenting of soccer matches had been, for a decade or so around 1985, one of the leading research motifs in Germany's young AI research landscape.

- Input signal: the radiowaves emitted from a transmitting antenna. Output signal: the radiowaves picked up by a receiving antenna. Physical system "in the middle": the physical world between the two antennas, inducing all kinds of static noise, echos, distortions, such that the received radio signal is a highly corrupted version of the cleanly transmitted one. Does it not seem hopeless to model the input-output transformation without including a model of the intervening physical *channel*? – There can hardly be a more

classical problem than this one; analysing signal transmission channels gave rise to Shannon's information theory.

Abstracting from these examples, consider how natural scientists and mathematicians describe dynamical systems. We stay in line with earlier parts of this section and consider only discrete-time models with a time index set is $T = \mathbb{N}$ or $T = \mathbb{Z}$. Three timeseries are considered simultaneously:

- an *input signal* $\mathbf{u}(t)$, where $\mathbf{u}(t) \in \mathbb{R}^k$ (as before),
- an *output signal* $\mathbf{y}(t)$, where $\mathbf{y}(t) \in \mathbb{R}^m$ (as before),
- a *dynamical system state* sequence $\mathbf{x}(t)$, where $\mathbf{x}(t) \in \mathbb{R}^n$ (this is new).

In soccer reporting example, $\mathbf{x}(t)$ would refer to some kind of brain state — for instance, the vector of activations of all the reporter's brain's neurons. In the signal transmission example, $\mathbf{x}(t)$ would be the state vector of some model of the physical world stretched out between the sending and receiving antenna.

A note in passing: variable naming conventions are a little confusing. In the machine learning literature, x's and y's in $(\mathbf{x}, \mathbf{y})$ pairs usually mean the arguments and values (or inputs and outputs) of classification/regression functions. Both $\mathbf{x}$ and $\mathbf{y}$ are observable. In the dynamical systems literature (mathematics, physics and engineering), the variable name x typically is reserved for the state of a signal-generating dynamical system – this state is normally not fully observable and not part of training data. Only the input and output signals $\mathbf{u}(t), \mathbf{y}(t)$ are observable "data".

In a discrete-time setting, the temporal evolution of $\mathbf{u}(t), \mathbf{x}(t), \mathbf{y}(t)$ is governed by two functions, the *state update map*

$$\mathbf{x}(t+1) = f(\mathbf{x}(t), \mathbf{u}(t+1)) \tag{22}$$

and the *observation function*

$$\mathbf{y}(t) = g(\mathbf{x}(t)). \tag{23}$$

The input signal $\mathbf{u}(t)$ is not specified by some equation, it is just "given".

Figure 12 visualizes the structural difference between the signal-based and the state-based input-output transformation models.

There are many other types of state update maps and observation functions, for instance ODEs and PDEs for continuous-time systems, automata models for discrete-state systems, or a host of probabilistic formalisms for random dynamical systems. For our present discussion, considering only discrete-time state update maps is good enough.

A core difference between signal-based and state-based timeseries transformations is the achievable memory timespans. In windowed signal transformations through regression functions, the memory depth is bounded by the window length.

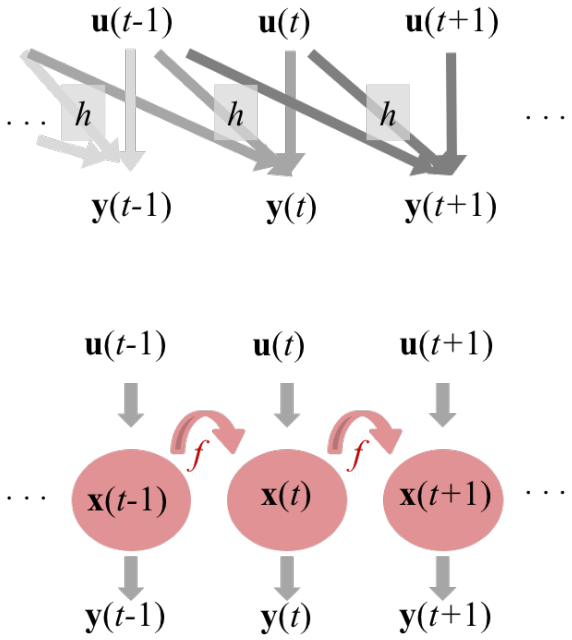

Figure 12: Contrasting signal-based with state-based timeseries transformations. **Top:** Window-based determination of output signal through a regression function h (here the window size is 3). **Bottom:** Output signal generation by driving in intermediary dynamical system with an input signal. The state $\mathbf{x}(t)$ is updated by f.

In contrast, the dynamical system state $\mathbf{x}(t)$ of the intermediary system is potentially co-determined by input that was fed to the dynamical system in an arbitrary deep past – the memory span can be unbounded! This may seem counterintuitive if one looks at Figure 12 because at each time point t, only the input data point $\mathbf{u}(t)$ from that same timepoint is fed to the dynamical system. But $\mathbf{u}(t)$ leaves some trace on the state $\mathbf{x}(t)$, and this effect is forwarded to the next timestep through f, thus $\mathbf{x}(t+1)$ is affected by $\mathbf{u}(t)$, too; and so forth. Thus, if one expects long-range or even unbounded memory effects, using state-based transformation models is often the best way to go.

Machine learning offers a variety of state-based models for timeseries transformations, together with learning algorithms. The most powerful ones are hidden Markov models (which we'll get to know in this course) and other dynamical graphical models (which we will not touch), and recurrent neural networks (which we'll briefly meet I hope).

In some applications it is important that the input-output transformation can be learnt in an *online adaptive* fashion. The input-output transformation is not trained just once, on the basis on a given, fixed training dataset. Instead, training never ends; while the system is being used, it continues to adapt to *changing* input-

output relationships in the data that it processes. My favourite example is the online adaptive filtering (denoising, echo cancellation) of the radio signal received by a mobile phone. When the phone is physically moving while it is being used (phonecall in a train, or just while walking up and down in a room), the signal channel from the transmitter antenna to the phone's antenna keeps changing. The denoising, echo-cancelling filter is re-learnt every few milliseconds. This is done with a window-based linear regression (window size several tens of thousands) and ingeniously simplified/accelerated algorithms. Because this is powerful stuff, we machine learners should not leave that only to the electrical engineers (who invented it) but learn to use it ourselves. I will devote a session later in this course to these online adaptive signal processing methods.

3.5 Takens' theorem

From what I just explained it may seem that signal-based and state-based input-output transformations are two quite different things. However, surprising connections exist. In certain ways and for certain systems, the two even conincide. This was discovered by the Dutch mathematician Floris Takens (1940-2010). His celebrated theorem (Takens 1981), now universally called *Takens Theorem*, is deep and beautiful, and enabled novel data analysis methods which triggered a flood of work in the study of complex system dynamics (in all fields biological, physical, metereological, economical, social, engineering). Also, Takens was a professor in Groningen, and founded a tradition of dynamical systems theory research in our mathematics department. Plus, finally, Takens-like theorems have very recently (not yet published) been used to analyse why/how certain recurrent neural networks of the "reservoir computing" brand function so surprisingly well in machine learning. These are all good enough causes for me to end this section with an intuitive explanation of Takens theorem, although this is not normally a part of a machine learning course.

Since the following contains allusions to mathematical concepts which I cannot assume are known by all course participants, the material in this section will not be tested in exams.

Floris Takens' original theorem was formulated in a context of continuous-time dynamics governed by differential equations. Many variants and extensions of Takens theorem are known. To stay in tune with earlier parts of this section I present a discrete-time version. Consider the input-free dynamical system

$$\begin{aligned} \mathbf{x}(t+1) &= f(\mathbf{x}(t)), \\ y(t) &= g(\mathbf{x}(t)), \end{aligned} \tag{24}$$

where $\mathbf{x}(t) \in \mathbb{R}^n$ and $y(t) \in \mathbb{R}$ (a one-dimensional output). The background intuition behind this set-up is that $\mathbf{x}$ models some physical dynamical system — possibly quite high-dimensional, for instance $\mathbf{x}$ being a brain state vector — while y is a physical quantity that is "measured", or "observed", from $\mathbf{x}$.

If the state update dynamics (24) is run for a long time, in many systems the state vector sequence $\mathbf{x}(t)$ will ultimately become confined to an *attracting* subset $A \subset \mathbb{R}^n$ of the embedding space $\mathbb{R}^n$. In some cases, this subset will be a low-dimensional manifold of dimension m; in other cases ("chaotic attractors") it will have a fractal geometry which is characterized by a *fractal dimension*, a real number which I will likewise call m and which typically is also small compared to the embedding space dimension n.

Now let us look at the observation sequence $y(t)$ recorded when the system has "relaxed" to the attracting subset. It is a scalar timeseries. For any $k > 1$, this scalar timeseries can be turned into a k-dimensional timeseries $\mathbf{y}(t)$ by *delay embedding*, as follows. Choose a delay of δ timesteps. Then set $\mathbf{y}(t) = (y(t), y(t-\delta), y(t-2\delta), \ldots, y(t-(k-1)\delta)'$. That is, just stack a few consecutive observations (spaced in time by δ) on top of each other. This gives a sequence of k-dimensional vectors $\mathbf{y}(t)$. You will recognize them as what we called "observation windows" earlier in this section.

Takens-like theorems now state that, under conditions specific to the particular version of the theorem, the geometry of the dynamics of the delay-embedded vectors is the same as the geometry of the dynamics of the original system, up to a smooth bijective transformation between the two geometries. I think a picture is really helpful here! Figure 13 gives a visual demo of Takens theorem at work.

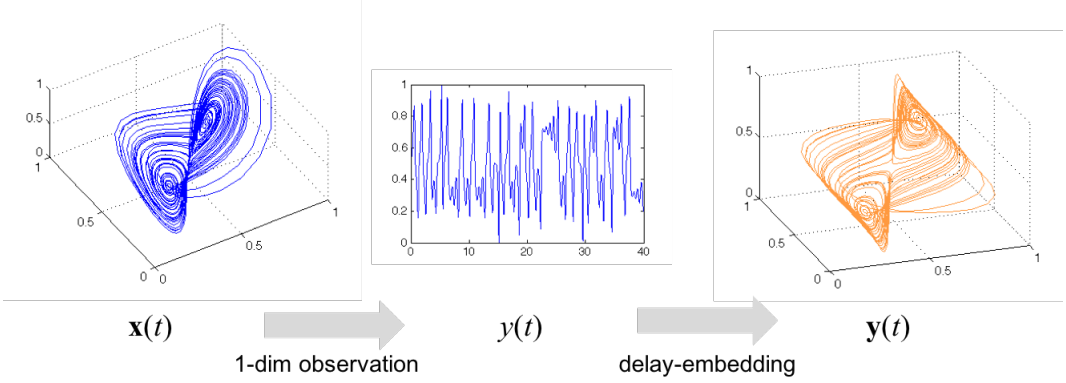

Figure 13: Takens theorem visualized. Left plot shows the Lorenz attractor, a chaotic attractor with a state sequence $\mathbf{x}(t)$ defined in an $n = 3$ dimensional state space. The center plot shows a 1-dimensional observation $y(t)$ thereof. The right plot (orange) shows the state sequence $\mathbf{y}(t)$ obtained from $y(t)$ by three-dimensional delay embedding (I forget which delay δ I used).

When I just said, "the geometry ... is the same ... up to smooth bijective transformation", I mean the following. Imagine that in Figure 13 (left) the blue trajectory lines were spun into a transparent 3-dimensional substrate which has rubber-like qualities. Then, by pushing and pulling and shearing this substrate (without rupturing it), the blue lines would take on new positions in 3D space — until they would *exactly* coincide with the orange ones in the right panel.

Even without applying such a "rubber-sheet transformation" (a term used in dynamical systems textbooks), some geometric characteristics are identical between the left and the right panel in the figure. Specifically, the so-called *Lyapunov exponents*, which are indicators for the stability (noise robustness) of the dynamics, and the (possibly fractal) dimension of the attracting set A are identical in the original dynamics and its delay-embedded reconstruction.

The deep, nontrivial message behind Takens-like theorems is that one can trade time for space in certain dynamical systems. If by "space" one means dimensions of state vectors, and by "time" lengths of observation windows of a scalar observable, Takens-like theorems typically state that if the dimension of the original attractor set (manifold or fractal) is m, then using a delay embedding of an integer dimension larger or equal than $2m + 1$ will always recuperate the original geometry; and sometimes smaller delay embedding dimensions suffice. Just for completeness: the fractal dimension of the Lorenz attractor is about $m = 2.06$, thus any delay embedding dimension exceeding $2m + 1 = 5.12$ would be certainly sufficient for reconstruction from a scalar observation; it turns out in Figure 13 that an embedding dimension of 3 is already working.

In timeseries prediction tasks in machine learning, Takens theorem gives a justification why in deterministic, autonomous dynamical systems it should be possible to predict the future of a scalar timeseries $y(t)$ from its past. If the timeseries in question has been produced from a system like (24), Takens theorem establishes that the information contained in the last $2m + 1$ timesteps before the prediction point t comprises the full information about the state of the system that generated $y(t)$ and thus knowledge of the last $2m + 1$ timesteps is enough to predict $y(t + 1)$ with absolute accuracy.

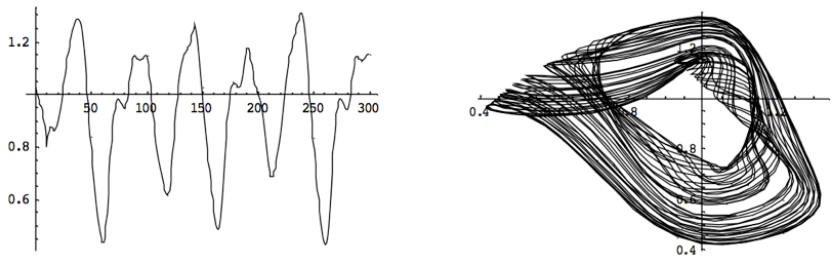

Figure 14: Getting nice graphics from delay embeddings. Left: a timeseries recorded from the "Mackey-Glass" chaotic attractor. Right: plotting the trajectory of a delay-embedded version of the left signal.

Even if you forget about the Takens theory background, it is good to be familiar with delay-embeddings of scalar timeseries, because they help creating instructive graphics. If you transform a one-dimensional scalar timeseries $y(t)$ into a 2-dimensional one by a 2-element delay embedding, plotting this 2-dimensional trajectory $\mathbf{y}(t) = (y(t - \delta), y(t))'$ in its delay coordinates $(y(t - \delta), y(t)$ will often give revealing insight into the structure of the timeseries – our visual system is

optimized for seeing patterns in 2-D images, not in 1-dimensional timeseries plots. See Figure 14 for a demo.

4 Basic methods for dimension reduction

One way to take up the fight with the "curse of dimensionality" which I briefly highlighted in Section 1.2.2 is to reduce the dimensionality of the raw input data before they are fed to subsequent learning algorithms. The dimension reduction ratio can be enormous.

In this Section I will introduce three standard methods for dimension reduction: K-means clustering, principal component analysis, and self-organizing feature maps. They all operate on raw vector data which come in the form of points $\mathbf{x} \in \mathbb{R}^n$, that is, this section is only about dimension reduction methods for numerical data. Dimension reduction is the archetypical unsupervised learning task.

4.1 Set-up, terminology, general remarks

We are given a family $(\mathbf{x}_i)_{i=1,\ldots,N}$ of "raw" data points, where $\mathbf{x}_i \in \mathbb{R}^n$. The goal of dimension reduction methods is to compute from each (high-dimensional) "raw" data vecor $\mathbf{x}_i$ a (low-dimensional) vector $\mathbf{f}(\mathbf{x}_i) \in \mathbb{R}^m$, such that

- $m < n$, that is, we indeed reduce the number of dimensions — maybe even dramatically;
- the low-dimensional vectors $\mathbf{f}(\mathbf{x}_i)$ should preserve from the raw data the specific information that is needed to solve the learning task that comes after this dimension-reducing data "preprocessing".

Terminology: The m component functions which constitute $\mathbf{f}(\mathbf{x})$ are called *features*. A feature is just a (any) function $f : \mathbb{R}^n \to \mathbb{R}$ which computes a scalar characteristic of input vectors $\mathbf{x} \in \mathbb{R}^n$. If one bundles together m such features $f_1, \ldots, f_m$ one obtains a *feature map* $(f_1, \ldots, f_m)' =: \mathbf{f} : \mathbb{R}^n \to \mathbb{R}^m$ which maps input vectors to *feature vectors*.

It is very typical, almost universal, for ML systems to include an initial data processing stage where raw, high-dimensional input patterns are first projected from their original pattern space $\mathbb{R}^n$ to a lower-dimensional feature space. In TICS, for example, a neural network was trained in a clever way to reduce the 1,440,000-dimensional raw input patterns to a 4,096-dimensional feature vector.

The ultimate quality of the learning system clearly depends on a good choice of features. Unfortunately there does not exist a unique or universal method to identify "good" features. Depending on the learning task and the nature of the data, different kinds of features work best. Accordingly, ML research has come up with a rich repertoire of *feature extraction* methods.

On an intuitive level, a "good" set of features $\{f_1, \ldots, f_m\}$ should satisfy some natural conditions:

- The number m of features should be small — after all, one of the reasons for using features is dimension reduction.

- Each feature f_i should be *relevant* for the task at hand. For example, when the task is to distinguish helicopter images from winged aircraft photos (a 2-class classification task), the brightness of the background sky would be an irrelevant feature; but the binary feature "has wings" would be extremely relevant.

- There should be *little redundancy* — each used feature should contribute some information that the others don't.

- A general intuition about features is that they should be rather cheap and easy to compute at the front end where the ML system meets the raw data. The "has wings" feature for helicopter vs. winged aircraft classification more or less amounts to actually solving the classification task and presumably is neither cheap nor easy to compute. Such highly informative, complex features are sometimes called *high-level features*; they are usually computed on the basis of more elementary, *low-level* features. Often features are computed stage-wise, low-level features first (directly from data), then stage by stage more complex, more directly task-solving, more "high-level cognition" features are built by combining the lower-level ones. *Feature hierarchies* are often found in ML systems. Example: in face recognition from photos, low-level features might extract coordinates of isolated black dots from the photo (candidates for the pupils of the person's eyes); intermediate features might give distance ratios between eyes, nose-tip, center-of-mouth; high-level features might indicate gender or age.

To sharpen our intuitions about features, let us hand-design some features for use in a simple image classification task. Consider a training dataset which consists of grayscale, low-resolution pictures of handwritten digits (Figure 15). Here and further in this section I will illustrate dimension reduction techniques with the simple "Digits" benchmark dataset which was first described in Kittler et al. 1998. This dataset contains 2000 grayscale images of handwritten digits, 200 from each class. The images are 15×16 sized, making for $n = 240$ dimensional image vectors $\mathbf{x}$. We assume they have been normalized to a real-valued pixel value range in $[0, 1]$ with 0 = white and 1 = black. The Digits benchmark task is to train a classifier which classifies such images into the ten digit classes.

Here are some candidates for features that might be useful for this task.

Mean brightness. $f_1(\mathbf{x}) = 1'_n \mathbf{x} \,/\, n$ (1_n is the vector of n ones). This is just the mean brightness of all pixels. Might be useful e.g. for distinguishing "1" images from "8" images because we might suspect that for drawing an "8" one needs more black ink than for drawing a "1". Cheap to compute but not very class-differentiating.

Radiality. An image $\mathbf{x}$ is assigned a value $f_2(\mathbf{x}) = 1$ if and only if two conditions are met: (i) the center horizontal pixel line crossing the image from left to

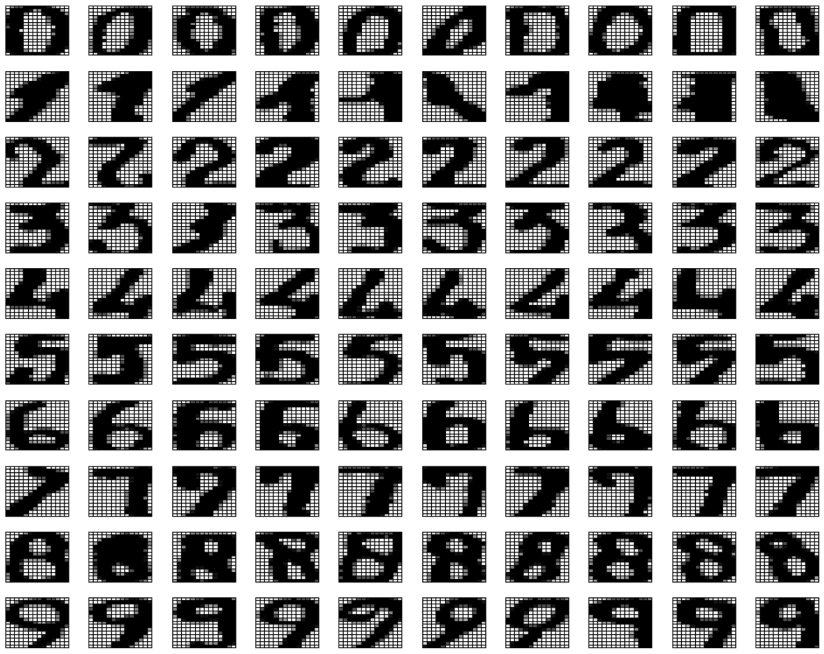

Figure 15: Some examples from the Digits dataset.

right has a sequence of pixels that changes from black to white to black; (ii) same for the center vertical pixel line. If this double condition is not met, the image is assigned a feature value of $f_2(\mathbf{x}) = 0$. f_2 thus has only two possible values; it is called a *binary feature*. We might suspect that only the "0" images have this property. This would be a slightly less cheap-to-compute feature compared to f_1 but more informative about classes.

Prototype matching. For each of the 10 classes c_j $(j = 1, \ldots, 10)$ define a *prototype vector* π_j as the mean image vector of all examples of that class contained in the training dataset: $\pi_j = 1/N_j \sum_{\mathbf{x} \text{ is training image of class } j} \mathbf{x}$. Then define 10 features f_3^j by match with these prototype vectors: $f_3^j(\mathbf{x}) = \pi_j' \mathbf{x}$. We might hope that f_3^j has a high value for patterns of class j and low values for other patterns.

Hand-designing features can be quite effective. Generally speaking, human insight on the side of the data engineer is a success factor for ML systems that can hardly be overrated. In fact, the classical ML approach to speech recognition was for two decades relying on low-level acoustic features that had been hand-designed by insightful phonologists. The MP3 sound coding format is based on features that reflect characteristics of the human auditory system. Many of the first functional computer vision and optical character recognition systems relied heavily on visual feature hierarchies which grew from the joint efforts of signal processing engineers and cognitive neuroscience experts.

However, since hand-designing good features means good insight on the side of the engineer, and good engineers are rare and have little time, the practice of ML today relies much more on features that are obtained from learning algorithms. Numerous methods exist. In the following subsections we will inspect three such methods.

4.2 K-means clustering

K-means clustering is an algorithm which allows one to split a collection of training data points $(\mathbf{x}_i)_{i=1,\dots,N} \in \mathbb{R}^n$ into K *clusters* $C_1, \dots, C_K$, such that points from the same cluster lie close to each other while being further away from points in other clusters. Each cluster C_j is represented by its *codebook* vector c_j, which is the vector pointing to the mean of all vectors in the cluster — that is, to the cluster's center of gravity.

The codebook vectors can be used in various ways to compress n-dimensional test data points $\mathbf{x}^{\text{test}}$ into lower-dimensional formats. The classical method, which also explains the naming of the c_j as "codebook" vectors, is to represent $\mathbf{x}^{\text{test}}$ simply by the index j of the codebook vector c_j which lies closest to $\mathbf{x}^{\text{test}}$, that is, which has the minimal distance $\alpha_j = \|\mathbf{x}^{\text{test}} - c_j\|$. The high-dimensional point $\mathbf{x}^{\text{test}}$ becomes represented by a single number, thus here we would have $m = 1$. This method is clearly very economical and it is widely used for data compression. But it is also clear that relevant information contained in vectors $\mathbf{x}^{\text{test}}$ may be lost — maybe too much information for many ML applications.

Another, less lossy, way to make use of the codebook vectors for dimension reduction is to compute the distances α_j between $\mathbf{x}^{\text{test}}$ and the codebook vectors, and reduce $\mathbf{x}^{\text{test}}$ to the K-dimensional distance vector $(\alpha_1, \dots, \alpha_K)'$. When $K \ll n$, the dimension reduction is substantial. The vector $(\alpha_1, \dots, \alpha_K)'$ can be considered a feature vector.

We can be brief when explaining the K-means clustering algorithm, because it is almost self-explaining. The rationale for defining clusters is that points within a cluster should have small metric distance to each other, points in different clusters should have large distance from each other. The procedure runs like this:

Given: a training data set $(\mathbf{x}_i)_{i=1,\dots,N} \in \mathbb{R}^n$, and a number K of clusters that one maximally wishes to obtain.
Initialization: randomly assign the training points to K sets S_j $(j = 1, \dots, K)$.
Repeat: For each set S_j, compute the mean $\mu_j = |S_j|^{-1} \sum_{\mathbf{x} \in S_j} \mathbf{x}$. This mean vector μ_j is the "center of gravity" of the vector cluster S_j. Create new sets S'_j by putting each data point $\mathbf{x}_i$ into that set S'_j where $\|\mathbf{x}_i - \mu_j\|$ is minimal. If some S'_j remains empty, dismiss it and reduce K to K' by subtractring the number of dismissed empty sets (this happens rarely). Put $S_j = S'_j$ (for the nonempty sets) and $K = K'$.
Termination: Stop when in one iteration the sets remain unchanged.

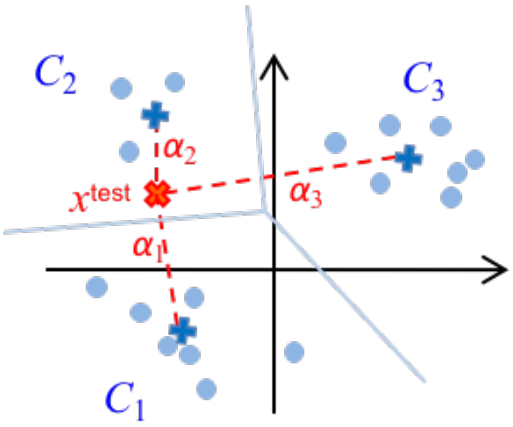

Figure 16: Clusters obtained from K-means clustering (schematic): For a training set of data points (light blue dots), a spatial grouping into clusters C_j is determined by the K-means algorithm. Each cluster becomes represented by a codebook vector (dark blue crosses). The figure shows three clusters. The light blue straight lines mark the cluster boundaries. A test data point $\mathbf{x}^{\text{test}}$ (red cross) may then become coded in terms of the distances α_j of that point to the codebook vectors. Since this $\mathbf{x}^{\text{test}}$ falls into the second cluster C_2, it could also be compressed into the codebook index "2" of this cluster.

It can be shown that at each iteration, the error quantity

$$J = \sum_{j=1}^{K} \sum_{\mathbf{x} \in S_j} \|\mathbf{x} - \mu_j\|^2 \tag{25}$$

will not increase. The algorithm typically converges quickly and works well in practice. It finds a local minimum or saddle point of J. The final clusters S_j may depend on the random initialization. The clusters are bounded by straight-line boundaries; each cluster forms a *Voronoi cell*. K-means cannot find clusters defined by curved boundaries. Figure 17 shows an example of a clustering run using K-means.

K-means clustering and other clustering methods have many uses besides dimension reduction. Clustering can also be seen as a stand-alone technique of unsupervised learning. The detected clusters and their corresponding codebook vectors are of interest in their own right. They reveal a basic structuring of a set of patterns $\{\mathbf{x}_i\}$ into subsets of mutually similar patterns. These clusters may be further analyzed individually, given meaningful names and helping a human data analyst to make useful sense of the original unstructured data cloud. For instance, when the patterns $\{\mathbf{x}_i\}$ are customer profiles, finding a good grouping into subgroups may help to design targetted marketing strategies.

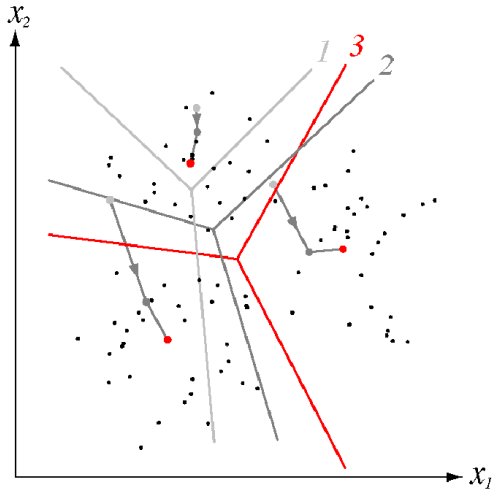

Figure 17: Running K-means with $K = 3$ on two-dimensional training points. Thick dots mark cluster means μ_j, lines mark cluster boundaries. The algorithm terminates after three iterations, whose boundaries are shown in light gray, dark gray, red. (Picture taken from Chapter 10 of the textbook Duda, Hart, and Stork 2001).

4.3 Principal component analysis

Like clustering, principal component analysis (PCA) is a basic data analysis technique that has many uses besides dimension reduction. But here we will focus on this use.

Generally speaking, a good dimension reduction method, that is, a good feature map $\mathbf{f} : \mathbb{R}^n \to \mathbb{R}^m$, should preserve much information contained in the high-dimensional patterns $\mathbf{x} \in \mathbb{R}^n$ and encode it robustly in the feature vectors $y = \mathbf{f}(\mathbf{x})$. But, what does it mean to "preserve information"? A clever answer is this: a feature representation $\mathbf{f}(\mathbf{x})$ preserves information about $\mathbf{x}$ to the extent that $\mathbf{x}$ can be *reconstructed* from $\mathbf{f}(\mathbf{x})$. That is, we wish to have a *decoding function* $\mathbf{d} : \mathbb{R}^m \to \mathbb{R}^n$ which leads back from the feature vector encoding $\mathbf{f}(\mathbf{x})$ to $\mathbf{x}$, that is we wish to achieve

$$\mathbf{x} \approx \mathbf{d} \circ \mathbf{f}(\mathbf{x})$$

And here comes a fact of empowerment: when $\mathbf{f}$ and $\mathbf{d}$ are confined to *linear* functions and when the similarity $\mathbf{x} \approx \mathbf{d} \circ \mathbf{f}(\mathbf{x})$ is measured by mean square error, the optimal solution for $\mathbf{f}$ and $\mathbf{d}$ can be easily and cheaply computed by a method that is known since the early days of statistics, *principal component analysis* (PCA). It was first found, in 1901, by Karl Pearson, one of the fathers of modern mathematical statistics. The same idea has been independently rediscovered under many other names in other fields and for a variety of purposes (check out `https://en.wikipedia.org/wiki/Principal_component_analysis`

for the history). Because of its simplicity, analytical transparency, modest computational cost, and numerical robustness PCA is widely used — it is the first-choice default method for dimension reduction that is tried almost by reflex, before more elaborate methods are maybe considered.

PCA is best explained alongside with a visualization (Figure 18). Assume the patterns are 3-dimensional vectors, and assume we are given a sample of $N = 200$ raw patterns $\mathbf{x}_1, \ldots, \mathbf{x}_{200}$. We will go through the steps of a PCA to reduce the dimension from $n = 3$ to $m = 2$.

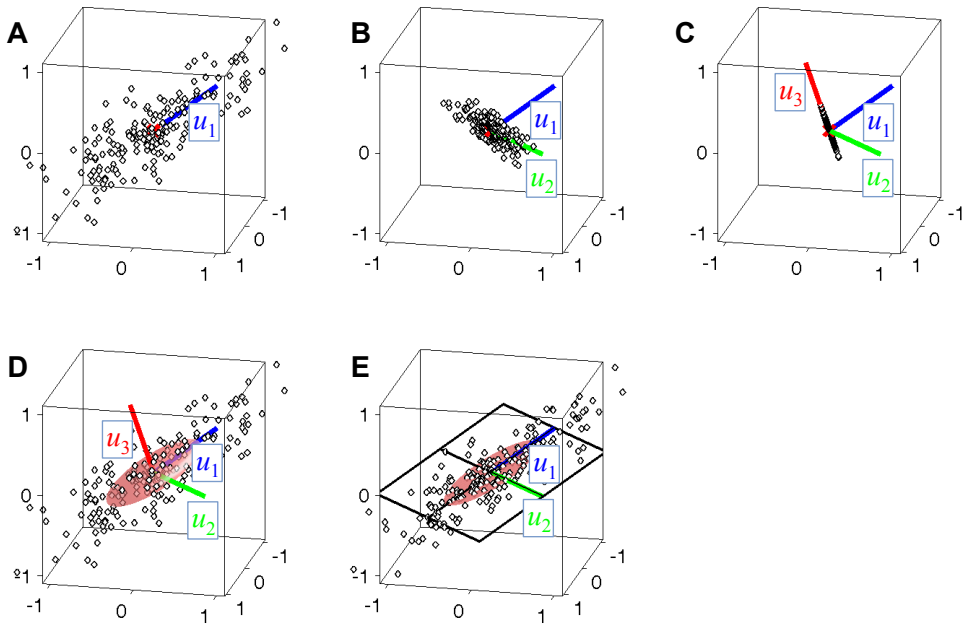

Figure 18: Visualization of PCA. **A.** Centered data points and the first principal component vector u_1 (blue). The origin of $\mathbb{R}^3$ is marked by a red cross. **B.** Projecting all points to the orthogonal subspace of u_1 and computing the second PC u_2 (green). **C.** Situation after all three PCs have been determined. **D.** Summary visualization: the original data cloud with the three PCs and an ellipsoid aligned with the PCs whose main axes are scaled to the standard deviations of the data points in the respective axis direction. **E.** A new dimension-reduced coordinate system obtained by the projection of data on the subspace U_m spanned by the m first PCs (here: the first two).

The first step in PCA is to *center* the training patterns $\mathbf{x}_i$, that is, subtract their mean $\mu = 1/N \sum_i \mathbf{x}_i$ from each pattern, obtaining centered patterns $\bar{\mathbf{x}}_i = \mathbf{x}_i - \mu$. The centered patterns form a point cloud in $\mathbb{R}^n$ whose center of gravity is the origin (see Figure 18**A**).

This point cloud will usually not be perfectly spherically shaped, but instead extend in some directions more than in others. "Directions" in $\mathbb{R}^n$ are characterized by unit-norm "direction" vectors $u \in \mathbb{R}^n$. The distance of a point $\bar{\mathbf{x}}_i$ from the origin

in the direction of u is given by the projection of $\bar{\mathbf{x}}_i$ on u, that is, the inner product $u' \bar{\mathbf{x}}_i$ (see Figure 19).

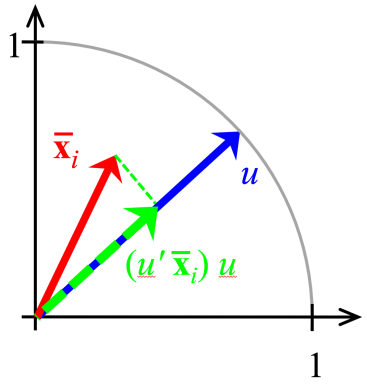

Figure 19: Projecting a point $\bar{\mathbf{x}}_i$ on a direction vector u: the inner product $u' \bar{\mathbf{x}}_i$ is the distance of $\bar{\mathbf{x}}_i$ from the origin along the direction given by u.

The "extension" of a centered point cloud $\{\bar{\mathbf{x}}_i\}$ in a direction u is defined to be the mean squared distance to the origin of the points $\bar{\mathbf{x}}_i$ in the direction of u. The direction of the largest extension of the point cloud is hence the direction vector given by

$$u_1 = \underset{u,\, \|u\|=1}{\operatorname{argmax}} \; 1/N \; \sum_i (u' \bar{\mathbf{x}}_i)^2. \tag{26}$$

Notice that since the cloud $\bar{\mathbf{x}}_i$ is centered, the mean of all $u' \bar{\mathbf{x}}_i$ is zero, and hence the number $1/N \; \sum_i (u' \bar{\mathbf{x}}_i)^2$ is the variance of the numbers $u' \bar{\mathbf{x}}_i$.

Inspecting Figure 18**A**, one sees how u_1 points in the "longest" direction of the pattern cloud. The vector u_1 is called the first *principal component* (PC) of the centered point cloud.

Next step: project patterns on the $(n-1)$-dimensional linear subspace of $\mathbb{R}^n$ that is orthogonal to u_1 (Figure 18**B**). That is, map pattern points $\bar{\mathbf{x}}$ to $\bar{\mathbf{x}}^* = \bar{\mathbf{x}} - (u_1' \bar{\mathbf{x}}) \cdot u_1$. Within this "flattened" pattern cloud, again find the direction vector of greatest variance

$$u_2 = \underset{u, \|u\|=1}{\operatorname{argmax}} \; 1/N \; \sum_i (u' \bar{\mathbf{x}}_i^*)^2$$

and call it the second PC of the centered pattern sample. From this procedure it is clear that u_1 and u_2 are orthogonal, because u_2 lies in the orthogonal subspace of u_1.

Now repeat this procedure: In iteration k, the k-th PC u_k is constructed by projecting pattern points to the linear subspace that is orthogonal to the already computed PCs $u_1, \ldots, u_{k-1}$, and u_k is obtained as the unit-length vector pointing in the "longest" direction of the current $(n-k+1)$-dimensional pattern point distribution. This can be repeated until n PCs $u_1, \ldots, u_n$ have been determined. They

form an orthonormal coordinate system of $\mathbb{R}^n$. Figure 18**C** shows this situation, and Figure 18**D** visualizes the PCs plotted into the original data cloud.

Now define features f_k (where $1 \leq k \leq n$) by

$$f_k : \mathbb{R}^n \to \mathbb{R}, \quad \mathbf{x} \mapsto u_k' \, \bar{\mathbf{x}}, \tag{27}$$

that is, $f_k(\bar{\mathbf{x}})$ is the projection component of $\bar{\mathbf{x}}$ on u_k. Since the n PCs form an orthonormal coordinate system, any point $\mathbf{x} \in \mathbb{R}^n$ can be perfectly reconstructed from its feature values by

$$\mathbf{x} = \mu + \sum_{k=1,\ldots,n} f_k(\mathbf{x}) \, u_k. \tag{28}$$

The PCs and the corresponding features f_k can be used for dimension reduction as follows. We select the first ("leading") PCs $u_1, \ldots, u_m$ up to some index m. Then we obtain a feature map

$$\mathbf{f} : \mathbb{R}^n \to \mathbb{R}^m, \quad \mathbf{x} \mapsto (f_1(\mathbf{x}), \ldots, f_m(\mathbf{x}))'. \tag{29}$$

At the beginning of this section I spoke of a decoding function $\mathbf{d} : \mathbb{R}^m \to \mathbb{R}^n$ which should recover the original patterns $\mathbf{x}$ from their feature vectors $\mathbf{f}(\mathbf{x})$. In our PCA story, this decoding function is given by

$$\mathbf{d} : (f_1(\mathbf{x}), \ldots, f_m(\mathbf{x}))' \mapsto \mu + \sum_{k=1}^{m} f_k(\mathbf{x}) \, u_k. \tag{30}$$

How "good" is this dimension reduction, that is, how similar are the original patterns $\mathbf{x}_i$ to their reconstructions $\mathbf{d} \circ \mathbf{f}(\mathbf{x}_i)$?

If dissimilarity of two patterns $\mathbf{x}_1, \mathbf{x}_2 \in \mathbb{R}^n$ is measured in the square error sense by

$$\delta(\mathbf{x}_1, \mathbf{x}_2) := \|\mathbf{x}_1 - \mathbf{x}_2\|^2,$$

a full answer can be given. Let

$$\sigma_k^2 = 1/N \, \sum_i f_k(\mathbf{x}_i)^2$$

denote the variance of the feature values $f_k(\mathbf{x}_i)$ (notice that the mean of the $f_k(\mathbf{x}_i)$, taken over all patterns, is zero, so σ_k^2 is indeed their variance). Then the mean square distance between patterns and their reconstructions is

$$1/N \, \sum_i \|\mathbf{x}_i - \mathbf{d} \circ \mathbf{f}(\mathbf{x}_i)\|^2 = \sum_{k=m+1}^{n} \sigma_k^2. \tag{31}$$

A derivation of this result is given in Appendix E.

Equation (31) gives an absolute value for dissimilarity. For applications however the relative amount of dissimilarity compared to the mean variance of patterns is more instructive. It is given by

$$\frac{1/N \ \sum_i \|\mathbf{x}_i - \mathbf{d} \circ \mathbf{f}(\mathbf{x}_i)\|^2}{1/N \ \sum_i \|\bar{\mathbf{x}}_i\|^2} = \frac{\sum_{k=m+1}^{n} \sigma_k^2}{\sum_{k=1}^{n} \sigma_k^2}. \tag{32}$$

Real-world sets of patterns often exhibit a rapid (roughly exponential) decay of the feature variances as their index k grows. The ratio (32) then is very small compared to the mean size $E[\|\bar{X}\|^2]$ of patterns, that is, only very little information is lost by reducing the dimension from n to m via PCA. Our visualization from Figure 18 is not doing justice to the amount of compression savings that is often possible. Typical real-world, high-dimensional, centered data clouds in $\mathbb{R}^n$ are often very "flat" in the vast majority of directions in $\mathbb{R}^n$ and these directions can all be zeroed without much damage by the PCA projection.

Note. Using the word "variance" above is not mathematically correct. Variance is the *expected* squared deviation from a *population* mean, a statistical property which is different from the *averaged* squared deviation from a *sample* mean. It would have been more proper to speak of an "empirical variance" above, or an "estimated variance". Check out Appendix D!

4.4 Mathematical properties of PCA and an algorithm to compute PCs

The key to analysing and computing PCA is the $(n \times n)$-dimensional covariance matrix $C = 1/N \ \sum_i \bar{\mathbf{x}}_i \, \bar{\mathbf{x}}_i'$, which can be easily obtained from the centered training data matrix $\bar{X} = [\bar{\mathbf{x}}_1, \ldots, \bar{\mathbf{x}}_N]$ by $C = 1/N \ \bar{X} \, \bar{X}'$. C is very directly related to PCA by the following facts:

1. The PCs $u_1, \ldots, u_n$ form a set of orthonormal, real eigenvectors of C.

2. The feature variances $\sigma_1^2, \ldots, \sigma_n^2$ are the eigenvalues of these eigenvectors.

A derivation of these facts can be found in my legacy ML lecture notes, Section 4.4.1 (`https://www.ai.rug.nl/minds/uploads/LN_ML_Fall11.pdf`). Thus, the principal component vectors u_k and their associated data variances σ_k^2 can be directly gleaned from C.

Computing a set of unit-norm eigenvectors and eigenvalues from C can be most conveniently done by computing the *singular value decomposition* (SVD) of C. Algorithms for computing SVDs of arbitrary matrices are shipped with all numerical or statistical mathematics software packages, like Matlab, R, or Python with numpy. At this point let it suffice to say that every covariance matrix C is a so-called *positive semi-definite* matrix. These matrices have many nice properties. Specifically, their eigenvectors are orthogonal and real, and their eigenvalues are real and nonnegative.

In general, when an SVD algorithm is run on an n-dimensional positive semi-definite matrix C, it returns a factorization

$$C = U\,\Sigma\,U',$$

where U is an $n \times n$ matrix whose columns are the normed orthogonal eigenvectors $u_1, \ldots, u_n$ of C and where Σ is an $n \times n$ diagonal matrix which has the eigenvalues $\lambda_1, \ldots, \lambda_n$ on its diagonal. They are usually arranged in descending order. Thus, computing the SVD of $C = U\,\Sigma\,U'$ directly gives us the desired PC vectors u_k, lined up in U, and the variances σ_k^2, which appear as the eigenvalues of C, collected in Σ.

This enables a convenient control of the goodness of similarity that one wants to ensure. For example, if one wishes to preserve 98% of the variance information from the original patterns, one can use the r.h.s. of (32) to determine the "cutoff" m such that the ratio in this equation is about 0.02.

4.5 Summary of PCA based dimension reduction procedure

Data. A set $(\mathbf{x}_i)_{i=1,\ldots,N}$ of n-dimensional pattern vectors.

Result. An n dimensional mean pattern vector μ and m principal component vectors arranged column-wise in an $n \times m$ sized matrix U_m.

Procedure.

Step 1. Compute the pattern mean μ and center the patterns to obtain a centered pattern matrix $\bar{X} = [\bar{\mathbf{x}}_1, \ldots, \bar{\mathbf{x}}_N]$.

Step 2. Compute the SVD $U\,\Sigma\,U'$ of $C = 1/N\ \bar{X}\bar{X}'$ and keep from U only the first m columns, making for a $n \times m$ sized matrix U_m.

Usage for compression. In order to compress a new n-dimensional pattern to a m dimensional feature vector $\mathbf{f}(\mathbf{x})$, compute $\mathbf{f}(\mathbf{x}) = U_m'\,\bar{\mathbf{x}}$.

Usage for uncompression (decoding). In order to approximately restore $\mathbf{x}$ from its feature vector $\mathbf{f}(\mathbf{x})$, compute $\mathbf{x}_{\text{restored}} = \mu + U_m\,\mathbf{f}(\mathbf{x})$.

4.6 Eigendigits

For a demonstration of dimension reduction by PCA, consider the "3" digit images. After reshaping the images into 240-dimensional grayscale vectors and centering and computing the PCA on the basis of $N = 100$ training examples, we obtain 240 PCs u_k associated with variances σ_k^2. Only the first 99 of these variances are

nonzero (because the 100 image vectors $\mathbf{x}_i$ span a 100-dimensional subspace in $\mathbb{R}^{240}$; after centering the $\bar{\mathbf{x}}_i$ however span only a 99-dimensional subspace – *why? homework exercise!* – thus the matrix $C = 1/N\ \bar{X}\ \bar{X}'$ has rank at most the rank of $\bar{X}$, which is 99), thus only the first 99 PCs are useable. Figure 20 **A** shows some of these eigenvectors u_i rendered as 15×16 grayscale images. It is customary to call such PC re-visualizations *eigenimages*, in our case "eigendigits". (If you have some spare time, do a Google image search for "eigenfaces" and you will find weird-looking visualizations of PC vectors obtained from PCA carried out on face pictures.)

Figure 20 **B** shows the variances σ_i^2 of the first 99 PCs. You can see the rapid (roughly exponential) decay. Aiming for a dissimilarity ratio (Equation 32) of 0.1 gives a value of $m = 32$. Figure 20 **C** shows the reconstructions of some "3" patterns from the first m PC features using (30).

4.7 Self-organizing maps

Nature herself has been facing the problem of dimension reduction when She was using evolution as a learning algorithm to obtain well-performing brains. Specifically, in human visual processing the input dimension n is in the order of a million (judging from the number of axons in the optical nerve), but the "space" where the incoming n-dimensional raw visual signal is processed has only $m = 2$ dimensions: it is the walnut-kernel-curly surface of the brain, the *cortical sheet*. Now this is certainly an over-simplified view of biological neural information processing, but at least in some brain areas and for some kinds of input projecting into those areas, it seems fairly established in neuroscience that an incoming high-dimensional signal becomes mapped on an $m = 2$ dimensional representation on the cortical sheet.

In the 1980 decade, Teuvo Kohonen developed an artificial neural network model which (i) could explain how this neural dimension reduction could be learnt in biological brains; and (ii) which could be used as a practical machine learning algorithm for dimension reduction. His model is today known as *Kohonen Network* or *Self-Organizing Map (SOM)*. The SOM model is one the very few and precious instances of a neural information processing model which is anchored in, and can bridge between, both neuroscience and machine learning. It made a strong impact in both communities. In the machine learning / data analysis world SOMs have been superseded in later years by other methods, and in my perception they are only rarely used today. But this may again change when non-digital neuromorphic microchip technologies will mature. In neuroscience research, SOM-inspired models continue to be explored. Furthermore, the SOM model is simple and intuitive. I think all of this is reason enough to include them in this lecture.

The learning task for SOMs is defined as follows (for the case of $m = 2$):

Given: a pattern collection $\mathcal{P} = (\mathbf{x}_i)_{i=1,\ldots,N}$ of points in $\mathbb{R}^n$.

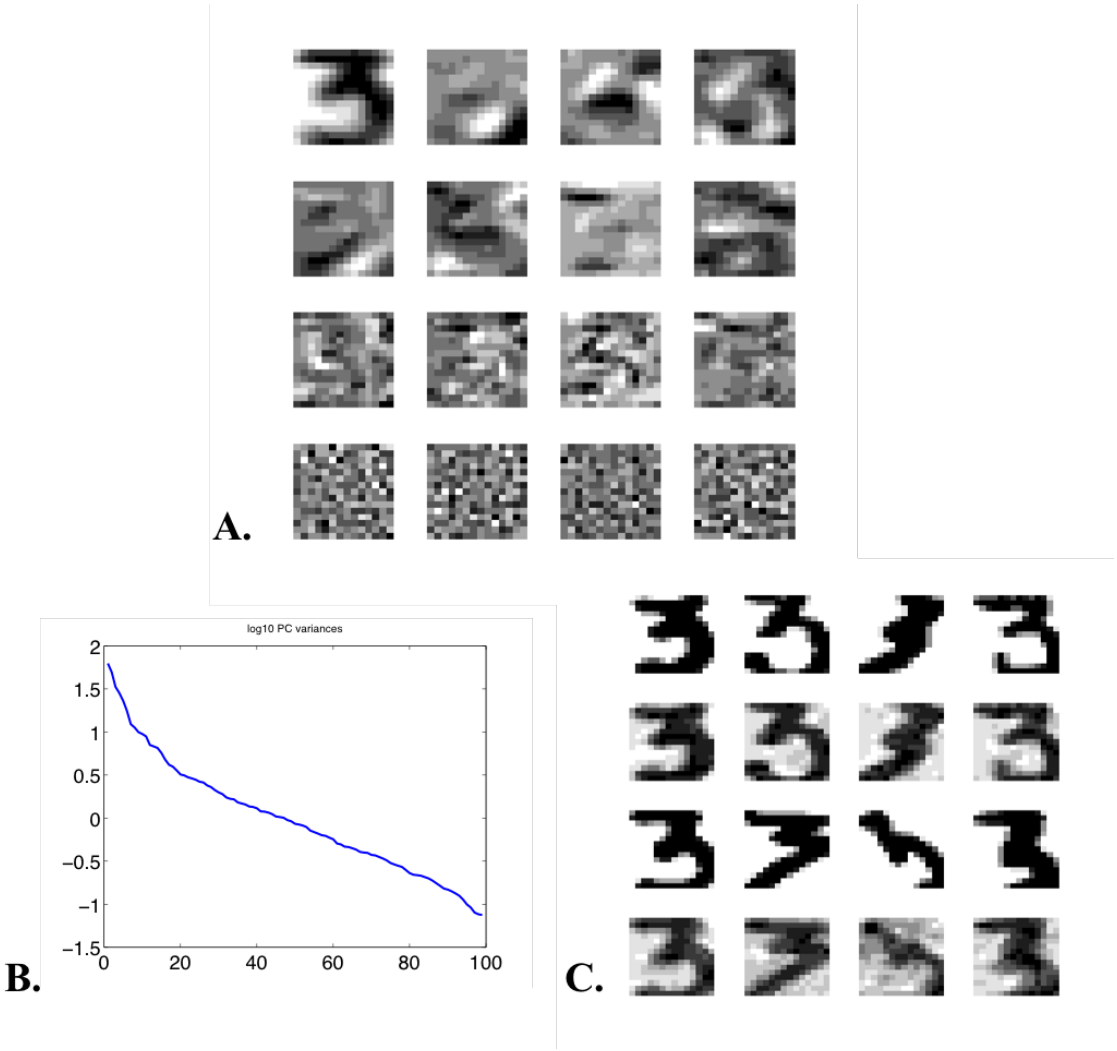

Figure 20: **A.** Visualization of a PCA computed from the "3" training images. Top left panel shows the mean μ, the next 7 panels (row-wise) show the first 7 PCs. Third row shows PCs 20–23, last row PCs 96-99. Grayscale values have been automatically scaled per panel such that they spread from pure white to pure black; they do not indicate absolute values of the components of PC vectors. **B.** The (log10 of) variances of the PC features on the "3" training examples. **C.** Reconstructions of digit "3" images from the first $m = 32$ features, corresponding to a re-constitution of 90% of the original image dataset variance. First row: 4 original images from the training set. Second row: their reconstructions. Third row: 4 original images from the test set. Last row: their reconstruction.

Given: a 2-dimensional grid of "neurons" $\mathcal{V} = (v_{kl})_{1 \le k \le K,\, 1 \le l \le L}$, where k, l are the grid coordinates of neuron v_{kl}.

Learning objective: find a map $\kappa : \mathcal{P} \to \mathcal{V}$ which

1. preserves input space topology (the metric topology of $\mathbb{R}^n$), that is, points $\mathbf{x}_j$ in the neighborhood of a point $\mathbf{x}_i$ should be mapped to $\kappa(\mathbf{x}_i)$ or to grid neighbors of $\kappa(\mathbf{x}_i)$, and which
2. covers the pattern collection $\mathcal{P}$ evenly, that is, all grid neurons v_{kl} should have approximately the same number of κ-preimages.

Two comments: (i) Here I use a grid with a rectangular neighborhood structure. Classical SOM papers and many applications of SOMs use a hexagonal neighborhood structure instead, where each neuron has 6 neighbors, all at the same distance. (ii) The "learning objective" sounds vague. It is. At the time when Kohonen introduced SOMs, tailoring learning algorithms along well-defined loss functions was not standard. Kohonen's modeling attitude was biological modeling oriented and a mathematical analysis of the SOM algorithm was not part of his agenda. In fact the problem to find a loss function which is minimized by the original SOM algorithm was still unsolved in the year 2008 (Yin 2008). I don't know what the current state of research in this respect is — I would guess not much has happened since.

In a trained SOM, each grid neuron v_{kl} is connected to the input pattern space $\mathbb{R}^n$ by an n-dimensional weight vector $\mathbf{w}(v_{kl})$. If a new test pattern $\mathbf{x} \in \mathbb{R}^n$ arrives, its κ-image is computed by

$$\kappa(\mathbf{x}) = \operatorname*{argmax}_{v_{kl} \in \mathcal{V}} \mathbf{w}'(v_{kl})\mathbf{x}. \tag{33}$$

In words, the neuron v whose weight vector $\mathbf{w}(v)$ best matches the input pattern $\mathbf{x}$ is chosen. In the SOM literature this neuron is called the *best matching unit* (BMU). Clearly the map κ is determined by the weight vectors $\mathbf{w}(v)$. In order to train them on the training data set $\mathcal{P}$, a basic SOM learning algorithm works as follows:

Initialization: The weights $\mathbf{w}(v_{kl})$ are set to small random values.

Iterate until convergence:

1. Randomly select a training pattern $\mathbf{x} \in \mathcal{P}$.
2. Determine the BMU v_{BMU} for this pattern, based on the current weight vectors $\mathbf{w}(v)$.
3. Update all the grid's weight vectors $\mathbf{w}(v_{kl})$ according to the formula

$$\mathbf{w}(v_{kl}) \leftarrow \mathbf{w}(v_{kl}) + \lambda\, f_r(d(v_{kl}, v_{\mathsf{BMU}}))\, (\mathbf{x} - \mathbf{w}(v_{kl})). \tag{34}$$

4. Make r a little smaller before entering the next interation.

In this sketch of an algorithm, λ is a *learning rate* — a small number, for instance $\lambda = 0.01$, plugged in for numerical stability. The function d is the Euclidean distance (between two neurons positions on the grid). $f_r : \mathbb{R}^{\geq 0} \to \mathbb{R}^{\geq 0}$ is a non-negative, monotonously decreasing function defined on the nonnegative reals which satisfies $f_r(0) = 1$ and which goes to zero as its argument grows. The function is parametrized by a radius parameter $r > 0$, where greater values of r spread out the range of f_r. A common choice is to use a Gaussian-like function $f_r(x) = \exp(-x^2/r^2)$.

Here is an intuitive explanation of this learning algorithm. When a new training pattern $\mathbf{x}$ has been presented and the BMU has been determined, each weight vector $\mathbf{w}(v_{kl})$ is adapted a little bit. The weight update formula (34) adds to $\mathbf{w}(v_{kl})$ a small multiple of $\mathbf{x} - \mathbf{w}(v_{kl})$. This pulls $\mathbf{w}(v_{kl})$ into the direction of $\mathbf{x}$. How strong this pull is depends on how close v_{kl} is to v_{BMU} — the closer, the stronger. This is regulated by the distance-dependent factor $f_r(d(v_{kl}, v_{\mathsf{BMU}}))$. Obviously the adaptation is strongest for the BMU. When (in the early phases of the algorithm) r is large, neurons in the wider vicinity of the BMU will likewise receive rather strong weight adjustments, while only far-away neurons remain more or less unaffected.

This mechanics has the effect that after convergence, the training dataset $\mathcal{P}$ will be covered by grid neurons rather evenly (see objective nr. 2 stated above). To get an intuition why this is so, let us consider a specific scenario. Assume that the pattern set $\mathcal{P}$ contains a dense cluster of mutually quite similar patterns $\mathbf{x}$, besides a number of other, dissimilar patterns. Furthermore assume that we are in an early stage of the learning process, where the radius r is still rather large, and also assume that at this early stadium of learning, each pattern from the cluster yields the same BMU v_0. Due to the large number of members in the cluster, patterns from that cluster will be drawn for the learning algorithm rather often. With r large, this will have the effect that neurons in the wider neighborhood of the BMU v_0 will grow their weight vectors toward $\mathbf{w}(v_0)$. After some time, v_0 will be surrounded by grid neurons whose weight vectors are all similar to $\mathbf{w}(v_0)$, and $\mathbf{w}(v_0)$ will roughly be the mean of all patterns $\mathbf{x}$ in the cluster. Now, some patterns $\mathbf{x}'$ in the cluster will start to have as their BMU not v_0 any longer, but some of its surrounding neighbors (why?). As a consequence, increasingly many patterns in the cluster will best-match the weight vectors of an increasing number of neighbors of v_0: the subpopulation of grid neurons which respond to cluster patterns has grown from the singleton population $\{v_0\}$ to a larger one. This growth will continue until the population of grid neurons responding to cluster patters has become so large that each member's BMU-response-rate has become too low to further drive this population's expansion.

The radius r is set to large values initially in order to let all (or most) patterns in $\mathcal{P}$ compete with each other, leading to a coarse global organization of the emerging map κ. In later iterations, increasingly smaller r leads to a fine-balancing of the BMU responses of patterns that are similar to each other.

SOM learning algorithms come in many variations. I sketched an arbitrary exemplar. The core idea is always the same. Setting up a SOM learning algorithm and tuning it is not always easy – the weight initialization, the decrease schedule for r, the learning rate, the random sampling strategy of training patterns from $\mathcal{P}$, the grid dimension (2 or 3 or even more... 2 is the most common choice), or the pattern preprocessing (for instance, normalizing all patterns to the same norm) are all design decisions that can have a strong impact on the convergence properties and final result quality of the learning process.

Yin 2008 includes a brief survey of SOM algorithm variants. I mention in passing an algorithm which has its roots in SOMs but is quite significantly different: The *Neural Gas* algorithm (good brief intro in `https://en.wikipedia.org/wiki/Neural_gas`), like SOMs, leads to a collection of neurons which respond to patterns from a training set through trainable weight vectors. The main difference is that the neurons are not spatially arranged on a grid but are spatially uncoupled from each other (hence, neural "gas"). The spatially defined distance d appearing in the adaptation efficacy term $f_r(d(v_{kl}, v_{\mathsf{BMU}}))$ is replaced by a rank ordering: the neuron with the best response to training pattern $\mathbf{x}$ (i.e., the BMU) is adapted most, the unit v with the second best response (i.e., second largest value of $\mathbf{w}(v)\,\mathbf{x}$) is adapted second most strongly, etc.

For a quick SOM demo I used a version of a legacy Matlab toolbox published by Kohonen's own research group (I downloaded it almost 20 years ago). As a pattern dataset $\mathcal{P}$ I used the Digits dataset that I also used before in this section. I used 100 examples from each digit class. Figure 21 shows the result of training an 8×8 neuron grid on this dataset. As expected, the ten digit classes become represented each by approximately the same number of grid neurons, reflecting the fact that the classes were represented in $\mathcal{P}$ in equal shares.

Just for the fun of it, I also generated an unbalanced pattern set that had 180 examples of class "5" and 20 examples of every other class. The result is shown in Figure 22. As it should be, roughly half of the SOM neurons are covering the "5" class examples, while the other SOM neurons reach out their weight vectors into the remaining classes.

Practical uses of SOMs appear to have been mostly as visualization tools for exploring (labelled) high-dimensional datasets in two-dimensional graphics. Specifically, such SOM visualizations can give insight into metric similiarities between pattern classes. For instance, inspecting the bottom right 3×3 panels in Figure 21, one finds "morphable" similarities between certain versions of "5" and "9" patterns.

What I find more relevant and interesting about SOMs is their use in neurosciences. Learning mechanisms similar to the SOM learning algorithm have been (and are being) invoked to explain the 2-dimensional spatial organization of *cortical maps*. They can explain how neurons on a surface patch of the cortical sheet align their specific responsiveness to high-dimensional input (from sensors or other brain areas) with their local 2-dimensional metric neighborhood. Pictures which

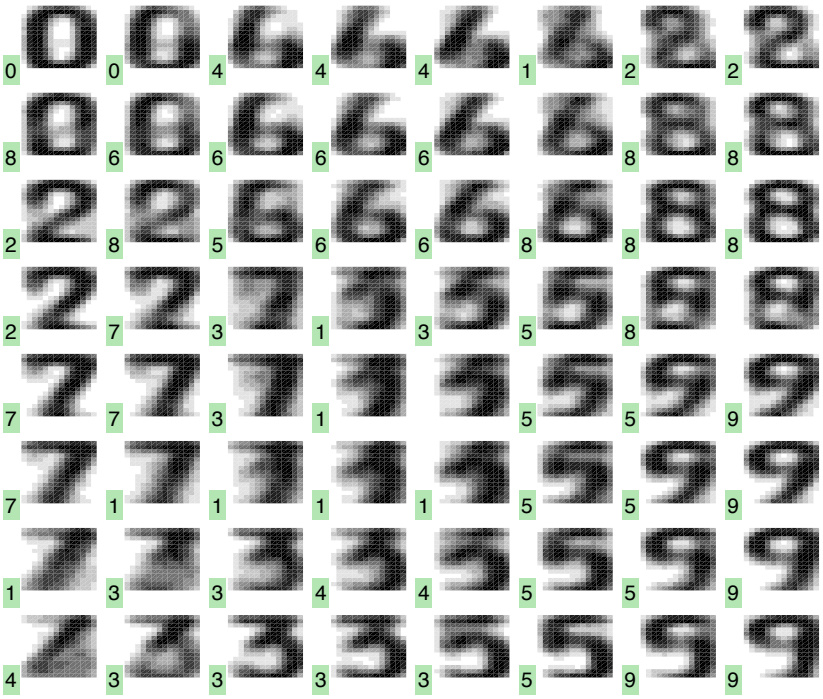

Figure 21: An 8×8 SOM representation of the Digits training dataset. The grayscale images show the weight vectors $\mathbf{w}(v_{kl})$, reshaped back to the rectangular pixel image format. The numbers in the small green insets give the most frequent class label of all training patterns which had the respective grid neuron as BMU. If this number is missing, the grid neuron never fired as BMU for any training pattern.

put synthetic SOM grids side to side with images recorded from small patches of cortical surface have variously been published. Figure 23 gives an example from a study by Swindale and Bauer 1998.

If you are interested in such themes, I can recommend the recent review Bednar and Wilson 2016 on cortical maps as a starting point.

4.8 Summary discussion. Model reduction, data compression, dimension reduction

Reducing the dimensionality of patterns which are represented by vectors is important not only in machine learning but everywhere in science and engineering, where you find it explored under different headline names and for different purposes:

Dimension reduction is a term used in machine learning and statistics. The core motivation is first, that statistical and machine learning models typically depend on a estimate of a probability distribution over some "pattern"

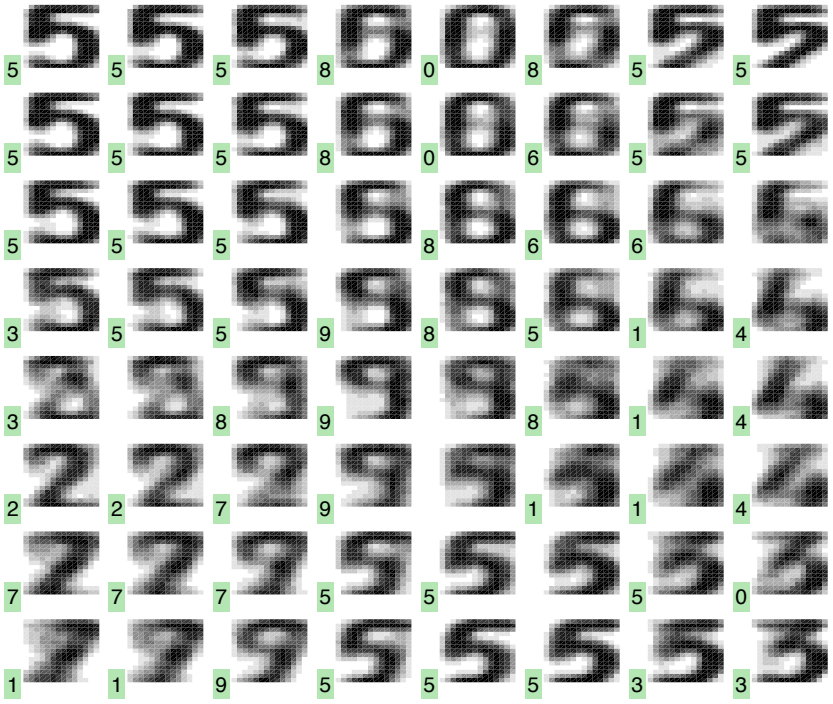

Figure 22: Similar to previous figure, but with an unbalanced pattern set where the number of "5" examples was the same as the total number of all other classes.

space (this distribution estimate may remain implicit); second, that the curse of dimensionality makes it intrinsically hard to estimate distributions from training data points in high-dimensional vector spaces, such that third, a key to success is to reduce the dimension of the "raw" patterns. Typically, the low-dimensional target format is again real-valued vectors ("feature vectors").

Data compression is a term used in signal processing and communication technology. The practical and economical importance of being able to compress and uncompress bulky data is obvious. The compressed data may have a different type than the raw data. For instance, in vector quantization compression, a real-valued vector will become encoded in a natural number, the index of its associated codebook vector. Again there is a close connection with probability, established through Shannon information theory.

Model reduction is a term used when it comes to trim down not just static "data points" but entire dynamical "system models". All branches of science and engineering today deal with models of complex physical dynamical systems which are instantiated as systems of coupled differential equations — often millions, sometimes billions ... or more ... of them. One obtains such gargantuan systems of coupled ODEs almost immediately when one discretizes system models expressed in PDEs. Such sytems cannot be nu-

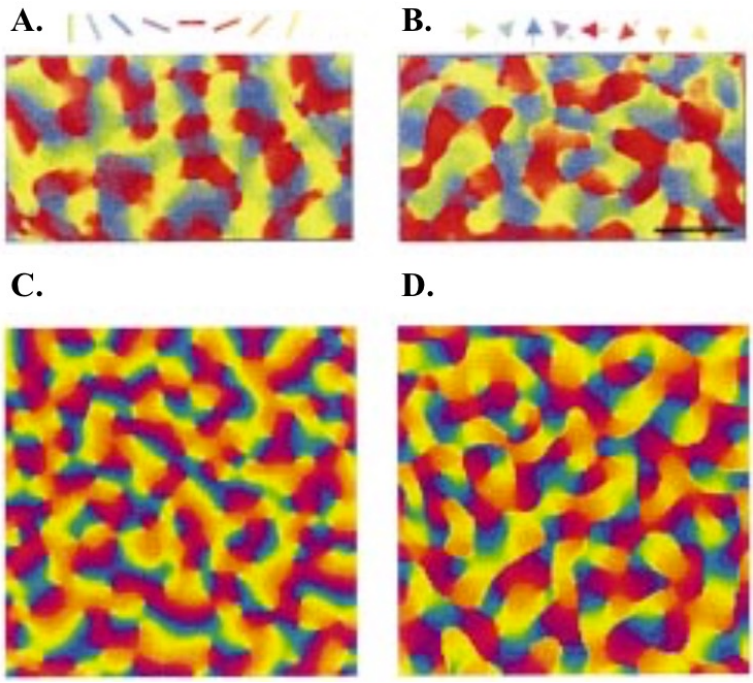

Figure 23: The SOM algorithm reproducing biological cortical response patterns. The scenario: an anaesthesized but eye-open ferret is shown moving images of a bar with varying orientation and direction of movement, while response activity from neurons on a patch (about 10 square mm) of visual cortex is recorded. **A.** A color-coded recording of neural response activity depending on the orientation of the visually presented bar. For instance, if the bar was shown in horizontal orientation, the neurons who responded to this orientation with maximal activity are rendered in red. **B.** Like in panel A., but for the motion direction of the bar (same cortical patch). **C., D.** Artificial similies of A., B. generated with a SOM algorithm. Figures taken from Swindale and Bauer 1998, who in turn took the panels A. and B from Weliky, Bosking, and Fitzpatrick 1996.

merically solved on today's computing hardware and need to be dramatically shrunk before a simulation can be attempted. I am not familiar with this field. The mathematical tools and leading intuitions are different from the ones that guide dimension reduction in machine learning. I mention this field for completeness and because the name "model reduction" invites misleading analogies with dimension reduction. Antoulas and Sorensen 2001 give a tutorial overview with instructive examples.

In this section we took a look at three methods for dimension reduction of high-dimensional "raw" data vectors, namely K-means clustering, PCA, and SOMs. While at first sight these methods appear quite different from each other, there is a unifying view which connects them. In all three of them, the reduction was done by introducing a comparatively simple kind of geometric object in the original high-dimensional pattern space $\mathbb{R}^n$, which was then used to re-express raw data points in a lightweight encoding:

1. In K-means-clustering, this object is the set of codebook vectors, which can be used to compress a test data point to the mere natural number index of its associated codebook vector; or which can be used to give a reduced K-dimensional vector comprised of the distances α_j to the codebook vectors.

2. In PCA, this object is the m-dimensional linear (affine) hyperplane spanned by the first m eigenvectors of the data covariance matrix. An n-dimensional test point is represented by its m coordinates in this hyperplane.

3. In SOMs, this object is the grid of SOM neurons v, including their associated weight vectors $\mathbf{w}(v)$. A new test data point can be compressed to the natural number index of its BMU. This is entirely analog to how the codebook vectors in K-means clustering can be used. Furthermore, if an m-dimensional neuron grid is used (we considered only $m = 2$ above), the grid plane is nonlinearly "folded" into the original dataspace $\mathbb{R}^n$, in that every grid point v becomes projected to $\mathbf{w}(v)$. It thus becomes an m-dimensional manifold embedded in $\mathbb{R}^n$, which is characterized by codebook vectors. This can be seen as a nonlinear generalization of the m-dimensional linear affine hyperplanes embedded in $\mathbb{R}^n$ in PCA.

Thus, the SOM shares properties with both K-means clustering and PCA. In fact, one can systematically explore a whole spectrum of dimension reduction / data compression algorithms which are located between K-means clustering and PCA, in the sense that they describe m-dimensional manifolds of different degrees of nonlinearity through codebook vectors. K-means clustering is the extreme case that uses only codebook vectors and no manifolds; PCA is the other extreme with only manifolds and no codebook vectors. The extensive Preface to the collection volume *Principal Manifolds for Data Visualization and Dimension Reduction* (Gorban et al. 2008) gives a readable intro to this interesting field.

In today's deep learning practice one often ignores the traditional methods treated in this section. Instead one immediately fires the big cannon, training a deep neural network wired up in an *auto-encoder* architecture. An autoencoder network is a multilayer feedforward network whose ouput layer has the same large dimension n as the input layer. It is trained in a supervised way, using training data $(\mathbf{x}_i, \mathbf{y}_i)$ to approximate the identity function: the training output data $\mathbf{y}_i$ are identical to the input patterns $\mathbf{x}_i$ (possibly up to some noise added to the inputs). The trick is to insert a "bottleneck" layer with only $m \ll n$ neurons into the layer sequence of the network. In order to achieve a good approximation of the n-dimensional identity map on the training data, the network has to discover an $n \to m$-dimensional compression mapping which preserves most of the information that is needed to describe the training data points. I will not give an introduction to autoencoder networks in this course (it's a topic for Marco Wiering's "Deep Learning" course). The Deep Learning standard reference I. Goodfellow, Bengio, and Courville 2016 has an entire section on autoencoders.

5 Discrete symbolic versus continuous real-valued

I hope this section will be as useful as it will be short and simple. Underneath it, however, lurks a mysterious riddle of mathematics, philosophy and the neurosciences.

Some data are given in symbolic form, for instance

- texts of all sorts,
- yes/no or rating scale questionnaire items,
- DNA and protein sequence data,
- records of chess or Go matches,
- large parts in public administration databases.

Others are real-valued (scalar, vector, matrix or array formatted) in principle, notwithstanding the circumstance that on digital machines real real numbers must be approximated by finite-length binary strings. Examples of data that are best understood as "continuous" are

- images, video, speech,
- measurement data from technical systems, e.g. in production process control or engine monitoring,
- financial data,
- environmental and weather data,
- signals used in robot motion control.

Many mathematical formalisms can be sorted in two categories: "discrete" and "continuous". Mathematicians, in fact, come in two kinds – ask one, and he/she will be able to tell you whether he/she feels more like a discrete or continuous mathematician. Discrete sorts of mathematics and discrete mathematicians typically operate in areas of number theory, set theory, logic, algebra, graph theory, automata theory. Continuous maths / mathematicians, that is linear algebra, functional analysis, and calculus.

Computer scientists are almost always discrete-math-minded: 0 and 1 and algorithms and Boolean circuits and AI knowledge representation formalisms are eminently discrete.

Physicists are almost always continuous-math minded, because their world is made of continuous space, time, matter, forces and fields.

There are some mathematical domains that are neither, or open to both, especially topology and probability. Some of the most advanced and ingenious modern

fields of mathematics arise from crossover formalisms between the Discrete and the Continuous. The fundamental difference between the two is not dissolved in these theories, but the tension between the Discrete and the Continuous sets free new forms of mathematical energy. Sadly, these lines of research are beyond what I understand and what I can explain (or even name), and certainly beyond what is currently used in machine learning.

The hiatus (an educated word of latin origin, meaning "dividing gap") between the Discrete and the Continuous is also the source of one of the great unresolved riddles in the neurosciences, cognitive science and AI: how can symbolic reasoning (utterly discrete) emerge from the continuous matter and signal processing in our material brains (very physical, very continuous)? This question has kept AI researchers and philosophers busy (and sometimes aggressively angry with one another) for 5 decades now and is not resolved; if you are interested, you can get a first flavor in the Wikipedia article on "Physical symbol system" or by reading up on the overview articles listed in `http://www.neural-symbolic.org/`.

Back to our down-to-earth business. Machine learning formalisms and algorithms likewise are often either discrete-flavored or continuous-flavored. The former feed on symbolic data and create symbolic results, using tools like decision trees, Bayesian networks and graphical models (including hidden Markov models), inductive logic, and certain sorts of neural networks where neurons have 0-1-valued activations (Hopfield networks, Boltzmann machines). The latter digest vector data and generate vector output, with deep neural network methods currently being the dominating workhorse which overshadow more traditional ones like support vector machines and various sorts of regression learning "machines".

The great built-in advantage of discrete formalisms is that they lend themselves well to *explainable*, human-understandable solutions. Their typical disadvantage is that learning or inference algorithms are often based on combinatorial search, which quickly lets computing times explode. In contrast, continuous formalisms typically lead to results that cannot be intuitively interpreted – vectors don't talk – but lend themselves to nicely, smoothly converging optimization algorithms.

When one speaks of "machine learning" today, one mostly has vector processing methods in mind. Also this RUG course is focussing on vector data. The discrete strands of machine learning are more associated with what one often calls "data mining". This terminology is however not clearly defined. I might mention that I have a brother, Manfred Jaeger (`http://people.cs.aau.dk/~jaeger/`), who is also a "machine learning" prof, but he is from the discrete quarters while I am more on the continuous side. We often meet and talk, but not about science, because we don't understand what the respective other researches; we publish in different journals and go to different conferences.

Sometimes one has vector data but wants to exploit benefits that come with discrete methods, or conversely, one has symbolic data and wants to use a neural network (because everybody else seems to be using them, or because one doesn't want to fight with combinatorial explosions). Furthermore, many an interesting

dataset comes as a mix of symbolic-discrete and numerical-continuous data – for instance, data originating from questionnaires or financial/business/admin data often are mixed-sort.

Then, one way to go is to *convert* discrete data to vectors or vice versa. It is a highly empowering professional skill to know about basic methods of discrete $\leftrightarrow$ continuous conversions.

Here are some discrete-to-continuous transformations:

One-hot encodings. Given: data points a_ν that are symbols from a finite "alphabet" $A = \{a_1, \ldots, a_k\}$. Examples: yes/no answers in a questionnaire; words from a vocabulary; nucleic acids A, C, G, T occuring in DNA. Turn each a_ν into the k-dimensional binary vector $v_\nu \in \{0,1\}^k$ which is zero everywhere except at position ν. This is a very common way to present symbolic input to neural networks. On the output side of a neural network (or any other regression learning machine), one-hot encodings are also often used to give vector teacher data in classification tasks: if $(\mathbf{x}_i, c_i)$ is a classification-task training dataset, where c_i is a symbolic class label from a class set $C = \{c_1 \ldots, c_k\}$, transform each c_i to its k-dimensional one-hot vector v_i and get a purely vector-type training dataset $(\mathbf{x}_i, v_i)$.

Binary pattern encodings. If the symbol alphabet A is of a large size k, one might shy away from one-hot encoding because it gives large vectors. Instead, encode each a_ν into a binary vector of length $\lceil \log_2 k \rceil$, where $\lceil \log_2 k \rceil$ is the smallest integer larger or equal to $\log_2 k$. Advantage: small vectors. Disadvantage: subsequent vector-processing algorithms must invest substantial nonlinear effort into decoding this essentially arbitrary encoding. This will mostly be crippling, and binary pattern encodings should only be considered if there is some intuitive logic in the encoding.

Linear scale encoding. If there is some natural ordering in the symbols $a_\nu \in A$, encode every a_ν by the index number ν. Makes sense, for instance, when the a_ν come from a Likert-scale questionnaire item, as in

$$A = \{\mathsf{certainly\ not}, \mathsf{rather\ not}, \mathsf{don't\ know}, \mathsf{rather\ yes}, \mathsf{certainly\ yes}\}.$$

Semantic word vectors. This is a technique which enabled breakthroughs in deep learning for text processing (I mentioned it in the Introduction; it is used in the TICS demo). By a nontrivial machine learning algorithm pioneered by Mikolov et al. 2013, convert words a_ν from a (large) vocabulary A into vectors of some reasonably large size, say 300-dimensional, such that semantically related words become mapped to vectors that are metrically close to each other.

For instance, code vectors v, v' for words $w = \mathsf{airplane}$ and $w' = \mathsf{aircraft}$ should have small distance, wheras the code vector v'' for $w'' = \mathsf{rose}$ should

lie at a great distance to both v and v'. So the goal is to find vectors v, v', v'' in this example that have small distance $\|v-v'\|$ and large distances $\|v-v''\|$, $\|v'-v''\|$. This is achieved by measuring the similarity of two words w, w' through counting how often they occur in similar locations in training texts. A large collection of English texts is processed, collecting statistics about similar sub-phrases in those texts that differed only in the two words whose similarity one wished to assess (plus, there was another trick: can you think of an important improvement of this basic idea?). – Mikolov's paper has been (Google-scholar) cited 24,000 times in merely seven years!

And here are some continuous-to-discrete transformations:

One-dimensional discretization, also known as binning. Given: a real number dataset $\{x_i\}$ where $x_i \in \mathbb{R}$. Divide the real line into k segments

$$A_1, A_2, \ldots, A_{k-1}, A_k = (-\infty, a_1], (a_1, a_2], \ldots, (a_{k-2}, a_{k-1}], (a_{k-1}, \infty)$$

. Then transform each x_i to that symbol A_ν for which $x_i \in A_\nu$. Comments:

- The segments $(a_\nu, a_{\nu+1}]$ are called *bins*.
- In the simplest case, the range $[\min\{x_i\}, \max\{x_i\}]$ of the data points is split into k bins of equal length.
- Alternatively, another way of splitting the range $[\min\{x_i\}, \max\{x_i\}]$ is to define the bins such that each bin will contain an approximately equal number of data points from the set $\{x_i\}$.
- Often the best way of splitting the data range into bins depends on the task. This can turn out to be a delicate optimization problem. For instance, there is a sizeable literature in deep learning which is concerned with the question of how one can reduce the numerical precision of weight parameters in neural networks. One first trains the neural network using standard high-precision learning algorithms, obtaining weight matrices in floating-point precision. In order to speed up computing, use small microchips on hand-held devices, or reduce energy consumption when using the trained network, one wishes to reduce the bit precision of the weight matrices. In extreme cases, one wants to end up with only three weight values $\{-1, 0, 1\}$, which would lead to very cheap neural network computations at use time. This amounts to the splitting the range of floating-point precision weights obtained after training into just three bins. The goal is to ensure that the reduced-precision network performs approximately as well as the high-precision original. This is a nontrivial problem. Check out the (randomly chosen) reference Indiveri 2015 if you want to get a taste of the flavor.

Multi-dimensional discretization by hierarchical refinement. If one wants to discretize a set $\{\mathbf{x}_i\}$ of n-dimensional vectors, one has to split the n-dimensional volume which contains the points $\{\mathbf{x}_i\}$ into a finite set of discrete regions R_ν. A common approach is to let these regions be n-dimensional hypercubes. By a process of hierarchical refinement one constructs these regions R_ν such that in areas where there is a higher point density, or in areas where there is much fine-grained information encoded in the local point distribution, one uses smaller hypercubes to increase resolution. This leads to a tree structure, which in the case $n = 2$ is called a *quadtree* (because every non-leaf node has four children) and in the case $n = 3$ an *octree* of hierarchically nested hypercubes. This tree structure enables a computationally efficient indexing of the hypercubes. The left panel in Figure 24 shows an example. The Wikipedia article on quadtrees is quite instructive. One may also opt for regions R_ν of other polygonal shape (see right panel in Figure 24). There are many such *mesh refinement* methods, with task-specific optimization criteria. They are not typically used in machine learning but rather in methods for simulating spatiotemporal (fluid) dynamics by numerically solving PDEs. Still, it is good to know that such methods exist.

Vector quantization. Using K-means or other clustering algorithms, the vector set $\{\mathbf{x}_i\}$ is partitioned into k cells whose center of gravity vectors are indexed and the indices are used as symbolic encodings of the $\{\mathbf{x}_i\}$. We have seen this in Section 4.2. This *is* a typical machine learning method for discretization.

Turning neural dynamics into symbol sequences. When we (I really mean "we", = us humans!) speak or write, the continuous-time, continuous-valued neural brain dynamics leads to a discrete sequence of words. Somehow, this symbolic sequence is encoded in the "subsymbolic", analog brain dynamics. It is unknown *how*, exactly, this encoding is realized. Numerous proposals based on nonlinear dynamical systems theory have been made. This is an area of research in which I am personally engaged. If you are interested: partial selections of some approaches are listed in Durstewitz, Seamans, and Sejnowski 2000, Pascanu and Jaeger 2011, Fusi and Wang 2016. In machine learning, the problem of transforming continuous-valued neural state sequences to sequences of words (or letters) arises in applications like speech recognition ("speech-to-text") or gesture recognition. Here the most common solution (which is not necessarily biologically plausible) is to use the core neural network to generate a sequence of continuous-valued *hypothesis* output vectors with as many components as there are possible target symbols. At each point in time, the numerical value of each vector component reflects a current "degree of belief" about which symbol should be generated. With some postprocessing mechanism (not easy to set up), this hypothesis stream is denoised and turned into a symbol sequence, for instance by selecting at each point in time the symbol that has the largest

degree of belief.

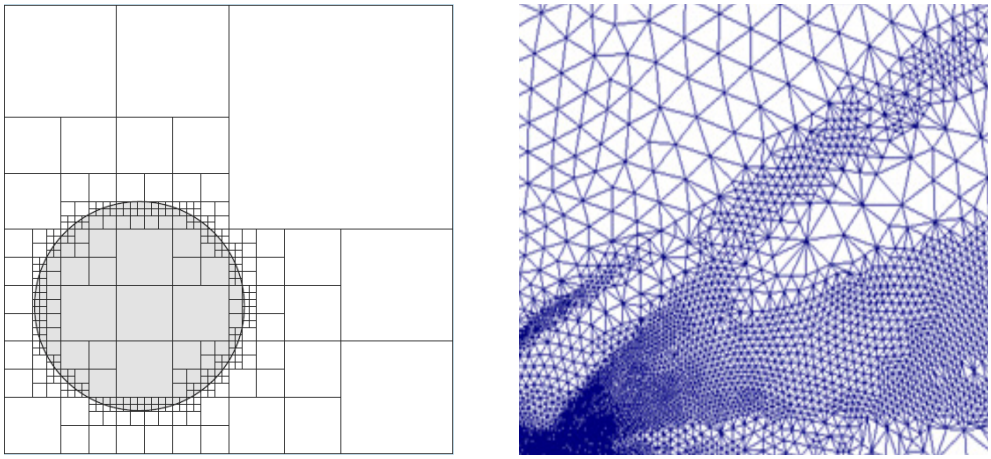

Figure 24: Left: A hierarchical hypercube mesh for a 2-dimensional dataset consisting of points homogeneously distributed inside a circle. Right: adaptive non-orthogonal meshing, here used in an airflow simulation. Sources: left panel: `http://www.questinygroup.com/tag/quad-tree/`; right panel: Luchinsky and al. 2012.

6 The bias-variance dilemma and how to cope with it

Reality is rich in detail and surprises. Measuring reality gives a finite number of data points – and the reality between and beyond these data points remains unmeasured, a source of unforseeable surprises. Furthermore, measuring is almost always "noisy" – imprecise or prone to errors. And finally, each space-time event point of reality can be measured in innumerable ways, of which only a small choice is actually measured. For instance, the textbook measurement of "tossing a coin" events is just to record "heads" or "tail". But one *could* also measure the weight and color of coin, the wind speed, the falling altitude, the surface structure of the ground where the coin falls, and ... everything else. In summary, any dataset will capture only a supremely scarce coverage of space-time events whose unfathomable qualitative richness has been reduced to a ridiculously small number of "observables". From this empoverished, punctuated information basis, called "training data", a machine learning algorithm will generate a "model" of a part of reality. This model will then be used to predict properties of *new* space-time events, called "test inputs". How should it be ever possible for a model to "know" anything about those parts of reality that lie between the pinpoints hit by the training data?

This would be a good point to give up.

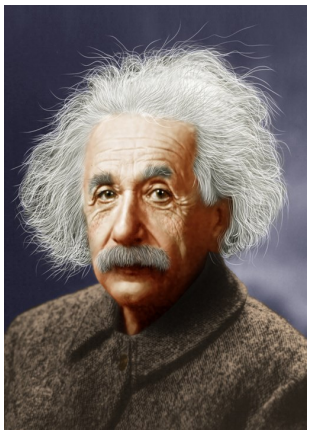

Figure 25: He gave the reason why machine learning works (from `https://commons.wikimedia.org/wiki/File:Albert_Einstein_-_Colorized.jpg`)

But ... quoting Einstein: *"Subtle is the Lord, but malicious He is not"* (`https://en.wikiquote.org/wiki/Albert_Einstein`). Reality is co-operative. Between measurement points, reality changes not arbitrarily but in a lawful manner. The question is, *which* law. In machine learning, this question is known as the problem of *overfitting*, or in more educated terms, the *bias-variance dilemma*. Welcome to this chapter which is all about this question. For all your practical exploits

of machine learning in your professional future, this is the most important and enabling chapter in this course. If you feel this menace is staring at you, this chapter shows you how to speak to it and tame it, and your final trained model will be so much better in generalizing from your training data to the data that your customers will have.

6.1 Training and testing errors

Let us take a closer look at the archetypical machine learning task of classifying handwritten digits. We use the simple Digits benchmark data which you know from Section 4.1. The task is specified as follows:

Training data. $(\mathbf{x}_i^{\mathsf{train}}, c_i^{\mathsf{train}})_{i=1,\ldots,1000}$ where the $\mathbf{x}_i^{\mathsf{train}} \in [0,1]^{240}$ are 240-dimensional image vectors, whose components correspond to the 15×16 pixels which have normalized grayscale values ranging in $[0,1]$; and where the c_i^{train} are class labels from the set $\{0,1,\ldots,9\}$. There are 100 examples from each class in the training data set.

Test data. Another set $(\mathbf{x}_i^{\mathsf{test}}, c_i^{\mathsf{test}})_{i=1,\ldots,1000}$, also having 100 exemplars of each digit.

Task specification. This is a benchmark dataset with a standardized task specification: train a classifier using (only) the training data, then test it on the test data and report the rate of misclassifications. The loss function is thus the count loss given in Equation 4.

An elementary but professionally structured learning pipeline which uses methods that we have already described in this course goes as follows (it may be a welcome rehearsal to give a step-by-step instruction):

First stage: dimension reduction by PCA:

1. Center the set of image vectors $(\mathbf{x}_i^{\mathsf{train}})_{i=1,\ldots,1000}$ by subtracting the mean vector μ, obtaining $(\bar{\mathbf{x}}_i^{\mathsf{train}})_{i=1,\ldots,1000}$.
2. Assemble the centered image vectors column-wise in a 240×1000 matrix $\bar{X}$. Compute the covariance matrix $C = 1/1000\ X\,X'$ and factorize C into its SVD $C = U\Sigma U'$. The columns of U are the 240 principal component vectors of C.
3. Decide how strongly you want to reduce the dimension, shrinking it from $n = 240$ to $m < n$. Let U_m be the matrix made from the first m columns from U.
4. Project the centered patterns $\bar{\mathbf{x}}_i^{\mathsf{train}}$ on the m first principal components, obtaining m-dimensional feature vectors $\mathbf{f}_i^{\mathsf{train}} = U_m'\,\bar{\mathbf{x}}_i^{\mathsf{train}}$.

Vectorize the class labels by one-hot encoding: Each c_i^{train} is re-written as a binary 10-dimensional vector v_i^{train} which has a 1 entry in the corresponding class c_i. Assemble these vectors column-wise in a 10×1000 matrix V.

Compute a linear regression classifier: Assemble the 1000 m-dimensional feature vectors $\mathbf{f}_i^{\mathsf{train}}$ into a $m \times 1000$ dimensional matrix F and obtain a $10 \times m$ dimensional regression weight matrix W by

$$W' = (F\,F')^{-1}\,F\,V'.$$

Compute the training MSE and training error rate: The training mean square error (MSE) is given by

$$\mathrm{MSE}^{\mathrm{train}} = 1/1000 \sum_{i=1}^{1000} \|v_i^{\mathrm{train}} - W\,(\mathbf{f}_i^{\mathrm{train}})\|^2.$$

The training misclassification rate is

$$\varrho^{\mathrm{train}} = 1/1000\;|\{i \mid \mathrm{maxInd}\;W\,\mathbf{f}_i^{\mathrm{train}} - 1 \neq c_i^{\mathrm{train}}\}|,$$

where maxInd picks the index of the maximal element in a vector. (Note: the "-1 is owed to the fact that the vector indices range from 1 to 10, while the class labels go from 0 to 9).

Similarly, compute the test MSE and error rates by

$$\mathrm{MSE}^{\mathrm{test}} = 1/1000 \sum_{i=1}^{1000} \|v_i^{\mathrm{test}} - W\,(\mathbf{f}_i^{\mathrm{test}})\|^2$$

and

$$\varrho^{\mathrm{test}} = 1/1000\;|\{i \mid \mathrm{maxInd}\;W\,\mathbf{f}_i^{\mathrm{test}} - 1 \neq c_i^{\mathrm{test}}\}|,$$

where $\mathbf{f}_i^{\mathrm{test}} = U'_m\,(\mathbf{x}_i^{\mathsf{test}} - \mu)$. Note: for centering the test data, use the mean μ obtained from the training data!

This is a procedure made from basic linear operations that you should command even when sleepwalking; with some practice the entire thing should not take you more than 30 minutes for programming and running. Altogether a handy quick-and-not-very-dirty routine that you should consider carrying out in every classification task, in order to get a baseline before you start exploring more sophisticated methods.

And now - let us draw what is probably the most helpful and worth burning into your subconscious graphics in these lecture notes. Figure 26 shows these diagnostics for all possible choices of the number $m = 1, \ldots, 240$ of PC features used.

This plot visualizes one of the most important issues in (supervised) machine learning and deserves a number of comments.

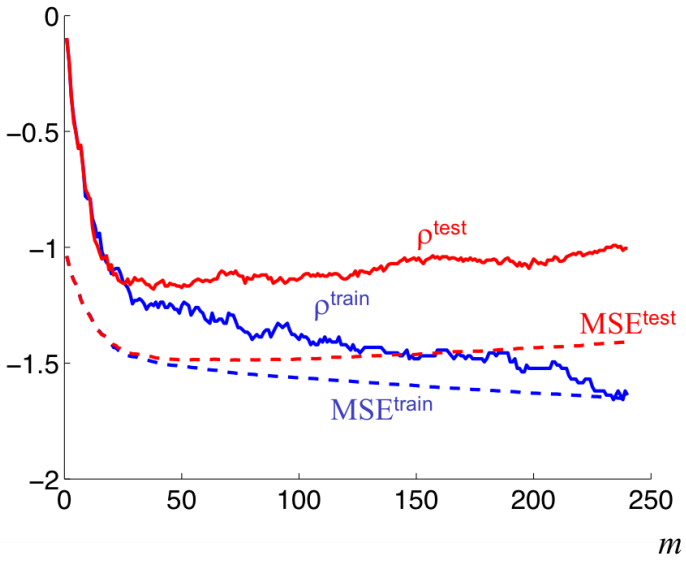

Figure 26: Dashed: Train (blue) and test (red) MSE obtained for $m = 1, \ldots, 240$ PCs. Solid: Train (blue) and test (red) misclassification rates. The y-axis is logarithmic base 10.

- As m increases (the x-axis in the plot), the number of parameters in the corresponding linear regression weight matrices W grows by $10 \cdot m$. More model parameters means more degree of freedoms, more "flexible" models. With greater m, models can increasingly better solve the linear regression learning equation (20). This is evident from the monontonous decrease of the train MSE curve. The training misclassification rate also decreases persistently except for a jitter that is due to the fact that we optimized models only indirectly for low misclassification.

- The analog performance curves for the testing MSE and misclassification first exhibit a decrease, followed by an increasing tail. The testing misclassification rate is minimal for $m = 34$.

- This "first decrease, then increase" behavior of testing MSE (or classification rate) is *always* observed in supervised learning tasks when models are compared which have growing degrees of data fitting flexibility. In our digit example, this increase in flexibility was afforded by growing numbers of PC features, which in turn gave the final linear regression a richer repertoire of feature values to combine into the hypothesis vectors.

- The increasing tail of testing MSE (or classification rate) is the hallmark of *overfitting*. When the learning algorithm admits too much flexibility, the resulting model can fit itself not only to what is "lawful" in the training data,

but also to the random fluctuations in the training data. Intuitively and geometrically speaking, a learning algorithm that can shape many degrees of freedom in its learnt models allows the models to "fold in curls and wiggles to accomodate the random whims of the training data". But then, the random curls and wiggles of the learnt model will be at odds with fresh testing data.

6.2 The menace of overfitting – it's real, it's everywhere

ML research has invented a great variety of model types for an even larger variety of supervised and unsupervised learning tasks. How exactly overfitting (mis-)functions in each of these model types will need a separate geometrical analysis in each case. Because overfitting is such a fundamental challenge in machine learning, I illustrate its geometrical manifestations with four examples.

6.2.1 Example 1: polynomial curve-fitting

This example is *the* standard textbook example for demonstrating overfitting. Let us consider a one-dimensional input, one-dimensional output regression task of the kind where the training data are of form $(x_i, y_i) \in \mathbb{R} \times \mathbb{R}$. Assume that there is some systematic relationship $y = h(x)$ that we want to recover from the training data. We consider a simple artificial case where the x_i range in $[0, 1]$ and the to-be-discovered true functional relationship is $y = \sin(2\,\pi\,x)$. The training data, however, contain a noise component, that is, $y_i = \sin(2\,\pi\,x_i) + \nu_i$, where ν_i is drawn from a normal distribution with zero mean and standard deviation σ. Figure 27 shows a training sample $(x_i, y_i)_{i=1,\ldots,11}$, where $N = 11$ training points x_i are chosen equidistantly.

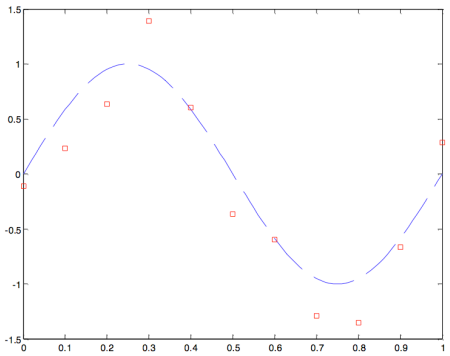

Figure 27: An example of training data (red squares) obtained from a noisy observation of an underlying "correct" function $sin(2\,\pi\,x)$ (dashed blue line).

We now want to solve the task of learning a good approximation for h from the training data (x_i, y_i) by applying polynomial curve fitting, an elementary technique you might be surprised to meet here as a case of machine learning. Consider an

m-th order polynomial

$$p(x) = w_0 + w_1 x + \cdots + w_m x^m. \tag{35}$$

We want to approximate the function given to us via the training sample by a polynomial, that is, we want to find ("learn") a polynomial $p(x)$ such that $p(x_i) \approx y_i$. More precisely, we want to minimize the mean square error on the training data

$$\mathrm{MSE}^{\mathrm{train}} = \frac{1}{N} \sum_{i=1}^{N} (p(x_i) - y_i)^2.$$

At this moment we don't bother how this task is solved computationally but simply rely on the Matlab function *polyfit* which does exactly this job for us: given data points (x_i, y_i) and polynomial order m, find the coefficients w_j which minimize this MSE. Figure 28 shows the polynomials found in this way for $m = 1, 3, 10$.

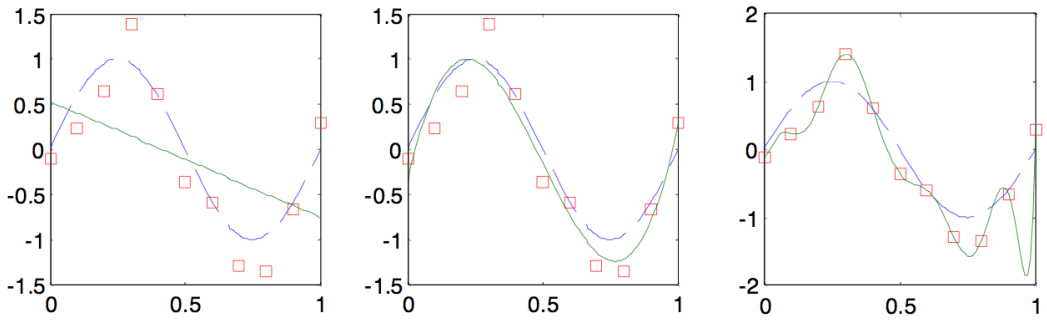

Figure 28: Fitting polynomials (green lines) for polynomial orders 1, 3, 10 (from left to right).

If we compute the MSE's for the three orders $m = 1, 3, 10$, we get $\mathrm{MSE}^{\mathrm{train}} = 0.4852, 0.0703, 0.0000$ respectively. Some observations:

- If we increase the order m, we get increasingly lower $\mathrm{MSE}^{\mathrm{train}}$.
- For $m = 1$, we get a linear polynomial, which apparently does not represent our original sine function well (underfitting).
- For $m = 3$, we get a polynomial that hits our target sine apparently quite well.
- For $m = 10$, we get a polynomial that perfectly matches the training data, but apparently misses the target sine function (overfitting).

The modelling flexibility is here defined through the polynomial order m. If it is too small, the models are too inflexible and *underfit*; if it is too large, we see overfitting.

However, please switch now into your most critical thinking mode and reconsider what I have just said. *Why*, indeed, should we judge the linear fit "underfitting", the order-3 fit "seems ok", and the order-10 fit "overfitting"? There is no other ground for justifying these judgements than our visual intuition! In fact, the order-10 fit might be the right one if the data contain no noise! the order-1 fit might be the best one if the data contain a lot of noise! We don't know!

6.2.2 Example 2: pdf estimation

Let us consider the task of estimating a 2-dimensional pdf over the unit square from 6 given training data points $\{x_i\}_{i=1,...,6}$, where each x_i is in $[0,1] \times [0,1]$. This is an elementary unsupervised learning task, the likes of which frequently occur as a subtask in more involved learning tasks, but which is of interest in its own right too. Figure 29 shows three pdfs which were obtained from three different learning runs with models of increasing flexibility (I don't explain the modeling method here — for the ones who know about it: simple Gaussian Parzen-window models where the degree of admitted flexibility was tuned by kernel width). Again we encounter the fingerprints of under/overfitting: the low-flexibility model seems too "unbending" to resolve any structure in the training point cloud (underfitting), the high-flexibility model is so volatile that it can accomodate each individual training point (presumably overfitting).

But again, we don't really know...

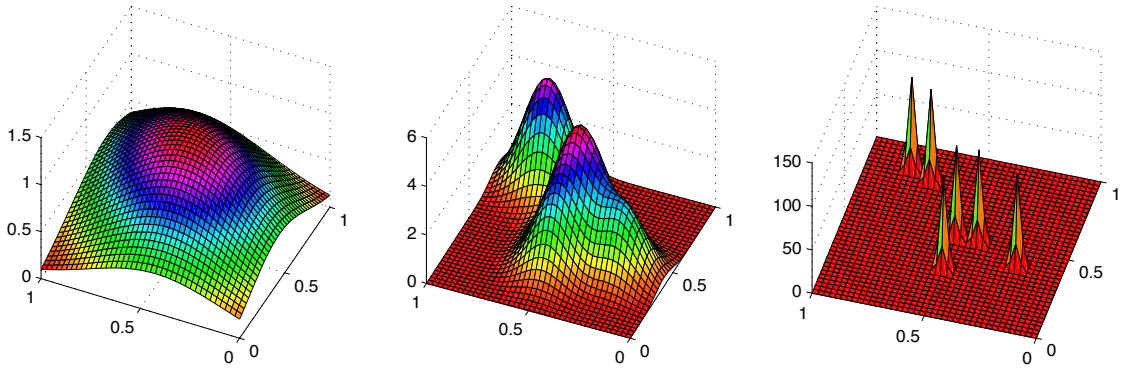

Figure 29: Estimating a pdf from 6 data points. Model flexibility grows from left to right. Note the different scalings of the z-axis: the integral of the pdf is 1 in each of the three cases.

6.2.3 Example 3: learning a decision boundary

Figure 30 shows a schematic of a classification learning task where the training patterns are points in $\mathbb{R}^2$ and come in two classes. When the trained model is too inflexible (left panel), the decision boundary is confined to be a straight line,

presumably underfitting. When the flexibility is too large, each individual training point can be "lasso-ed" by a sling of the decision boundary, presumably overfitting.

Do I need to repeat that while these graphics *seem* to indicate under- or overfitting, we do not actually *know*?

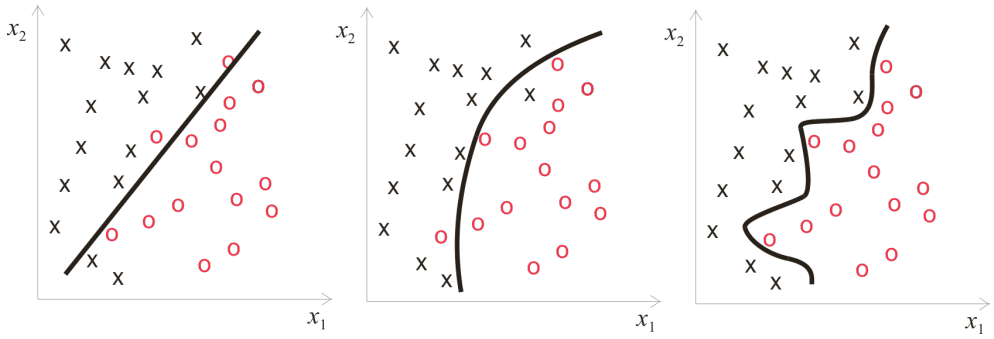

Figure 30: Learning a decision boundary for a 2-class classification task of 2-dimensional patterns (marked by black "x" and red "o").

6.2.4 Example 4: furniture design

Overfitting can also hit you in your sleep, see Figure 31.

Again, while this looks like drastic overfitting, it would be just right if all humans sleep in the same folded way as the person whose sleep shape was used for training the matrass model did.

6.2.5 Interim summary

The four examples stem from different learning tasks (function approximation, pdf learning, classification learning, furniture optimization), and correspondingly the overfitting problem manifests itself in different geometrical ways. But the flavor is the same in all cases. The model flexibility determines how "wiggly" the geometry of the learnt model can become. Very large flexibility ultimately admits to adapt the model to each individual training point. This leads to small, even zero, training error; but it is likely disastrous for generalization to new test data points. Very low flexibility can hardly adapt to the structure of the training data at all, likewise leading to poor test performance (and poor training performance too). Some intermediate flexibility is likely to strike the best balance.

Properly speaking, flexibility is not a characteristic of the final model that one obtains after learning, but of the learning algorithm. If one uses the term precisely, one should speak, for example, of "the flexibility of the procedure to train a third-order polynomial function", or of "the flexibility of the PCA-based linear regression learning scheme which uses m PCA features".

I introduced this way of speaking about "flexibility" ad hoc. In statistics and machine learning textbooks you will hardly find this term. Instead, specific

Figure 31: A nightmare case of overfitting. Picture spotted by Yasin Cibuk (2018 ML course participant) on `http://dominicwilcox.com/portfolio/bed/`, designed and crafted by artist Dominic Wilcox, 1999. Quote from the artist's description of this object: "I used my own body as a template for the mattress". From a ML point of view, this means a size $N = 1$ training data set.

methods to measure and tune the flexibility of a learning algorithm have their specific names, and it is these names that you will find in the literature. The most famous among them is *model capacity*. This concept has been developed in a field now called *statistical learning theory*, and (not only) I consider it a highlight of modern ML theory. We will however not treat it in this lecture, since it is not an easy concept and it needs to be spelled out in different versions for different types of learning tasks and algorithms. Check out `en.wikipedia.org/wiki/Vapnik-Chervonenkis_theory` if you want to get an impression. Instead, in Sections 6.4.1 and 6.4.2 I will present two simpler methods for handling modeling flexibility which, while they lack the analytical beauty and depth of the model capacity concept, are immensely useful in practice.

I emphasize that finding the right flexibility for a learning algorithm is ab-so-lu-te-ly crucial for good performance of ML algorithms. Our little visual examples do not do justice to the dismal effects that overfitting may have in real-life learning tasks where a high dimension of patterns is combined with a small number of training examples — which is a situation faced very often by ML engineers in practical applications.

6.3 An abstract view on supervised learning

Before I continue with the discussion of modeling flexibility, it is helpful to introduce some standard theoretical concepts and terminology. Before you start reading this section, make sure that you understand the difference between the

expectation of a random variable and the *sample mean* (explained in Appendix D).

In supervised learning scenarios, one starts from a training sample of the form $(x_i, y_i)_{i=1,\ldots,N}$, which is drawn from a joint distribution $P_{X,Y}$ of two random variables X and Y. So far, we have focussed on tasks where the x_i were vectors and the y_i were class labels or numbers or vectors, but supervised learning tasks can be defined for any kind variables. In this subsection we will take an abstract view and just consider any kind of supervised learning based on a training sample $(x_i, y_i)_{i=1,\ldots,N}$. We then call the x_i the *arguments* and the y_i the *targets* of the learning task. The target RV Y is also sometimes referred to as the *teacher* variable.

The argument and target variables each come with their specific *data value space* – a set of possible values that the RVs X and Y may take. For instance, in our digit classification example, the data value space for X was $\mathbb{R}^{240}$ (or more constrained, $[0,1]^{240}$) and the data value space for Y was the set of class labels $\{0, 1, \ldots, 9\}$. After the extraction of m features and turning the class labels to class indicator vectors, the original picture–label pairs (x_i, y_i) turned into pairs $(\mathbf{f}_i, v_i)$ with data value spaces $\mathbb{R}^m, \{0,1\}^k$ respectively. In English-French sentence translation tasks, the data value spaces of the random variables X and Y would be a (mathematical representation of a) set of English and French sentences. We now abstract away from such concrete data value spaces and write $\mathcal{E}_X, \mathcal{E}_Y$ for the data value spaces of X and Y.

Generally speaking, the aim of a supervised learning task is to derive from the training sample a function $h : \mathcal{E}_X \to \mathcal{E}_Y$. We called this function a *decision function* earlier in these lecture notes, and indeed that is the term which is used in abstract statistical learning theory.

Some of the following I already explained before (Section 2.3) but it will be helpful if I repeat this here, with a little more detail.

The decision function h obtained by a learning algorithm should be optimized toward some objective. One introduces the concept of a *loss function*. A loss function is a function

$$L : \mathcal{E}_Y \times \mathcal{E}_Y \to \mathbb{R}^{\geq 0}. \tag{36}$$

The idea is that a loss function measures the "cost" of a mismatch between the target values y and the values $h(x)$ returned by a decision function. Higher cost means lower quality of h. We have met two concrete loss functions so far:

- A loss that counts misclassifications in pattern classification: when the decision function returns a class label, define

$$L(h(x), y) = \begin{cases} 0, & \text{if } h(x) = y \\ 1, & \text{if } h(x) \neq y \end{cases} \tag{37}$$

- A loss that penalizes quadratic errors of vector-valued targets:

$$L(h(x), y) = \|h(x) - y\|^2. \tag{38}$$

This loss is often just called "quadratic loss". We used it as a basis for deriving the algorithm for linear regression in Section 3.1.

The decision function h is the outcome of a learning algorithm, which in turn is informed by a sample $(x_i, y_i)_{i=1,\ldots,N}$. Learning algorithms should minimize the *expected* loss, that is, a good learning algorithm should yield a decision function D whose *risk*

$$R(h) = E[L(h(X), Y)] \tag{39}$$

is small. The expectation here is taken with respect to the true underlying joint distribution $P_{X,Y}$. For example, in a case where X and Y are numerical RVs and their joint distribution is described by a pdf f, the risk of a decision function h would be given by

$$R(h) = \int_{\mathcal{E}_X \times \mathcal{E}_Y} L(h(x), y)\, f(x, y)\, d(x, y).$$

However, the true distribution f is unknown. The mission to find a decision function h which minimizes (39) is, in fact, hopeless. The only access to $P_{X,Y}$ that the learning algorithm affords is the scattered reflection of $P_{X,Y}$ in the training sample $(x_i, y_i)_{i=1,\ldots,N}$.

A natural escape from this impasse is to tune a learning algorithm such that instead of attempting to minimize the risk (39) it tries to minimize the *empirical risk*

$$R^{\text{emp}}(h) = 1/N \sum_{i=1}^{N} L(h(x_i), y_i), \tag{40}$$

which is just the mean loss calculated over the training examples. Minimizing this empirical risk is an achievable goal, and a host of optimization algorithms for all kinds of supervised learning tasks exist which do exactly this, that is, they find

$$h_{\text{opt}} = \operatorname*{argmin}_{h \in \mathcal{H}} \; 1/N \sum_{i=1}^{N} L(h(x_i), y_i). \tag{41}$$

The set $\mathcal{H}$ is the *hypothesis space* – the search space within which a learning may look for an optimal h.

It is important to realize that every learning algorithm comes with a specific hypothesis space. For instance, in decision tree learning $\mathcal{H}$ is the set of all decision trees that use a given set of properties and attributes. Or, in linear regression, $\mathcal{H}$ is the set of all affine linear functions from $\mathbb{R}^n$ to $\mathbb{R}^k$. Or, if one sets up a neural network learning algorithm, $\mathcal{H}$ is typically the set of all neural networks that have a specific connection structure (number of neuron layers, number of neuros per layer); the networks in $\mathcal{H}$ then differ from each other by the weights associated with the synaptic connections.

The empirical risk is often – especially in numerical function approximation tasks – also referred to as *training error*.

While minimizing the empirical loss is a natural way of coping with the impossibility of minimizing the risk, it may lead to decision functions which combine a low empirical risk with a high risk. This is the ugly face of overfitting which I highlighted in the previous subsection. In extreme cases, one may learn a decision function which has zero empirical risk and yet has a extremely large expected testing error which makes it absolutely useless.

There is no easy or general solution for this conundrum. It has spurred statisticians and mathematicians to develop a rich body of theories which analyze the relationships between risk and empirical risk, and suggest insightful strategies to manage as well as one can in order to keep the risk within provable bounds. These theories, sometimes referred to as *statistical learning theory* (or better, theor*ies*), are beyond the scope of this lecture.

If you are in a hardcore mood and if you have some background in probability theory, you can inspect Section 18 of lecture notes of my legacy "Principles of Statistical Modeling" course (online at `https://www.ai.rug.nl/minds/uploads/LN_PSM.pdf`). You will find that the definitions of loss and risk given there in the spirit of mathematical statistics are a bit more involved than what I presented above, but the definitions of loss and risk that I gave here are used in textbooks on machine learning.

6.4 Tuning model flexibility

In order to deal with the overfitting problem, one must have ways to tune the flexibility of the learning algorithm and set it to the "right" value.

Let us briefly return to the overfitting diagram in Figure 26. In that demo, the flexibility regulation (moving left or right on the horizontal axis) was effected by moving in a model class inclusion hierarchy. But similar diagrams would be obtained in any other ML exercise where other methods for navigating on the flexibility axis might be used. Because the essential message of Figure 26 is universal across all machine learning tasks, I redraw that figure and annotate it generically (Figure 32).

Summarizing and emphasizing the main messages of this figure:

- Increasing the model flexibility leads to monotonous decrease of the empirical risk - because training data can be fitted better and better.
- Increasing the model flexibility from very low to very high will lead to a risk that first decreases (less and less underfitting) and then rises again (more and more overfitting).
- The best model flexibility is where the risk curve reaches its minimum. The problem is that the risk is defined on the distribution of "test" data which one does not have at training time.

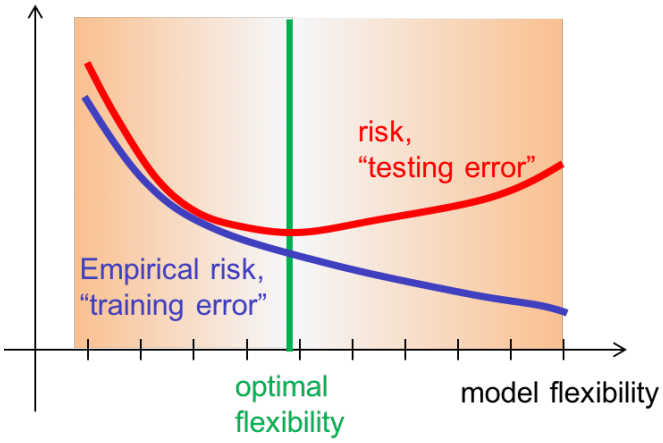

Figure 32: The generic, universal, core challenge of machine learning: finding the right model flexibility which gives the minimal risk.

There are many, quite different, ways of tuning flexibility of a learning algorithm (that is, an algorithm that solves the optimization problem (41)). Note that the word “flexibility” is only intuitive; how this is concretely formalized, implemented and measured differs between the methods of adjusting this “flexibility”. I proceed to outline the most common ones.

6.4.1 Tuning learning flexibility through model class size

In the Digits classification demo from Section 6.1, we tuned flexibility by changing the dimension of the PCA features. In the polynomial curve fitting demo in Section 6.2.1 we changed the order of polynomials. Let us re-consider these two examples to get a clearer picture:

- In the Digits example (Figure 26) we found that the number m of principal component features that were extracted from the raw image vectors was decisive for the testing error. When m was too small, the resulting models were too simple to distinguish properly between different digit image classes (underfitting). When m was too large, overfitting resulted. Fixing a particular m determines the class $\mathcal{H}$ of candidate decision functions within which the empirical risk (41) is minimized. Specifically, using a fixed m meant that the optimal decision function h_{opt} was selected from the set $\mathcal{H}_m$ which contains all decision functions which first extract m principal component features before carrying out the linear regression. It is clear that $\mathcal{H}_{m-1}$ is contained in $\mathcal{H}_m$, because decision functions that only combine the first $m-1$ principal component features into the hypothesis vector can be regarded as special cases of decision functions that combine m principal component features into the hypothesis vector, namely those whose linear combination weight for the m-th feature is zero.

- In the polynomial curve fitting example from Section 6.2.1, the model parameters were the monomial coefficients $w_0, \ldots, w_m$ (compare Equation 35). After fixing the polynomial order m, the optimal decision function $p(x)$ was selected from the set $\mathcal{H}_m = \{p : \mathbb{R} \to \mathbb{R} \,|\, p(x) = \sum_{j=0}^{m} w_j \, x^j\}$. Again it is clear that $\mathcal{H}_{m-1}$ is contained in $\mathcal{H}_m$.

A note on terminology: I use the words "decision function" and "model" as synonyms, meaning the (classification) algorithm h which results from a learning procedure. The word "decision function" is standard in theoretical statistics, the word "model" is more common in machine learning.

Generalizing from these two examples, we are now in a position to draw a precise picture of what it may mean to consider learning algorithms of "increasing flexibility". A *model class inclusion sequence* is a sequence $\mathcal{H}_1 \subset \mathcal{H}_2 \subset \ldots \subset \mathcal{H}_L$ of sets of candidate models. Since there are more candidate models in classes that appear later in the sequence, "higher" model classes have more possibilities to fit the training data, thus the optimal model within class $\mathcal{H}_{m+1}$ can achieve an empirical risk that is at least as low as the optimal model in class $\mathcal{H}_m$, — but gets you closer to overfitting.

There are many ways how one can set up a sequence of learning algorithms which pick their respective optimal models from such a model class inclusion sequence. In most cases – such as in our two examples – this will just mean to admit larger models with more tuneable parameters for "higher" classes.

From now on we assume that a class inclusion sequence $\mathcal{H}_1 \subset \ldots \subset \mathcal{H}_L$ is given. We furthermore assume we have a loss function L and are in possession of a learning algorithm which for every class $\mathcal{H}_m$ can solve the optimization problem of minimizing the empirical risk

$$h_{\text{opt } m} = \underset{h \in \mathcal{H}_m}{\text{argmin}} \;\; 1/N \sum_{i=1}^{N} L(h(x_i), y_i). \tag{42}$$

So... how can we find the best model class m_{opt} which gives us the best *risk* – note: *not* the best *empirical* risk? Or stated in more basic terms, which model class will give us the smallest expected test error? Expressed formally, how can we find

$$m_{\text{opt}} = \underset{m}{\text{argmin}} \;\; R(h_{\text{opt } m})? \tag{43}$$

6.4.2 Using regularization for tuning modeling flexibility

The flexibility tuning mechanism explained in this subsection is simple, practical, and in widespread use. It is called *model regularization*.

When one uses regularization to vary the modeling flexibility, one does not vary the model class $\mathcal{H}$ at all. Instead, one varies the optimization objective (41) for minimizing the training error.

The basic geometric intuition behind modeling flexibility is that low-flexibility models should be "smooth", "more linear", "flatter", admitting only "soft curvatures" in fitting data; whereas high-flexibility models can yield "peaky", "rugged", "sharply twisted" curves (see again Figures 28, 29, 30).

When one uses model regularization, one fixes a single model structure and size with a fixed number of trainable parameters, that is, one fixes $\mathcal{H}$. Structure and size of the considered model should be rich and large enough *to be able to overfit* (!) the available training data. Thus one can be sure that the "right" model is contained in the search space $\mathcal{H}$. For instance, in our evergreen digit classification task one would altogether dismiss the dimension reduction through PCA (which has the same effect as using the maximum number $m = 240$ of PC components) and directly use the raw picture vectors (padded by a constant 1 component to enable affine linear maps) as argument vectors for a training a linear regression decision function. Or, in polynomial curve-fitting, one would fix a polynomial order that clearly is too large for the expected kind of true curve.

The models in $\mathcal{H}$ are typically characterized by a set of trainable parameters. In our example of digit classification through linear regression from raw images, these trainable parameters are the elements of the regression weight matrix; in polynomial curve fitting these parameters are the monomial coefficients. Following the traditional notation in the machine learning literature we denote this collection of trainable parameters by θ. This is a vector that has as many components as there are trainable parameters in the chosen kind of model. We assume that we have M tuneable parameters, that is $\theta \in \mathbb{R}^M$.

Such a high-flexibility model type would inevitably lead to overfitting when an "optimal" model would be learnt using the basic learning equation (41) which I repeat here for convenience:

$$h_{\text{opt}} = \underset{h \in \mathcal{H}}{\text{argmin}} \ \ 1/N \ \sum_{i=1}^{N} L(h(x_i), y_i).$$

In order to dampen the exaggerated flexibility of this baseline learning algorithm, one adds a *regularization term* (also known as *penalty term*, or simply *regularizer*) to the loss function. A regularization term is a cost function $R : \mathbb{R}^M \to \mathbb{R}^{\geq 0}$ which penalizes model parameters θ that code models with a high degree of geometrical "wiggliness".

The learning algorithm then is constructed such that it solves, instead of (41), the regularized optimization problem

$$h_{\text{opt}} = \underset{h \in \mathcal{H}}{\text{argmin}} \ 1/N \ \sum_{i=1}^{N} L(h(x_i), y_i) + \alpha^2 \ R(\theta_h). \tag{44}$$

where θ_h is the collection of parameter values in the candidate model h.

The design of a useful penalty term is up to your ingenuity. A good penalty term should, of course, assign high penalty values to parameter vectors θ which

represent "wiggly" models; but furthermore it should be easy to compute and blend well with the algorithm used for empirical risk minimization.

Two examples of such regularizers:

1. In the polynomial fit task from Section 6.2.1 one might consider for $\mathcal{H}$ all 10th order polynomials, but penalize the "oscillations" seen in the right panel of Figure 28, that is, penalize such 10th order polynomials that exhibit strong oscillations. The degree of "oscillativity" can be measured, for instance, by the integral over the (square of the) second derivative of the polynomial p,

$$R(\theta) = R((w_0, \ldots, w_{10})) = \int_0^1 \left(\frac{d^2\, p(x)}{dx^2} \right)^2 dx.$$

   Investing a little calculus (good exercise! not too difficult), it can be seen that this integral resolves to a quadratic form $R(\theta) = \theta'\, C\, \theta$ where C is an 11×11 sized positive semi-definite matrix. That format is more convenient to use than the original integral version.

2. A popular regularizer that often works well is just the squared sum of all model parameters,

$$R(\theta) = \sum_{w \in \theta} w^2.$$

   This regularizer favors models with small absolute parameters, which often amounts to "geometrically soft" models. This regularizer is popular among other reasons because it supports simple algorithmic solutions for minimizing risk functions that contain it. It is called the *L_2-norm regularizer* because it measures the (squared) L_2-norm of the parameter vector θ.

Computing a solution to the minimization task (44) means to find a set of parameters which simultaneously minimizes the original risk and the penalty term. The factor α^2 in (44) controls how strongly one wishes the regularization to "soften" the solution. Increasing α means downregulating the model flexibility. For $\alpha^2 = 0$ one returns to the original un-regularized empirical risk (which would likely mean overfitting). For $\alpha^2 \to \infty$ the regularization term entirely dominates the model optimization and one gets a model which does not care anymore about the training data but instead only is tuned to have minimal regularization penalty. In case of the L_2 norm regularizer this means that all model parameters are zero – the ultimate wiggle-free model; one should indeed say the model is dead.

When regularization is used to steer the degree of model flexibility, the x-axis in Figure 32 would be labelled by α^2 (highest α^2 on the left, lowest at the right end of the x-axis).

Using regularizers to vary model flexibility is often computationally more convenient than using different model sizes, because one does not have to tamper with differently structured models. One selects a model type with a very large

(unregularized) flexibility, which typically means to select a big model with many parameters (maybe hundreds of thousands). Then all one has to do (and one *must* do it – it is a *most crucial* part of any professionally done machine learning project) is to find the optimal degree of flexibility which minimizes the risk. At this moment we don't know how to do that – the secret will be revealed later in this section.

I introduced the word "regularization" here for the specific flexibility-tuning method of adding a penalty term to the loss function. The same word is however often used in a generalized fashion to denote *any* method used for steering model flexibility.

6.4.3 Ridge regression

Let us briefly take a fresh look at linear regression, now in the light of general supervised learning and regularization. Linear regression should always be used in conjunction with regularization. Because this is such a helpful thing to know, I devote this separate subsection to this "trick". Recall from Section 3.1 that the learning task solved by linear regression is to find

$$\mathbf{w}_{\text{opt}} = \underset{\mathbf{w}\in\mathbb{R}^n}{\text{argmin}} \sum_{i=1}^{N} (\mathbf{w}\,\mathbf{x}_i - y_i)^2, \tag{45}$$

where $(\mathbf{x}_i, y_i)_{i=1,\ldots,N}$ is a set of training data with $\mathbf{x}_i \in \mathbb{R}^n, y_i \in \mathbb{R}$. Like any other supervised learning algorithm, linear regression may lead to overfitting solutions $\mathbf{w}_{\text{opt}}$. It is *always* advisable to control the flexibility of linear regression with an L_2 norm regularizer, that is, instead of solving (45) go for

$$\mathbf{w}_{\text{opt}} = \underset{\mathbf{w}\in\mathbb{R}^n}{\text{argmin}} \frac{1}{N} \sum_{i=1}^{N} (\mathbf{w}\,\mathbf{x}_i - y_i)^2 + \alpha^2 \|\mathbf{w}\|^2 \tag{46}$$

and find the best regularization coefficient α^2. The optimization problem (46) admits a closed-form solution, namely the *ridge regression* formula that we have already met in Equation 21. Rewriting it a little to make it match with the current general scenario, here it is again:

$$\mathbf{w}'_{\text{opt}} = (\frac{1}{N}\, X\, X' + \alpha^2\, I_{n\times n})^{-1}\, \frac{1}{N}\, X\, Y = (X\, X' + \alpha^2\, I_{n\times n})^{-1}\, X\, Y, \tag{47}$$

where $X = [x_1, \ldots, x_N]$ and $Y = (y_1, \ldots, y_N)'$.

In Section 3.1 I motivated to use the ridge regression formula because it warrants numerical stability. Now we see that a more fundamental reason to prefer ridge regression over the basic kind of regression (45) is that it implements L_2 norm regularization. The usefulness of ridge regression as an allround simple baseline tool for supervised learning tasks can hardly be overrated.

6.4.4 Tuning model flexibility through adding noise

Another way to tune model flexibility is to add noise. Noise can be added at different places. Here I discuss three scenarios.

Adding noise to the training input data. If we have a supervised training dataset $(\mathbf{x}_i, y_i)_{i=1,\dots,N}$ with vector patterns $\mathbf{x}_i$, one can enlarge the training dataset by adding more patterns obtained from the original patterns $(\mathbf{x}_i, y_i)_{i=1,\dots,N}$ by adding some noise vectors to each input pattern $\mathbf{x}_i$: for each $\mathbf{x}_i$, add l variants $\mathbf{x}_i + \nu_{i1}, \dots, \mathbf{x}_i + \nu_{il}$ of this pattern to the training data, where the ν_{ij} are i.i.d. random vectors (for instance, uniform or Gaussian noise). This increases the number of training patterns from N to $(l+1)N$. The more such noisy variants are added and the stronger the noise, the more difficult will it be for the learning algorithm to fit all data points, and the smoother the optimal solution becomes – that is, the more one steers to the left (underfitting) side of Figure 32. Adding noise to training patterns is a very common strategy.

Adding noise while the optimization algorithm runs. If the optimization algorithm used for minimizing the empirical risk is iterative, one can "noisify" it by jittering the intermediate results with additive noise. We have not seen an iterative algorithm in this course so far, therefore I cannot demonstrate this by example here. The "dropout regularization" trick which is widely used in deep learning is of this kind. The effect is that the stronger the algorithm is noisified, the stronger the regularization, that is the further one steers to the left end of Figure 32.

Use stochastic ensemble learning. We have seen this strategy in the presentation of random forests. A stochastic learning algorithm is repeatedly executed with different random seeds (called Θ in Section 2.7). The stronger the randomness of the stochastic learning algorithm, and the more members are included in the ensemble, the stronger the regularization effect.

6.5 Finding the right modeling flexibility by cross-validation

Statistical learning theory has come up with a few analytical methods to approximately solve (43). But these methods are based on additional assumptions which are neither easy to verify nor always granted. By far the most widely used method to determine an (almost) optimal model flexibility (that is, determine the position of the green line in Figure 32) is a rather simple scheme called *cross-validation*. Cross-validation is a generic method which does not need analytical insight into the particulars of the learning task at hand. Its main disadvantage is that it may be computationally expensive.

Here is the basic idea of cross-validation.

In order to determine whether a given model is under- or overfitting, one would need to run it on test data that are "new" and not contained in the training data. This would allow one to get a hold on the red curve in Figure 32.

However, at training time only the training data are available.

The idea of cross-validation is to artificially split the training data set $D = (x_i, y_i)_{i=1,\dots,N}$ into two subsets $T = (x_i, y_i)_{i \in I}$ and $V = (x'_i, y'_i)_{i \in I'}$. These two subsets are then pretended to be a "training" and a "testing" dataset. In the context of cross-validation, the second set is called a *validation* set.

A bit more formally, let the flexibility axis in Figure 32 be parametrized by m, where small m means "strong regularization", that is, "go left" on the flexibility axis. Let the range of m be $m = 1, \dots, L$.

For each setting of regularization strength m, the data in T is used to train an optimal model $h_{\text{opt}\,m}$. The test generalization performance on "new" data is then tested on the validation set, for each $m = 1, \dots, L$. It is determined which model $h_{\text{opt}\,m}$ performs best on the validation data. Its regularization strength m is then taken to be the sought solution m_{opt} to (43). After this screening of model classes for the best test performance, a model within the found optimal regularization strength is then finally trained on the original complete training data set D.

This whole procedure is called cross-validation. Notice that nothing has been said so far about how to split D into T and V. This is not a trivial question: how should D be best partitioned?

A clever way to answer this question is to split D into many subsets D_j of equal size ($j = 1, ..., K$). Then carry out K complete screening runs via cross validation, where in the j-th run the subset D_j is withheld as a validation set, and the remaining $K - 1$ sets joined together make for a training set. After these K runs, average the validation errors in order to find m_{opt}. This is called *K-fold cross-validation*. Here is the procedure in detail:

Given: A set $(x_i, y_i)_{i=1,\ldots,N}$ of training data, and a loss function L.

Also given: Some method which allows one to steer the model flexibility along a regularization strength parameter m. The weakest regularization should be weak enough to allow overfitting.

Step 1. Split the training data into K disjoint subsets $D_j = (x_i, y_i)_{i \in I_j}$ of roughly equal size $N' = N/K$.

Step 2. Repeat for $m = 1, \ldots, L$:

Step 2.1 Repeat for $j = 1, \ldots, K$:

Step 2.2.1 Designate D_j as validation set V_j and the union of the other $D_{j'}$ as training set T_j.

Step 2.2.1 Compute the model with minimal training error on T_j

$$h_{\mathrm{opt}\,m\,j} = \operatorname*{argmin}_{h \in \mathcal{H}_m} 1/|T_j| \sum_{(x_i, y_i) \in T_j} L(h(x_i), y_i),$$

where $\mathcal{H}_m$ is the model search space for the regularization strength m.

Step 2.2.2 Test $h_{\mathrm{opt}\,m\,j}$ on the current validation set V_j by computing the validation risk

$$R^{\mathrm{val}}_{m\,j} = 1/|V_j| \sum_{(x_i, y_i) \in V_j} L(h_{\mathrm{opt}\,m\,j}(x_i), y_i).$$

Step 2.2 Average the K validation risks $R^{\mathrm{val}}_{m\,j}$ obtained from the "folds" carried out for this m, obtaining

$$R^{\mathrm{val}}_m = 1/K \sum_{j=1,\ldots,K} R^{\mathrm{val}}_{m\,j}.$$

Step 3. Find the optimal class by looking for that m which minimizes the averaged validation risk:

$$m_{\mathrm{opt}} = \operatorname*{argmin}_m R^{\mathrm{val}}_m.$$

Step 4. Compute $h_{m_{\mathrm{opt}}}$ using the complete original training data set:

$$h_{m_{\mathrm{opt}}} = \operatorname*{argmin}_{h \in \mathcal{H}_{m_{\mathrm{opt}}}} 1/N \sum_{i=1,\ldots,N} L(h(x_i), y_i).$$

This procedure contains two nested loops and looks expensive. For economy, one starts with the low-end m and increases it stepwise, assessing the generalization quality through cross-validation for each regularization strength m, until the

validation risk starts to rise. The strength m_{opt} reached at that point is likely to be about the right one.

The best assessment of the optimal class is achieved when the original training data set is split into singleton subsets – that is, each D_j contains just a single training example. This is called *leave-one-out cross-validation*. It looks like a horribly expensive procedure, but yet it may be advisable when one has only a small training data set, which incurs a particularly large danger of ending up with poorly generalizing models when a wrong model flexibility was used.

K-fold cross validation is widely used – it is a factual standard procedure in supervised learning tasks when the computational cost of learning a model is affordable.

6.6 Why it is called the bias-variance dilemma

We have seen that a careful adjustment of the flexibility of a supervised learning algorithm is needed to find the sweet spot between underfitting and overfitting. A more educated way to express this condition is to speak of the *bias-variance tradeoff*, also known as *bias-variance dilemma*. In this subsection I want to unravel the root cause of the under/overfitting phenomenon in a little more mathematical detail. We will find that it can be explained in terms of a bias and a variance term in the expected error of estimated models.

Again I start from a training data set $(x_i, y_i)_{i=1,\dots,N}$ drawn from a joint distribution $P_{X,Y}$, with $x_i \in \mathbb{R}^n, y_i \in \mathbb{R}$. Based on these training data I consider the learning task to find a decision function $h : \mathbb{R}^n \to \mathbb{R}$ which has a low quadratic risk

$$R(h) = E_{X,Y}[(h(X) - Y)^2], \tag{48}$$

where the notation $E_{X,Y}$ indicates that the expectation is taken with respect to the joint distribution of X and Y. We assume that we are using some fixed learning algorithm $\mathcal{A}$ which, if it is given a training sample $(x_i, y_i)_{i=1,\dots,N}$, estimates a model $\hat{h}$. The learning algorithm $\mathcal{A}$ can be anything, good or bad, clever or stupid, overfitting or underfitting; it may be close to perfect or just be always returning the same model without taking the training sample into account – we don't make any assumptions about it.

The next consideration leads us to the heart of the matter, but it is not trivial. In mathematical terms, the learning algorithm $\mathcal{A}$ is just a *function* which takes a training sample $(x_i, y_i)_{i=1,\dots,N}$ as input and returns a model $\hat{h}$. Importantly, if we would run $\mathcal{A}$ repeatedly, but using freshly sampled training data $(x_i, y_i)_{i=1,\dots,N}$ in each run, then the returned models $\hat{h}$ would be varying from trial to trial – because the input samples $(x_i, y_i)_{i=1,\dots,N}$ are different in different trials. Applying these varying $\hat{h}$ to some fixed pattern $x \in \mathbb{R}^n$, the resulting values $\hat{h}(x)$ would show a random behavior too. The distribution of these variable values $\hat{h}(x)$ is a distribution over $\mathbb{R}$. This distribution is determined by the distribution $P_{X,Y}$ and the chosen learning algorithm $\mathcal{A}$ and the training sample size, and a good

statistician could give us a formal derivation of the distribution of $\hat{h}(x)$ from $P_{X,Y}$ and knowledge of $\mathcal{A}$, but we don't need that for our purposes here. The only insight that we need to take home at this point is that for a fixed x, $\hat{h}(x)$ is a random variable whose value is determined by the drawn training sample $(x_i, y_i)_{i=1,\ldots,N}$, and which has an expectation which we write as $E_{\mathsf{retrain}}[\hat{h}(x)]$ to indicate that the expectation is taken over all possible training runs with freshly drawn training data.

Understanding this point is the key to understanding the inner nature of under/overfitting.

If you feel that you have made friends with this $E_{\mathsf{retrain}}[\hat{h}(x)]$ object, we can proceed. The rest is easy compared to this first conceptual clarification.

Without proof I note the following, intuitively plausible fact. Among *all* decision functions (from any candidate space $\mathcal{H}$), the quadratic risk (48) is minimized by the function

$$\Delta(x) = E_{Y|X=x}[Y], \tag{49}$$

that is, by the expectation of Y given x. This function $\Delta : \mathbb{R}^n \to \mathbb{R}, x \mapsto E[Y|X = x]$ is the gold standard for minimizing the quadratic risk; no learning algorithm can give a better result than this. Unfortunately, of course, Δ remains unknown because the underlying true distribution $P_{X,Y}$ cannot be exactly known.

Now fix some x and ask by how much $\hat{h}(x)$ deviates, on average and in the squared error sense, from the optimal value $\Delta(x)$. This expected squared error is

$$E_{\mathsf{retrain}}[(\hat{h}(x) - \Delta(x))^2].$$

We can learn more about this error if we re-write $(\hat{h}(x) - \Delta(x))^2$ as follows:

$$\begin{aligned}(\hat{h}(x) - \Delta(x))^2 &= (\hat{h}(x) - E_{\mathsf{retrain}}[\hat{h}(x)] + E_{\mathsf{retrain}}[\hat{h}(x)] - \Delta(x))^2 \\ &= (\hat{h}(x) - E_{\mathsf{retrain}}[\hat{h}(x)])^2 + (E_{\mathsf{retrain}}[\hat{h}(x)] - \Delta(x))^2 \\ &\quad +2\,(\hat{h}(x) - E_{\mathsf{retrain}}[\hat{h}(x)])\,(E_{\mathsf{retrain}}[\hat{h}(x)] - \Delta(x)).\end{aligned} \tag{50}$$

Now observe that

$$E_{\mathsf{retrain}}\left[(\hat{h}(x) - E_{\mathsf{retrain}}[\hat{h}(x)])\,(E_{\mathsf{retrain}}[\hat{h}(x)] - \Delta(x))\right] = 0, \tag{51}$$

because the second factor $(E_{\mathsf{retrain}}[\hat{h}(x)] - \Delta(x))$ is a constant, hence

$$\begin{aligned}&E_{\mathsf{retrain}}\left[(\hat{h}(x) - E_{\mathsf{retrain}}[\hat{h}(x)])\,(E_{\mathsf{retrain}}[\hat{h}(x)] - \Delta(x))\right] = \\ &= E\left[\hat{h}(x) - E_{\mathsf{retrain}}[\hat{h}(x)]\right]\,(E_{\mathsf{retrain}}[\hat{h}(x)] - \Delta(x)),\end{aligned}$$

and

$$\begin{aligned}E_{\mathsf{retrain}}\left[\hat{h}(x) - E_{\mathsf{retrain}}[\hat{h}(x)]\right] &= E_{\mathsf{retrain}}[\hat{h}(x)] - E_{\mathsf{retrain}}[E_{\mathsf{retrain}}[\hat{h}(x)]] \\ &= E_{\mathsf{retrain}}[\hat{h}(x)] - E_{\mathsf{retrain}}[\hat{h}(x)] \\ &= 0.\end{aligned}$$

Inserting (51) into (50) and taking the expectation on both sides of (50) of finally gives us

$$E_{\mathsf{retrain}}[(\hat{h}(x) - \Delta(x))^2] = \\ = \underbrace{\left(E_{\mathsf{retrain}}[\hat{h}(x)] - \Delta(x)\right)^2}_{\text{(squared) bias}} + \underbrace{E_{\mathsf{retrain}}\left[\left(\hat{h}(x) - E_{\mathsf{retrain}}[\hat{h}(x)]\right)^2\right]}_{\text{variance}}. \tag{52}$$

The two components of this error are conventionally named the *bias* and the *variance* contribution to the expected squared mismatch $E_{\mathsf{retrain}}[(\hat{h}(x)-\Delta(x))^2]$ between the learnt-model decision values $\hat{h}(x)$ and the optimal decision value $\Delta(x)$. The bias measures how strongly the average learning result deviates from the optimal value; thus it indicates a systematic error component. The variance measures how strongly the learning results $\hat{h}(x)$ vary around their expected value $E_{\mathsf{retrain}}[\hat{h}(x)]$; this is an indication of how strongly the particular training data sets induce variations on the learning result.

When the model flexibility is too low (underfitting), the bias term dominates the expected modeling error; when the flexibility is too high (overfitting), the variance term is the main source of mismatch. This is why the underfitting versus overfitting challenge is also called the bias-variance tradeoff (or dilemma).

7 Representing and learning distributions

Almost all machine learning tasks are based on training data that have some random component. Having completely noise-free data from deterministic sources observed with high-precision measurements is a rare exception. Thus, machine learning algorithms are almost all designed to cope with stochastic data. Their ultimate functionality (classification, prediction, control, ...) will be served well or poorly to the extent that the probability distribution of the training data has been properly accounted for. We have seen this in the previous section. If one (wrongly) believes that there is little randomness in the training data, one will take the given training points as almost correct – and end up with an overfitted model. Conversely, if one (wrongly) thinks the training data are almost completely "white noise randomness", the learnt model will under-exploit the information in the training data and underfit. Altogether it is fair to say that machine learning is the art of probability distribution modeling (plus subsequent use of that learnt distribution for classification etc.)

In many machine learning algorithms, the distribution model remains implicit – there is no place or data structure in the algorithm which explicitly models the data distribution. In some algorithms however, and for some tasks, the probability distribution of the training data is explicitly modeled. We will encounter some of these algorithms later in this course (hidden Markov models, Bayesian networks, Boltzmann machines are of that kind). At any rate, it is part of the standard knowledge of a machine learning professional to know some ways to represent probability distributions and to estimate these representations from data.

7.1 Optimal classification

The grand role which is played by modeling a data distribution accurately can be demonstrated very nicely in classification learning. We have met this basic task several times now – and in your professional future you will meet it again, dozens of times if you will seriously work in machine learning. We consider again a scenario where the input patterns are vectors $\mathbf{x} \in \mathbf{P} \subseteq \mathbb{R}^n$, which belong to one of k classes which we represent by their class labels $C = \{c_1, \ldots, c_k\}$. The set $\mathbf{P}$ is the "possible pattern space", usually a bounded subset of $\mathbb{R}^n$ (for instance, when the patterns $\mathbf{x}$ are photographic pixel vectors and the pixel color values are normalized to a range between 0 and 1, $\mathbf{P}$ would be the n-dimensional unit hypercube). We furthermore introduce a random variable (RV) X for the patterns and a RV Y for the class labels.

Many different decision functions $h : \mathbf{P} \to C$ exist, some of which can be learnt from training data using some known learning algorithm. We will not deal with the learning problem in this subsection, but ask (and answer!) the fundamental question:

Among all possible decision functions $h : \mathbf{P} \to C$, which one has the lowest risk in the sense of giving the lowest possible rate of misclassifications on test

data? Or, expressing the same question in terms of a loss function, which decision function minimizes the risk connected to the counting loss

$$L(y, c) = \begin{cases} 1 & \text{if } y \neq c, \\ 0 & \text{if } y = c? \end{cases}$$

It turns out that the minimal-risk decision function is in fact well-defined and unique, and it can (and must) be expressed in terms of the distribution of our data-generating RVs X and Y.

Our starting point is the true joint distribution $P_{X,Y}$ of patterns and labels. This joint distribution is given by all the probabilities of the kind

$$P(X \in A, Y = c), \tag{53}$$

where A is some subvolume of $\mathbf{P}$ and $c \in \mathbf{C}$. The subvolumes A can be n-dimensional hypercubes within $\mathbf{P}$, but they also can be arbitrarily shaped "volume bodies", for instance balls or donuts or whatever. Note that the probabilities $P(X \in A, Y = c)$ are numbers between 0 and 1, while the distribution $P_{X,Y}$ is the *function* which assigns to every choice of $A \subseteq \mathbf{P}, c \in C$ the number $P(X \in A, Y = c)$ (probability theory gives us a rigorous formal way to define and handle this strange object, $P_{X,Y}$, which I will explain in depth, step by step, in the tutorial.)

The joint distribution $P_{X,Y}$ is the "ground truth" – it is the real-world statistical distribution of pattern-label pairs of the kind we are interested in. In the Digits example, it would be the distribution of pairs made of (i) a handwritten digit and (ii) a human-expert provided class label. Test digit images and their class labels would be randomly "drawn" from this distribution.

A decision function $h : \mathbf{P} \to \{c_1, \ldots, c_k\}$ partitions the pattern space $\mathbf{P}$ into k disjoint *decision regions* $R_1, \ldots, R_k$ by

$$R_i = \{\mathbf{x} \in \mathbf{P} \,|\, h(\mathbf{x}) = c_i\}. \tag{54}$$

A test pattern $\mathbf{x}^{\text{test}}$ is classified by h as class i if and only if it falls into the decision region R_i.

Now we are prepared to analyze and answer our ambitious question, namely which decision functions yield the lowest possible rate of misclassifications. Since two decision functions yield identical classifications if and only if their decision regions are the same, we will focus our attention on these regions and reformulate our question: which decision regions yield the lowest rate of misclassifications, or expressed in its mirror version, which decision regions give the highest probability of correct classifications?

Let f_i be the pdf for the conditional distribution $P_{X \,|\, Y=c_i}$. It is called the *class-conditional* distribution.

The probability to obtain a correct classification for a random test pattern, when the decision regions are R_i, is equal to $\sum_{i=1}^{k} P(X \in R_i, Y = c_i)$. Rewriting this expression using the pdfs of the class conditional distributions gives

$$
\begin{aligned}
&\sum_{i=1}^{k} P(X \in R_i, Y = c_i) = \\
&\quad = \sum_{i=1}^{k} P(X \in R_i \,|\, Y = c_i)\, P(Y = c_i) \\
&\quad = \sum_{i=1}^{k} P(Y = c_i) \int_{R_i} f_i(\mathbf{x})\, d\mathbf{x} \\
&\quad = \sum_{i=1}^{k} \int_{R_i} P(Y = c_i)\, f_i(\mathbf{x})\, d\mathbf{x}. \qquad (55)
\end{aligned}
$$

Note that the integral is taken over a region that possibly has curved boundaries, and the integration variable $\mathbf{x}$ is a vector. The boundaries between the decision regions are called *decision boundaries*. For patterns $\mathbf{x}$ that lie exactly on such boundaries, two or more classifications are equally probable. For instance, the digit pattern shown in the last but third column in the second row in Figure 15 would likely be classified by humans as a "1" or "4" class pattern with roughly the same probability; this pattern would lie close to a decision boundary.

The expression (55) obviously becomes maximal if the decision regions are given by

$$
R_i = \{\mathbf{x} \in \mathbf{P} \,|\, i = \operatorname*{argmax}_j P(Y = c_j)\, f_j(\mathbf{x})\}. \qquad (56)
$$

Thus we have found the decision function which is optimal in the sense that it maximizes the probability of correct classifications: namely

$$
h_{\text{opt}} : \mathbf{P} \to C,\ \mathbf{x} \mapsto c_{\operatorname{argmax}_j P(Y=c_j)\, f_j(\mathbf{x})}. \qquad (57)
$$

A learning algorithm that finds the optimal decision function (or some function approximating it) *must* learn (implicitly or explicitly) estimates of the the class-conditional distributions $P_{X \,|\, Y=c_i}$ and the class probabilities $P(Y = c_i)$.

The class probabilities are also called the class *priors*. Figure 33 visualizes optimal decision regions and decision boundaries. In higher dimensions, the geometric shapes of decision regions can become exceedingly complex, fragmented and "folded into one another" — disentangling them during a learning process is one of the eternal challenges of ML.

7.2 Representing and learning distributions

The optimal classifier described in the previous subsection is optimal because it is shaped along the true distribution of pattern and class label random variables.

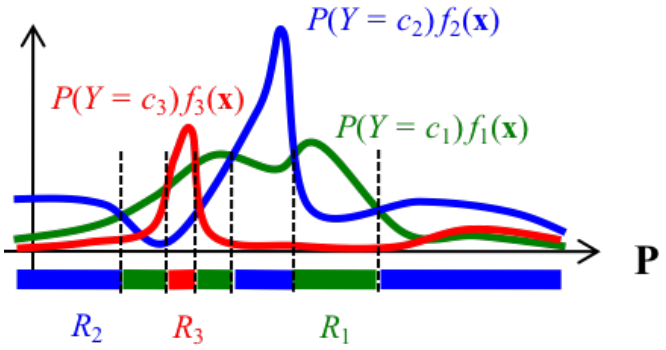

Figure 33: Optimal decision regions R_i. A case with a one-dimensional pattern space $\mathbf{P}$ and $k = 3$ classes is shown. Broken lines indicate decision boundaries. Decision regions need not be connected!

Quite generally, *any* machine learning task can be solved "optimally" (in terms of minimizing some risk) only if the solution takes the true distribution of all task-relevant RVs into account. As I mentioned before, many learning algorithms estimate a model of the underlying data distribution only implicitly. But some ML algorithms generate explicit models of probability distributions, and in the wider fields of statistical modeling, explicit models of probability distributions are often the final modeling target.

Representing a probability distribution in mathematical formalism or by an algorithm is not always easy. Real-world probability distributions can be utterly complex and high-dimensional objects which one cannot just "write down" in a formula. Over the last 60 or so years, ML and statistics research has developed a wide range of formalisms and algorithms for representing and estimating ("learning") probability distributions. A machine learning professional should know about some basic kinds of such formalisms and algorithms. In this section I present a choice, ranging from elementary to supremely complex, powerful — and computationally costly.

7.2.1 Some classical probability distributions

In this section we describe a few distributions which arise commonly in application scenarios. They have standard names and one should just know them, and under which conditions they arise.

We start with distributions that are defined over discrete sample spaces $S = \{s_1, \ldots, s_k\}$ (finite sample space) or $S = \{s_1, s_2, s_3 \ldots\}$ (countable infinite sample space). These distributions can all be represented by their *probability mass function* (pmf):

Definition 7.1 *Given a discrete sample space S (finite or countable infinite), a* probability mass function *on S is a function $p : S \to [0, 1]$ whose total mass is 1,*

that is, which satisfies $\sum_{s\in S} p(s) = 1$.

Bernoulli distribution. The Bernoulli distribution arises when one deals with observations that have only two possible outcomes, like tail – head, female – male, pass – fail, 0 – 1. This means a two-element sample space $S = \{s_1, s_2\}$ equipped with the power set σ-field, on which a Bernoulli distribution is defined by its pmf, which in this case has its own standard terminology:

Definition 7.2 *The distribution of a random variable which takes values in* $S = \{s_1, s_2\}$ *with probability mass function*

$$p(s_i) = \begin{cases} 1-q & \text{for } i = 1 \\ q & \text{for } i = 2 \end{cases}$$

is called a Bernoulli distribution *with* success parameter q, *where* $0 \le q \le 1$.

A Bernoulli distribution is thus specified by a single parameter, q.
Learning / estimation: Given a set of training data $\{x_1, \ldots, x_N\}$ where $x_i \in \{s_1, s_2\}$, the parameter q can be estimated by $\hat{q} = (1/N)\,|\{i \,|\, x_i = s_2\}|$.

Binomial distribution. The binomial distribution describes the counts of successes if a binary-outcome "Bernoulli Experiment" is repeated N times. For a simple example, consider a gamble where you toss a coin N times, and every time the head comes up, you earn a Dollar (not Euro; gambling is done in Las Vegas). What is the distribution of Dollar earnings from such N-repetition games, if the coin comes up with head ($= s_2$; outcome tail is s_1) with a success probability of q? Clearly the range of possible earnings goes from 0 to N Dollars. These earnings are distributed according to the *binomial distribution*:

Definition 7.3 *Let* N *be the number of trials of independent Bernoulli experiments with success probability* q *in each trial. The distribution of the number of successes is called the* binomial distribution *with parameters* N *and* q *and its pmf is given by*

$$p(s) = \binom{N}{s} q^s (1-q)^{N-s} = \frac{N!}{s!\,(N-s)!} q^s (1-q)^{N-s}, \quad s = 0, 1, 2, ..., N.$$

We write $Bi(N, q)$ *to denote the binomial distribution with parameters* N *and* q.

The factor $\binom{N}{s}$ is called *binomial coefficient*. Figure 34 shows some binomial pmf's.

A note on notation: it is customary to write

$$X \sim Bi(10, 0.25)$$

as a shorthand for the statement "X is distributed according to $Bi(10, 0.25)$".
Learning / estimation: Depends on the format of available training data. In most cases the data will be of the same form as in the Bernoulli distribution, which gives rise to an estimate $\hat{q}$ of the success parameter. The number N of repetitions will usually be given by the context in which the modeling task arises and need not be estimated.

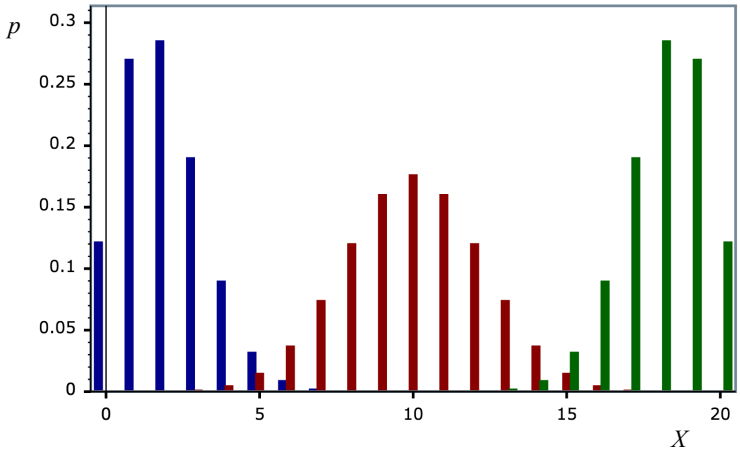

Figure 34: The pmf's of $Bi(20, 0.1)$ (blue), $Bi(20, 0.5)$ (red), and $Bi(20, 0.9)$ (green). Figure taken from `www.boost.org`.

Poisson distribution. This distribution is defined for $S = \{0, 1, 2, \ldots\}$. $p(s)$ is the probability that a particular kind of event occurs k times within a given time interval. Examples (except the last one taken from `https://en.wikipedia.org/wiki/Poisson_distribution`): $p(k)$ might be the probability that

- k meteorites impact on the earth within 100 years,
- a call center receives k calls in an hour,
- a block of uranium emits k alpha particles in a second,
- k patients arrive in an emergency ward between 10 and 11 pm,
- a piece of brain tissue sends s neural spike signals within a second.

Similarly, instead of referring to a time interval, k may count spatially or otherwise circumscribed events, for instance

- the number of dust particles found in a milliliter of air,
- the number of diamonds found in a ton of ore.

The expected number of events $E[X]$ is called the *rate* of the Poisson distribution, and is commonly denoted by λ. The pmf of a Poisson distribution with rate λ is given by

$$p(k) = \frac{\lambda^k \, e^{-\lambda}}{k!}. \tag{58}$$

Figure 35 depicts the pmf's for three different rates.

Learning / estimation: For concreteness consider the call center example. Training data would be N 1-hour protocols of incoming calls, where n_i $(i =$

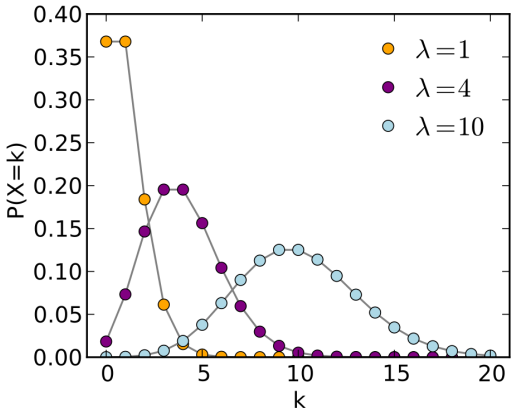

Figure 35: The pmf of the Poisson distribution for various values of the parameter λ. The connecting lines bewteen the dots are drawn only for better visual appearance (image source: `https://commons.wikimedia.org/wiki/File:Poisson_pmf.svg`).

$1, \ldots, N$) is the number of calls received in the respective hour. Then λ is estimated by $\hat{\lambda} = (1/N) \sum_i n_i$.

We continue with a few distributions on continuous sample spaces ($\mathbb{R}^n$ or subsets thereof). These distributions are most often characterized by their *probability density functions* (pdf's).

Definition 7.4 *Let X be a RV which takes values in $S \subseteq \mathbb{R}^n$. A pdf for the distribution of X is a function $f : S \to \mathbb{R}^{\geq 0}$ which satisfies the following condition: For every subvolume $A \subseteq S$ of S, the probability $P(X \in A)$ that X gives a value in A is equal to*

$$P(X \in A) = \int_A f(\mathbf{x}) d\mathbf{x}. \tag{59}$$

Point distributions. There exist continuous-valued distributions for which a description through a pdf is impossible. One kind of such "non-pdf-able" continuous distributions occurs quite often: *point distributions*. Here, the probability mass is concentrated in a few (finitely many or countably infinitely many) points in $\mathbb{R}^n$. The simplest point distribution is defined on the real line $S = \mathbb{R}$ and has the defining property that for any subset $A \subseteq \mathbb{R}$ it holds that

$$P(X \in A) = \begin{cases} 1 & \text{if } 0 \in A \\ 0 & \text{if } 0 \notin A. \end{cases}$$

There are several ways to write down such a distribution in mathematical formalism. In the machine learning literature (and throughout the natural sciences,

especially physics), the above point distribution would be represented by a weird kind of pdf-like function, called the *Dirac delta function* δ (the Wikipedia article `https://en.wikipedia.org/wiki/Dirac_delta_function` is recommendable if you want to understand this function better). The Dirac delta function is used inside an integral just like a normal pdf is used in (59). Thus, for a subset $A \subseteq \mathbb{R}$ one has

$$P(X \in A) = \int_A \delta(x)\, dx.$$

The Dirac delta is also used in $\mathbb{R}^n$, where likewise it is a "pdf" which describes a probability distribution concentrated in a single point, the origin.

If one wants to have a multi-point distribution one can combine Dirac deltas. For example, if you want to create a probability measure on the real line that places a probability of 1/2 on the point 1.0, and probabilities 1/4 each on the points 2.0 and 3.0, you can do this by a linear combination of shifted Dirac deltas:

$$P(X \in A) = \int_A 1/2\ \delta(x-1) + 1/4\ \delta(x-2) + 1/4\ \delta(x-3)\, dx.$$

Point distributions arise frequently in Bayesian machine learning, where they are needed to express and compute certain "hyperdistributions". We will meet them later in this course.

We now take a look at a small choice of common continuous distributions which can be characterized by pdfs.

The uniform distribution. We don't need to make a big fuzz about this. If $I = [a_1, b_1] \times \ldots \times [a_n, b_n]$ is a n-dimensional interval in $\mathbb{R}^n$, the uniform distribution on I is given by the pdf

$$p(x) = \begin{cases} \frac{1}{(b_1-a_1)\cdot\ldots\cdot(b_n-a_n)} & \text{if } x \in I \\ 0 & \text{if } x \notin I. \end{cases} \tag{60}$$

Learning / estimation: This distribution is not normally "learnt". There is also nothing about it that could be learnt: the uniform distribution has no "shape" that would be specified by learnable parameters.

The exponential distribution. This distribution is defined for $S = [0, \infty)$ and could be paraphrased as "the distribution of waiting times until the next of these things happens". Consider any of the kinds of temporal events listed for the Poisson distribution, for instance the event "meteorite hits earth". The exponential distribution characterizes how long you have to wait for the next impact, given that one impact has just happened. Like in the Poisson distribution, such random event processes have an average *rate* events / unit reference time interval. For instance, meteorites of a certain minimum size hit the earth with a rate of 2.34 per year

(just guessing). This rate is again denoted by λ. The pdf of the exponential distribution is given by

$$p(x) = \lambda\, e^{-\lambda x} \quad \text{(note that } x \geq 0\text{)}. \tag{61}$$

It is (almost) self-explaining that the expectation of an exponential distribution is the reciprocal of the rate, $E(X) = 1/\lambda$. Figure 36 shows pdf's for some rates λ.

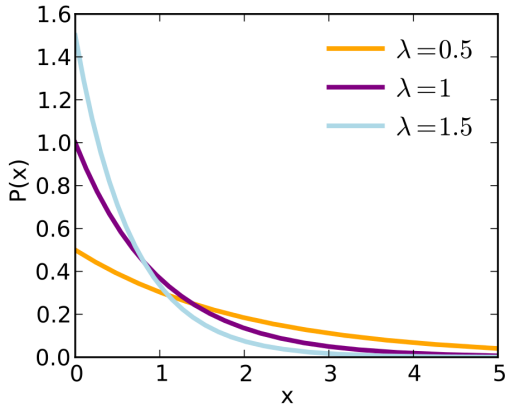

Figure 36: The pdf of the exponential distribution for various values of the parameter λ (image source: `https://commons.wikimedia.org/wiki/File:Exponential_pdf.svg`).

The exponential distribution plays a big role in spiking neural networks (SNNs). Biological neurons communicate with each other by sending short "point-like" electrical pulses, called *spikes*. Many people believe that Nature invented communication by spikes to let the brain save energy – your head shouldn't perceptibly warm up (like your PC does) when you do a hefty thinking job! For the same reason, microchip engineers have teamed up with deep learning researchers to design novel kinds of microchips for deep learning applications. These microchips contain neuron-like processing elements which communicate with each other by spikes. IBM and Intel have actually built such chips (check out "IBM TrueNorth" and "Intel Loihi") if you want to learn more). Research about artificial SNNs for machine learning applications goes hand in hand with research in neuroscience. In both domains, one often uses models based on the assumption that the temporal pattern in a spike sequence sent by a neuron is a stochastic process called a *Poisson process*. In a Poisson process, the waiting times between two consecutive spikes are exponentially distributed. Recordings from real biological neurons often show a temporal randomness of spikes that can be almost perfectly modeled by a Poisson process.

Learning / estimation: The rate λ is the only parameter characterizing an exponential distribution. Training data: a sequence $t_1, t_2, \ldots, t_N$ of time points where the event in question was observed. Then the rate can be estimated by $\hat{\lambda} = (1/(N-1)) \sum_{i=1,\ldots,N-1} t_{i+1} - t_i$.

The one-dimensional normal distribution. Enter the queen of distributions! Bow in reverence! I am sure you know her from the media and facebook... For royal garments, as everybody knows, she wears the pdf

$$p(x) = \frac{1}{\sqrt{2\pi}\sigma} e^{-\frac{(x-\mu)^2}{2\sigma^2}}, \tag{62}$$

which is fully specified by its mean μ and standard deviation (square root of variance) σ, has the famous bell shape with μ being the location of the maximum and $\mu \pm \sigma$ being the locations of the zeros of the second derivative (Fig. 37).

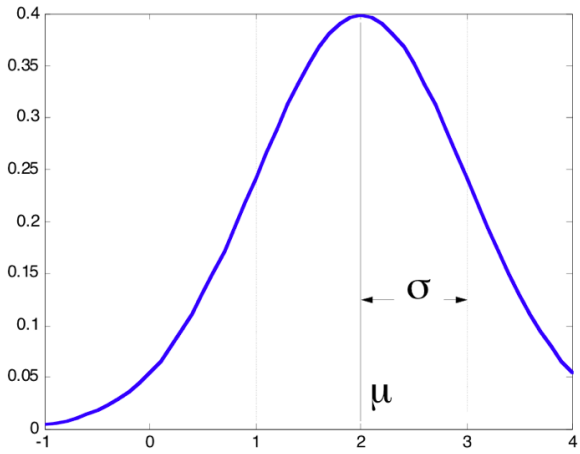

Figure 37: pdf of a normal distribution with mean 2 and standard deviation 1.

The normal distribution with mean μ and variance σ^2 is denoted by $\mathcal{N}(\mu, \sigma^2)$. The normal distribution with zero mean and unit variance, $\mathcal{N}(0, 1)$, is called the *standard normal distribution*. The normal distribution is also called *Gaussian distribution* or simply *Gaussian*.

The normal distribution has a number of nice properties that very much facilitate calculations and theory. Specifically, linear combinations of normal distributed, independent normal RVs are again normal distributed:

Proposition 7.1 *Let $X, Y : \Omega \to \mathbb{R}$ be two independent, normally distributed RVs with means μ and ν and variances σ^2 and τ^2. Then the weighted sum $a\,X + b\,Y$ is normally distributed with mean $a\,\mu + b\,\nu$ and variance $a^2\,\sigma^2 + b^2\,\tau^2$.*

The majestic power of the normal distribution, which makes her reign almost universally over almost all natural phenomena, comes from one of the most central theorems of probability theory, the *central limit theorem*. It is stated in textbooks in a variety of (not always exactly equivalent) versions. It says, in brief, that one gets the normal distribution whenever random effects of many independent small-sized causes sum up to large-scale observable effects. The following definition — which I do not expect you to fully understand (which would need a substantial

training in probability theory), but you should at least have seen it — makes this precise:

Definition 7.5 *Let $(X_i)_{i\in\mathbb{N}}$ be a sequence of independent, real-valued, square integrable random variables with nonzero variances $Var(X_i) = E[(X_i - E[X_i])^2]$. Then we say that* the central limit theorem holds for $(X_i)_{i\in\mathbb{N}}$ *if the distributions P_{S_n} of the standardized sum variables*

$$S_n = \frac{\sum_{i=1}^n (X_i - E[X_i])}{\sigma\left(\sum_{i=1}^n X_i\right)} \tag{63}$$

converges weakly to $\mathcal{N}(0,1)$.

Explanations:

- A real-valued random variable with pdf p is *square integrable* if its [uncentered] second moment, that is the integral $E[X^2] = \int_{\mathbb{R}} x^2\, p(x)dx$ is finite.
- If $(P_n)_{n\in\mathbb{N}}$ is a sequence of distributions over $\mathbb{R}$, and P a distribution (all over the same measure space $(\mathbb{R}, \mathcal{B})$), then $(P_n)_{n\in\mathbb{N}}$ is said to *converge weakly* to P if
$$\lim_{n\to\infty} \int f(x)\, P_n(dx) = \int f(x) P(dx) \tag{64}$$
for all continuous, bounded functions $f : \mathbb{R} \to \mathbb{R}$. You will find the notation of these integrals unfamiliar, and indeed you see here cases of *Lebesgue integrals* – a far-reaching generalization of the *Riemann integrals* that you know. Lebesgue integrals can deal with a far greater range of functions than the Riemann integral. Mathematical probability theory is formulated exclusively with the Lebesgue integral. We cannot give an introduction to Lebesgue integration theory in this course. Therefore, simply ignore the precise meaning of "weak convergence" and take home that sequences of distributions are required to converge to a target distribution in some subtly defined way.

A sequence $(X_i)_{i\in\mathbb{N}}$ of random variables (or, equivalently, its associated sequence of distribution $(P_{X_i})_{i\in\mathbb{N}}$) obeys the central limit theorem under rather weak conditions – or in other words, for many such sequences the central limit theorem holds.

A simple, important class of (X_i) for which the central limit theorem holds is obtained when the X_i are identically distributed (and, of course, are independent, square integrable and have nonzero variance). Notice that regardless of the shape of the distribution of each X_i, the distribution of the normalized sums converges to $\mathcal{N}(0,1)$!

The classical demonstration of the central limit theorem is the *Galton board*, named after Sir Francis Galton (1822–1911), an English multi-scientist. The idea

is to let little balls (or beans, hence this device is sometimes called "bean machine") trickle down a grid of obstacles which randomly deflect the ball left or right (Figure 38). It does not matter how, exactly, these deflections act — in the simplest case, the ball is just kicked right or left by one space grid unit with equal probability. The deeper the trickling grid, the closer will the resulting distribution be to a normal distribution. A nice video can be watched at `https://www.youtube.com/watch?v=PM7z_03o_kk`.

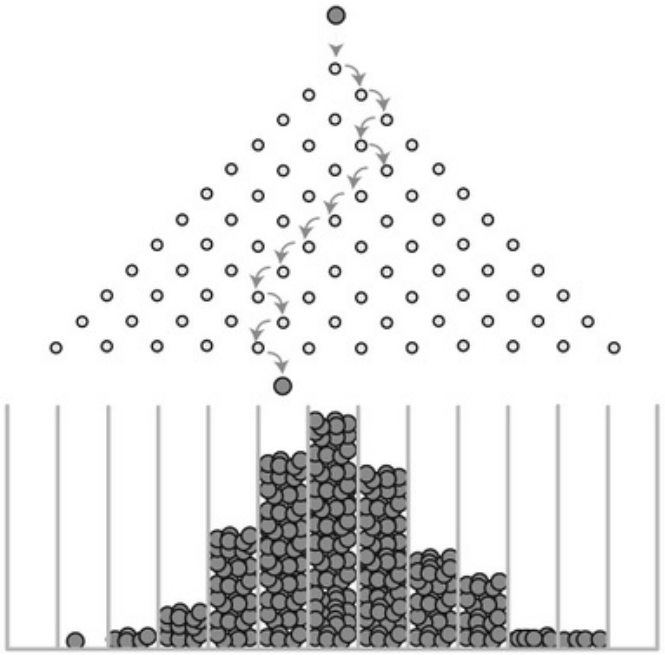

Figure 38: The Dalton board. Compare text for explanation. Figure taken from `https://janav.wordpress.com/2013/09/26/power-law/`.

However, this simple case does not explain the far-reaching, general importance of the central limit theorem (rather, property). In textbooks one often finds statements like, "if the outcomes of some measurement procedure can be conceived to be the combined effect of many independent causal effects, then the outcomes will be approximately normal distributed". The "many independent causal effects" that are here referred to are the random variables (X_i); they will typically not be identically distributed at all. Still the central limit theorem holds under mild assumptions. Intuitively, all that one has to require is that none of the individual random variables X_i dominates all the others – the effects of any single X_i must asymptotically be "washed out" if an increasing number of other $X_{i'}$ is entered into the sum variable S_n. In mathematical textbooks on probability you may find numerous mathematical conditions which amount to this "washing out". A special case that captures many real-life cases is the condition that the X_i are uniformly bounded, that is, there exists some $b > 0$ such that $|X_i(\omega)| < b$ for all i and ω. However, there exist much more general (nontrivial to state) conditions that like-

wise imply the central limit theorem. For our purposes, a good enough take-home message is

if (X_i) is a halfway reasonably behaved sequence of numerical RV's, then the normalized sums converge to the standard normal distribution.

The normal distribution plays an overwhelming role in applied statistics. One often has to actually compute integrals of the pdf (62):

Task: compute the numerical value of $\int_a^b \frac{1}{\sqrt{2\pi}\sigma} e^{-\frac{(x-\mu)^2}{2\sigma^2}} dx$.

There is no closed-form solution formula for this task. Instead, the solution is found in a two-step procedure:

1. Transform the problem from its original version $\mathcal{N}(\mu, \sigma^2)$ to the standard normal distribution $\mathcal{N}(0, 1)$, by using

$$\int_a^b \frac{1}{\sqrt{2\pi}\sigma} e^{-\frac{(x-\mu)^2}{2\sigma^2}} dx = \int_{\frac{a-\mu}{\sigma}}^{\frac{b-\mu}{\sigma}} \frac{1}{\sqrt{2\pi}} e^{-\frac{(x)^2}{2}} dx. \tag{65}$$

   In terms of probability theory, this means to transform the original, $\mathcal{N}(\mu, \sigma^2)$-distributed RV X to a $\mathcal{N}(0, 1)$-distributed variable $Z = (X - \mu)/\sigma$. (The symbol Z is often used in statistics for standard normal distributed RVs.).

2. Compute the numerical value of the r.h.s. in (65) by using the cumulative density function of $\mathcal{N}(0, 1)$, which is commonly denoted by Φ:

$$\int_{\frac{a-\mu}{\sigma}}^{\frac{b-\mu}{\sigma}} \frac{1}{\sqrt{2\pi}} e^{-\frac{(x)^2}{2}} dx = \Phi(\frac{b-\mu}{\sigma}) - \Phi(\frac{a-\mu}{\sigma}).$$

   Since there is no closed-form solution for calculating Φ, in former times statisticians found the solution in books where Φ was tabulated. Today, statistics software packages call fast iterative solvers for Φ.

Learning / estimation: The one-dimensional normal distribution is characterized by two parameters, μ and σ^2. Given a dataset $(x_i)_{i=1,\ldots,N}$ of points in $\mathbb{R}$, the estimation formulas for these two parameters are

$$\begin{aligned} \hat{\mu} &= \frac{1}{N} \sum_i x_i, \\ \hat{\sigma}^2 &= \frac{1}{N-1} \sum_i (x_i - \hat{\mu})^2. \end{aligned}$$

The n–dimensional normal distribution. If data points are not just real numbers but vectors $\mathbf{x} = (x_1, \ldots, x_n)' \in \mathbb{R}^n$, whose component RVs X_i which give the vector components x_i fulfill the central limit theorem, the joint distribution of the RVs $X_1, \ldots, X_n$ is the multidimensional normal distribution which has the pdf

$$p(\mathbf{x}) = \frac{1}{(2\pi)^{n/2}\,\det(\Sigma)^{1/2}}\,\exp\left(-\frac{1}{2}(\mathbf{x}-\mu)'\,\Sigma^{-1}(\mathbf{x}-\mu)\right). \tag{66}$$

Here μ is the expectation $E[(X_1, \ldots, X_n)']$ and Σ is the covariance matrix of the n component variables, that is $\Sigma(i,j) = E[(X_i - E[X_i])(X_j - E[X_j])]$. Figure 39 shows the pdf of a 2-dimensional normal distribution. In geometrical terms, a multidimensional normal distribution is shaped as an *ellipsoid*, whose main axes coincide with the eigenvectors $\mathbf{u}_i$ of the covariance matrix Σ. Like in PCA one can obtain them from the SVD: if $UDU' = \Sigma$ is the singular value decomposition of Σ, the eigenvectors $\mathbf{u}_i$ are the columns of U.

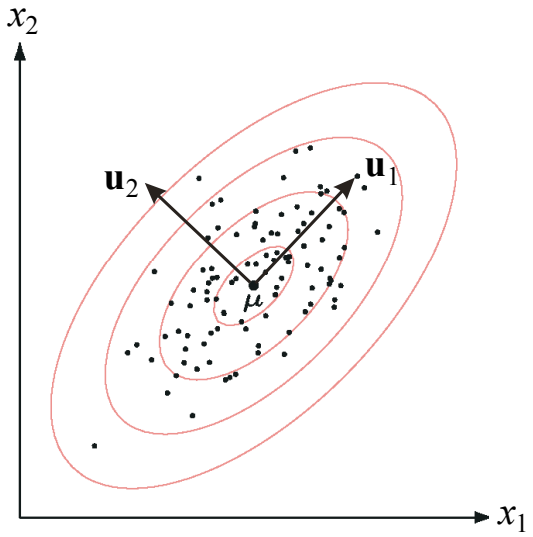

Figure 39: A pdf (indicated by contour lines) of a 2-dimensional normal distribution with expectation μ. The vectors $\mathbf{u}_1, \mathbf{u}_2$ are the principal axes of the ellipses which characterize the geometry of this pdf.

Multidimensional normal distributions (or simply, "Gaussians") are major players in machine learning. On the elementary end, one can use weighted combinations of Gaussians to approximate complex distributions - we will see this later in today's lecture. At the advanced end, there is an entire modern branch of ML, *Gaussian processes*, where complex distributions (and hyperdistributions) are modeled by infinitely many, interacting Gaussians. This is quite beyond the scope of our course.

Learning / estimation: Given a set of n-dimensional training data points $(\mathbf{x}_i)_{i=1,\ldots,N}$, the expectation μ and the covariance matrix Σ can be estimated from

the training data in the obvious way:

$$\hat{\mu} = 1/N \sum_i \mathbf{x}_i \text{ and } \hat{\Sigma} = 1/(N-1) \sum_i (\mathbf{x}_i - \hat{\mu})(\mathbf{x}_i - \hat{\mu})'$$

.

... and many more! The few common, named distributions that I displayed in this section are only meant to be illustrative picks from a much, much larger reservoir of well-known, completely analyzed, tabulated, pre-computed, and individually named distributions. The online book "Field Guide to Continuous Probability Distributions" Crooks 2017 attempts a systematic overview. You should take home the following message:

- In 100 years or so of research, statisticians have identified hundreds of basic mechanisms by which nature generates random observations. In this subsection we only looked at only two of them – (i) intermittent rare "impact events" coming from large numbers of independent sources which hit some target system with a mean frequency λ, giving rise to Poisson and exponential distributions; and (ii) stochastic physical measurables that can be understood as the additive effect of a large number of different causes, which leads to the normal distribution.
- One way of approaching a statistical modeling task for a target distribution P_X is to
    1. first analyze and identify the nature of the physical (or psychological or social or economical...) effects that give rise to this distributions,
    2. then do a literature search (e.g. check out what G. E. Crooks says) or ask a statistics expert friend which known and named distribution is available that was tailored to capture exactly these effects, – which will likely give you a distribution formula that is shaped by a small number of parameters θ,
    3. then estimate θ from available observation data, getting a distribution estimate $\hat{\theta}$, and
    4. use the theory that statisticians have developed in order to calculate confidence intervals (or similar accuracy tolerance measures) for $\hat{\theta}$, which
    5. finally allows you to state something like, *"given the observation data, with a probability of 0.95, the true distribution θ^{true} differs from the estimate $\hat{\theta}$ by less than 0.01 percent."*
- In summary, a typical classical statistical modeling project starts from well-argued assumptions about the type of the true distribution, then estimates

the parameters of the distribution, then reports the estimate together with a quantification of the error bound or confidence level (or the like) of the estimate.

- Professionally documented statistical analyses will *always* state not only the estimated model, but also in addition quantify how accurate the model estimate is. This can take many forms, like error bars drawn around estimated parameters or stating "significance levels".

- If you read a report that only reports a model estimate, without any such quantification of accuracy levels, then this report has not been written by a professional scientist. There are two kinds of such reports. Either the author was ignorant about how to carry out a statistical analysis – then trash the report and forget it. Or the report was written by a machine learner in a task context where accuracy levels are not important and/or cannot be technically obtained because it is not possible to identify the distribution kind of the data generating system.

7.3 Mixture of Gaussians; maximum-likelihood estimates by EM algorithms

Approximating a distribution of points $\mathbf{x} \in \mathbb{R}^n$ by a single n-dimensional Gaussian will be a far too coarse approximation which wipes out most of the interesting structure in the data. Consider, for a demonstration, the probability distribution of points in a rectangular subset of $\mathbb{R}^2$ visualized in Figure 40. The true distribution shown in panel **A** could not be adequately approximated by a single 2-dimensional Gaussian, but if one invests a mixture of twenty of them, the resulting model distribution (panel **D**) starts to look useful.

Approximating a complex probability distribution by such *mixtures of Gaussians* (MoG's) is a widely used technique. It comes with a transparent and robust optimization algorithm which locates, scales and orients the various Gaussians such that all together they give an optimal approximation. This optimization algorithm is an *expectation-maximization* (EM) algorithm. EM algorithms appear in many variants in machine learning, but all of them are designed according to the same basic optimization principle, which every machine learning professional should know. I will use this occasion of optimizing MoGs to introduce you to the world of EM algorithms as a side-effect.

Let us first fix notation for MoGs. We consider probability distribtions in $\mathbf{R}^n$. A Gaussian (multi-dimensional normal distribution) in $\mathbf{R}^n$ is characterized by its mean μ and its n-dimensional covariance matrix Σ. We lump all the parameters inside μ and Σ together and denote the resulting parameter vector by θ. We denote the pdf of the Gaussian with parameters θ by $p(\cdot|\theta)$. Now we can write

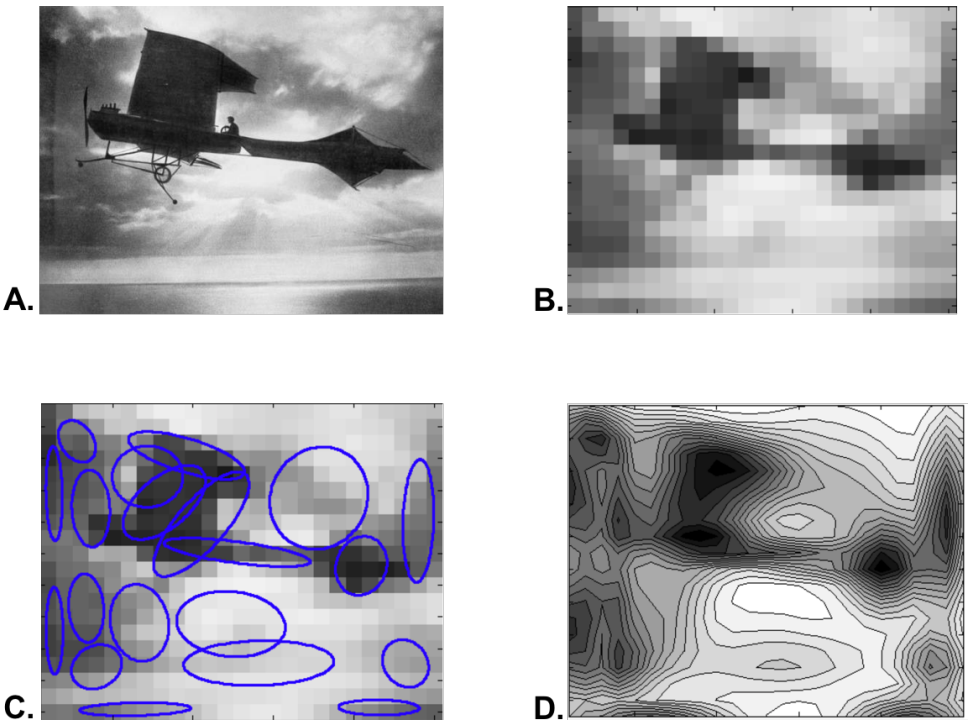

Figure 40: **A.** A richly structured 2-dimensional pdf (darker: larger values of pdf; white: zero value of pdf). **B.** Same, discretized to a pmf. **C.** A MoG coverage of the pmf with 20 Gaussians, showing the ellipsoids coresponding to standard deviations. **D.** Contour plot of the pdf represented by the mixture of Gaussians. (The picture I used here is an iconic photograph from the history of aviation, July 1909. It shows Latham departing from Calais, attempting to cross the Channel in an aeroplane for the first time in history. The motor of his Antoinette IV monoplane gave up shortly before he reached England and he had to water. A few days later his rival Blériot succeeded. `https://en.wikipedia.org/wiki/Hubert_Latham`

down the pdf p of a MoG that is assembled from m different Gaussians as

$$p : \mathbb{R}^n \to \mathbb{R}^{\geq 0}, \;\; \mathbf{x} \mapsto \sum_{j=1}^{m} p(\mathbf{x}|\theta_j)\; P(j), \tag{67}$$

where $\theta_j = (\mu_j, \Sigma_j)$ are the parameters of the jth Gaussian, and where the *mixture coefficients* $P(j)$ satisfy

$$0 \leq P(j) \quad \text{and} \quad \sum_{j=1}^{m} P(j) = 1.$$

For notational simplification we will mostly write $\sum_{j=1}^{m} p(\mathbf{x}|j)\; P(j)$ instead of $\sum_{j=1}^{m} p(\mathbf{x}|\theta_j)\; P(j)$.

MoG's are used in unsupervised learning situations: given a data set $(\mathbf{x}_i)_{i=1,\ldots,N}$ of points in $\mathbb{R}^n$, one wants to find a "good" MoG approximation of the distribution from which the $\mathbf{x}_i$ have been sampled. But... what does "good" mean?

This is the point to introduce the loss function which is invariably used when the task is to find a "good" distribution model for a set of training data points. Because this kind of loss function and this way of thinking about optimizing distribution models is not limited to MoG models but is the universal way of handling distribution modeling throughout machine learning, I devote a separate subsection to it and discuss it in general terms.

7.3.1 Maximum likelihood estimation of distributions

We consider the following general modeling problem: Given a dataset $D = (\mathbf{x}_i)_{i=1,\ldots,N}$ of points in $\mathbb{R}^n$ and a hypothesis set $\mathcal{H}$ of pdf's p over $\mathbb{R}^n$, where each pdf $p \in \mathcal{H}$ is parametrized by θ_p, we want to select that $p_{\mathsf{opt}} \in \mathcal{H}$ which "best" models the distribution from which the data points $\mathbf{x}_i$ were sampled.

In supervised learning scenarios, we formalized this modeling task around a loss function which compared model outputs with teacher outputs. But now we find ourselves in an unsupervised learning situation. How can a pdf p be a "good" or "bad" model for a given set of training points?

In order to answer this question, one turns the question around: assuming the true distribution is given by a pdf p, how "likely" is it to get the training dataset $D = (\mathbf{x}_i)_{i=1,\ldots,N}$? That is, how well can the training datapoints be "explained" by p?

To make this precise, one considers the probability that the dataset D was drawn, *given* that the true distribution has the pdf p (which is characterized by parameters θ) Since the probability of drawing D is a probability over the set of N datapoints from $\mathbb{R}^n$, the probability of drawing D is described by a pdf $f(D|\theta)$ over $(\mathbb{R}^n)^N$. At this point one assumes that the datapoints in D have been drawn independently (and each of them from a distribution with pdf p), which leads to

$$f(D|\theta) = \prod_{i=1}^{N} p(\mathbf{x}_i \,|\, \theta). \tag{68}$$

This pdf $f(D|\theta)$ value measures the probability of getting the sample D if the underlying distribution is the one modeled by θ. Conversely, one says that this value $f(D|\theta)$ is the *likelihood* of the distribution θ given the data D, and writes $L(\theta \,|\, D)$. The words "probability" and "likelihood" are two different words which refer to the same mathematical object, namely $f(D|\theta)$, but this object is read from left to right when speaking of "probability":

- "the probability to get data D given the distribution is modeled by θ", written $f(D|\theta)$,

and it is read from right to left when speaking of "likelihood":

- "the likelihood of the model θ given a dataset D", written $L(\theta \,|\, D)$.

A correct usage of the words "probability" vs. "likelihood" is a sign of a good education in machine learning.

The likelihood pdf (68) is not suitable for doing numerical computations, because a product of very many small numbers (the $p(\mathbf{x}_i \,|\, \theta)$) will lead to numerical underflow and become squenched to zero on digital computers. To avoid this, one always works with the *log likelihood*

$$\mathcal{L}(\theta|D) = \log \prod_{i=1}^{N} p(\mathbf{x}_i \,|\, \theta) = \sum_{i=1}^{N} \log\, p(\mathbf{x}_i \,|\, \theta) \tag{69}$$

instead. A model θ is "good" if it has a high (log)likelihood. Machine learning algorithms for finding the best model p in a hypothesis set $\mathcal{H}$ are designed to find the *maximum likelihood* model

$$\theta^{\mathsf{ML}} = \operatorname*{argmax}_{\theta \in \mathcal{H}} \mathcal{L}(\theta \,|\, D). \tag{70}$$

Machine learners like to think of their learning procedures as minimizing some cost or loss. Thus one also finds in the literature the sign-inverted version of (70)

$$\theta^{\mathsf{ML}} = \operatorname*{argmin}_{\theta \in \mathcal{H}} \; -\mathcal{L}(\theta \,|\, D), \tag{71}$$

which obviously is equivalent. If one writes out the $\mathcal{L}(\theta \,|\, D)$ one sees the structural similarity of this unsupervised learning task with the supervised loss-minimization task which we met earlier in this course (e.g. (41)):

$$\theta^{\mathsf{ML}} = \operatorname*{argmin}_{\theta \in \mathcal{H}} \; -\sum_{i=1}^{N} \log\, p(\mathbf{x}_i \,|\, \theta).$$

7.3.2 Maximum-likelihood estimation of MoG models by an EM algorithm

Back to our concrete business of modeling a distribution represented by a dataset $D = (\mathbf{x}_i)_{i=1,\ldots,N}$ by a MoG. In order to to find a maximum-likelihood solution for this MoG modeling task, one has to answer two questions:

1. What is the appropriate number m of mixture components? Setting m determines the class of candidate solutions in which an optimization algorithm can search for the maximum-likelihood solution. The set $\mathcal{H}_m$ contains all mixtures of m Gaussians. We have here a case of a model class inclusion sequence as discussed in Section 6.4. For determining an appropriate model flexibility m the routine way would be to carry out a cross-validation.

2. If an appropriate m has been determined, how should the parameters θ_j (where $j = 1, \ldots, m$) of the participating Gaussians be set in order to solve the optimization problem

$$\theta^{\mathsf{ML}} = \operatorname*{argmax}_{\theta \in \mathcal{H}_m} \mathcal{L}(\theta \mid D)? \tag{72}$$

The second question is answered by employing an expectation-maximization (EM) algorithm. EM algorithms can be often designed for maximizing the (log) likelihoods of parametrized distributions. There is a general scheme for designing such algorithms, and general theorems concerning their convergence properties. The EM principle had been introduced by Dempster, Laird, and Rubin 1977 — one of these classical landmark papers that will forever continue to be continuously cited (as of 2019, 57K Google cites).

EM algorithms are widely used in computational statistics when it comes to estimate model parameters θ from *incomplete* or *partially observable* data. The principle of designing EM algorithms is a cornerstone of many important machine learning algorithms that are using "incomplete" training data. What "incomplete" means depends on the specific case. For instance, it might mean missing data points in time series measurements, or measurements of physical systems where the available sensors give only a partial account of the system state. The general idea is that the observed data have been caused by some "hidden" mechanism which

- for filling in "best guesses" for missing values in time series data where observations are unavailable for certain time points (like handwritten texts with unreadable words in them);

- for estimating *hidden Markov models* (HMMs) of stochastic timeseries; HMMs are the most widely used models for stochastic processes with memory;

- for estimating models of complex systems that are described by many interacting random variables, some of which are not observable — an example

from human-machine interfacing: modeling the decisions expected from a user assuming that these decisions are influenced by emotional states that are not directly observable; such models are called *Bayesian networks* or more generally, *graphical models*;

- for a host of other practical modeling tasks, like our MoG optimization task.

Because of the widespread usefulness of EM algorithms I will now carry you through a general, abstract explanation of the underlying principle. This is not easy stuff but worth the effort. I follow the modern exposition given in Roweis and Ghahramani 1999, which also covers other versions of EM for other machine learning problems. I use however another notation than these authors and I supply more detail. In blue font I will insert how the abstract picture translates into our specific MoG case. The following treatment will involve a lot of probability formalism — I consider it a super exercise in becoming friends with random variables and products of random variables! try not to give up on the way! I suggest that in a first reading you skip the blue parts and concentrate on the abstract picture alone.

The general situation is the following. Let X be an observable random variable and let Y be a hidden random variable, which take values in value sets ("sample spaces") S_X and S_Y, respectively. X produces the visible training data D and Y produces the hidden data which have a causal impact on D but cannot be observed. Note: the words *visible* and *hidden* are the common technical terms in the EM literature.

In the MoG case, X would be the random variable which generates the entire training sample $(\mathbf{x}_i)_{i=1,\dots,N}$, thus here $S_X = (\mathbb{R}^n)^N$. Y would be a random variable that decides which of the m Gaussians is used to generate $\mathbf{x}_i$, thus $S_Y = \{1,\dots,m\}^N$. The RV Y is a product $Y = \bigotimes Y_i$ of i.i.d. RVs Y_i, where Y_i takes values $j \in \{1,\dots,m\}$. Concretely, Y_i selects one of the m Gaussians by a random choice weighted by the probability vector $(P(1),\dots,P(m))$. Thus the value of Y_i is j_i, an element of $\{1,\dots,m\}$.

The RV X is a product $X = \bigotimes X_i$ of i.i.d. RVs X_i, where X_i generates the i-th training data point $\mathbf{x}_i$ by a random draw from the j_i-th Gaussian, that is from the normal distribution $\mathcal{N}(\mu_{j_i}, \Sigma_{j_i})$.

Figure 7.3.2 illustrates what it means not to know the values of the hidden variable Y.

Let θ be a vector of parameters describing the joint distribution $P_{X,Y}$ of hidden and visible RVs.

In our MoG case, $\theta = (\mu_1,\dots,\mu_m,\Sigma_1,\dots,\Sigma_m,P(1),\dots,P(m))'$.

Let D be the observable sample, that is, the result from a random draw with X.

In the MoG scenario, $D = (\mathbf{x}_i)_{i=1,\dots,N}$.

The objective of an EM algorithm is to determine θ such that the likelihood $L(\theta) = P(X = D \,|\, \theta)$ becomes maximal, or equivalently, such that the log likeli-

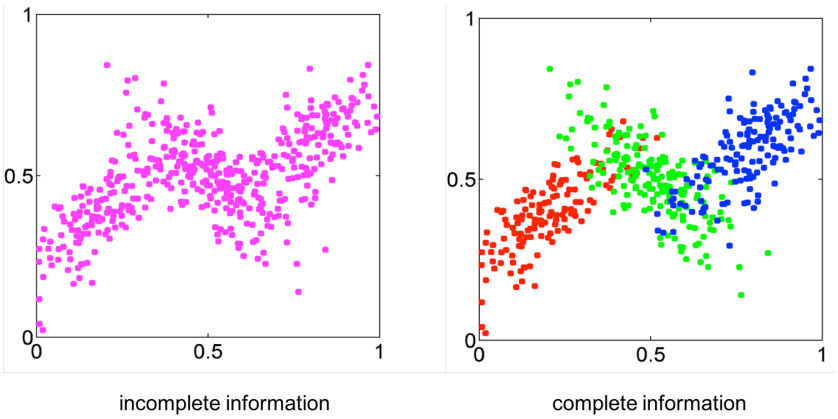

Figure 41: A point set sampled from a mixture of Gaussians. Left: what we (don't) know if we don't know from which Gaussian a point was drawn. Right: the "hidden" variable made visible. (Figure copied from an online presentation of Christopher M. Bishop, no longer accessible)

hood

$$\mathcal{L}(\theta \,|\, D) = \log\, P(X = D \,|\, \theta)$$

becomes maximal.

At this point we would have to start using different notations (pmf's versus pdf's) depending whether X and Y are discrete or continuous RVs. I will carry out the formal description only for the case that both X and Y are continuous, which means that their joint distribution can be described by a pdf $p_{X,Y}$ defined on $S_X \times S_Y$. The marginal distributions of X and Y are then given by parametrized pdf's $p_X(x|\theta) = \int_Y p_{X,Y}(x, y|\theta)dy$ and $p_Y(y|\theta) = \int_X p_{X,Y}(x, y|\theta)dx$. We can then switch to a description of distributions using only pdfs, that is, the distribution of samples D is described by the pdf $p_X(D|\theta)$.

In the case of all-continuous distributions, the log likelihood of θ becomes

$$\mathcal{L}(\theta \,|\, D) = \log\, p_X(D|\theta). \tag{73}$$

The MoG case has a mix of types: X gives values in the continuous space $(\mathbb{R}^n)^N$ and Y gives values in the discrete space $\{1, \ldots, m\}^N$. This makes it necessary to use a mix of pdf's and pmf's when working out the MoG case in detail.

The difficulty we are facing is that the pdf value $p_X(D|\theta)$ depends on the values that the hidden variables take, that is,

$$\mathcal{L}(\theta \,|\, D) = \log\, p_X(D|\theta) = \log \int_{S_Y} p_{X,Y}(D, y \,|\, \theta)\, dy.$$

In the MoG case, the integral over S_Y becomes a sum over S_Y:

$$\begin{aligned} p_X(D|\theta) &= \sum_{(j_1,\ldots,j_N)\in\{1,\ldots,m\}^N} P(Y=(j_1,\ldots,j_N))\, p_{X|Y=(j_1,\ldots,j_N)}(D) \\ &= \sum_{(j_1,\ldots,j_N)\in\{1,\ldots,m\}^N} \prod_{i=1,\ldots,N} P(Y_i=j_i)\, p_{X_i|Y_i=j_i}(\mathbf{x}_i), \end{aligned}$$

where $p_{X|Y=(j_1,\ldots,j_N)}$ is the pdf of the conditional distribution of X given that the hidden variables take the value $(j_1,\ldots,j_N)$ and $p_{X_i|Y_i=j_i}$ is the pdf of the conditional distribution of X_i given that the hidden variable Y_i takes the value j_i.

Now let q be *any* pdf for the hidden variables Y. Then we can obtain a lower bound on $\log p_X(D|\theta)$ by

$$\begin{aligned} \mathcal{L}(\theta\,|\,D) &= \log \int_{S_Y} p_{X,Y}(D,y\,|\,\theta)\,dy = \\ &= \log \int_{S_Y} q(y)\,\frac{p_{X,Y}(D,y\,|\,\theta)}{q(y)}\,dy \\ &\geq \int_{S_Y} q(y)\,\log\,\frac{p_{X,Y}(D,y\,|\,\theta)}{q(y)}\,dy \\ &= \int_{S_Y} q(y)\,\log\,p_{X,Y}(D,y\,|\,\theta)\,dy - \int_{S_Y} q(y)\,\log\,q(y)\,dy \qquad (74) \\ &=: \mathcal{F}(q,\theta), \qquad (75) \end{aligned}$$

where the inequality follows from a version of Jensen's inequality which states that

$$E[f\circ Y] \leq f(E[Y])$$

for any concave function f (the log is concave).

EM algorithms maximize the lower bound $\mathcal{F}(q,\theta)$ by alternatingly and iteratively maximizing $\mathcal{F}(q,\theta)$ first with respect to q, then with respect to θ, starting from an initial guess $q^{(0)},\theta^{(0)}$ which is then updated by:

$$\textbf{E}\text{xpectation step:} \qquad q^{(k+1)} = \operatorname*{argmax}_q \mathcal{F}(q,\theta^{(k)}), \qquad (76)$$

$$\textbf{M}\text{aximization step:} \qquad \theta^{(k+1)} = \operatorname*{argmax}_\theta \mathcal{F}(q^{(k+1)},\theta). \qquad (77)$$

The maximum in the E-step is obtained when q is the conditional pdf of Y given the data D,

$$q^{(k+1)} = p_{Y|X=D,\theta^{(k)}}, \qquad (78)$$

because then $\mathcal{F}(q^{(k+1)},\theta^{(k)}) = \mathcal{L}(\theta^{(k)}\,|\,D)$:

$$
\begin{aligned}
&\mathcal{F}(p_{Y|X=D,\theta^{(k)}}, \theta^{(k)}) = \\
&= \int_{S_Y} p_{Y|X=D,\theta^{(k)}}(y)\ \log\ p_{X,Y}(D, y \,|\, \theta^{(k)})\, dy - \int_{S_Y} p_{Y|X=D,\theta^{(k)}}(y)\ \log\ p_{Y|X=D,\theta^{(k)}}(y)\, dy \\
&= \int_{S_Y} p_{Y|X=D,\theta^{(k)}}(y)\ \log\ \frac{p_{X,Y}(D, y \,|\, \theta^{(k)})}{p_{Y|X=D,\theta^{(k)}}(y)}\, dy \\
&= \int_{S_Y} p_{Y|X=D,\theta^{(k)}}(y)\ \log\ p_X(D \,|\, \theta^{(k)})\, dy \\
&= \int_{S_Y} \frac{p_{X,Y}(D, y|\theta^{(k)})}{p_X(D \,|\, \theta^{(k)})}\ \log\ p_X(D \,|\, \theta^{(k)})\, dy \\
&= \frac{\log\ p_X(D \,|\, \theta^{(k)})}{p_X(D \,|\, \theta^{(k)})} \int_{S_Y} p_{X,Y}(D, y|\theta^{(k)})\, dy \\
&= \log\ p_X(D \,|\, \theta^{(k)}) \\
&= \mathcal{L}(\theta^{(k)} \,|\, D).
\end{aligned}
$$

In concrete algorithms, the conditional distribution $p_{Y|X=D,\theta^{(k)}}$ is computed as the expectation of Y given data D and parameters $\theta^{(k)}$, which is why this step has its name, the **E**xpectation step.

The maximum in the M-step is obtained if the first term in (74) is maximized, because the second term does not depend on $\theta^{(k)}$:

$$
\begin{aligned}
\theta^{(k+1)} &= \operatorname*{argmax}_{\theta} \int_{S_Y} q^{(k+1)}(y)\ \log\ p_{X,Y}(D, y \,|\, \theta)\, dy \\
&= \operatorname*{argmax}_{\theta} \int_{S_Y} p_{Y|X=D,\theta^{(k)}}(y)\ \log\ p_{X,Y}(D, y \,|\, \theta)\, dy \qquad (79) \\
& \qquad\qquad (80)
\end{aligned}
$$

How the M-step is concretely computed depends on the particular kind of model. Because we have $\mathcal{F} = \mathcal{L}(\theta^{(k)} \,|\, D)$ before each M-step, and the E-step does not change $\theta^{(k)}$, and $\mathcal{F}$ cannot decrease in an EM-double-step, the sequence $\mathcal{L}(\theta^{(0)} \,|\, D), \mathcal{L}(\theta^{(1)} \,|\, D), \ldots$ monotonously grows toward a supremum. The iterations are stopped when $\mathcal{L}(\theta^{(k)} \,|\, D) = \mathcal{L}(\theta^{(k+1)} \,|\, D)$, or more realistically, when a predefined number of iterations is reached or when the growth rate falls below a predetermined threshold. The last parameter set $\theta^{(k)}$ that was computed is taken as the outcome of the EM algorithm.

It must be emphasized that EM algorithms steer toward a local maximum of the likelihood. If started from another initial guess, another final parameter set may be found. Here is a summary of the EM principle:

E-step: Estimate the distribution $p_{Y|X=D,\theta^{(k)}}(y)$ of the hidden variables, given data D and the parameters $\theta^{(k)}$ of a preliminary model. This can be intu-

itively understood as inferring knowledge about the hidden variables, thereby *completing* the data.

M-step: Use the (preliminary) "knowledge" of the complete data (given by D for the visibles and by $p_{Y|X=D,\theta^{(k)}}(y)$ for the hidden variables) to compute a maximum likelihood model $\theta^{(k+1)}$.

There are other ways to compute maximum likelihood solutions in tasks that involve visible and hidden variables. Specifically, one can often invoke a gradient descent optimization. A big advantage of EM over gradient descent is that EM does not need a careful tuning of algorithm control parameters (like learning rates, an eternal bummer in gradient descent methods), simply because there are no tuning parameters. Furthermore, EM algorithms are typically numerically robust, which cannot be said about gradient descent algorithms.

Now let us put EM to practice for the MoG estimation. For better didactic transparency, I will restrict my treatment to a special case where we require all Gaussians to be spheric, that is, their covariance matrices are of the form $\Sigma = \sigma^2 I_n$ where σ^2 is the variance of the Gaussian in every direction and I_n is the n-dimensional identity matrix. The general case of mixtures of Gaussians composed of member Gaussians with arbitrary Σ is described in textbooks, for instance Duda, Hart, and Stork 2001. And anyway, you would probably use a ready-made online tool for MoG estimation... Here we go.

A MoG pdf with m spherical components is given by the vector of parameters $\theta = (\mu_1, \ldots, \mu_m, \sigma_1^2, \ldots, \sigma_m^2, P(1), \ldots, P(m))'$. This gives the following concrete optimization problem:

$$\begin{aligned} \theta^{\mathsf{ML}} &= \operatorname*{argmax}_{\theta \in \mathcal{H}_m} \mathcal{L}(\theta \,|\, D) \\ &= \operatorname*{argmax}_{\theta \in \mathcal{H}_m} \sum_{i=1}^{N} \log \left(\sum_{j=1}^{m} \frac{1}{(2\pi\sigma_j^2)^{n/2}} \exp\left(-\frac{\|\mathbf{x}_i - \mu_\mathbf{j}\|^2}{2\sigma_j^2} \right) P(j) \right) \end{aligned} \tag{81}$$

Assume that we are after iteration k and want to estimate $\theta^{(k+1)}$. In the E-step we have to compute the conditional distribution of the hidden variable Y, given data D and the preliminary model

$$\theta^{(k)} = (\mu_1^{(k)}, \ldots, \mu_m^{(k)}, \sigma_1^{2\,(k)}, \ldots, \sigma_m^{2\,(k)}, P^{(k)}(1), \ldots, P^{(k)}(m))'.$$

Unlike in the treatment that I gave for the general case, where we assumed Y to be continuous, now Y is discrete. Its conditional distribution is given by the probabilities $P(Y_i = j_i \,|\, X_i = \mathbf{x}_i, \theta^{(k)})$. These probabilities are

$$P(Y_i = j_i \,|\, X_i = \mathbf{x}_i, \theta^{(k)}) = \frac{p^{(k)}(\mathbf{x}_i \,|\, Y_i = j_i)\; P^{(k)}(j_i)}{p_X^{(k)}(\mathbf{x}_i)}, \tag{82}$$

where $p^{(k)}(\mathbf{x}_i \,|\, Y_i = j_i)$ is the pdf of the j_i-th Gaussian with parameters $\mu_{j_i}^{(k)}, \sigma_{j_i}^{2\,(k)}$ and

$$p_X^{(k)}(\mathbf{x}_i) = \sum_{j=1}^{m} P^{(k)}(j)\; p^{(k)}(\mathbf{x}_i \,|\, Y_i = j).$$

In the M-step we have to find maximum likelihood estimates for all parameters in θ. I do not give a derivation here but just report the results, which are intuitive enough:

$$\begin{aligned}
\mu_j^{(k+1)} &= \frac{\sum_{i=1}^N P(Y_i = j_i \,|\, X_i = \mathbf{x}_i, \theta^{(k)})\, \mathbf{x}_i}{\sum_{i=1}^N P(Y_i = j_i \,|\, X_i = \mathbf{x}_i, \theta^{(k)})}, \\
\sigma_j^{2\,(k+1)} &= \frac{1}{n} \frac{\sum_{i=1}^N P(Y_i = j_i \,|\, X_i = \mathbf{x}_i, \theta^{(k)}) \|\mu_j^{(k+1)} - \mathbf{x}_i\|^2}{\sum_{i=1}^N P(Y_i = j_i \,|\, X_i = \mathbf{x}_i, \theta^{(k)})}, \quad \text{and} \\
P^{(k+1)}(j) &= \frac{1}{N} \sum_{i=1}^N P(Y_i = j_i \,|\, X_i = \mathbf{x}_i, \theta^{(k)}).
\end{aligned}$$

I conclude this sudorific (look this up in a dictionary) subsection with a little EM-for-MoG demo that I copied from an online presentation of Christopher Bishop (now apparently no longer online). The sample data $\mathbf{x}_i \in \mathbb{R}^2$ come from observations of the Old Faithful geysir in the Yellowstone National Park (Figure 42).

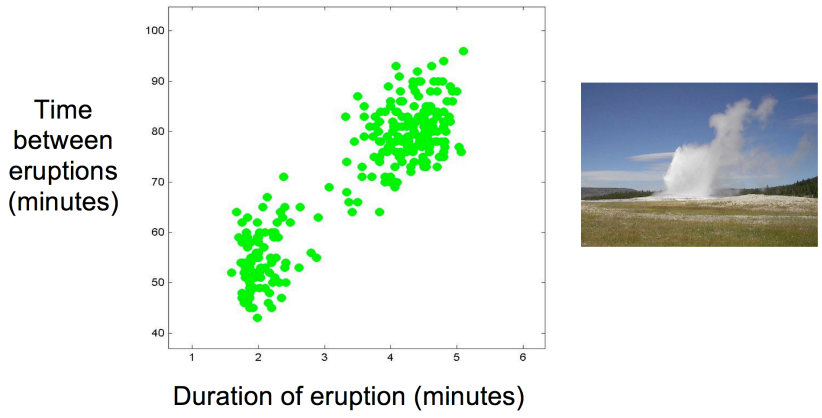

Figure 42: A two-dimensional dataset.

Figure 43 shows 20 EM iterations with $m = 2$ Gaussian components. The first panel shows the initial guess. Color codes are the estimated probabilities $P(Y_i = j_i \,|\, X_i = \mathbf{x}_i, \theta^{(k)})$. The MoG modeling of the aeroplane image in Figure 40 was also done with the EM algorithm, in a version that allowed for arbitrary covariance matrices Σ_j. I did it myself, programming it from scratch, just to prove to myself that all of this really works. It does!

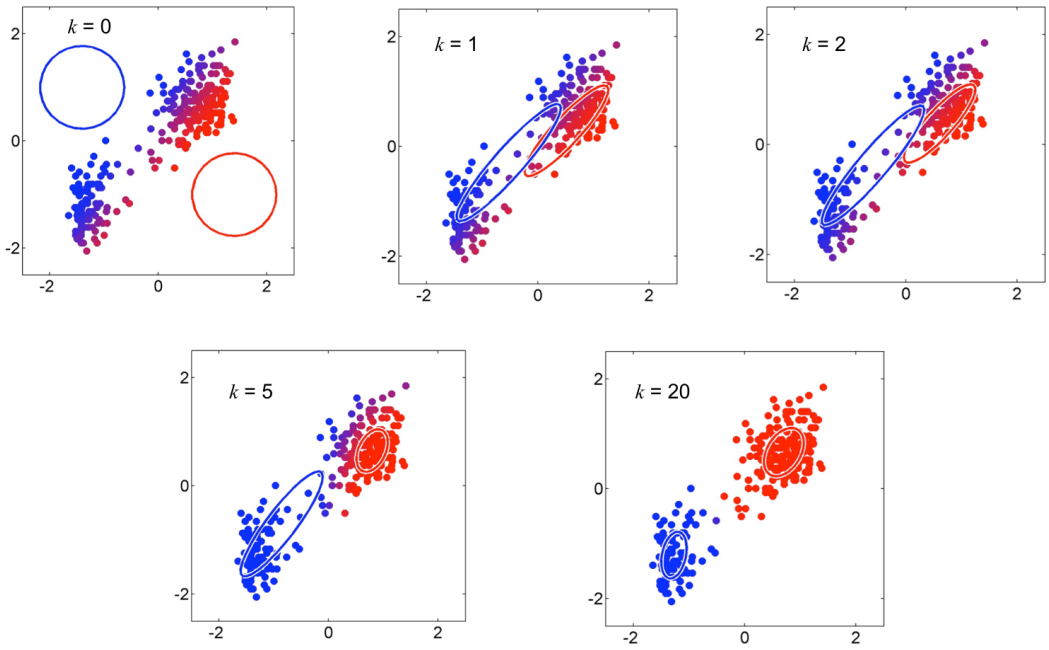

Figure 43: The EM algorithm at work on the Old Faithful dataset.

7.4 Parzen windows

After the heavy-duty work of coming to grips with the EM algorithm, let us finish this section with something easy, for chilling out. Parzen windows!

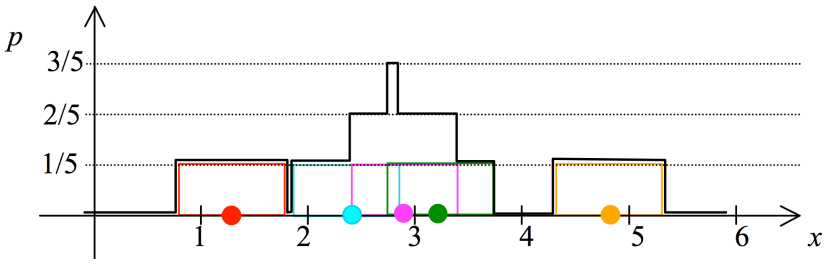

Figure 44: Rectangular Parzen window representation of a distribution given by a sample of 5 real numbers. The sample points are marked by colored circles. Each data point lies in the middle of a square "Parzen window", that is, a rectangular pdf centered on the point. Weighted by 1/5 (colored rectangles) and summed (solid black staircase line) they give a pdf.

Parzen windows are a simple representative of the larger class of *kernel-based* representations, providing an alternative to mixture models for representing pdf's. These representations are *non-parametric* — there is no parameter vector θ for specifying a Parzen window approximation to a pdf. To introduce Parzen windows, consider a sample of 5 real-valued points shown in Figure 44. Centered at each

sample point we place a unit square area on the x-axis. Weighing them each by 1/5 and summing them gives an intuitively plausible representation of a pdf.

To make this example more formal and general, consider n-dimensional data points $\mathbf{x}_i$. Instead of a unit-length square, we wish to make these points the centers of n-dimensional hypercubes of side length d. We need a function H that indicates which points around $\mathbf{x}_i$ fall into the hypercube centered at $\mathbf{x}_i$. To this end we introduce a *kernel function*, also known as *Parzen window*,

$$H : \mathbb{R}^n \to \mathbb{R}^{\geq 0}, \quad (x_1, \ldots, x_n)' \mapsto \begin{cases} 1, & \text{if } |x_j| < 1/2 \text{ for } j = 1, \ldots, n \\ 0, & \text{else} \end{cases} \tag{83}$$

which makes H the indicator function of a unit hypercube centered at the origin. Using H, we get the n-dimensional analog of the staircase pdf in Figure 44 for a sample $D = (\mathbf{x}_i)_{i=1,\ldots,N}$ by

$$p^{(D)}(\mathbf{x}) = \frac{1}{N} \sum_{i=1}^{N} \frac{1}{d^n} H\left(\frac{\mathbf{x} - \mathbf{x}_i}{d}\right), \tag{84}$$

observing that the volume of such a cube is d^n. The superscript (D) in $p^{(D)}$ is meant to indicate that the pdf depends on the sample D.

Clearly, given some sample $(\mathbf{x}_i)_{i=1,\ldots,N}$, we do not believe that such a rugged staircase reflects the true probability distribution the sample was drawn from. We would rather prefer a smoother version. This can be easily done if we use smoother kernel functions. A standard choice is to use multivariate Gaussians with diagonal covariance matrix and uniform standard deviations $\sigma =: d$ for H. This turns (84) into

$$\begin{aligned} p^{(D)}(\mathbf{x}) &= \frac{1}{N} \sum_{i=1}^{N} \frac{1}{(2\pi d^2)^{n/2}} \exp\left(-\frac{\|\mathbf{x} - \mathbf{x}_i\|^2}{2d^2}\right) \\ &= \frac{1}{N} \sum_{i=1}^{N} \frac{1}{d^n} \frac{1}{(2\pi)^{n/2}} \exp\left(-\frac{1}{2} \|\frac{\mathbf{x} - \mathbf{x}_i}{d}\|^2\right) \end{aligned} \tag{85}$$

where the second line brings the expression to a format that is analog to (84).

It is clear that any nonnegative kernel function H which integrates to unity can be used in an equation of this sort such that the resulting $p^{(D)}$ will be a pdf. The scaling factor d determines the width of the Parzen window and thereby the amount of smoothing. Figure 45 illustrates the effect of varying d.

Comments:

- Parzen window representations of pdfs are "non-parametric" in the sense that the shape of such a pdf is determined by a sample (plus, of course, by the shape of the kernel function, which however mainly serves a smoothing purpose). This fact also can render Parzen window representations computationally expensive, because if the sample size is large, a large number of data points have to be stored (and accessed if the pdf is going to be used).

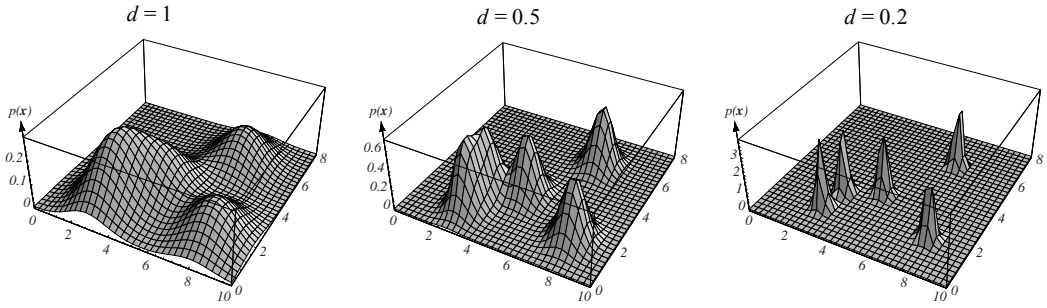

Figure 45: The effect of choosing different widths d in representing a 5-point, 2-dimensional sample by Gaussian windows. (Taken from the online set of figures of the book by Duda, Hart & Stork, `ftp://ftp.wiley.com/public/sci_tech_med/pattern/`)

- The basic Parzen windowing scheme, as introduced here, can be refined in many ways. A natural way to improve on it is to use different widths d for different sample points $\mathbf{x}_i$. One then makes d narrow in regions of the sample set which are densely populated, and wide in regions that are only thinly covered by sample points. One way of doing that (which I invented while I was writing this — there are many ways to go) would be to (i) choose a reasonably small integer K; (ii) for each sample point $\mathbf{x}_i$ determine its K nearest neighbors $\mathbf{x}_{i1}, ..., \mathbf{x}_{iK}$; (iii) compute the mean squared distance δ of $\mathbf{x}_i$ from these neighbors, (iv) set d proportional to this δ for this sample point $\mathbf{x}_i$.

- As Figure 45 demonstrates, the width d has a strong effect on the Parzen pdf. If d is too large, the smoothing becomes too strong, and information contained in the sample is smoothed away — underfitting! In contrast, when d is too small, all that we see in the resulting Parzen pdf is the individual data points — the pdf then models not a distribution, but just the sample. Overfitting! Here one should employ a cross-validation scheme to optimize d, minimizing the validation loss defined by $-\sum_{\mathbf{v}\in V} \log\, p^{(T)}(\mathbf{v}\,|\,d)$, where V is the validation set, T the training set, and $p^{(T)}(\mathbf{v}\,|\,d)$ the Parzen pdf obtained from the training set using width d.

- The Parzen-window based distribution (85) will easily lead to numerical underflow problems for arguments $\mathbf{x}$ which are not positioned close to a sample point, especially if d is set to small values. A partial solution is to use log probabilities instead, i.e. use

$$\log\, p^{(D)}(\mathbf{x}) = \log\left(\frac{1}{N}\,\sum_{i=1}^{N}\frac{1}{(2\pi d^2)^{n/2}}\,\exp\left(-\frac{\|\mathbf{x}-\mathbf{x}_i\|^2}{2d^2}\right)\right). \qquad (86)$$

  Still this will not usually solve all underflow problems, because the sum-exp

terms within the log still may underflow. Here is a trick to circumvent this problem, known as the "log-sum-exp" trick. Exploit the following:

$$\begin{aligned}
&\log(\exp(-A) + \exp(-B)) = \\
&\quad = \log\left(\exp(-A + C)\exp(-C) + \exp(-B + C)\exp(-C)\right) \\
&\quad = -C + \log\left(\exp(-A + C) + \exp(-B + C)\right),
\end{aligned}$$

where you use $C = \max(A, B)$.

8 Bayesian model estimation

Machine learning is based on probability, and probability is ... ? — We don't know what probability is! After centuries of thinking, philosophers and mathematicians have not arrived to a general consensus of how to best understand randomness. The proposals can be broadly grouped into *objectivistic* and *subjectivistic* interpretations of "probability".

According to the objectivistic view, probability resides physically in the real world — it is a phenomenon of nature, as fundamentally a property of physical reality as for instance "time" or "energy".

According to the subjectivistic view, probability describes an observer's subjective opinion on something observed — a degree of belief, of uncertainty, of plausibility of judgement, or missing information etc.

Calling the two views "objectivistic" versus "subjectivistic" is the philosophers' terminology. Statisticians and machine learners rather call it *frequentist statistics* versus *Bayesian statistics*.

The duality of understandings of "probability" has left a strong mark on machine learning. The two ways of thinking about probability lead to two different ways of designing learning algorithms. Both are important and both are in daily use. A machine learning professional should be aware of the fundamental intuitions behind the two sorts of algorithms and when to use which sort. In this section I explain the fundamental ideas behind the two understandings of probability, outline the general principles of constructing Bayesian algorithms, and demonstrate them in a case study of great importance in bioinformatics, namely the classification of proteins.

8.1 The ideas behind frequentist statistics

When probability is regarded as a phenomenon of nature, there should be ways to *measure* it. The standard proposition of how one can measure probability is by *relative frequency counting*. For instance, in the textbook example of a loaded (unfair) die, a loaded die may have the physical property that $P(X = 6) = 1/5$ (as opposed to $P(X = 6) = 1/6$ for a fair die), where X is the RV which gives the outcomes of throwing-the-die experiments. This property of the die could be experimentally measured by *repeating* the die-throwing act many times. This would give a sequence of outcomes $x_1, x_2, x_3, \ldots$ where $x_i \in \{1, \ldots, 6\}$. After N such throws, an estimate of the quantity $P(X = 6)$ is calculated by

$$\hat{P}_N(X = 6) = \frac{\text{number of outcomes } x_i = 6}{N}, \tag{87}$$

where N is the number of throws that the experimentalist measuring this probability has carried out.

We generally use the hat symbol $\hat{\cdot}$ on top of some variable to denote a numerical estimate based on a finite amount of observation data. The true probability $P(X =$

6) = 1/5 would then become "measurable in principle" by

$$(^*) \qquad P(X = 6) = \lim_{N\to\infty} \hat{P}_N(X = 6). \tag{88}$$

A fundamental mathematical theorem in frequentist probability theory — actually, *the* fundamental law which justifies frequentist probability theory in the first place — is the *law of large numbers*. It states that if one carries out an infinite sequence of repeating the same numerical measurement, obtaining a sequence of measurement values $x_1, x_2, \ldots$, where $x_i \in \mathbb{R}$, then the mean value $\mu_N = (1/N) \sum_{i=1}^{N} x_i$ of initial sequences up N will "almost always" converge to the same number $\mu = E[X]$, called the expectation of X. Stating and proving this theorem in formal rigor has taken mathematicians a long time and was achieved by Kolmogorov not earlier than in the early 1930's. A precise formulation needs the full apparatus of measure-theoretic probability theory (which I partly introduce in the tutorial sessions).

More generally, considering some random variable X which takes values in a sample space S, one considers subsets $A \subseteq S$ (called *events*) and then defines

> **The frequentist view of probability:** The probability $P(X \in A)$ that the outcome of sampling a datapoint with procedure X gives an outcome in A is the relative frequency (in the limit of carrying out infinitely many unbiased trials of enacting a measurement procedure X) of obtaining a measurement value in A.

If one looks at this "definition" with a critical mind one will find that it is loaden with difficulties.

First, it defines a "measurement" process that is not feasible in reality because one cannot physically carry out infinitely many measurement trials. This is maybe not really disturbing because *any* measurement in the sciences (say, of a voltage) is imprecise and one gets measurements of increasing precision by repeating the measurement, just as when one measures a probability.

Second, it does not inform us about how, exactly, the "repeated trials" of executing X should be done in order to be "unbiased". What does that mean in terms of experimental procedures? This is a very critical issue. To appreciate its impact, consider the example of a bank who wishes to estimate the probability that a customer will fail to pay back a loan. In order to get an estimate of this probability, the bank can only use customer data collected in the *past*, but wants to base creditworthyness decisions for *future* customers on those data. Picking only past data points to base probability estimates on hardly can qualify as an "absolutely unbiased" sampling of data, and in fact the bank may grossly miscalculate credit risks when

the general customer body or their economical conditions change over time. These difficulties have of course been recognized in practical applications of statistics. Textbooks and statistics courses for psychologists and economists contain entire chapters with instructions on how to create "random samples" or "unbiased samples".

Third, if one repeats the repeated measurement, say by carrying out one measurement sequence giving $x_1, x_2, \ldots$ and then (or in parallel) another one giving $x'_1, x'_2, \ldots$, the values $\hat{P}_N$ from Equation (88) are bound to differ between the two series. The limit indicated in Equation (88) must somehow be robust against different versions of the $\hat{P}_N$. Mathematical probability theory offers several ways to rigorously define limits of series of probability quantities which we do not present here. Equation (88) is suggestive only and I marked it with a $(^*)$ to indicate that it is not technically complete.

Among these three difficulties, only the second one is really problematic. The first one is just a warning that in order to measure a probability with increasing precision we need to invest an increasingly large effort, — but that is the same for other measurables in the sciences. The third difficulty can be fully solved by a careful definition of suitable limit concepts in mathematical probability theory. But the second difficulty is fundamental and raises its ugly head whenever statistical assertions about reality are made.

In spite of these difficulties, the objectivist view on probability in general and the frequentist account of how to measure it in particular is widely shared among empirical scientists. It is also the view of probability which is commonly taught in courses of statistics for mathematicians. A student of mathematics may not even have heard of Bayesian statistics at the end of his/her studies. In machine learning, the frequentist view often leads to learning algorithms which are based on the principle of maximum likelihood estimation of distributions — as we have seen in Section 7.3.1. In fact, all what I wrote in these lecture notes up to now was implicitly based on a frequentist understanding of probability.

8.2 The ideas behind Bayesian statistics

Subjectivist conceptions of probability also have led to mathematical formalisms that can be used in statistical modeling. A hurdle for the student here is that a number of different formalisms exist which reflect different modeling goals and approaches, and tutorial texts are rare.

The common starting point for subjectivist theories of probability is to cast "probability" as a subjective degree of belief, of certainty of judgement, or plausibility of assertions, or similar — instead of as an objective property of real-world systems. Subjectivist theories of probability do not develop analytical tools to describe randomness in the world. Instead they provide formalisms that code how rational agents (you, I, and AI systems) should *think about* the world, in the face of

various kinds of uncertainty in their knowledge and judgements. The formalisms developed by subjectivists can by and large be seen as generalizations of classical *logic*. Classical logic only knows two truth values: true or false. In subjectivist versions of logic formalisms, a proposition can be assigned graded degrees of "belief", "plausibility", etc. For a very first impression, contrast a classical-logic syllogism like

$$\frac{\begin{array}{c}\textit{if } A \textit{ is true, then } B \textit{ is true} \\ A \textit{ is true}\end{array}}{\textit{therefore, } B \textit{ is true}}$$

with a "plausibility reasoning rule" like

$$\frac{\begin{array}{c}\textit{if } A \textit{ is true, then } B \textit{ becomes more plausible} \\ B \textit{ is true}\end{array}}{\textit{therefore, } A \textit{ becomes more plausible}}$$

This example is taken from Jaynes 2003, where a situation is described in which a policeman sees a masked man running away from a juweler's shop whose window was just smashed in. The plausibility rule captures the policeman's inference that the runner is a thief (A) because if a person is a thief, it is more likely that the person will run away from a smashed-in shop window (B) than when the person isn't a thief. From starting points like this, a number of logic formalisms have been devised which enrich/modify classical two-valued logic in various ways. If you want to explore these areas a little further, the Wikipedia articles probabilistic logic, Dempster-Shafer theory, fuzzy logic, or Bayesian probability are good entry points. In some of these formalisms the Kolmogorov axioms of frequentist probability reappear as part of the respective mathematical apparatus. Applications of such formalisms arise in artificial intelligence (modeling reasoning under uncertainty), human-machine interfaces (supporting discourse generation), game theory and elsewhere.

The discipline of statistics has almost entirely been developed in an objectivist spirit, firmly rooted in the frequentist interpretation of probability. Machine learning also in large parts roots in this view. However, a certain subset of machine learning models and computational procedures have a subjectivist component. These techniques are referred to as *Bayesian model estimation* methods. Bayesian modeling is particulary effective and important when training datasets are small. I will explain the principle of Bayesian model estimation with a super-simple synthetic example. A more realistic but also more complex example will be given in a separate subsection.

Consider the general statistical modeling task, here discussed for real-valued random variables only to simplify the notation. A measurement which yields real-valued outcomes (like measuring the speed of a diving falcon) is repeated N times, giving a measurement sequence $x_1, \ldots, x_N$. The ith measurement value is obtained from a RV X_i. These RVs X_i which model the individual measurements are i.i.d. We assume that the distribution of each X_i can be represented by a pdf $p_{X_i} : \mathbb{R} \to \mathbb{R}^{\geq 0}$. The i.i.d. property of the family $(X_i)_{i=1,\ldots,N}$ implies that all these p_{X_i} are the same, and we call that pdf p_X. We furthermore assume that p_X is a parametric pdf, that is, it is a function which is parametrized by a parameter vector θ, for which we often write $p_X(\theta)$. Then, the statistical modeling / machine learning task is to estimate θ from the sample data $x_1, \ldots, x_N$. We have seen that this set-up naturally leads to maximum-likelihood estimation algorithms which need to be balanced with regards to bias-variance using some regularization and cross-validation scheme.

For concreteness let us consider a case where $N = 2$, that is two observations (*only* two!) have been collected, forming a training sample $D = (x_1, x_2) = (0.9, 1.0)$. We assume that the pdf p_X is a normal distribution with unit standard deviation, that is, the pdf has the form $p_X(x) = 1/\sqrt{2\pi}\exp(-(x-\mu)^2/2)$. This leaves the expectation μ as the only parameter, thus $\theta = \mu$. The learning task is to estimate μ from $D = (x_1, x_2) = (0.9, 1.0)$.

The classical frequentist answer to this question is to estimate the μ by the sample mean (which, by the way, is the maximum-likelihood estimator for the expectation μ). That is, one computes

$$\hat{\mu} = \frac{1}{N} \sum_{i=1}^{N} x_i, \tag{89}$$

which in our example gives $\hat{\mu} = (0.9 + 1.0)/2 = 0.95$.

This is the best a classical-frequentist modeler can do. In a certain well-defined sense which we will not investigate, the sample mean is the optimal estimator for the true mean of a real-valued distribution. But "best" is not "good": with only two data points, this estimate is quite shaky. It has a high variance: if one would repeat the observation experiment, getting a new sample x'_1, x'_2, very likely one would obtain a quite different sample and thus an estimate $\hat{\mu}'$ that is quite different from $\hat{\mu}$.

Bayesian model estimation shows a way how to do better. It is a systematic method to make use of *prior knowledge* that the modeler may have beforehand. This prior knowledge takes the form of "beliefs" which parameter vectors θ are more or less plausible. This belief is cast in the form of a probability distribution over the space Θ of possible parameter vectors θ. In our super-simple example let us assume that the modeler knows or believes that

- the true expectation μ can't be negative and it can't be greater than 1.

That's all as far as prior knowledge goes. In the absence of more detailed insight, this belief that the range of μ is limited to $[0, 1]$ is cast in the *Bayesian prior* distribution h:

- the degrees of plausibility for μ are described by the uniform distribution h on $[0, 1]$ (see Figure 46).

This kind of prior knowledge is often available, and it can be quite weak (as in our example). Abstracting from our example, this kind of knowledge means to fix a "belief profile" (in the mathematical format of a probability distribution) over the space Θ of possible parameters θ for a model family. In our mini-example the modeler felt confident to restrict the possible range of the single parameter $\theta_1 = \mu$ to the interval $[0, 1]$, with a uniform (= non-committing) distribution of "belief" over this interval.

Before I finish the treatment of our baby example, I will present the general schema of Bayesian model estimation.

To start the Bayesian model estimation machinery, available prior knowledge about parameters θ is cast into the form of a distribution over parameter space. For a K-parametric pdf p_X, the parameter space is $\mathbb{R}^K$. Two comments:

- The distribution for model parameters θ is not a distribution in the classical sense. It is not connected to a random variable and does not model a real-world outcome of observations. Instead it captures subjective beliefs that the modeler has about how the true distribution P_{X_i} of data points *should* look like. It is here that subjectivistic aspects of "probability" intrude into an otherwise classical-frequentist picture.

- Each parameter vector $\theta \in \mathbb{R}^K$ corresponds to one specific pdf $p_X(\theta)$, which in turn represents one possible candidate distribution $\hat{P}_X$ for empirical observation values x_i. A distribution over parameter vectors $\theta \in \mathbb{R}^K$ is thus a distribution over distributions. It is called a *hyperdistribution*.

In order to proceed with our discussion of general principles, we need to lift our view from the pdf's $p_{X_i}(\theta)$, which model the distribution of single data points, to the the N-dimensional pdf $p_{\bigotimes X_i} : \mathbb{R}^N \to \mathbb{R}^{\geq 0}$ for the distribution of the product RV $\bigotimes_i X_i$. It can be written as

$$p_{\bigotimes X_i}((x_1, \ldots, x_N)) = p_{X_1}(x_1) \cdot \ldots \cdot p_{X_N}(x_N). \tag{90}$$

or in another notation (observing that all pdfs p_{X_i} are identical, so we can use the generic RV X with $p_X = p_{X_i}$ for all i), as

$$p_{\bigotimes_i X}((x_1, \ldots, x_N)) = \prod_i p_X(x_i). \tag{91}$$

We write $p_{\bigotimes_i X}(D \mid \theta)$ to denote the pdf value $p_{\bigotimes_i X}(\theta)((x_1, \ldots, x_N)) = p_{\bigotimes_i X}(\theta)(D)$ of $p_{\bigotimes_i X}(\theta)$ on a particular training data sample D.

Summarizing:

- The pdf $h(\theta)$ encodes the modeler's prior beliefs about how the parametrized distribution $p_X(\theta)$ should look like. Parameters θ where $h(\theta)$ is large correspond to data distributions that the modeler a priori finds more plausible. The distribution represented by $h(\theta)$ is a hyperdistribution and it is often called the (*Bayesian*) *prior*.

- If θ is fixed, $p_{\bigotimes_i X}(D \,|\, \theta)$ can be seen as a function of data vectors D. This function is a pdf over the training sample data space. For each possible training sample $D = (x_1, \ldots, x_N)$ it describes how probable this particular outcome is, assuming the true distribution of X is $p_X(\theta)$.

- If, conversely, D is fixed, then $p_{\bigotimes_i X}(D \,|\, \theta)$ can be seen as a function of θ. Seen as a function of θ, $p_{\bigotimes_i X}(D \,|\, \theta)$ is *not* something like a pdf over θ-space. Its integral over θ will not usually be one. Seen as a function of θ, $p_{\bigotimes_i X}(D \,|\, \theta)$ is called a *likelihood function* — given data D, it reveals certain models θ as being more likely than others. A model (characterized by θ) "explains" given data D better if $p_{\bigotimes_i X}(D \,|\, \theta)$ is higher. We have met the concept of a likelihood function before in Section 7.3.1.

We thus have two sources of information about the sought-after, unknown true distribution $p_X(\theta)$: the likelihood $p_{\bigotimes_i X}(D \,|\, \theta)$ of θ given data, and the prior plausibility encoded in $h(\theta)$. These two sources of information are independent of each other: the prior plausibility is settled by the modeler *before* data have been observed, and should not be informed by data. Because the two sources of information come from "independent" sources of information (belief and data), it makes sense to combine them by multiplication and consider the product

$$p_{\bigotimes_i X}(D \,|\, \theta)\ h(\theta).$$

This product combines the two available sources of information about the sought-after true distribution $p_X(\theta)$. When data D are given, this product is a function of model candidates θ. High values of this product mean that a candidate model θ is a good estimate, low values mean it's bad — in the light of both observed data and prior assumptions.

With fixed D, the product $p_{\bigotimes_i X}(D \,|\, \theta)\ h(\theta)$ is a non-negative function on the K-dimensional parameter space $\theta \in \mathbb{R}^K$. It will not in general integrate to unity and thus is not a pdf. Dividing this product by its integral however gives a pdf, which we denote by $h(\theta \,|\, D)$:

$$h(\theta \,|\, D) = \frac{p_{\bigotimes_i X}(D \,|\, \theta)\ h(\theta)}{\int_{\mathbb{R}^K} p_{\bigotimes_i X}(D \,|\, \theta)\ h(\theta)\ d\theta} \tag{92}$$

The distribution on model parameter space represented by the pdf $h(\theta|D)$ is called the *posterior distribution* or simply the *posterior*. The formula (92) shows how Bayesians combine the subjective prior $h(\theta)$ with empirical information $p_{\bigotimes_i X}(D|\theta)$ to get a posterior distribution over candidate models. Comments:

- The posterior distribution $h(\theta \,|\, D)$ is the final result of a Bayesian model estimation procedure. It is a *probability distribution over candidate models*, which is a richer and often a more useful thing than the single model that is the result of a classical frequentist model estimation (like the sample mean from Equation 89).

- Here I have considered real-valued distributions that can be represented by pdfs throughout. If some of the concerned distributions are discrete or cannot be represented by pdfs for some reason, one gets different versions of (92).

- If one wishes to obtain a single, definite model estimate from a Bayesian modeling exercise, a typical procedure is to compute the mean value of the posterior. The resulting model $\hat{\theta}$ is called the *posterior mean estimate*

$$\hat{\theta} = \theta^{\mathsf{PME}} = \int_{\mathbb{R}^K} \theta \; h(\theta \,|\, D) \; d\theta.$$

- Compared to classical-frequentist model estimation, generally Bayesian model estimation procedures are computationally more expensive and also more difficult to design properly, because one has to invest some thinking into good priors. With diligently chosen priors, Bayesian model estimates may give far better models than classical-frequentist ones, especially when sample sizes are small.

- If one abbreviates the normalization term $\int_{\mathbb{R}^K} p_{\bigotimes_i X}(D \,|\, \theta) \; h(\theta) \; d\theta$ in (92) as $p(D)$ ("probability density of seeing data D, averaged over candidate model parameters θ"), the formula (92) looks like a version of Bayes' rule:

$$h(\theta \,|\, D) = \frac{p_{\bigotimes_i X}(D \,|\, \theta) \; h(\theta)}{p(D)}, \tag{93}$$

  which is why the this entire approach is called "Bayesian". Note that while Bayes' rule is a *theorem* that can be proven from the axioms of classical probability theory, (93) is a *definition* (of $h(\theta \,|\, D)$).

- A note on terminology. There exists a family of models in machine learning named *Bayesian networks*. This name does not imply that Bayesian networks are estimated from data using "subjectivist" Bayesian statistics. Bayesian networks are parametrized models and their parameter vectors can be estimated with classical frequentist *or* with Bayesian methods.

Let us conclude this section with a workout of our simple demo example. For the given sample $D = (0.9, 1.0)$, the likelihood function becomes

$$\begin{aligned} p_{\bigotimes_i X}(D \,|\, \mu) &= \frac{1}{\sqrt{2\pi}} \exp\left(\frac{-(0.9-\mu)^2}{2}\right) \cdot \frac{1}{\sqrt{2\pi}} \exp\left(\frac{-(1.0-\mu)^2}{2}\right) \\ &= \frac{1}{2\pi} \exp\left(-0.905 + 1.9\,\mu - \mu^2\right) \end{aligned}$$

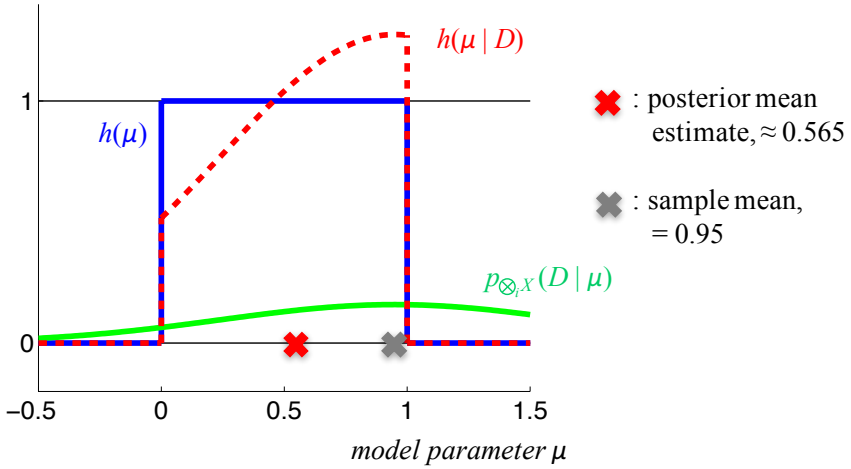

Figure 46: Bayesian model estimation. Compare text.

The green line in Figure 46 gives a plot of $p_{\bigotimes_i X}(D \mid \mu)$, and the red broken line a plot of the posterior distribution $h(\mu \mid D)$. A numerical integration of $\int_{\mathbb{R}} \mu \; h(\mu \mid D) \; d\mu$ yields a posterior mean estimate of $\hat{\theta} \approx 0.565$. This is quite different from the sample mean 0.95, revealing the strong influence of the prior distribution on possible models.

8.3 Case study: modeling proteins

I will now discuss in some detail an elementary modeling task that is easily stated and ubiquitously met in practical applications — yet it needs a surprisingly subtle treatment if training data are scarce.

In as general formulation, the task is to estimate a probability mass function for a finite, discrete distribution, given a histogram from a sample.

For example, one might want to estimate the probabilities that a coin comes up with head or tail after tossing (formally modeled by a RV X). Tossing the coin 100 times gives a histogram over the two symbolic measurement outcomes `H` and `T`, say, (55, 45). Based on these training data, one wants to estimate the probabilities $P(X = \mathtt{H})$ and $P(X = \mathtt{T})$. A maximum likelihood estimate is the pmf $\hat{p} = (P(X = \mathtt{H}), P(X = \mathtt{T}))' = (0.55, 0.45)'$. Easy and obvious.

But things become not-so-easy and non-obvious when the number of symbolic categories is large and the number of available observations is small. I will highlight this with an example taken from a textbook of bioinformatics (Durbin et al. 2000).

Proteins are sequences of amino acids, of which there are 20 different ones which occur in proteins. They are standardly tagged by 20 capital symbols, giving an alphabet $S = \{\mathtt{A}, \mathtt{C}, \mathtt{D}, ..., \mathtt{Y}\}$, intimately familiar to biologists. Proteins come in classes. Some protein in one animal or plant species has typically close relatives in other species. Related proteins differ in detail but generally can be *aligned*, that

is, corresponding sites in the amino acid string can be detected, put side by side, and compared. For instance, consider the following short section of an alignment of 7 amino acids, all from the class of "globuline" proteins:

```
...GHGK...
...AHGK...
...KHGV...
...THAN...
...WHAE...
...AHAG...
...ALGA...
```

A basic task in bioinformatics is to estimate the probability distribution of the amino acids in each column in a protein class. These 20-dimensional pmf's (one for each site in the protein) are needed for deciding whether some newly found protein belongs into the class — that is, for carrying out protein classifications, a fundamental and bulk-volume task in bioinformatics.

This task is rendered difficult by the fact that the sample of aligned proteins used to estimate these pmf's is typically rather small — here we have only 7 individuals in the sample. As can be seen in the segment of the alignment shown above, some columns have widely varying entries (e.g. the last column has `K K V N E G A`). In such a small sample, chances are high that an amino acid, which is generally rare at a given site in the animal/plant kingdom, will not appear in the training data set. The column `K K V N E G A` only features 6 out of 20 possible amino acids; 14 amino acids are missing at this site in the training data.

But the class of related proteins is huge: in every animal species one would expect at least one class member and typically many more — millions of members in the family of globulines! This implies that at every site, every amino acid will occur in *some* species, though maybe with low probability. A low-probability-in-a-specific-site amino acid, call it `X`, will often not be represented in that site's training data. Consequences: (1) a maximum-likelihood estimate of the pmf for that site will assign zero probability to `X` which in turn implies (2), when this model is used for protein classification and a new test protein *does* have `X` in that site, it will turn out that the test protein cannot possibly be a globuline because it has `X` at that site and in globulines the probability for this is zero. This wrong decision will be made for all test proteins which are globulines but happen to host one of the 14 amino acids not in the training set on that site. Since there are many sites in a protein (dozens to hundreds), chances are high for any test sequence to have a zero-probability amino-acid in some site. Most of the test sequences which are, in fact, globulines, would be rejected.

Thus, maximum likelihood estimates of pmf's for sites of proteins cannot be used. A Bayesian approach is mandatory.

The following lengthy derivations show how the general formula (93) for Bayesian

model estimation is worked out in the case of amino acid distribution estimation.

The 20-dimensional pmf for the amino acid distribution at a given site is characterized by a 20-dimensional parameter vector

$$\theta = (\theta_1, \ldots, \theta_{20})' = (P(X = \mathtt{A}), \ldots, P(X = \mathtt{Y})'$$

(actually 19 parameters would be enough — why?).

We start with the probability of observed data, given that the true distribution is θ. This corresponds to the pdf factor $p_{\bigotimes_i X}(D \,|\, \theta)$ in (93), but here we have discrete counting data and hence use a probability instead of a pdf. The observation data D consist in counts $n_1, \ldots, n_{20}$ of the different amino acids found at a given site in the training population. These count vectors are distributed according to the *multinomial distribution*

$$P(D \,|\, \theta) = \frac{N!}{n_1! \cdots n_{20}!} \prod_{j=1}^{20} \theta_j^{n_j}, \tag{94}$$

where $N = n_1 + \ldots + n_{20}$ is the total number of observations.

Next we turn to the Bayesian prior $h(\theta)$ in (93). The "subjective" background knowledge which is inserted into the picture is the general belief held by biologists that every amino acid *can* appear in any site in a protein of a given class, though maybe with small probability.

The Bayesian prior which reflects the biologists' insight that zero probabilities should not occur in θ is expressed in a hyperdistribution over the hypothesis space $\mathcal{H}$ of possible θ vectors. $\mathcal{H}$ is the subset of $\mathbb{R}^{20}$ which contains all positive vectors whose components sum to one:

$$\mathcal{H} = \{(\theta_1, \ldots, \theta_{20})' \in \mathbb{R}^{20} \mid \theta_j \in (0, 1) \text{ and } \sum_j \theta_j = 1\}.$$

This is a 19-dimensional hypervolume in $\mathbb{R}^{20}$ (try to imagine its shape — impossible for $\mathbb{R}^{20}$, but you can do it for embedding spaces $\mathbb{R}^2, \mathbb{R}^3, \mathbb{R}^4$).

$\mathcal{H}$ is a continuous space, thus a Bayesian prior distribution on $\mathcal{H}$ can be represented by a pdf. But which distribution makes a reasonable prior? For reasons that will become clear later, one uses the *Dirichlet* distribution. The Dirichlet distribution is parametrized itself, with (in our case) a 20-dimensional parameter vector $\alpha = (\alpha_1, \ldots, \alpha_{20})'$ (where all α_i are positive reals). The Bayesian prior pdf $h(\theta|\alpha)$ of the Dirichlet distribution with parameters α is defined as

$$h(\theta|\alpha) = \frac{1}{Z(\alpha)} \prod_{j=1}^{20} \theta_j^{\alpha_j - 1}, \tag{95}$$

where $Z(\alpha) = \int_{\mathcal{H}} \prod_{j=1}^{20} \theta_j^{\alpha_j - 1} \, d\theta$ is the normalization constant which ensures that the integral of h over $\mathcal{H}$ is one.

Finally, the normalization denominator $p(D)$ in (93) need not be analyzed in more detail because it will later cancel out.

Now we have everything together to calculate the Bayesian posterior distribution on $\mathcal{H}$:

$$\begin{aligned} p(\theta \mid D, \alpha) &= \frac{P(D \mid \theta)\, h(\theta|\alpha)}{p(D)} \\ &= \frac{1}{p(D)} \frac{N!}{n_1! \cdots n_{20}!} \prod_{j=1}^{20} \theta_j^{n_j} \frac{1}{Z(\alpha)} \prod_{j=1}^{20} \theta_j^{\alpha_j - 1} \\ &= \frac{1}{p(D)} \frac{N!}{n_1! \cdots n_{20}!} \frac{1}{Z(\alpha)} \prod_{j=1}^{20} \theta_j^{n_j + \alpha_j - 1} \\ &= \frac{1}{p(D)} \frac{N!}{n_1! \cdots n_{20}!} \frac{Z(D+\alpha)}{Z(\alpha)} h(\theta \mid D + \alpha), \end{aligned} \tag{96}$$

where $D + \alpha = (n_1 + \alpha_1, \ldots, n_{20} + \alpha_{20})'$. Because both $p(\theta \mid D, \alpha)$ and $h(\theta \mid D + \alpha)$ are pdfs, the product of the three first factors in (96) must be one, hence the posterior distribution of models θ is

$$p(\theta \mid D, \alpha) = h(\theta \mid D + \alpha). \tag{97}$$

In order to get the posterior mean estimate, we integrate over the model candidates θ with the posterior distribution. I omit the derivation (can be found in Durbin et al. 2000) and only report the result:

$$\theta_j^{\mathsf{PME}} = \int_{\mathcal{H}} \theta_i \; h(\theta \mid D + \alpha) \; d\theta = \frac{n_j + \alpha_j}{N + A}, \tag{98}$$

where $N = n_1 + \cdots n_{20}$ and $A = \alpha_1 + \cdots + \alpha_{20}$. If one compares this to the maximum-likelihood estimates

$$\theta_j^{\mathsf{ML}} = \frac{n_j}{N}, \tag{99}$$

we can see that the α_j parameters of the Dirichlet distribution can be understood as "pseudo-counts" that are added to the actually observed counts. These pseudocounts reflect the subjective intuitions of the biologist, and there is no formal rule of how to set them correctly.

Adding the α_j pseudocounts in (98) can also be considered just as a regularization tool in a frequentist setting. One would skip the Bayesian computations that give rise to the Bayesian posterior (97) and directly use (98), optimizing α to navigate on the model flexibility scale in a cross-validation scheme. With α set to all zero, one gets the maximum-likelihood estimate (99) which will usually be overfitting; with large values for α one smoothes out the information contained in the data — underfitting.

You may ask, why go through all this complex Bayesian thinking and calculating, and not just do a regularized maximum-likelihood estimation with a solid

K-fold cross-validation scheme to get the regularizers α_j's right? The reason is that the two methods will not give the same results, although both ultimately use the same formula $\hat{\theta}_j = \frac{n_j+\alpha_j}{N+A}$. But: in the frequentist, regularized, maximum-likelihood approach, the *only information* that is made use of is the data D, which is scarce and the careful cross-validation will merely make sure that the estimated model $\hat{\theta} = \theta^{\mathsf{ML}}$ will be the best (with regards to not over- or underfitting) among the ones that can be estimated from D. In contrast, a Bayesian modeler inserts *additional information* by fixing the α_j's beforehand. If the Bayesian modeler has the right intuitions about these α_j's, the found model $\hat{\theta} = \theta^{\mathsf{PME}}$ will generalize better than θ^{ML}, possibly *much* better.

The textbook of Durbin et al, from which this example is taken, shares some thoughts on to how a biosequence modeler should select the pseudo-counts. The proper investment of such soft knowledge makes all the difference in real-life machine learning problems.

8.4 Terminology

I conclude this section with a brief summary:

The objectivistic view sees probabilities as measurable properties of physical systems. This *frequentist* view is the classical view represented in mathematics textbooks. "Frequentist" and "objectivistic" are more or less synonymous. Its deep-rooting anchor is the Law of Large Numbers. There is one commonly accepted set of axioms for frequentist probability theory, the Kolmogorov axioms.

Subjectivistic views cast probability as degrees of belief or confidence held by a rational reasoning agent when he/she/it makes statements. Rigorous formalizations take the shape of logic-like formalisms, of which there are several. Probability is thus a property of statements — generalizations of the True and False properties in classical logic —, not a property of the reality described by statements. Such logic system are not taught to mathematicians and also not to psychology students in their dreaded statistics courses. Students of philosphy will hear about them (or they should at least), and students of AI and linguistics are likely to learn a little about them. The Kolmogorov axioms can be *derived* in most subjectivist-probabilistic logic systems, sometimes in somewhat weaker versions. When it comes to calculation rules, there is thus much agreement between objectivist and subjectivist accounts of probability.

Bayesian statistics (or Bayesian modeling) can be seen as a very special case of subjectivist probability. Bayesian modeling does not appear in the format of a logic-like calculus. It has developed into an bundle of very useful algorithmic techniques in machine learning. The subjectivist-philosophical

heritage has been more or less been lost from sight. The link to the subjectivist philosophical attitude is the way how the modeler's private beliefs are inserted into the model estimation via hyperdistributions — the "Bayesian priors". Furthermore, prominent current modeling approaches in the cognitive and neurosciences posit that human cognitive processing (Clark 2013; Tenenbaum, Griffiths, and Kemp 2006) and even the brain "hardware" (Friston 2003) are organized in hierarchies of Bayesian priors.

9 Sampling algorithms

Many tasks that arise in machine learning (and in mathematical modeling of complex systems in general) require one to "draw" random samples from a probability distribution. Algorithms which compute "random" samples from a distribution are needed, for instance (very incomplete listing),

- when *noise* is needed, e.g. for regularization of learning algorithms,
- when *ensembles* of models are computed for better accuracy and generalization (as in random forests),
- generally, when natural or social or economical systems are *simulated*,
- when certain stochastic *neural network* models are trained and exploited (Hopfield networks, Boltzmann machines).

Sampling algorithms are an essential "fuel" which powers many modern computational techniques. Entire branches of physics, chemistry, biology (and meteorology and economics and ...) could only grow after efficient sampling algorithms became available.

Designing algorithms which produce (pseudo-) random numbers from a given distribution are not easy to design. Even something that looks as elementary as sampling from the uniform distribution — with pseudo-random number generating algorithms — becomes mathematically and algorithmically involved if one wants to do it well.

In this section I describe a number of design principles for sampling algorithms that you should know about.

9.1 What is "sampling"?

"Sampling" means to artificially simulate the process of randomly taking measurements from a distribution given by a pmf or pdf. A "sampler" is an algorithm for doing this. Of samplers there are many, and I am not aware of a universally agreed definition. Here is my own definition (only for the ones of you with probability theory background; will not be asked in exams):

Definition 9.1 *Let P_X be a distribution on a measure space $(E, \mathcal{B})$. A sequence $X_1, X_2, \ldots$ of random variables is a* sampler *for P_X, if for all $A \in \mathcal{B}$*

$$P_X(A) = \lim_{N\to\infty} \frac{1}{N} \sum_{i=1}^{N} 1_A \circ X_i \qquad P\text{-almost surely,}$$

where 1_A is the indicator function for A.

The notion of a sample must be clearly distinguished from the notion of a sampler. A "sample" is more often than not implied to be an "i.i.d. sample", that is, it results from independent random variables $X_1, \ldots, X_N$ that all have the same distribution as X, the random variable whose distribution P_X the sample is drawn from. This i.i.d. assumption is standardly made for real-world training data.

In contrast, the random variables $X_1, X_2, \ldots$ of a "sampler" for P_X need not individually have the same distribution as X, and they need not be independent. For instance, let P_X be the uniform distribution on the binary event space $E = 0, 1$, that is, $P(X = 1) = P(X = 0) = 1/2$. Here are some samplers:

- All X_i are i.i.d. with each of them being uniformly distributed on $[0, 1]$. This is a dream of a sampler...
- The subset X_{2i} of RVs with even indices are identically and uniformly distributed on $[0, 1]$. The RVs X_{2i+1} repeat the value of X_{2i}. Here the RVs X_i are identically but not independently distributed.
- The subset X_{2i} of RVs with even indices are identically and uniformly distributed on $[0, 1/2]$ and the subset of X_{2i+1} are identically and uniformly distributed on $[1/2, 1]$. Here the RVs X_i are independently but not identically distributed.
- X_1 is always evaluating to 0, and the other X_i are inductively and deterministically defined to give the value $x_i = x_{i-1} + \sqrt{2} \pmod 1$. This is a deterministic sequence.
- Let Y_i be an i.i.d. sequence where each Y_i draws a value y_i from $\mathcal{N}(0, 1)$, and let ε be a small positive real number. X_1 is always evaluating to 0, and following X_i are inductively and stochastically defined by $x_i = x_{i-1} + \varepsilon\, y_i \pmod 1$. This gives a *random walk* (more specifically, a *Brownian motion* process) whose paths are slowly and randomly migrating across $[0, 1]$. This kind of samplers will turn out to be the most important type when it comes to sampling from complex distributions — this is a *Markov chain Monte Carlo* (MCMC) sampler.

9.2 Sampling by transformation from the uniform distribution

There is one sampler that you know very well and have often used: the random function that comes by different names in different programming languages (and is internally implemented in many different ways). In Matlab it is called `rand`, which draws a random double-precision number from the continuous, uniform distribution over the interval $[0, 1]$; in C it's also called `rand` but here generates a

random integer from the discrete uniform distribution between 0 and some maximal value. At any rate, a *pseudo-random number generator* of almost uniformly distributed numbers over some interval is offered by every programming language that I know, including Microsoft Word. And that's about it; the only sampler you can directly call in most programming environments is just that, a uniform sampler.

By the way, it is by no means easy to program a good pseudo-random number generator – in fact, designing such generators is an active field of research. If you are interested – the practical guide to using pseudorandom number generators by Jones 2010 is fun to read and very illuminating.

Assume you have a sampler U_i for the uniform distribution on $[0,1]$, but you want to sample from another distribution P_X on the measure space $E = \mathbb{R}$, which has a pdf $f(x)$. Then you can use the sampler U_i indirectly to sample from P_X by a *coordinate transformation*, as follows.

First, compute the cumulative density function $\varphi : \mathbb{R} \to [0,1]$, which is defined by $\varphi(x) = \int_{-\infty}^{x} f(u)\,du$, and its inverse φ^{-1}. The latter may be tricky or impossible to do analytically – then, numerical approximations must be used. Now obtain a sampler X_i for P_X from the uniform sampler U_i by

$$X_i = \varphi^{-1} \circ U_i.$$

Here is a brief proof why X_i indeed samples from P_X. Let $A = [a,b]$ be an interval on the real line. We have to show that

$$P_X(A) = \lim_{N\to\infty} \frac{1}{N} \sum_{i=1}^{N} 1_A \circ X_i = \lim_{N\to\infty} \frac{1}{N} \sum_{i=1}^{N} 1_A \circ \varphi^{-1} \circ U_i.$$

This follows from

$$\lim_{N\to\infty} \frac{1}{N} \sum_{i=1}^{N} 1_A \circ \varphi^{-1} \circ U_i = \lim_{N\to\infty} \frac{1}{N} \sum_{i=1}^{N} 1_{\varphi(A)} \circ U_i = P_U\varphi(A) = P_X(A).$$

Figure 47 illustrates this.

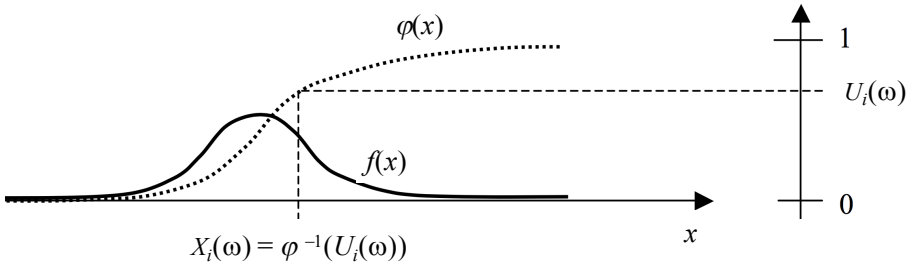

Figure 47: Sampling by transformation from the uniform distribution.

The remainder of this subsection is optional reading and will not be tested in exams.

Out of curiosity, I explored a little bit how one can sample from the standard normal distribution $\mathcal{N}(0,1)$. Computing it by transformation from the uniform distribution, as outlined above, appears not to be done because the inverse cumulative density function φ^{-1} for $\mathcal{N}(0,1)$ can only be represented through a power series which converges slowly (my source, I must confess, is Wikipedia). Instead, special algorithms have been invented for sampling from $\mathcal{N}(0,1)$, which exploit mathematical properties of this distribution. One algorithm (see `http://en.wikipedia.org/wiki/Normal_distribution#Generating_values_for_normal_random_variables`) which I found very elegant is the *Box-Muller algorithm*, which produces a $\mathcal{N}(0,1)$ distributed RV C from *two* independent uniform-[0,1]-distributed RVs A and B:

$$C = \sqrt{-2\,\ln A}\,\cos(2\,\pi\,B).$$

The computational cost is to compute a logarithm and a cosine. An even (much) faster, but more involved (and very tricky) method is the *Ziggurat algorithm* (check Wikipedia for "Ziggurat_algorithm" for an article written with tender care). All in all, there exist wonderful things under the sun.

Sampling by coordinate transformation can be generalized to higher-dimensional distributions. Here is the case of a 2-dimensional pdf $f(x_1, x_2)$, from which the general pattern should become clear. First define the cumulative density function in the first dimension as the cumulative density function of the marginal distribution of the first coordinate x_1

$$\varphi_1(x_1) = \int_{-\infty}^{x_1} \left(\int_{-\infty}^{\infty} f(u,v)\,dv \right) du$$

and the conditional cumulative density function on x_2 given x_1

$$\varphi_2(x_2 \,|\, x_1) = \frac{\int_{-\infty}^{x_2} f(x_1,v)\,dv}{\int_{-\infty}^{\infty} f(x_1,v)\,dv}.$$

Then, for sampling one value (x_1, x_2), sample two values u_1, u_2 from the uniform sampler U, and transform

$$x_1 = \varphi_1^{-1}(u_1), \quad x_2 = \varphi_2^{-1}(u_2 \,|\, x_1).$$

A widely used method for drawing a random vector $\mathbf{x}$ from the n-dimensional multivariate normal distribution with mean vector μ and covariance matrix Σ works as follows:

1. Compute the Cholesky decomposition (matrix square root) of Σ, that is, find the unique lower triangular matrix A such that $A\,A' = \Sigma$.

2. Sample n numbers $z_1, \ldots, z_n$ from the standard normal distribution.

3. Output $\mathbf{x} = \mu + A(z_1, \ldots, z_n)'$.

9.3 Rejection sampling

Sampling by transformation from the uniform distribution can be difficult or impossible if the pdf f one wishes to sample from has no simple-to-compute cumulative density function, or that has no simple-to-compute inverse. If this happens, it is sometimes possible to sample from a simpler distribution with pdf g that is related to the target pdf f and for which sampling by transformation works, and by a simple trick end up with a sampler for the pdf of interest, f. To understand this *rejection sampling* (also known as *importance sampling* we first need to generalize the notion of a pdf:

Definition 9.2 *A* proto-pdf *on* $\mathbb{R}^n$ *is any nonnegative function* $g_0 : \mathbb{R}^n \to \mathbb{R}$ *with a finite integral* $\int_{\mathbb{R}^n} g_0(\mathbf{x})\, d\mathbf{x}$.

If one divides a proto-pdf g_0 by its integral, one obtains a pdf g. Now consider a pdf f on $\mathbb{R}^n$ that you want to sample from, but sampling by transformation doesn't work. However, you find a proto-pdf $g_0 \geq f$ for whose associated pdf g you know how to sample from, that is, you have a sampler for g. With that in your hands you can construct a sampler X_i for f as follows. In order to generate a random value x for X_i, carry out the following procedure:

Initialize: set `found_x` $= 0$

While `found_x` $== 0$ **do**

1. sample a *candidate* $\tilde{x}$ from g.
2. with probability $f(\tilde{x})/g_0(\tilde{x})$, *accept* $\tilde{x}$; otherwise, *reject* $\tilde{x}$.

   If $\tilde{x}$ is accepted
   (a) set `found_x` $= 1$
   (b) return $\tilde{x}$

Rejection sampling becomes immediately clear if you re-conceptualize "sampling from a pdf f" as "piling up the pdf by many grains of sand that you let fall at the various positions x of $\mathbb{R}^n$ with a frequency proportional to $f(x)$". Look at Figure 48 where g_0 and f are plotted. Think of the g_0 curve as a sand dune that you get when sampling for g in this sand metaphor. Now, when you drop a grain of sand for modelling the g_0 "sand curve", imagine you paint it orange with a probability of $f(\tilde{x})/g_0(\tilde{x})$ before you let it fall down. I think this saves you a mathematical proof.

The computational efficiency of rejection sampling clearly depends on how close g_0 is to f. If the ratio f/g_0 is on average small, there will be many rejections which slow down the algorithm. In high-dimensional spaces it is often quite difficult to avoid this.

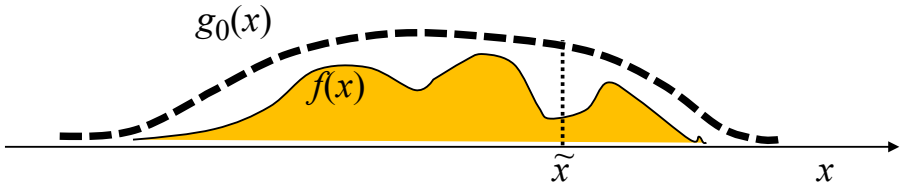

Figure 48: The principle of rejection sampling. Candidates $\tilde{x}$ are first sampled from g, then accepted ("painted orange") with probability $f(\tilde{x})/g_0(\tilde{x})$.

9.4 Proto-distributions

The pdf's of parametrized continuous distributions over $\mathbb{R}^k$ are typically represented by a formula of the kind

$$p(\mathbf{x} \,|\, \theta) = \frac{1}{\int_{\mathbb{R}^k} p_0(\mathbf{x} \,|\, \theta)\, d\mathbf{x}}\, p_0(\mathbf{x} \,|\, \theta), \tag{100}$$

where $p_0 : \mathbb{R}^k \to \mathbb{R}^{\geq 0}$ defines the shape of the pdf and the factor $1/(\int_{\mathbb{R}^k} p_0(\mathbf{x} \,|\, \theta)\, d\mathbf{x})$ normalizes p_0 to integrate to 1. For example, in the pdf

$$p(\mathbf{x} \,|\, \mu, \Sigma) = \frac{1}{(2\pi)^{k/2}\, \det(\Sigma)^{1/2}}\, \exp\left(-\frac{1}{2}(\mathbf{x}-\mu)'\, \Sigma^{-1}(\mathbf{x}-\mu)\right)$$

for the multidimensional normal distribution, the shape is given by $p_0(\mathbf{x}|\mu, \Sigma) = \exp\left(-\frac{1}{2}(\mathbf{x}-\mu)'\, \Sigma^{-1}(\mathbf{x}-\mu)\right)$ and the normalization prefactor $1/((2\pi)^{k/2}\, \det(\Sigma)^{1/2})$ is equal to $1/\int_{\mathbb{R}^k} p_0(\mathbf{x} \,|\, \mu, \Sigma)\, d\mathbf{x}$.

It is a quite general situation in machine learning that a complex model of a distribution is only known up to an undetermined scaling factor — that is, one has a proto-distribution but not a distribution proper. This is often good enough. For instance, in our initial TICS demo (Section 1.2.1), we saw that the TICS system generated a list of captions, ordered by plausibility. In order to produce this list, the TICS system did not need to command on a proper probability distribution on the space of possible captions — a proto-distribution is good enough to determine the best, second-best, etc. caption.

Proto-distributions are not confined to continuous distributions on $\mathbb{R}^k$, where they appear as proto-pdf's. In discrete sample spaces $S = \{s_1, \ldots, s_N\}$ or $S = \{s_1, s_2, \ldots,\}$ where the distribution is given by a parametrized pmf $p(\theta)$, the normalization factor becomes a sum over S:

$$p(x \,|\, \theta) = \frac{1}{\sum_{s \in S} p_0(s)}\, p_0(x),$$

where again $p_0 : S \to \mathbb{R}^{\geq 0}$ is a shape-giving function which must have a finite sum. When S is large and p_0 is analytically intractable, the normalization factor $1/\sum_{s \in S} p_0(s)$ cannot be computed and one is limited to work with the proto-pmf

p_0 only. Very large S appear standardly in systems which are modeled by many interacting random variables. We will meet with such proto-pmf's in the next section on graphical models.

This is also a good moment to mention the *softmax* function. This is a ubiquitously used machine learning trick to transform any vector $\mathbf{y} = (y_1, \ldots, y_n)' \in \mathbb{R}^n$ into an n-dimensional probability vector $\mathbf{p}$ by

$$\mathbf{p} = \frac{1}{\sum_{i=1,\ldots,n} \exp(\alpha\, y_i)}\, (\exp(\alpha\, y_1), \ldots, \exp(\alpha\, y_n))'.$$

The softmax is standardly used, for instance, to transform the output vector of a neural network into a probability vector, which is needed when one wants to interpret the network output probabilistically.

The factor $\alpha \geq 0$ determines the entropy of the resulting probability vector. If $\alpha = 0$, $\mathbf{p}$ is the uniform distribution on $\{1, \ldots, n\}$, and in the limit $\alpha \to \infty$, $\mathbf{p}$ becomes the binary vector which is zero everywhere except at the position i where $\mathbf{y}$ is maximal.

Notes:

1. The word "proto-distribution" is not in general use and can be found in the literature only rarely.

2. Proto-distributions occur always in Bayesian modeling (compare Section 8.3, Equation 96). The Bayesian posterior distribution $p(\theta \,|\, D)$ is shaped by the product $P(D \,|\, \theta)\, h(\theta)$, whose integral will not usually be one. The functions $P(D \,|\, \theta)\, h(\theta)$ are proto-distributions on θ-space.

3. Many algorithms exist that allow sampling from proto-distributions, without the need of normalizing them. Rejection sampling is a point in case, but also the Gibbs and Metropolis sampler presented below work with proto-pdfs. The case study in Section 9.6 crucially relies on sampling from a proto-pdf.

4. There exists a large and important class of probability distributions on generic sample spaces S which are defined by an *energy function* $E : S \to \mathbb{R}^{\geq 0}$, or more generally, by a *cost function* $C : S \to \mathbb{R}$. In *energy-based models of probability distributions*, such an energy or cost function is turned into a probability distribution on S by defining the *Boltzmann distribution* which has the pdf

$$p(s \,|\, T) = \frac{1}{\int_S \exp(-C(s)/T)\, ds}\, \exp(-C(s)/T), \tag{101}$$

where T is a *temperature* parameter. In this context, the normalization factor $\frac{1}{\int_S \exp(-C(s)/T)\, ds}$ is often written as $1/Z(T)$, and $Z(T)$ is called the *partition function* of the distribution. The notation $1/Z(\theta)$ and the name "partition function" are sometimes also used in a generalized fashion for

other distributions given by a shape-defining proto-pdf. Boltzmann distributions are imported from statistical physics and thermodynamics, where they play a leading role. In machine learning, Boltzmann distributions occur, for instance, in *Markov random fields* which are a generalization of Markov chains to spatial patterns that are used (among other applications) in image analysis. They are a core ingredient for *Boltzmann machines* (Ackley, Hinton, and Sejnowski 1985), a type of neural network which I consider one of the most elegant and fundamental models for general learning systems. A computationally simplified version, *restricted Boltzmann machines*, became the starting point for what today is known as deep learning (Hinton and Salakuthdinov 2006). Furthermore, Boltzmann distributions also are instrumental for *free-energy models* of intelligent agents, a class of models of brain dynamics popularized by Karl Friston (for example, Friston 2005) which explain the emergence of adaptive, hierarchical information representations in biological brains and artificial intelligent "agents", and which today are a mainstream approach in the cognitive neurosciences and cognitive science to understanding adaptive cognition. And last but not least, the Boltzmann distribution is the root mechanism in *simulated annealing* (Kirkpatrick, Gelatt, and Vecchi 1983), a major general-purpose strategy for finding minimal-cost solutions in complex search spaces.

Sadly in this course there is no time for treating energy-based models of information processing. I will present this material in my course on neural networks in the Summer semester (lecture notes remain to be written).

9.5 MCMC sampling

We now turn to Markov Chain Monte Carlo (MCMC) sampling techniques. These samplers are the only choice when one wants to sample from complex distributions of which one only knows a proto-pdf g_0. Inventing MCMC sampling techniques was a breakthrough in theoretical physics because it made it possible to simulate stochastic physical systems on computers. The original article *Equation of state calculations by fast computing machines* (Metropolis et al. 1953) marks a turning point in physics (Wikipedia has an article devoted to this paper). In later decades, MCMC techniques were adopted in machine learning, where today they are used in several places, in particular for working with *graphical models*, which constitute the high-end modeling approach for complex real-world systems that are described by a multitude of interacting RVs. We will get a glimpse of graphical models in the next session of this course. A long tutorial paper (essentially, the PhD thesis) of Radford Neal 1993 was instrumental for establishing MCMC methods for statistical inference applications. This tutorial paper established not only MCMC methods in machine learning, but also established the professional reputation of Radford Neal (`http://www.cs.utoronto.ca/~radford/`). If you ever want to implement MCMC samplers in a serious way, this tutorial is mandatory reading.

And if you want to inform yourself about the use of MCMC in deep learning (advanced stuff), a talk of Radford Neal that he recently delivered in honor of Geoffrey Hinton (Neal 2019) gives you an orientation. And if you think of entering a spectacular academic career, it is not a bad idea to write a PhD thesis which "only" gives the first readable, coherent, comprehensive tutorial introduction to some already existing kind of mathematical modeling method which until you write that tutorial has been documented only in disparate technical papers written from different perspectives and using different notations, thus nobody could really understand or use it.

9.5.1 Markov chains

Before we can start with MCMC we need to refresh some basics of Markov chains.

Definition 9.3 *A* Markov chain *is a sequence of random variables $X_1, X_2, \ldots$, all taking values in the same sample space S, such that X_{n+1} depends only on X_n and is conditionally independent on all earlier values:*

$$P(X_{n+1} = x_{n+1} \,|\, X_1 = x_1, \ldots, X_n = x_n) = P(X_{n+1} = x_{n+1} \,|\, X_n = x_n). \quad (102)$$

Intuitively, a Markov chain is a discrete-time stochastic process which generates sequences of measurements/observations, where the next observation only depends on the current one; earlier observations are "forgotten". Markov chains are "stochastic processes without memory".

Do not confound the notion of a Markov chain with the notion of a *path* (or *realization* or *trajectory*) of a Markov chain. The Markov chain is the generative mechanism which can be "executed" or "run" as often as one wishes, and at every run one will obtain a different concrete sequence $x_1, x_2, \ldots$ of observations. The possible values $x \in S$ are called the *states* of a Markov chain.

A Markov chain on S is fully characterized by the initial distribution P_{X_1} and the conditional *transition distributions*

$$P_n(X_{n+1} = x \,|\, X_n = y) \quad \text{for all } x, y \in S, \quad (103)$$

for which we also write (following Neal's notation)

$$T_n(x \,|\, y). \quad (104)$$

A common name for $T_n(x \,|\, y)$ is *transition kernel*. If $T_n(x|y) = T_{n'}(x|y)$ for all n, n', the Markov chain's transition law does not itself change with time; we then call the Markov chain *homogeneous*. With homogeneous Markov chains, the index n can be dropped from $T_n(x|y)$ and we write $T(x|y)$.

In order to generate a path from a homogeneous Markov chain with initial distribution P_{X_1} and transition kernel $T(x|y)$, one carries out the following recursive procedure:

1. Generate the first value x_1 by a random draw from P_{X_1}.

2. If x_n has been generated, generate x_{n+1} by a random draw from the distribution $P_{X_{n+1}|X_n=x_n}$ which is specified by the transition kernel $T(x|x_n)$.

A note on notation: a mathematically correct and general definition and notation for transition kernels on arbitrary observation spaces S requires tools from measure theory which we haven't introduced. Consider the notation $T(x|y)$ as a somewhat sloppy shorthand. When dealing with discrete distributions where S is finite, say, $S = \{s_1, \ldots, s_k\}$, then consider $T(x|y)$ as a $k \times k$ Markov transition matrix M where $M(i,j) = P(X_{n+1} = s_j \,|\, X_n = s_i)$. The i-th row of M has the vector of the probabilities by which the process will transit from state s_j to the states $s_1, \ldots, s_k$ indexing the columns.

When dealing with continuous distributions of x (given y) which have a pdf, regard $T(x|y)$ as denoting the conditional pdf $p_{X|Y=y}$ of x. Note that when we write $T(x|y)$, we refer not to a single pdf but to a family of pdf's; for every y we have another conditional pdf $T(x|y)$.

If a Markov chain with finite state set $S = \{s_1, \ldots, s_k\}$ and Markov transition matrix M is executed m times, the transition probabilities to transit from state s_i to state s_j can be found in the m-step transition matrix M^m:

$$P(X_{n+m} = s_j \,|\, X_n = s_i) = M^m(i,j), \tag{105}$$

where $M^m = M \cdot M \cdot \ldots \cdot M$ (m times).

We now consider the sample space $S = \mathbb{R}^k$, and assume that all distributions of interest are specified by pdf's. We consider a homogeneous Markov chain. Its transition kernel $T(\mathbf{x}|\mathbf{y})$ can be identified with the pdf $p_{X_{n+1}|X_n=\mathbf{y}}$, and in the remainder of this section, we will write $T(\mathbf{x}|\mathbf{y})$ for this pdf. Such a Markov chain with continuous sample space $\mathbb{R}^k$ is specified by an initial distribution on $\mathbb{R}^k$ which we denote by its pdf $g^{(1)}$. The pdf's $g^{(n+1)}$ of distributions of subsequent RVs X_{n+1} can be calculated from the pdf's $g^{(n)}$ of the preceding RV X_n by

$$g^{(n+1)}(\mathbf{x}) = \int_{\mathbb{R}^k} T(\mathbf{x}|\mathbf{y})\; g^{(n)}(\mathbf{y})\; d\mathbf{y}. \tag{106}$$

Please make sure you understand this equation. It is the key to everything which follows.

For the theory of MCMC sampling, a core concept is an *invariant distribution* of a homogenous Markov chain.

Definition 9.4 *Let g be the pdf of any distribution on $\mathbb{R}^k$, and let $T(\mathbf{x}|\mathbf{y})$ be the (pdf of the) transition kernel of a homogeneous Markov chain with values in $\mathbb{R}^k$. Then g is the pdf of an* invariant distribution of $T(\mathbf{x}|\mathbf{y})$ *if*

$$g(\mathbf{x}) = \int_{\mathbb{R}^k} T(\mathbf{x}|\mathbf{y})\, g(\mathbf{y})\; d\mathbf{y}. \tag{107}$$

Except for certain pathological cases, a transition kernel has generically at least one invariant distribution.

Furthermore, it is often the case that there exists exactly one invariant distribution g of $T(\mathbf{x}|\mathbf{y})$, and the sequence of distributions $g^{(n)}$ converges to g from any initial distribution. We will call the transition kernel $T(\mathbf{x}|\mathbf{y})$ *ergodic* if it has this property. The (unique) invariant distribution g of an ergodic Markov chain is also called its *asymptotic distribution* or its *stationary distribution* or its *equilibrium distribution.*

9.5.2 Constructing MCMC samplers through detailed balance

Let g be the pdf of some (usually very complex) distribution on $\mathbb{R}^k$. The goal is to design an MCMC sampler for g. The core idea is to find a transition kernel $T(\mathbf{x}|\mathbf{y})$ for a homogenous, ergodic Markov chain which has g as its invariant distribution. Then, by of certain deep mathematical theorems (suitable versions of *ergodic theorems*), which we will not endeavour to explain, the Markov chain will be a sampler for g.

There will be many different ways to design such a transition kernel. However, they will differ from each other with regards to computational cost. Quoting from the Neal's survey,

"The amount of computational effort required to produce a good Monte Carlo estimate using the states generated by a Markov chain will depend on three factors: first, the amount of computation required to simulate each transition; second, the time for the chain to converge to the equilibrium distribution, which gives the number of states that must be discarded from the beginning of the chain; third, the number of transitions needed to move from one state drawn from the equilibrium distribution to another state that is almost independent, which determines the number of states taken from the chain at equilibrium that are needed to produce an estimate of a given accuracy. The latter two factors are related..."

A brief explanation: The best possible sampler for g would be one where each new sampled value is independent from the previous ones — in other words, one would like to have an i.i.d. sampler. If observations x_n obtained from a sampler depend on previous observations x_{n-d}, there is redundant information in the sample path. But the paths $(x_n)_{n=1,2,\ldots}$ obtained from running an MCMC sampler will have more or less strong dependencies between subsequent values. The initial values will depend, in a decreasing degree, on the arbitrary initial value x_1 and should be discarded. After this initial "washout" phase, one usually keeps only those values $x_n, x_{n+d}, x_{n+2d}, \ldots$ whose distance d from each other is large enough to warrant that the dependency of x_{n+d} on x_n has washed out to a neglible amount.

One standard way to construct an MCMC transition kernel $T(\mathbf{x}|\mathbf{y})$ which leads to a Markov chain that has the target distribution g as its invariant distribution is to ensure that the Markov chain $(X_n)_{n=1,2,\ldots}$ has the property of *detailed balance* with respect to g. Detailed balance connects $X_1, X_2, \ldots$ to g in a strong way. It says that if we pick some state $\mathbf{x} \in \mathbb{R}^k$ with the probability given by g and

multiply its probability $g(\mathbf{x})$ with the transition probability density $T(\mathbf{y}|\mathbf{x})$ — that is, we consider the probability density of transiting from $\mathbf{x}$ to $\mathbf{y}$ weighted with the probability density of $\mathbf{x}$ — then this is the same as the reverse weighted transiting probability density from $\mathbf{y}$ to $\mathbf{x}$:

Definition 9.5 *Let g be a pdf on $\mathbb{R}^k$ and let $T(\mathbf{y}|\mathbf{x})$ be the pdf of a transition kernel of a homogeneous Markov chain on $\mathbb{R}^k$. Then $T(\mathbf{y}|\mathbf{x})$ has the* detailed balance *property with respect to g if*

$$\forall \mathbf{x}, \mathbf{y} \in \mathbb{R}^k : \;\; T(\mathbf{y}|\mathbf{x})\; g(\mathbf{x}) = T(\mathbf{x}|\mathbf{y})\; g(\mathbf{y}). \tag{108}$$

If $T(\mathbf{x}|\mathbf{y})$ has detailed balance with respect to g, then g is an invariant distribution of the Markov chain given by $T(\mathbf{x}|\mathbf{y})$ because

$$\int_{\mathbb{R}^k} T(\mathbf{x}|\mathbf{y})\; g(\mathbf{y})\, d\mathbf{y} = \int_{\mathbb{R}^k} T(\mathbf{y}|\mathbf{x})\; g(\mathbf{x})\, d\mathbf{y} = g(\mathbf{x}) \int_{\mathbb{R}^k} T(\mathbf{y}|\mathbf{x})\, d\mathbf{y} = g(\mathbf{x}).$$

Detailed balance is sufficient but not necessary for a Markov chain to be a sampler for g. However, there are generally applicable, convenient and widely used recipies to design MCMC's based on detailed balance. I present two of them: the *Gibbs sampler* and the *Metropolis algorithm*.

9.5.3 The Gibbs sampler

Let g be a pdf on $\mathbb{R}^k$. For $i = 1, \ldots, k$ and $\mathbf{x} \in \mathbb{R}^k$, where $\mathbf{x} = (x_1, \ldots, x_k)'$, let

$$\begin{aligned} g_i(\cdot \,|\, \mathbf{x}) \quad &: \quad \mathbb{R} \to \mathbb{R}^{\geq 0} \\ g_i(y \,|\mathbf{x}) \quad &= \quad \frac{g((x_1, \ldots, x_{i-1}, y, x_{i+1}, \ldots x_k)')}{\int_{\mathbb{R}} g((x_1, \ldots, x_{i-1}, z, x_{i+1}, \ldots x_k)')\, dz} \end{aligned}$$

be the conditional density function of the coordinate i given the values of $\mathbf{x}$ on the other coordinates. Let $g^{(1)}$ be the pdf of an initial distribution on $\mathbb{R}^k$, and let an initial value $\mathbf{x}^{(1)} = (x_1^{(1)}, \ldots, x_k^{(1)})'$ be drawn from $g^{(1)}$. We define a Markov chain $X_1, X_2, \ldots$ through transition kernels as follows. The idea is to cycle through the k coordinates and at some time $\nu k + i$ $(0 \leq \nu, 1 \leq i \leq k)$ change the previous state $\mathbf{x}^{(\nu k+i-1)} = (x_1^{(\nu k+i-1)}, \ldots, x_k^{(\nu k+i-1)})'$ only in the i-th coordinate, by sampling from g_i. That is, at time $\nu k + i$ we set

$$\mathbf{x}^{(\nu k+i)} = (x_1^{(\nu k+i-1)}, \ldots, x_{i-1}^{(\nu k+i-1)}, y, x_{i+1}^{(\nu k+i-1)}, \ldots x_k^{(\nu k+i-1)})'$$

equal to the previous state except in coordinate i where the value y which is freshly sampled from g_i.

This method is known as the *Gibbs sampler*. It uses k different transition kernels $T_1, \ldots, T_k$, where T_i is employed at times $\nu k + i$ and updates only the i-th coordinate.

This Markov chain is not homogeneous because we cycle through different transition kernels. However, we can condense a sequence of k successive updates into a single update that affects all coordinates by putting $T = T_k \circ \cdots \circ T_1$, which yields a homogeneous Markov chain $(Y_n)_{n=1,2,\ldots}$ with transition kernel T whose path is derived from a path $(\mathbf{x}_n)_{n=1,2,\ldots}$ of the "cycling" Markov chain by

$$\begin{aligned} \mathbf{y}^{(1)} &= \mathbf{x}^{(1)}, \\ \mathbf{y}^{(2)} &= \mathbf{x}^{(n+1)}, \\ \mathbf{y}^{(3)} &= \mathbf{x}^{(2n+1)}, \ldots . \end{aligned}$$

It should be clear that g is an invariant distribution of this homogeneous Markov chain, because each transition kernel T_i leaves g invariant: only the i-th component of the observation vector is affected at all, and it is updated exactly according to the conditional distribution g_i for this component. It even holds that T has detailed balance w.r.t. g (exercise — do it!).

It remains to ascertain that the Markov chain with kernel T is ergodic. This is certainly the case when the support of g in $\mathbf{R}^k$ (that is, the subset of $\mathbf{R}^k$ where g is positive) is k-dimensionally connected. This means that for any points $\mathbf{x}, \mathbf{y} \in \mathbf{R}^k$ with $g(\mathbf{x}) > 0, g(\mathbf{y}) > 0$ there exists a finite sequence of k-dimensional balls B_m of positive radius, the first containing $\mathbf{x}$ and the last containing $\mathbf{y}$, such that B_m intersects with B_{m+1} with positive volume. However, if the support of g is not k-dimensionally connected, then T may or may not be ergodic, and determining whether it is needs to be done on a case by case basis. For instance, if g is a distribution on $\mathbb{R}^2$ whose support lies exclusively in the first and third orthant, T would not be ergodic, because the Gibbs sampler, when started from a point in the third orthant, would be unable to jump into the first orthant. This situation is depicted in Figure 49.

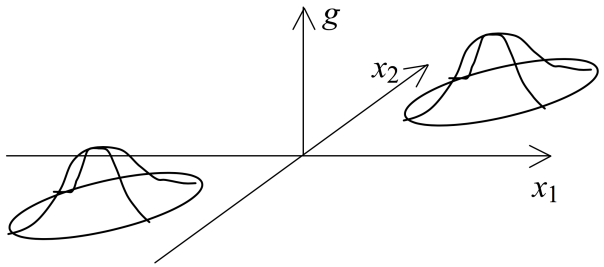

Figure 49: A bipartite pdf g where the Gibbs sampler would fail.

The Gibbs sampler is practically applicable only if one can easily sample from the 1-dimensional conditional distributions g_i. Therefore, the Gibbs sampler is mostly employed in cases where these g_i are parametric, analytical distributions, or in cases where S is finite and the g_i thus become simple probability vectors (and would be represented by pms, not pdfs). The Gibbs sampler is attractive for its

simplicity. A number of extensions and refinements of the basic idea is presented in Neal 1993.

9.5.4 The Metropolis algorithm

The Metropolis algorithm is more sophisticated than the Gibbs sampler and works in a much larger number of cases. The drawback is that it may be computationally more expensive. This algorithm explicitly constructs a Markov transition kernel with detailed balance. Like the Gibbs algorithm, the Metropolis algorithm can be cyclically applied to the k dimensions of the observation vectors in turn ("local" Metropolis algorithm) or it can be applied to all dimensions simultaneously ("global" algorithm). I describe the local version.

Like the Gibbs sampler, the local Metropolis algorithm updates the sample vector $\mathbf{x}^{(\nu k+i-1)} = (x_1^{(\nu k+i-1)}, \ldots, x_k^{(\nu k+i-1)})'$ only in the i-th coordinate, yielding an update

$$\mathbf{x}^{(\nu k+i)} = (x_1^{(\nu k+i-1)}, \ldots, x_{i-1}^{(\nu k+i-1)}, y, x_{i+1}^{(\nu k+i-1)}, \ldots x_k^{(\nu k+i-1)})'$$

in two substeps, which together ensure detailed balance w.r.t. the conditional distribution g_i:

Step 1: Randomly choose a candidate value y^* for y. Usually a *proposal distribution* $S_i(y^* \,|\, \mathbf{x}^{(\nu k+i-1)})$ is used (which may depend on $\mathbf{x}^{(\nu k+i-1)}$) which is symmetric in the sense that

$$\begin{aligned} S_i(y \,|(x_1^{(\nu k+i-1)}, \ldots, x_{i-1}^{(\nu k+i-1)}, y', x_{i+1}^{(\nu k+i-1)}, \ldots x_k^{(\nu k+i-1)})' = \\ S_i(y' \,|(x_1^{(\nu k+i-1)}, \ldots, x_{i-1}^{(\nu k+i-1)}, y, x_{i+1}^{(\nu k+i-1)}, \ldots x_k^{(\nu k+i-1)})' \end{aligned}$$

for all $y, y', \mathbf{x}$.

Step 2: Randomly *accept* or *reject* y^* as the new value for $x_i^{(\nu k+i)}$, in a fashion that ensures detailed balance. In case of acceptance, $x_i^{(\nu k+i)}$ is set to y^*; in case of rejection, $x_i^{(\nu k+i)}$ is set to $x_i^{(\nu k+i-1)}$, i.e., the observation vector is not changed at all and is identically repeated in the sampling sequence. The probability for accepting y^* is determined by an *acceptance probability* $A_i(y^*|\mathbf{x})$.

Note that $S_i(y^* \,|\, \mathbf{x}^{(\nu k+i-1)}$ is a probability distribution on the x_i coordinate space $\mathbb{R}$, while $A_i(y^*|\mathbf{x})$ is a number (a probability value).

The proposal distribution and the acceptance probability must be designed to warrant detailed balance, that is, to ensure

$$\begin{aligned} \forall \mathbf{x} = (x_1, \ldots, x_k)' \in \mathbb{R}^k, \forall y, y' \in \mathbb{R}: \\ g_i(y \,|\, \mathbf{x})\; T_i(y \,|\, (x_1, \ldots, x_{i-1}, y', x_{i+1}, \ldots, x_k)') = \\ g_i(y' \,|\, \mathbf{x})\; T_i(y \,|\, (x_1, \ldots, x_{i-1}, y, x_{i+1}, \ldots, x_k)'). \end{aligned} \tag{109}$$

There are several ways to ensure this. For instance, it is not difficult to see (exercise!) that if $S_i(y^* \,|\, \mathbf{x}^{(\nu k+i-1)})$ is symmetric, using

$$A_i(y^* \,|\, (x_1, \ldots, x_k)') = \frac{g_i(y^* \,|\, (x_1, \ldots, x_k)')}{g_i(y^* \,|\, (x_1, \ldots, x_k)') + g_i(x_i \,|\, (x_1, \ldots, x_k)')} \tag{110}$$

yields detailed balance. This is called the *Boltzmann acceptance function*. However, the Metropolis algorithm standardly uses another acceptance distribution, namely the *Metropolis acceptance distribution*

$$A_i(y^* \,|\, (x_1, \ldots, x_k)') = \min\left(1, \frac{g_i(y^* \,|\, (x_1, \ldots, x_k)')}{g_i(x_i \,|\, (x_1, \ldots, x_k)')}\right). \tag{111}$$

That is, whenever $g_i(y^* \,|\, (x_1, \ldots, x_k)') \geq g_i(x_i \,|\, (x_1, \ldots, x_k)')$, — the proposed observation in component i has no lower probability than the current one —, accept with certainty; else accept with probability $g_i(y^* \,|\, (x_1, \ldots, x_k)')/g_i(x_i \,|\, (x_1, \ldots, x_k)')$.

For symmetric proposal distributions, this strategy implies detailed balance. It is clear that in the rejection case, where the current observation is not changed, the detailed balance condition trivially holds. In the acceptance case we verify (108) as follows:

$$\begin{aligned}
&g_i(y^* \,|\, (x_1, \ldots, x_k)')\; T_i(x_i \,|\, (x_1, \ldots, y^*, \ldots, x_n)') = \\
&\quad = \; g_i(y^* \,|\, \mathbf{x})\; S_i(x_i \,|\, (x_1, \ldots, y^*, \ldots, x_n)')\; A_i(x_i \,|\, \mathbf{x}) \\
&\quad = \; S_i(x_i \,|\, (x_1, \ldots, y^*, \ldots, x_n)')\; \min\left(g_i(y^* \,|\, \mathbf{x}), g_i(x_i \,|\, \mathbf{x})\right) \\
&\quad = \; S_i(y^* \,|\, (x_1, \ldots, x_i, \ldots, x_n)')\; \min\left(g_i(y^* \,|\, \mathbf{x}), g_i(x_i \,|\, \mathbf{x})\right) \\
&\quad = \; g_i(x_i \,|\, \mathbf{x})\; S_i(y^* \,|\, (x_1, \ldots, x_i, \ldots, x_n)')\; A_i(y^* \,|\, \mathbf{x}) \\
&\quad = \; g_i(x_i \,|\, \mathbf{x})\; T_i(y^* \,|\, (x_1, \ldots, x_i, \ldots, x_n)')
\end{aligned}$$

Notes:

1. Both the Boltzmann and the Metropolis acceptance functions also work with proto-pdf's g_i. This is an invaluable asset because often it is infeasible to compute the normalization factor $1/Z$ needed to turn a proto-pdf into a pdf.

2. Like the Gibbs sampler, this local Metropolis algorithm can be turned into a global one, then having a homogeneous Markov chain with transition kernel T, by condensing one k-cycle through the component updates into a single observation update.

3. Detailed balance guarantees that g is an invariant distribution of the homogeneous Markov chain with transition kernel T. Before the resulting Metropolis sampler $Y_1, Y_2, \ldots$ can be used for sampling, it must in addition be shown that this Markov chain is ergodic. The same caveats that we met with the Gibbs sampler apply.

4. The Metropolis algorithm is more widely applicable than the Gibbs sampler because it obviates the need to sample from conditional distributions. The price one has to pay is a higher computational cost, because the rejection events lead to duplicate sample points which obviously leads to an undesirable "repetition redundancy" in the sample that has to be compensated by a larger sample size.

5. In statistical physics, the term "Monte Carlo Simulation" is almost synonymous with this Metropolis algorithm (says Neal — I am no physicist and couldn't check).

6. The quality of Metropolis sampling depends very much on the used proposal distribution. Specifically, the variance of the proposal distribution should neither be too small (then exploration of new states is confined to a narrow neighborhood of the current state, implying that the Markov chain traverses the distribution very slowly) nor too large (then one will often be propelled far out in the regions of g where it almost vanishes, leading to numerous rejection events). A standard choice is a normal distribution centered on the current state.

7. The Metropolis algorithm (and the Gibbs sampler, too) works best if the k state components are statistically maximally independent. Then the state space exploration in each dimension is independent from the exploration in the other dimensions, whereas if the components are statistically coupled, a fast exploration in one dimension is hindered by the fact that moving in this dimension entails a synchronized moving in the other dimensions, thus larger changes in one dimension have to wait for the correlated changes in the other dimensions. Thus if possible one should coordinate-transform the distribution before sampling with the aim to decorrelate the dimensions (which in principle does not imply making them independent but in practice is the best one can do).

8. I presented the Metropolis algorithm in the special case of sampling from a distribution over (a subset of) $\mathbb{R}^k$. This made the "cycle through dimensions" scheme natural which we also described for the Gibbs sampler. But the Metropolis algorithm also works on sample spaces S which do not have the vector space structure of $\mathbb{R}^k$; proposal distributions then have to be designed as the individual case requires. The application study from the next subsection is an example.

9.6 Application example: determining evolutionary trees

This section is a condensed version of a paper by Mau, Newton, and Larget 1999, *Bayesian Phylogenetic Inference via Markov Chain Monte Carlo Methods*. It is a

beautiful demonstration of how various modeling techniques are combined to characterize a highly complex pdf (namely, the conditional distribution of all possible evolutionary pasts, given DNA data from living species), and how the Metropolis algorithm is used to sample from it. The MCMC based method to determine evolutionary trees seems to have become a standard method in the field (I am not an expert to judge). A short paper (Huelsenbeck and Ronquist 2001) announcing a software toolbox for this method has been cited more than 20,000 times on Google Scholar. Methods to reconstruct phylogenetic trees from DNA obtained in surviving species are needed, in particular, for reconstructing trees of descendence for man; such studies often make it into the public press.

This application example is instructive in several respects. First, it uses Metropolis sampling on a sample space that is very different from $\mathbb{R}^k$ — the sample space will be a space of trees whose nodes are labelled with discrete symbols and whose edges are labelled with real numbers. This will highlight the flexibility and generality of Metropolis sampling. Second, the distribution from which will be sampled is a hyperdistribution — this application example also serves as a demonstration of the usefulness (in this case, even necessity) of Bayesian modeling. And third, the distribution from which will be sampled is represented in a format that is not normalized (the normalization factor $1/Z$ is unknown).

Data. DNA strings from related l living species, each string of length N, have been aligned without gaps. In the reported paper, $l = 32$ African fish species (cichlids from central African lakes except one cichlid species from America that served as a control) were represented by DNA sequences of length 1044. 567 of these 1044 sites were identical across all considered species and thus carried no information about phylogeny. The remaining $N = 477$ sites represented the data D that was entered into the analysis. Reminder: the DNA symbol alphabet is $\Sigma = \{A, C, G, T\}$.

Task. Infer from data D the most likely phylogenetic tree, assuming that the considered living species have a common ancestor from which they all descended.

Modeling assumptions. Mutations act on all sites independently. Mutations occur randomly according to a "molecular clock", i.e. a probability distribution of the form

$$P^{\mathsf{clock}}(y \,|\, x, t, \theta) \tag{112}$$

specifing the probability that the symbol $y \in \{A, C, G, T\}$ occurs at a given site where t years earlier the symbol x occurred. θ is a set of parameters specifying further modeling assumptions about the clock mechanism. Mau et al. used the molecular clock model proposed in Hasegawa, Kishino, and Yano 1985 which uses two parameters $\theta = (\phi, \kappa)$, the first quantifying an overall rate of mutation, and the second a difference of rates between the more frequent mutations that leave the type of nucleic acid (purine or pyrmidine) unchanged ("transitions") vs. change the type ("transversions"). All that we need to know here, not pretending to be biologists, is that (112) can be efficiently computed. Note that θ is not assumed to be known beforehand but has to be estimated/optimized in the modeling process,

based on the data D.

Representing phylogenetic trees. A phylogenetic tree is a binary tree Ψ. The nodes represent taxa (species); leaves are living taxa, internal nodes are extinct taxa, the root node is the assumed common ancestor. Mau et al. plot their trees bottom-up, root node at the bottom. Vertical distances between nodes metrically represent the evolutionary timespans t between nodes. Clades are subsets of the leaves that are children of a shared internal node. Figure 50 shows a schematic phylogenetic tree and some clades.

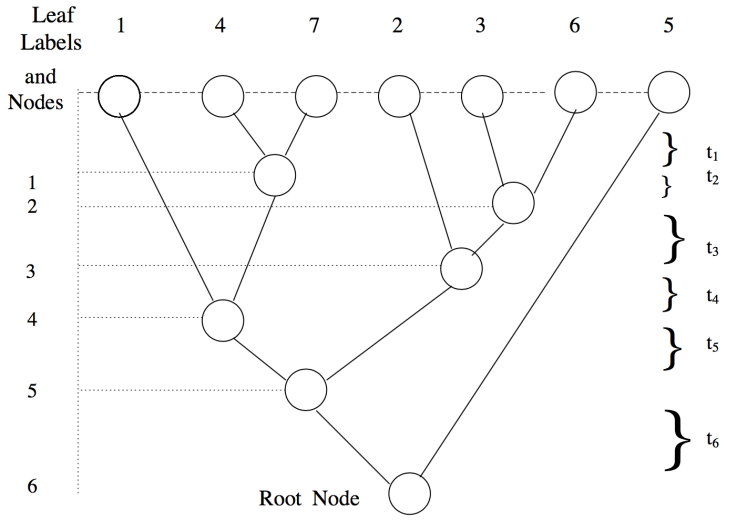

Figure 50: An examplary phylogenetic tree (from the Mau et al paper). {4,7}, {1 4 7}, {2, 3, 6} are examples of clades in this tree.

A given evolutionary history can be represented by trees in 2^{n-1} different but equivalent ways (where n is the number of living species), through permuting the two child branches of an internal node. For computational purposes a more convenient representation than a tree graph is given by

1. a specification of a left-to-right order σ of leaves (in Figure 50, $\sigma = (1, 4, 7, 2, 3, 6, 5)$), plus

2. a specification a of the graph distances between two successive leaves.

The graph distance is the length of the connecting path between the two leaves. In the example tree from Figure 50, the distances between leaves make the distance vector $a = 2(t_1 + t_2 + t_3 + t_4, t_1, t_1 + t_2 + t_3 + t_4 + t_5, t_1 + t_2 + t_3, t_1 + t_2, t_1 + t_2 + t_3 + t_4 + t_5 + t_6)$. A pair (σ, a) is a compact representation for a phylogenetic tree.

Likelihood of a phylogenetic tree. One subtask that must be solved in order to find the most probable evolutionary tree is to devise a fast method for computing the likelihood of a particular tree Ψ and molecular clock parameters θ, given the sequence data D:

$$L(\Psi, \theta) = P(D \mid \Psi, \theta). \tag{113}$$

Because the mutation processes at different sites are assumed to be independent, $P(D \mid \Psi, \theta)$ splits into a product of single-site probabilities $P(D_i \mid \Psi, \theta)$, where D_i are the symbols found in the sequences from D at site i. Thus D_i is a symbol vector of length l. Therefore, we only must find a way to compute

$$L_i(\Psi, \theta) = P(D_i \mid \Psi, \theta). \tag{114}$$

We approach this task sideways, assuming first that we know the symbols y_ν at the i-th site of the internal nodes ν of Ψ. Let ϱ be the root node and π_0 a reasonable distribution of symbols in ϱ in site i (for instance the global distribution of all symbols in all sites of all sequences in D). Then we get the probability of observed data D_i joined with the hypothetical data of these $(y_\nu)_{\nu \in \mathcal{I}}$ (where $\mathcal{I}$ is the set of internal nodes of Ψ) by

$$P(D_i, (y_\nu)_{\nu \in \mathcal{I}} \mid \Psi, \theta) = \pi_0(y_\varrho) \prod_{\nu \text{is non-root node of } \Psi} P^{\mathsf{clock}}(y_\nu \mid y_{\mathrm{par}(\nu)}, t_\nu, \theta), \tag{115}$$

where $\mathrm{par}(\nu)$ is the parent node of ν and t_ν is the timespan between $\mathrm{par}(\nu)$ and ν. From (115) we could obtain (114) by summing over all possible assignments of symbols to internal nodes, which is clearly infeasible. Fortunately there is a cheap recursive way to obtain (114), which works top-down from the leaves, inductively assigning conditional likelihoods $L_\nu(y) = P(D_i \restriction \nu \mid \Psi, \theta, \text{node } \nu = y)$ to nodes ν, where $y \in \Sigma$ and $D_i \restriction \nu$ is the subset of the D_i which are siblings of node ν, as follows:

$$\textbf{Case 1: } \nu \notin \mathcal{I}: \quad L_\nu(y) = \begin{cases} 1, & \text{if } y = y_\nu \\ 0, & \text{else} \end{cases}$$

$$\textbf{Case 2: } \nu \in \mathcal{I}: \quad L_\nu(y) = \left(\sum_{z \in \Sigma} L_\lambda(z) P^{\mathsf{clock}}(z|y, t_\lambda, \theta) \right) \left(\sum_{z \in \Sigma} L_\mu(z) P^{\mathsf{clock}}(z|y, t_\mu, \theta) \right),$$

where λ, μ are the two children of ν, t_λ is the timespan from ν to λ, and t_μ is the timespan from ν to μ. Then (114) is obtained from

$$L_i(\Psi, \theta) = \sum_{z \in \Sigma} \pi_0(z)\ L_\varrho(z),$$

from which (113) is obtained by

$$L(\Psi, \theta) = \prod_{i \text{ is site in } D} L_i(\Psi, \theta).$$

$O(N|\Sigma|l)$ flops are needed to compute $L(\Psi, \theta)$ – in our example, $N = 477$, $|\Sigma| = 4$, $l = 32$.

The posteriori distribution of trees and mutation parameters. We are actually not interested in the likelihoods $L(\Psi, \theta)$ but rather in the distribution

of Ψ, θ (a Bayesian hyperdistribution!) given D. Bayes theorem informs us that this desired distribution is proportional to the likelihood times the prior (hyper-)distribution $P(\Psi, \theta)$ of Ψ, θ:

$$P(\Psi, \theta \,|\, D) \sim P(D \,|\, \Psi, \theta)\ P(\Psi, \theta) = L(\Psi, \theta)\ P(\Psi, \theta).$$

Lacking a profound theoretical insight, Mau et al. assume for $P(\Psi, \theta)$ a very simple, uniform-like distribution (such uninformedness is perfectly compatible with the Bayesian approach!). Specifically:

1. They bound the total hight of trees by some arbitrary maximum value, that is, all trees Ψ with a greater hight are assigned $P(\Psi, \theta) = 0$.

2. All trees of lesser height are assigned the same probability. Note that this does *not* imply that all *topologies* are assigned equal prior probabilities. Figure 51 shows two topologies, where the one shown in **a.** will get a prior twice as large as the one shown in **b.** Reason: the two internal nodes of the first topology can be shifted up- and downwards independently, whereas this is not the case in the tree **b.**, thus there are twice as many trees of the topology **a.** than of **b.** Note that for evolutionary biologists it is the tree topology (which species derives from which species) rather than the tree metrics (how long took what) which is of prime interest!

3. The mutation parameters θ are assigned a prior distribution that is uniform on a range interval chosen generously large to make sure that all biologically plausible possibilities are contained in it.

Figure 51: Two tree topologies that get different prior probabilities. Topologies are defined by the parenthesis patterns needed to describe a tree. For instance, the tree **a.** would be characterized by a pattern ((x x)(x x)) and the tree **b.** by ((x (x x)) x).

The stage is now set. After all these preparations, for every Ψ, θ we can compute a pdf g (up to an unknown scaling factor) for $P(\Psi, \theta \,|\, D)$ with a small computational effort. (Of course, it will rather be the log of g which would be actually computed, avoiding underflow problems).

What is the structure and dimensionality of the (hyperdistribution) sample space S in which Ψ, θ lie? Remember that a tree Ψ can be specified by (σ, a), where σ is a permutation vector of $(1, \ldots, l)$ and a is a numerical vector of length $l1$. Noticing that there are $l!$ permutations, a pair (σ, a) reflects a point in a

product space $\{1,\ldots,l!\} \times \mathbb{R}^{l-1}$; together with the two real-valued parameters comprised in θ this brings us to a space $\{1,\ldots,l!\} \times \mathbb{R}^{l+1}$. However, there may be some constraints within the parameters of a that reduce the effective degrees of freedom to a number smaller than $l1$. This is hard to analyze (Mau et al. don't do it), and if the degrees of freedom are less than $l1$, we would not necessarily find a useful lower-dimensional representation. Be this as it may, all in all the support domain of our pdf for $P(\Psi, \theta \mid D)$ has a dimension in the order of l — in our example, 32 —, and a heterogeneous, complicated structure.

The target question that biologists want to get answered: what tree *topology* is the most probable, given DNA sequences D of living species?

The strategy to find out about the answer is brutally simple: sample a large number of trees Ψ_i from g, sort these sampled trees into sets defined by tree topology, then interpret the relative sizes of these sets as probability estimates.

The Metropolis algorithm at work. Mau et al. use the Metropolis algorithm (in a global version) to sample trees from g. A crucial design task is to find a good proposal distribution $S((\Psi^*, \theta^*)|(\Psi, \theta))$. It should lead from any plausible (Ψ, θ) [$g((\Psi, \theta))$ is not very small] to another plausible (Ψ^*, θ^*) which should be however as distinct from (Ψ, θ) as possible. The way how Mau et al. go about this task is one of the core contributions of their work.

The authors alternate between updating only θ and only Ψ. Proposing θ^* from θ is done in a straightforward way: the new *-parameters are randomly drawn from a rectangular distribution centered on the current settings θ.

The tricky part is to propose an as different as possible, yet "plausibility-preserving" new tree Ψ^* from Ψ. Mau et al. transform $\Psi = (\sigma, a)$ into $\Psi^* = (\sigma^*, a^*)$ in two steps:

1. The current tree Ψ is transformed into one of its $2n-1$ equivalent topological versions by randomly reversing with 0.5 probability every of its internal branches, getting $\Psi' = (\sigma', a')$.

2. In Ψ' the evolutionary inter-species time spans t are varied by changing the old values by a random increment drawn from the uniform distribution over $[\delta, \delta]$, where δ is a fixed bound (see Figure 52). This gives $\Psi^* = (\sigma', a^*)$.

Mau et al. show that this method yields a symmetric proposal distribution, and that every tree Ψ' can be reached from every other tree Ψ in a bounded number of such transformations – the Markov chain is thus ergodic.

Concretely, the Metropolis algorithm was run for 1,100,000 steps (20 hours CPU time on a 1998 Pentium 200 PC), the first 100,000 steps were discarded to wash out possible distortions resulting from the arbitrary starting tree, the remaining 1,000,000 trees were subsampled by 200 (reflecting the finding that after every 200 steps, trees were empirically independent [zero empirical cross-correlation at 200 step distance]), resulting in a final tree sample of size 5000.

Final findings. The 600 (!) most frequent topologies make up for 90% of the total probability mass. This high variability however is almost entirely due to

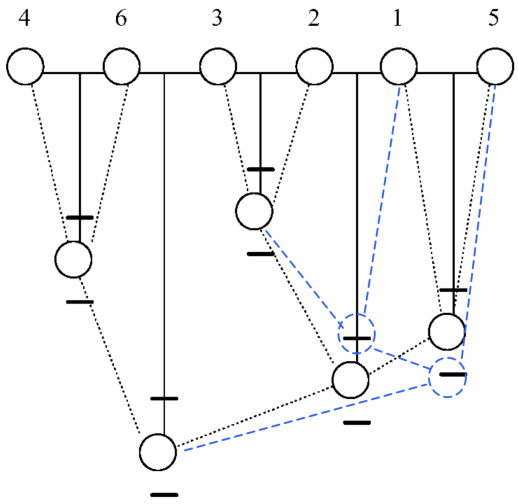

Figure 52: Proposal candidate trees, attainable from the current tree, are found within timeshift intervals of size 2δ, centered at the current internal nodes, that constrain the repositioning of the internal nodes. Note that if the two rightmost internal nodes are shifted such that their relative heights become reversed (dashed blue circles), the topology of the tree would change (dashed blue lines). Figure adapted from the Mau et al paper.

minute variations within 6 clades (labelled A, ..., F) that are stable across different topologies. Figure 53 shows the two most frequently found topologies resolved at the clade level, with a very strong posterior probability indication for the first of the two.

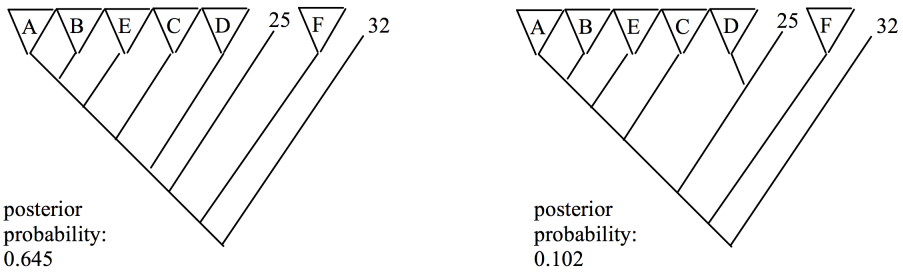

Figure 53: The two clade tree structures of highest posterior probability found by Mau et al.

For quality control, this was repeated 10 times, with no change of the final outcome, which makes the authors confident of their work's statistical reliability.

10 Graphical models

My favourite motivational example for introducing graphical models is the Space Shuttle. In the launch phase, the engineering staff in the control center and the astronauts on board have to make many critical decisions under severe time pressure. If anything on board of the roaring Space Shuttle seems to go wrong, it must be immediately determined, for instance, whether to shut down an engine (means ditching the Space Shuttle in the ocean but might save the astronauts) or not (might mean explosion of the engine and death of astronauts — or it might be just the right thing to do if it's a case of sensor malfunction and in fact all is fine with the engine). The functioning of the Space Shuttle is monitored with many dozens of sensors (more prone to malfunction than you would believe). They are delivering a massive flow of information which is impossible for human operators to evaluate for fast decision-making. So-called *decision support systems* are needed which automatically calculate probabilities for the actual system state from sensor readings and display to the human operators a condensed, human-understandable view of its most decision-critical findings. Read the original paper Horvitz and Barry 1995 on the probabilistic modeling of the combined SpaceShuttle-Pilots-GroundControlStaff system if you want to see how thrilling and potentially life-saving statistical modeling can be.

Such decision support systems are designed around hidden and visible random variables. The visible RVs represent observable variables, for instance the pressure or temperature readings from Space Shuttle engine sensors, but also actions taken by the pilot. The hidden RVs represent system state variables which cannot be directly measured but which are important for decision making, for instance a binary RV "Sensor 32 is functioning properly — yes / no", or "pilot-in-command is aware of excess temperature reading in engine 3 — yes / no". There are many causal chains between the hidden and visible RVs which lead to chains of conditional probability assessments, for instance "If sensor reading 21 is 'normal' and sensor reading 122 is 'normal' and sensor reading 32 is 'excess temperature', the probability that sensor 32 is misreading is 0.6". Such causal dependencies between RVs are mathematically represented by arrows between the participating RVs, which in total gives a directed graph whose nodes are the RVs. In such a graph, each RV X has its own sample space R_X which contains the possible values that X may take. When the graph is used (for instance, for decision support), for each RV a probability distribution P_X on R_X is computed. If $X_1, \ldots, X_k$ are RVs with arrows fanning in on a RV Y, the probability distribution P_Y on R_Y is calculated as a conditional distribution which depends on the distributions $P_{X_1}, \ldots, P_{X_k}$. These calculations quickly become expensive when the graph is large and richly connected (exact statistical inference in such graphs is NP-hard) and require approximate solution strategies. Despite the substantial complexity of algorithms in the field, such *graphical models* are today widely used. Many special sorts of graphical models have traditional special names and have been investi-

gated in a diversity of application contexts long before today's general, unifying theory of graphical models was developed. Such special kinds of graphical models or research traditions include

- *Hidden Markov models*, a basic model of stochastic processes with memory, for decades the standard machine learning model for speech and handwriting recognition and today still the reference model for DNA and protein sequences,
- models for *diagnostic reasoning* where a possible disease is diagnosed from symptoms and medical lab results (also in fault diagnostics in technical systems);
- *decision support systems*, not only in Space Shuttle launching but also in economics or warfare to name only two;
- *human-machine interfaces* where the machine attempts to infer the user's state of mind from the user's actions — the (in-)famous and now abolished Microsoft Office "paperclip" online helper was based on a graphical model;
- *Markov random fields* which model the interactions between local phenomena in spatially extended systems, for instance the pixels in an image;
- *Boltzmann machines*, a neural network model of hierarchical information processing.

In this section I will give an introduction to the general theory of graphical models and give a special treatment of Markov random fields and hidden Markov models.

This will be a long section. Graphical models are a heavyweight branch of machine learning and would best be presented in an entire course of their own. The course *Probabilistic Graphical Models* of Stefano Ermon at Stanford University is a (beautifully crafted) example. The course homepage `https://cs228.stanford.edu/` gives links to literature and programming toolboxes — and it serves you a transparently written set of lecture notes on `https://ermongroup.github.io/cs228-notes/` which culminates in explaining *deep variational autoencoders*, a powerful recent deep learning method which includes a number of techniques from graphical models.

10.1 Bayesian networks

Bayesian networks (BNs) are graphical models where the graph structure is a finite, directed, acyclic (that is, the arrows never form cycles) graph. Today's general theory of graphical models emerged from research on Bayesian networks, and many themes of graphical models can be best introduced with Bayesian networks.

The classical application domain for BNs is decision support, user modeling, and diagnostic systems. BN algorithms and fast computers have become indispensible for decision support because humans are simply bad at correctly combining pieces of evidence in uncertain systems. They tend to make gross, systematic prediction errors even in simple diagnostic tasks involving only two observables — which is why in good universities, future doctors must take courses in diagnostic reasoning —, let alone be capable of dealing with complex systems involving dozens of random variables.

In my condensed treatment I lean heavily on the two tutorial texts by Pearl and Russell 2003 and K. Murphy 2001.

For a first impression, we consider a classical example. Let $X_1, \ldots, X_5$ be five discrete random variables, indicating the following observations:

X_1 : indicates the season of the year, has values in $R_{X_1} = \{\text{Winter}, \text{Spring}, \text{Summer}, \text{Fall}\}$,

X_2 : indicates whether it rains, with values $\{0, 1\}$,

X_3 : indicates whether the lawn sprinkler is on, has values $\{0, 1\}$,

X_4 : indicates whether the pavement (close to the lawn) is wet, values $\{0, 1\}$,

X_5 : indicates whether the pavement is slippery, values from $\{0, 1\}$, too.

There are certain causal influences between some of these random variables. For instance, the season co-determines the probabilities for rain; the sprinkler state co-determines whether the pavement is wet (but one would not say that the wetness of the pavement has a causal influence on the sprinkler state), etc. Such influences can be expressed by arranging the X_i in a directed, acyclic graph (a DAG), such that each random variable becomes a node, with an edge (i, j) denoting that the fact measured by X_i has some causal influence on the fact measured by X_j. Of course there will be some subjective judgement involved in claiming a causal influence between two observables, and denying it for other pairs – such dependency graphs are not objectively "true", they are designed to represent one's view of a part of the world. Figure 54 is the DAG for our example which serves as standard example in many introductions to Bayesian nets.

The intuitive interpretation of arrows (i, j) in a Bayesian network as "causal influence" is mathematically captured by the following formal, semantic constraint that a DAG must satisfy in order to qualify as a Bayesian network:

Definition 10.1 *A directed acyclic graph with nodes labelled by RVs $\{X_1, \ldots, X_n\}$ (each with a separate sample space R_i) is a Bayesian network (BN) for the joint distribution $P_{\mathbf{X}}$ of $\mathbf{X} = X_1 \otimes \ldots \otimes X_n$ if every X_i is conditionally independent of its non-descendants in the graph given its parents.*

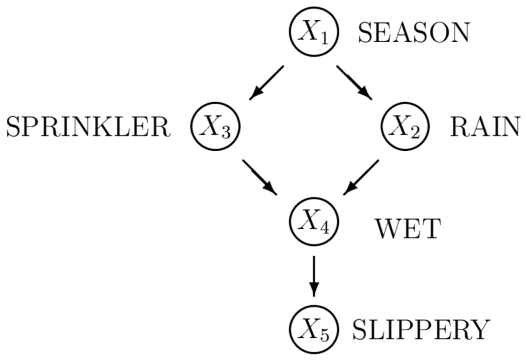

Figure 54: A simple Bayesian network. Image taken from Pearl and Russell 2003

For convenience of notation we often identify the nodes X_i of a BN with their indices i. The *descendants* of a node i in a DAG G are all nodes j that can be reached from i on a forward path in G. Descendance is a transitive relation: if j is a descendant of i and k a descendant of j, then k is a descendant of i. The nondescendants of i are all j that are not descendants of i.

The *parents* of a node i are all the *direct* graph predecessors of i, that is, all j such that (j, i) is an edge in the graph.

For instance, in the DAG shown in Figure 54, X_3 has parent X_1 and descendants X_4, X_5, and the condition stated in the definition requires that $P(X_3|X_1)$ is independent of X_2, that is $P(X_3|X_1) = P(X_3|X_1, X_2)$: our judgement whether the sprinkler is on or off is not influenced by our knowledge whether it rains or not if we know what season it is. Personal note: I always found this a weird old-times Californian way of behaving: those guys would set the sprinkler on or off just depending on the season; I guess in Summer all Californian sprinklers sprinkled all Summer, come rain come shine (in the year 2000 when that tutorial text was written).

The independence relations expressed in a BN in terms of parents and nondescendants need not be the only independence relations that are actually true in the joint distribution. In our example, for instance, it may be the case that the pavement is always slippery because it was made from polished marble. Then X_5 would be unconditionally independent from any of the other variables. The complete independence relations between the variables figuring in a BN depend on the particulars of the joint distribution and need not all be represented in the graph structure. A BN is only a partial model of the independence relations that may be present in the concerned variables.

Let's squeeze in a short note on notation here. By $P(X_4 \,|\, X_2, X_3)$ we denote the conditional *distribution* of X_4 given X_2 and X_3. In mathematical texts one would denote this distribution by $P_{X_4 \,|\, X_2, X_3}$ but I will follow the notation in the Pearl/Russell tutorial in this section. For discrete random variables, as in our example, such conditional distributions can be specified by a table — for

$P(X_4 \mid X_2, X_3)$ such a table might look like

X_2	X_3	$P(X_4 = 0)$	$P(X_4 = 1)$
0	0	1.0	0.0
0	1	0.1	0.9
1	0	0.1	0.9
1	1	0.01	0.99

(116)

For continuous-valued random variables, such conditional distributions cannot in general be specified in a closed form (one would have to specify pdf's for each possible combination of values of the conditioning variables), except in certain special cases, notably Gaussian distributions.

In contrast, I use lowercase $P(x_4 \mid x_2, x_3)$ as a shorthand for $P(X_4 = x_4 \mid X_2 = x_2, X_3 = x_3)$. This denotes a single probability number for particular values of our random variables. – End of the note on notation.

A Bayesian network can be used for reasoning about uncertain causes and consequences in many ways. Here are three kinds of arguments that are frequently made, and for which BNs offer algorithmic support:

Prediction. *"If the sprinkler is on, the pavement is wet with a probability* $P(X_4 = 1|X_3 = 1) = ###$*"*: reasoning from causes to effects, along the arrows of the BN in forward direction. Also called *forward reasoning* in AI contexts.

Abduction. *"If the pavement is wet, it is more probable that the season is spring than that it is summer, by a factor of ### percent"*: reasoning from effects to causes, that is, diagnostic reasoning, backwards along the network links. (By the way, for backward reasoning you need Bayes' formula, which is what gave Bayesian networks their name.)

Explaining away, and the rest. *"If the pavement is wet and we don't know whether the sprinkler is on, and then observe that it is raining, the probability of the sprinkler being on, too, drops by ### percent*: reasoning "sideways", of which there are many variants. In "explaining away" there are several possible causes $C_1, \ldots, C_k$ for some observed effect E, and when we learn that actually cause C_i holds true, then the probabilities drop that the other causes are likewise true in the current situation.

Bayesian networks offer *inference algorithms* to carry out such arguments and compute the correct probabilities, ratios of probabilities, etc. These inference algorithms are not trivial at all, and Bayesian networks have only begun to make their way into applications since efficient inference algorithms had been discovered in the mid-80'ies. I will explain a classical (and still widely used) algorithm in this section (a *join tree* algorithm for exact inference); it is still widely used and efficient

in BNs where the connectivity is not too dense. Because exact statistical inference in BNs is NP-hard, one has to take resort to approximate algorithms in many cases. There are two main families of such algorithms, one based on sampling and the other on *variational approximation*. I will give a hint on inference by sampling and omit variational inference.

In a sense, the most natural (the only?) thing you can do when it comes to handle the interaction between many random variables is to arrange them in a causal influence graph. So it is no surprise that related formalisms have been invented independently in AI, physics, genetics, statistics, and image processing. However, the most important algorithmic developments have been in AI / machine learning, where feasible inference algorithms for large-scale BNs have first been investigated. The unrivalled pioneer in this field is Judea Pearl `http://bayes.cs.ucla.edu/jp_home.html`, who laid the foundations for the algorithmic theory of BNs in the 1980's. These foundations were later developed to a more general theory of graphical models, a development promoted (among others) by Michael I. Jordan `https://people.eecs.berkeley.edu/~jordan/`. Michael Jordan not only helped to build the general theory of graphical models but also had a shaping influence on other areas in machine learning. He is a machine learning superpower. The list of his past students and postdocs on his homepage reads like a Who's Who of machine learning.

In the world of BNs (and graphical models in general) there exist two fundamental tasks:

Inference: Find algorithms that exploit the graph structure as ingeneously as possible to yield feasible algorithms for computing all the quantities asked for in prediction, abduction and explaining-away tasks.

Learning: Find algorithms to estimate a BN from observed empirical data. Learning algorithms typically call inference algorithms as a subroutine, so we will first treat the latter.

10.1.1 Brute-force inference in BNs

A Bayesian network is a probabilistic representation of a piece of reality – that piece which we observe through the visible RVs and that we hypothetically capture through the hidden RVs. A BN represents the *joint* probability distribution of all of these RVs. In inference tasks one computes distributions of target variables of interest ("probability that Space Shuttle engine will explode") as marginal or conditional probabilities derived from that joint distribution. In this subsection I will explain how such marginal or conditional distributions are mathematically connected to the joint distribution in cases where all RVs have a finite sample space, and how the graph structure can be exploited to *factorize* distributions of interest, which makes them computationally more tractable.

The joint distribution in our Californian pavement example is a distribution over the sample space

$$\{\text{Winter}, \text{Spring}, \text{Summer}, \text{Fall}\} \times \{0,1\} \times \{0,1\} \times \{0,1\} \times \{0,1\},$$

which has $4 \cdot 2 \cdot 2 \cdot 2 \cdot 2 = 64$ elements. Thus one would need a 64-dimensional pmf to characterize it, which has 63 degrees of freedom (one parameter we get for free because the pmf must sum to 1). This pmf would not be given in vector format but as a 5-dimensional probability array. We will now investigate brute-force methods for elementary inference in this joint probability table and see how the graph structure leads to a dramatic reduction in computational complexity (which however still is too high for practical applications with larger BNs – more refined algorithms will be presented later).

By a repeated application of the factorization formula (174) (in Appendix B), the joint distribution of our five random variables is

$$P(\mathbf{X}) = P(\bigotimes_{i=1,\ldots,5} X_i) = \\ P(X_1)\, P(X_2|X_1)\, P(X_3|X_1,X_2)\, P(X_4|X_1,X_2,X_3)\, P(X_5|X_1,X_2,X_3,X_4). \quad (117)$$

Exploiting the conditional independencies expressed in the BN graph, this reduces to

$$P(\mathbf{X}) = P(X_1)\, P(X_2|X_1)\, P(X_3|X_1)\, P(X_4|X_2,X_3)\, P(X_5|X_4). \quad (118)$$

For representing the factors on the right-hand side of (118) by tables like (116), one would need tables of sizes 1×4, 4×2, 4×2, 4×2, and 2×2, respectively. Because the entries per row in each of these tables must sum to 1, one entry per row is redundant, so these tables are specified by 3, 4, 4, 4 and 2 parameters, respectively. All in all, this makes 17 parameters needed to specify $P(\mathbf{X})$, as opposed to the 63 parameters needed for the naive representation $P(\mathbf{X})$ in a 5-dimensional array.

In general, the number of parameters required to specify the joint distribution of n discrete random variables with maximally ν values each arranged in a BN with a maximum fan-in of k is $O(n\,\nu^k)$ as opposed to the raw number of parameters $O(\nu^n)$ needed for a naive characterization of the joint distribution. This is a reduction from a space complexity that is exponential in n to a space complexity that is linear in n! This simple fact has motivated many a researcher to devote his/her life to Bayesian networks.

Any reasoning on BNs (predictive, abductive, sidestepping or other) boils down to calculate conditional or marginal probabilities. For instance, the abductive question, *"If the pavement is wet, by which factor y is it more probable that the season is spring than that it is summer"*, asks one to compute

$$y = \frac{P(X_1 = \text{spring} \,|\, X_4 = 1)}{P(X_1 = \text{summer} \,|\, X_4 = 1)}. \quad (119)$$

Such *probability ratios* are often sought in diagnostic reasoning — as for instance in *"by which factor is it more probable that my symptoms are due to cancer, than that they are due to a harmless cause"*.

Any conditional probability $P(y_1, \ldots, y_m \,|\, z_1, \ldots, z_l)$, where the Y_i and Z_j are among the RVs in the BN, can be computed from the joint distribution of all variables in the BN by first transforming $P(y_1, \ldots, y_m \,|\, z_1, \ldots, z_l)$ into a fraction of two marginal probabilities,

$$P(y_1, \ldots, y_m \,|\, z_1, \ldots, z_l) = \frac{P(y_1, \ldots, y_m, z_1, \ldots, z_l)}{P(z_1, \ldots, z_l)}$$

and then computing the denominator and the enumerator by marginalization from the joint distribution of all RVs in the BN, exploiting efficient BN factorizations of the kind exemplified in Equation 118. The probability $P(X_1 = \text{spring} \,|\, X_4 = 1)$, for instance, can be computed by

$$\begin{aligned} & P(X_1 = \text{spring} \,|\, X_4 = 1) = \qquad (120) \\ = \;& \frac{P(X_1 = \text{spring}, X_4 = 1)}{P(X_4 = 1)} \\ = \;& \frac{\sum\limits_{x_2,x_3,x_5} P(X_1 = \text{spring}, x_2, x_3, X_4 = 1, x_5)}{\sum\limits_{x_1,x_2,x_3,x_5} P(x_1, x_2, x_3, X_4 = 1, x_5)} \\ = \;& \frac{\sum\limits_{x_2,x_3,x_5} P(X_1 = \text{s})\, P(x_2|X_1 = \text{s})\, P(x_3|X_1 = \text{s})\, P(X_4 = 1|x_2, x_3)\, P(x_5|X_4 = 1)}{\sum\limits_{x_1,x_2,x_3,x_5} P(x_1)\, P(x_2|x_1)\, P(x_3|x_1) P(X_4 = 1|x_2, x_3)\, P(x_5|X_4 = 1)}, \end{aligned}$$

where I abbreviated "spring" to "s" in order to squeeze the expression into a single line.

(120) can be computed by a brute-force evaluation of the concerned summations. The sum to be taken in the denominator would run over $4{\times}2{\times}2{\times}2 = 32$ terms, each of which is a product of 5 subterms; we thus would incur 128 multiplications. It is apparent that this approach generally incurs a number of multiplications that is exponential in the size of the BN.

A speedup strategy is to try pulling the sum into the product as far as possible, and evaluate the resulting formula from the inside of bracketing levels. This is called the method of *variable elimination*. For example, an equivalent formula for the sum in the denominator of (120) would be

$$\sum_{x_1} \left(P(x_1) \sum_{x_2,x_3} \left(P(x_2|x_1) P(x_3|x_1) P(X_4 = 1|x_2, x_3) \left(\sum_{x_5} P(x_5|X_4 = 1) \right) \right) \right).$$

To evaluate this expression from the inside out, we note that the sum over x_5 in the innermost term is 1 and need not be explicitly calculated. For the remaining

calculations, 15 sums and 36 multiplications are needed, as opposed to the 31 sums and 128 multiplications needed for the naive evaluation of the denominator in (120). However, finding a summation order where this pulling-in leads to the minimal number of summations and multiplications is again NP-hard, although greedy algorithms for that purpose are claimed to work well in practice.

In this situation, computer scientists can choose between three options:

1. *Restrict the problem by suitable constraints, earning a tractable problem.* For BNs, this was the first strategy that was used with success: early (now classical) inference algorithms were defined only for BNs with *tree* graphs.

2. *Use heuristic algorithms, i.e. algorithms that embody human insight for computational shortcuts.* Heuristic algorithms need not always be successful in leading to short runtimes; if they do, their result is perfectly accurate. The goal is to find heuristics which lead to fast runtimes almost always and which run too long only rarely. The "join tree" algorithm which we will study later contains heuristic elements.

3. *Use approximate algorithms, i.e. algorithms that yield results always and fast, but with an error margin (which should be controllable).* For BN inference, a convenient class of approximate algorithms is based on sampling. In order to obtain an estimate of some marginal probability, one samples from the distribution defined by the BN and uses the sample as a basis to estimate the desired marginal. There is an obvious tradeoff between runtime and precision. Another class of approximate algorithms is to use *variational inference*. Variational algorithms need some insight into the shape of the conditional distributions in a BN. Their speedup results from restricting the admissible shapes of these distributions to analytically tractable classes. I will not go into this topic in this course. Jordan, Ghahramani, et al. 1999 gives a tutorial introduction.

10.1.2 BN inference with the join-tree algorithm

In this subsection I will unfold the classical exact inference algorithm that can compute conditional and marginal probabilities on BNs at (often) affordable cost. This algorithm is often referred to as *join tree algorithm*, or *junction tree algorithm*. It is an exact algorithm: it computes exact, not approximate values of the desired probabilities.

The join-tree algorithm isn't simple and this subsection will be long. I will follow the description given in Huang and Darwiche 1994.

Before the BN can be used with the join tree inference algorithm, the original DAG must be transformed into an auxiliary graph structure, called a *join tree*, by a rather involved process. This has to be done only once for a given BN however; the same join tree can be re-used for all subsequent inference calls. The transformation from a DAG to a join tree runs through 4 stages:

Given: A BN with DAG G_d with nodes $\mathbf{X} = \{X_1, \ldots, X_n\}$

Step 1: Transform G_d to an undirected graph G_m, called the *moral undirected graphical model* (moral UGM), which is an equivalent way of expressing the independencies expressed in G_d, but using another graph separation mechanism for expressing conditional independencies.

Step 2: Add some further undirected edges to G_m which *triangulate* G_m, obtaining G_t. This may destroy some of the original independence relations between $\{X_1, \ldots, X_n\}$ but will not introduce new ones.

Step 3: Detect all cliques $\mathbf{C}_i$ in G_t (while this is NP-complete for general undirected graphs, it can be done efficiently for triangulated undirected graphs).

Step 4: Build an undirected *join tree* $\mathcal{T}$ with nodes $\mathbf{C}_i$. This is the desired target structure. It represents an elegant factorization of the joint probability $P(\mathbf{X})$ which in turn can be processed with a fast, local inference algorithm known as *message passing*.

We will go through these steps in a mostly informal manner. The purpose of this presentation is not to provide you with a detailed recipe for building executable code. There exist convenient BN toolboxes. The purpose of this subsection is to provide you with a navigation guide to gain an overview of the general picture, then study the more detailed paper Huang and Darwiche 1994, then start using (and understanding) a toolbox.

Undirected graphical models. Before we can delve into the join tree algorithm, we have to introduce the concept of undirected graphical models (UGMs), because these will be constructed as intermediate data structures when a BN is transformed to a join tree.

The essence of BNs is that conditional independency relationships between RVs are captured by directed graph structures, which in turn guide efficient inference algorithms. But it is also possible to use undirected graphs. This leads to undirected graphical models (UGMs), which have a markedly different flavour from directed BNs. UGMs originated in statistical physics and image processing, while BNs were first explored in Artificial Intelligence. A highly readable non-technical overview and comparison of directed and undirected models is given in Smyth 1997.

We will use the following compact notation for statistical, conditional independence between two sets $\mathbf{Y}$ and $\mathbf{Z}$ of random variables, given a set $\mathbf{S}$ of random variables:

Definition 10.2 *Two sets* $\mathbf{Y}$ *and* $\mathbf{Z}$ *of random variables are* independent given $\mathbf{S}$*, if*

$$P(\mathbf{Y}, \mathbf{Z} \,|\, \mathbf{S}) = P(\mathbf{Y} \,|\, \mathbf{S})\ P(\mathbf{Z} \,|\, \mathbf{S}).$$

We write $\mathbf{Y} \perp \mathbf{Z} \,|\, \mathbf{S}$ *to denote this conditional independence.*

It is easy to see that if $\mathbf{Y} \perp \mathbf{Z} \,|\, \mathbf{S}$ and $\mathbf{Y}' \subseteq \mathbf{Y}, \mathbf{Z}' \subseteq \mathbf{Z}$, then $\mathbf{Y}' \perp \mathbf{Z}' \,|\, \mathbf{S}$.

In an UGM, independence relations between sets of random variables are defined in terms of a graph separation property:

Definition 10.3 *Let $G = (V, E)$ be an undirected graph with vertices V and edges $E \subseteq V \times V$. Let $Y, Z, S \subset V$ be disjoint, nonempty subsets. Then Y* is separated from *Z by S if every path from some vertex in Y to any vertex in Z contains a node from S. S is called a* separator *for Y and Z.*

And here is how statistical independence is reflected in a graph's separation properties:

Definition 10.4 *An undirected graph with nodes $\mathbf{X} = \{X_1, \ldots, X_n\}$ is an* undirected graphical model *(UGM) for $P(\mathbf{X})$ if for all $\mathbf{Y}, \mathbf{Z}, \subseteq \mathbf{X}$ it holds that if $\mathbf{Y}$ is separated from $\mathbf{Z}$ by $\mathbf{S}$, then $\mathbf{Y} \perp \mathbf{Z} \,|\, \mathbf{S}$.*

UGMs are sometimes defined in a slightly different but equivalent way. We formulate this other definition as a proposition:

Proposition 10.1 *An undirected graph with nodes $\mathbf{X} = \{X_1, \ldots, X_n\}$ is an UGM for $P(\mathbf{X})$ iff for all $i = 1, \ldots, n$ it holds that $P(X_i \,|\, (X_j)_{j \neq i}) = P(X_i \,|\, (X_j)_{j \in \mathcal{N}_i})$, where $\mathcal{N}_i$ is the set of all direct graph neighbors of node i.*

The set $\mathcal{N}_i$ which makes X_i independent from all other RVs in the model is also called the *Markov blanket* of X_i. Notice that Markov chains (see Section 9.5.1) can be considered as UGMs where the (only) edges are between subsequent X_n, X_{n+1} and the Markov blanket of X_n is given by its temporal neighbors $\{X_{n-1}, X_{n+1}\}$.

Step 1: The moral UGN. After this quick introduction of UGMs we return to the join tree algorithm for BNs. The first step is to transform the directed graph structure of BN into an UGM structure. This can be done in many ways. The art lies in transforming a BN into an UGM such that as few as possible of the valuable independence relations expressed in the BN get lost. The standard thing to do is to *moralize* the directed BN graph G_d into an undirected graph G_m by

1. converting all edges from directed to undirected ones,
2. for every node X_i, adding undirecting edges between all parents of X_i.

See Figure 55 for an example. The peculiar name "moralizing" comes from the act of "marrying" previously unmarried parents. The moral UGM G_m implies the same conditional independence relations as the BN G_d from which it was derived (proof omitted here).

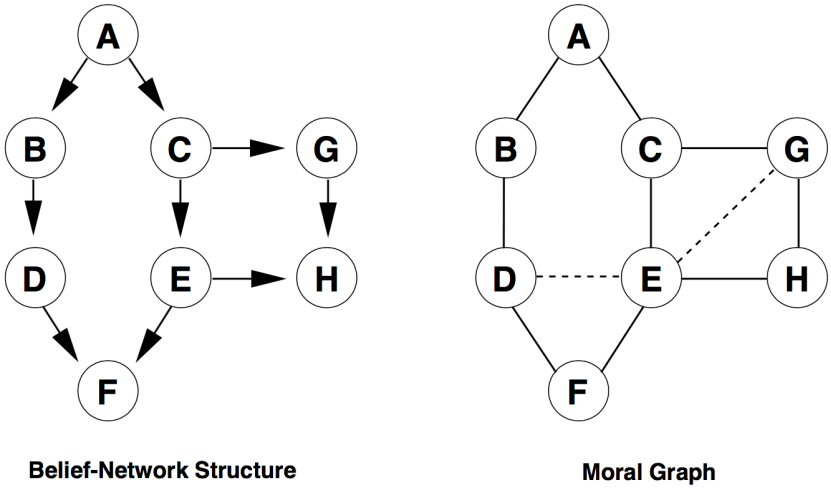

Figure 55: A BN and its associated moral UGM. Image taken from Huang and Darwiche 1994.

Step 2: Triangulation. An undirected graph is *triangulated* if every cycle of length at least 4 contains two nodes not adjacent in the cycle which are connected by an edge.

Any undirected graph can be triangulated by adding edges. There are in general many ways of doing so. For best efficiency of UGM inference algorithms, one should aim at triangulating in a way that minimizes the size of cliques of the triangulated graph. This is (again) an NP- complete problem. However there are heuristic algorithms which yield close to optimal triangulations in (fast) polynomial time. One of them is sketched in the Huang/Darwiche guideline for BN inference design.

After triangulation, we have an UGM graph G_t. Figure 56 shows a possible triangulation of the UGM from Figure 55.

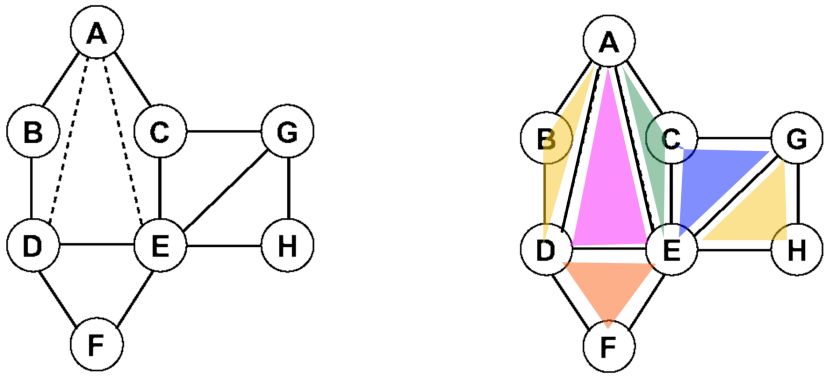

Figure 56: Left: A triangulated version G_t of the moral UGM G_m from Figure 55. Right: the 6 cliques in G_t. Image adopted from Huang and Darwiche 1994.

The reason for triangulating is that triangulated graphs can be decomposed into junction trees in Step 4.

Step 3: finding the cliques. For a change, finding all cliques in a triangulated graph is not NP-complete — efficient algorithms for finding all cliques in a triangulated graph are known. In our running example, we get 6 cliques, namely all the "triangles" ABD, ACE, ADE, DEF, CGE, and EGH (Figure 56 (right)). Our example conveys maybe a wrong impression that we always get cliques of size 3 in triangulated graphs. In general, one may find cliques of any size greater ≥ 2 in such graphs.

Step 4: Building the join tree. This is a more interesting and involved step. After BNs and UGMs, join trees are our third graph-based representation of independence relations governing a set $\mathbf{X}$ of random variables. We will discuss join trees in their own right first, and then consider how a join tree can be obtained from the cliques of a triangulated UGM.

Definition 10.5 *Let $\mathbf{X} = \{X_1, \ldots, X_n\}$ be a set of discrete random variables with joint distribution $P(\mathbf{X})$, where X_i takes values in a sample space R_{X_i}. A join tree for $P(\mathbf{X})$ is an undirected tree whose nodes are labelled with subsets $\mathbf{C}_i \subseteq \mathbf{X}$ (called* clusters*) and whose edges are labelled with subsets $\mathbf{S}_j \subseteq \mathbf{X}$ (called the separator sets or sepsets). Furthermore, each cluster $\mathbf{C} = \{Y_1, \ldots, Y_k\}$ is associated with a* belief potential *$\varphi_{\mathbf{C}} : R_{Y_1} \times \ldots \times R_{Y_k} \to \mathbb{R}^{\geq 0}$, and each sepset $\mathbf{S} = \{S_1, \ldots, S_l\}$ with a belief potential $\varphi_{\mathbf{S}} : R_{S_1} \times \ldots \times R_{S_l} \to \mathbb{R}^{\geq 0}$, such that the following conditions are satisfied:*

1. *The graph has the* running intersection property*, that is, given two cluster nodes labelled with $\mathbf{C}$ and $\mathbf{C}'$, all labels $\mathbf{C}^*$ of cluster nodes on the path between $\mathbf{C}$ and $\mathbf{C}'$ must have labels containing $\mathbf{C} \cap \mathbf{C}'$.*

2. *Each edge between two nodes labelled by $\mathbf{C}$ and $\mathbf{C}'$ is labelled by $\mathbf{S} = \mathbf{C} \cap \mathbf{C}'$.*

3. *For each cluster $\mathbf{C} = \{Y_1, \ldots, Y_k\}$ and neighboring sepset $\mathbf{S} = \{Y_1, \ldots, Y_l\}$ (not that $l \leq k$ because $\mathbf{S} \subseteq \mathbf{C}$), it holds that $\varphi_{\mathbf{C}}$ is* consistent *with $\varphi_{\mathbf{S}}$ in the sense that*

$$\sum_{y_{l+1}, \ldots, y_k} \varphi_{\mathbf{C}}(y_1, \ldots, y_k) = \varphi_{\mathbf{S}}(y_1, \ldots, y_l), \tag{121}$$

   that is, $\varphi_{\mathbf{S}}$ is obtained by marginalization from $\varphi_{\mathbf{C}}$.

4. *The joint distribution $P(\mathbf{X})$ is factorized by the belief potentials according to*

$$P(\mathbf{X}) = \frac{\prod_i \varphi_{\mathbf{C}_i}}{\prod_j \varphi_{\mathbf{S}_j}}. \tag{122}$$

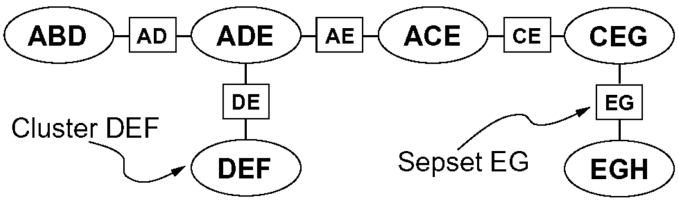

Figure 57: A join tree derived from the triangulated UGN shown in Figure 56. Image taken from Huang and Darwiche 1994.

I mention without proof how statistical independence relations are reflected in a join tree:

Proposition 10.2 *Let $\mathcal{T}$ be a join tree for $P(\mathbf{X})$ and $\mathbf{Y}, \mathbf{Z}, \mathbf{S} \subseteq \mathbf{X}$. Re-interpret the link labels as nodes (so the join tree from Figure 57 would become an undirected tree with 11 nodes and unlabelled links), obtaining a "homogenized" tree $\mathcal{T}'$. If for all $Y \in \mathbf{Y}, Z \in \mathbf{Z}$ the path from any node in $\mathcal{T}'$ containing X to any node containing Y passes through a node whose labels include $\mathbf{S}$, then $\mathbf{Y} \perp \mathbf{Z} \,|\, \mathbf{S}$.*

In join trees, the belief potentials are the marginal distributions of their variables:

Proposition 10.3 *Let $\mathcal{T}$ be a join tree for $P(\mathbf{X})$, and let $\mathbf{K} = \{X_1, \ldots, X_k\} \subseteq \mathbf{X} = \{X_1, \ldots, X_k, X_{k+1}, \ldots, X_n\}$ be a clique or sepset label set. Then for any value instantiation $x_1, \ldots, x_k$ of the variables from $\mathbf{K}$, it holds that*

$$\sum_{x_{k+1}, \ldots, x_n} P(x_1, \ldots, x_n) = \varphi_{\mathbf{K}}(x_1, \ldots, x_k), \tag{123}$$

that is, $\varphi_{\mathbf{K}}$ is the marginal distribution of the variables in $\mathbf{K}$.

A proof this proposition amounts to a medium difficult exercise. We will from now on use the shorthand notation

$$\sum_{\mathbf{X} \setminus \mathbf{K}} P(\mathbf{X}) = \varphi_{\mathbf{K}} \tag{124}$$

to denote marginalization.

Ok., now that we know what a join tree is, we return to Step 4: constructing a join tree from a triangulated moral UGM G_t. A join tree is specified through (i) its labelled graph structure and (ii) its belief potentials. We first treat the the question how one can derive the join tree's graph structure from G_t.

There is much freedom in creating a join tree graph from G_t. One goal for optimizing the design is that one strives to end with clusters that are as small as possible (because the computational cost of using a join tree for inference will turn out to grow exponentially in the maximal size of clusters). On the other hand,

in order to compute belief potentials later, any clique in G_t must be contained in some cluster. This suggests to turn the cliques identified in Step 3 into the cluster nodes of the join tree. This is indeed done in a general recipe for constructing a join tree from a triangulated UGM G_t, which I rephrase from Huang and Darwiche 1994:

1. Begin with an empty set SEP, and a completely unconnected graph whose nodes are the maximal cliques $\mathbf{C}_i$ found in Step 3.

2. For each distinct pair of cliques $\mathbf{C}_i, \mathbf{C_j}$ create a candidate sepset $\mathbf{S}_{ij} = \mathbf{C}_i \cap \mathbf{C_j}$, and put it into SEP. SEP will then contain $m\,(m-1)/2$ such $\mathbf{S}_{ij}$ (some of which may be the empty).

3. From SEP iteratively choose $m-1$ sepsets and use them to create connections in the node graph, such that each newly chosen sepset connects two subgraphs that were previously unconnected. This necessarily yields a tree structure.

A note on the word "tree structure": in most cases when a computer scientist talks about tree graphs, there is a special "root" node. Here we use a more general notion of trees to mean undirected graphs which (i) are connected (there is a path between any two nodes) and (ii) where these paths are unique, that is between any two nodes there is exactly one connecting path. In such tree graphs any node can be designated as "root" and one gets the familiar appearance of a tree.

This general recipe leaves much freedom in choosing the sepsets from SEP. Not all choices will result in a valid join tree. In order to ensure the join tree properties, we choose, at every step from 3., the candidate sepset that has the largest mass (among all those which connect two previously unconnected subgraphs). The mass of a sepset is the number of variables it contains.

This is not the only possible way of constructing a join tree, and it is still underspecified (there may be several maximal mass sepsets at our disposal in a step from 3.) Huang and Darwiche propose a full specification that heuristically optimizes the join tree with respect to the ensuing inference algorithms.

If the original BN was not connected, some of the sepsets used in the join tree will be empty; we get a join forest then.

We now turn to the second subtask in Step 4 and construct belief potentials $\varphi_{\mathbf{C}}, \varphi_{\mathbf{S}}$ for the clusters and sepsets, such that Equations 121 and 122 hold.

Belief potentials which account for (121) and (122) are constructed in two steps. First, the potentials are initialized in a way such that (122) holds. Second, by a sequence of *message passes*, local consistency (121) is achieved.

Initialization. Initialization works in two steps:

1. For each clique or sepset $\mathbf{K}$ (we use symbol $\mathbf{K}$ for cliques $\mathbf{C}$ or sepsets $\mathbf{S}$), set $\varphi_{\mathbf{K}}$ to the unit function

$$\varphi_{\mathbf{K}} \equiv 1.$$

2. For each variable X_k, do the following. Assign to X_k a clique $\mathbf{C}_{X_k}$ that contains X_k and its parents $\mathbf{\Pi}_{X_k}$ from the original BN. Note: due to the moralizing, such a clique must exist. Multiply $\varphi_{\mathbf{C}_{X_k}}$ by $P(X_k \,|\, \mathbf{\Pi}_{X_k})$:

$$\varphi_{\mathbf{C}_{X_k}} \leftarrow \varphi_{\mathbf{C}_{X_k}} P(X_k \,|\, \mathbf{\Pi}_{X_k}).$$

Make sure that you understand this operation: interpret $P(X_k \,|\, \mathbf{\Pi}_{X_k})$ as a function of *all* variables contained in $\mathbf{C}_{X_k}$.

After this initialization, the conditional distributions $P(X_k \,|\, \mathbf{\Pi}_{X_k})$ of all variables (and hence the information from the BN) have been multiplied into the clique potentials, and (122) is satisfied:

$$\frac{\prod_i \varphi_{\mathbf{C}_i}}{\prod_j \varphi_{\mathbf{S}_j}} = \frac{\prod\limits_{k=1,\ldots,n} P(X_k|\mathbf{C}_{X_k})}{1} = \prod_{k=1,\ldots,n} P(X_k|\mathbf{\Pi}_{X_k}) = P(\mathbf{X}),$$

where i ranges over all cliques, j over all sepsets, and k over all RVs.

After having initialized the join tree potentials, we make them locally consistent by propagating the information, which has been locally multiplied-in, across the entire join tree. This is done through a suite of *message passing* operations, each of which makes one clique/sepset pair consistent. We first describe a single message pass operation and then show how they can be scheduled such that a message pass does not destroy consistency of clique/sepset pairs that have been made consistent in an earlier message passing.

A single message pass. Consider two adjacent cliques $\mathbf{C}$ and $\mathbf{D}$ with an intervening sepset $\mathbf{S}$ and their associated belief potentials $\varphi_{\mathbf{C}}, \varphi_{\mathbf{D}}, \varphi_{\mathbf{S}}$. A message pass from $\mathbf{C}$ to $\mathbf{D}$ occurs in two steps:

1. "Projection": create a copy $\varphi_{\mathbf{S}}^{\mathsf{old}}$ of $\varphi_{\mathbf{S}}$ for later use, then recompute $\varphi_{\mathbf{S}}$ by marginalization from $\mathbf{C}$:

$$\varphi_{\mathbf{S}}^{\mathsf{old}} = \varphi_{\mathbf{S}}, \quad \varphi_{\mathbf{S}} = \sum_{\mathbf{C}\setminus\mathbf{S}} \varphi_{\mathbf{C}}.$$

This makes $\varphi_{\mathbf{S}}$ consistent with $\varphi_{\mathbf{C}}$ according to Equation 121. The joint distribution $P(\mathbf{X})$ becomes changed through this operation by a factor of $\varphi_{\mathbf{S}}^{\mathsf{old}}/\varphi_{\mathbf{S}}$ (notice that $\varphi_{\mathbf{S}}$ appears in the denominator of (122)).

2. "Absorption": multiply the belief potential of $\mathbf{D}$ by the inverse of $\varphi_{\mathbf{S}}^{\mathsf{old}}/\varphi_{\mathbf{S}}$ in order to restore the joint distribution:

$$\varphi_{\mathbf{D}} \leftarrow \varphi_{\mathbf{D}} \, \frac{\varphi_{\mathbf{S}}}{\varphi_{\mathbf{S}}^{\mathsf{old}}}.$$

A technical detail: if $\varphi_{\mathbf{S}}^{\mathsf{old}}(\mathbf{s}) = 0$, it can been shown that also $\varphi_{\mathbf{S}}(\mathbf{s}) = 0$; in this case set $\varphi_{\mathbf{S}}(\mathbf{s})/\varphi_{\mathbf{S}}^{\mathsf{old}}(\mathbf{s}) = 0$.

After this step, $\mathbf{C}$ is consistent with $\mathbf{S}$ in the sense of (121). To also make $\mathbf{D}$ consistent with $\mathbf{S}$, a message passing in the reverse direction must be carried out. An obvious condition is that this reverse-direction pass must preserve the consistency of $\mathbf{C}$ with $\mathbf{S}$. This is warrented if a certain order of passes is observed, to which we now turn our attention.

Coordinating all message passes. In order to achieve local consistency (121) for all neighboring clique-sepset pairs in the join tree, as many message passes as there are such pairs must be executed, one for each pair. In order to avoid that local consistency for a pair $\mathbf{C}$, $\mathbf{S}$ achieved by a message pass from $\mathbf{C}$ to $\mathbf{D}$ (where $\mathbf{S}$ is the sepset between $\mathbf{C}$ and $\mathbf{D}$) is not destroyed by a subsequent message pass in the reverse direction, the global order of these passes is crucial. We will motivate a global propagation scheme by considering some connection $\mathbf{C}$ – $\mathbf{S}$ – $\mathbf{D}$ within the tree, as depicted in Figure 58.

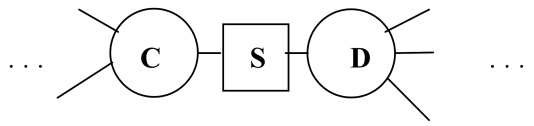

Figure 58: A connection $\mathbf{C}$ – $\mathbf{S}$ – $\mathbf{D}$ within the tree.

This connection will be hit twice by a message pass, one in each direction. Assume that the first of the two passes went from $\mathbf{C}$ to $\mathbf{D}$. After this pass, we have potentials $\varphi^0_{\mathbf{C}}, \varphi^0_{\mathbf{S}}, \varphi^0_{\mathbf{D}}$, and $\mathbf{C}$ is consistent with $\mathbf{S}$:

$$\varphi^0_{\mathbf{S}} = \sum_{\mathbf{C}\setminus\mathbf{S}} \varphi^0_{\mathbf{C}}.$$

At some later time, a message pass sweeps back from $\mathbf{D}$ to $\mathbf{C}$. Before this happens, the potential of $\mathbf{D}$ might have been affected by some other passes, so it is $\varphi^1_{\mathbf{D}}$ when the pass from $\mathbf{D}$ to $\mathbf{C}$ occurs. After this pass, we have

$$\varphi^1_{\mathbf{S}} = \sum_{\mathbf{D}\setminus\mathbf{S}} \varphi^1_{\mathbf{D}} \quad \text{and} \quad \varphi^1_{\mathbf{C}} = \varphi^0_{\mathbf{C}} \, \frac{\varphi^1_{\mathbf{S}}}{\varphi^0_{\mathbf{S}}}.$$

It turns out that still $\mathbf{S}$ is consistent with $\mathbf{C}$:

$$\varphi^1_{\mathbf{S}} = \varphi^0_{\mathbf{S}} \, \frac{\varphi^1_{\mathbf{S}}}{\varphi^0_{\mathbf{S}}} = \left(\sum_{\mathbf{C}\setminus\mathbf{S}} \varphi^0_{\mathbf{C}} \right) \frac{\varphi^1_{\mathbf{S}}}{\varphi^0_{\mathbf{S}}} = \sum_{\mathbf{C}\setminus\mathbf{S}} \left(\varphi^0_{\mathbf{C}} \, \frac{\varphi^1_{\mathbf{S}}}{\varphi^0_{\mathbf{S}}} \right) = \sum_{\mathbf{C}\setminus\mathbf{S}} \varphi^1_{\mathbf{C}}.$$

In summary, we see that if a connection $\mathbf{C}$ – $\mathbf{S}$ – $\mathbf{D}$ is hit by two passes, one for each direction, $\mathbf{S}$ will be consistent with $\mathbf{C}$ and $\mathbf{D}$. In order to ensure consistency for all connections in the tree, we must make sure that after some connection $\mathbf{C}$ –

S – **D** has been passed back and forth, neither **C** nor **D** take part in any further passes, as this might again disrupt the already achieved consistency. The following global scheduling scheme assures this condition:

1. To start, single out any clique **C** and call it the "center".
2. In a first phase ("collect evidence" in the Huang/Darwiche paper), carry out all passes that are oriented towards the center. Carry out these passes in any order such that a pass "leaves" some node on some connection only after all other "incoming" connections have been used for passes.
3. In a second phase ("distribute evidence"), carry out all passes that are oriented away from the center. Observe the same order constraint as in the first phase.

Figure 59 shows a possible global scheduling for our example join tree.

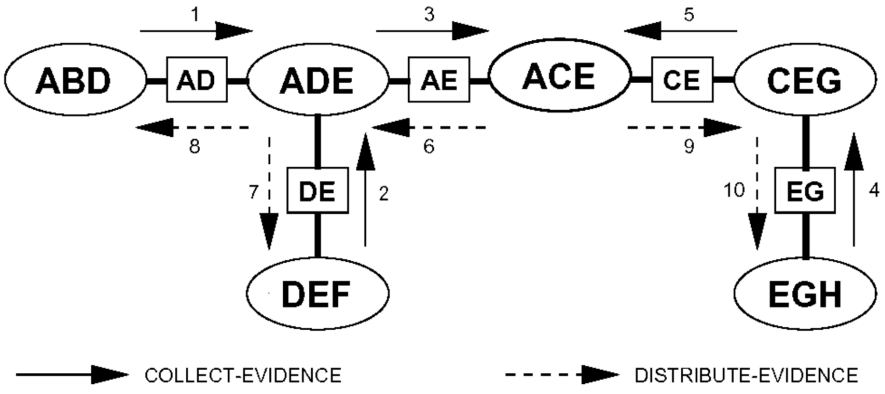

Figure 59: A scheduling for the global propagation of message passing. The center is ACE. Figure taken from the Huang/Darwiche paper.

After all of this toiling, we have a magic join tree $\mathcal{T}$ — a tree graph adorned with belief potentials that are locally consistent (Equation 121) and globally represent the joint distribution $P(\mathbf{X})$ (Equation 122). The join tree is now ready for use in inference tasks.

Inference task 1: compute a single marginal distribution. For any RV X in the BN, computing the marginal distribution $P(X)$ is a simple two-step procedure:

1. Identify a clique or sepset $\mathbf{K}$ which contains X.
2. Obtain $P(X)$ by marginalization

$$P(X) = \sum_{\mathbf{K}\setminus\{X\}} \varphi_{\mathbf{K}}.$$

This follows from Proposition 10.3.

Inference task 2: Compute conditional distributions. Most use-cases of BNs concern the calculation of probabilities for certain events, given that some information is known / measured / observed. For instance, in the Space Shuttle example, one wants to know the probability that the engine will explode given certain sensor readings; or in medical diagnostic one wants to know the probability that the patient has cancer given lab results.

In formal terms, this means to calculate conditional distributions of the kind $P(Z \mid E_1 = e_1, \ldots, E_k = e_k)$, where $Z, E_1, \ldots, E_k$ are variables in the BN, and current values for the E_i are known. The known facts $E_i = e_i$ are called *evidence*.

Let $e_1, \ldots, e_k = \mathbf{e}$ be an evidence, that is values for RVs $E_1, \ldots, E_k = \mathbf{E}$. To feed this information into $\mathcal{T}$, we introduce a new kind of belief potentials called (in this context) *likelihoods*. For each $E \in \mathbf{E}$ we define the likelihood $\Lambda_E : R_E \to \{0, 1\}$ by

$$\Lambda_E(e) = \begin{cases} 1 & \text{if } e \text{ is the observed value of } E \\ 0 & \text{for all other } e \in R_E \end{cases}$$

In order to compute $P(Z \mid E_1 = e_1, \ldots, E_k = e_k) = P(Z \mid \mathbf{e})$, we have to go through the routine of initializing $\mathcal{T}$ and making it consistent via global message propagation again, using an augmented version of the method described previously. Here is how.

Initialization: Exactly as described above. This yields initial belief potentials $\varphi_{\mathbf{C}}, \varphi_{\mathbf{S}}$ for all cliques and sepsets.

Observation entry: for each $E \in \mathbf{E}$, do the following:

1. Identify a clique $\mathbf{C}_E$ which contains E.
2. Update $\varphi_{\mathbf{C}_E} = \varphi_{\mathbf{C}_E} \, \Lambda_E$.

Here $\varphi_{\mathbf{C}_E} \, \Lambda_E$ is a shorthand for the function $\varphi_{\mathbf{C}_E} \, \Lambda_E : R_E \times R_{A_1} \times \ldots \times R_{A_l} \to \mathbb{R}^{\geq 0}$ defined by

$$\varphi_{\mathbf{C}_E} \, \Lambda_E(\tilde{e}, a_1, \ldots, a_l) = \varphi_{\mathbf{C}_E}(\tilde{e}, a_1, \ldots, a_l) \ \cdot \ \Lambda_E(\tilde{e}),$$

where $\mathbf{C}_E$ has labels $(E, A_1, \ldots, A_l)$, that is, $\varphi_{\mathbf{C}_E} \, \Lambda_E$ simply resets $\varphi_{\mathbf{C}_E}$ to zero for all arguments that have a different value for E than the observed one. With the new potentials, the tree globally encodes $P(\mathbf{X}) \, \mathbf{1}_{\mathbf{e}}$, where $\mathbf{1}_{\mathbf{e}} : R_{\bigotimes X_i} \to \{0, 1\}$ is the indicator function of the set $\{(x_1, \ldots, x_n) \in R_{\bigotimes X_i} \mid x_i = e_j \text{ for } X_i = E_j, j = 1, \ldots, k\}$:

$$\frac{\prod_i \varphi_{\mathbf{C}_i}}{\prod_j \varphi_{\mathbf{S}_j}} = P(\mathbf{X}) \, \Lambda_{E_1} \ldots \Lambda_{E_k} = P(\mathbf{X}) \, \mathbf{1}_{\mathbf{e}} =: P(\mathbf{X}, \mathbf{e}).$$

Note furthermore that

$$\sum_{\mathbf{X}\setminus\mathbf{E}} = P(\mathbf{e}).$$

Global propagation: Global propagation: exactly as before, but starting from the updated potentials obtained by observation entry. After this is completed, the join tree is locally consistent. Furthermore, each clique or sepset $\mathbf{K}$ has a potential satisfying

$$\varphi_{\mathbf{K}} = P(\mathbf{K}, \mathbf{e}).$$

Normalization: In order to compute $P(Z \mid \mathbf{e})$, determine a clique $\mathbf{C}_Z$ which contains Z. When we marginalize this clique's potential to Z, we obtain the probability of Z *and* $\mathbf{e}$:

$$\sum_{\mathbf{C}_Z\setminus\{X\}} \varphi_{\mathbf{C}_Z} = P(Z, \mathbf{e}).$$

But our goal is to compute $P(Z|\mathbf{e})$, the distribution of Z given $\mathbf{e}$. We obtain this by normalizing $P(Z|\mathbf{e})$:

$$P(Z \mid \mathbf{e}) = \frac{P(Z, \mathbf{e})}{P(\mathbf{e})} = \frac{P(Z, \mathbf{e})}{\sum\limits_{z \in S_Z} P(Z, \mathbf{e})}.$$

10.1.3 Learning Bayesian networks

We have seen how we can calculate statistical inferences on the basis of a given BN. But who gives it to us, and how?

A common approach, especially in AI, is to distil the conditional probability tables from interviews with experts of the target domain. Domain experts often have clear conceptions of local conditional probabilities that connect a few variables. You might ask, why use a BN if such experts are available? The answer is that while humans may have a good insight on local interdependencies between a few variables, they are psychologically and intellectually poorly equipped to use this local knowledge for making sound statistical inferences which connect many variables in a globally connected causal interaction system.

In other cases, empirical observations are available that allow one to estimate the conditional probability tables from data. For instance, the table shown in Equation (116) could have been estimated from counts # of observed outcomes as suggested in Figure 60.

Notice that each row in such a table is estimated independently from the other rows. The task of estimating such a row is the same as estimating a discrete distribution from data. When there is no abundance of data, Bayesian model estimation via Dirichlet priors is the way to go, as in the protein frequency estimation in Section 8.3.

X_2	X_3	$\#(X_4 = 0)$	$\#(X_4 = 1)$
0	0	7	0
0	1	2	18
1	0	1	9
1	1	2	198

frequency counts

X_2	X_3	$P(X_4 = 0)$	$P(X_4 = 1)$
0	0	1.0	0.0
0	1	0.1	0.9
1	0	0.1	0.9
1	1	0.01	0.99

maximum likelihood probability estimates

Figure 60: Example of estimating a probability table from frequency counts.

When data like in Figure 60 are available for all nodes in a BN, estimating the local conditional probabilities by the obvious frequency counting ratios gives maximum likelihood estimates of the local conditional probabilities. It can be shown that this is also the maximum likelihood estimate of the joint distribution $P(\mathbf{X})$ (not a deep result, the straightforward derivation can be found in the online lecture notes Ermon 2019, chapter "Learning in directed models").

It is very often the case that for some of the variables, neither empirical observations nor an expert's opinion is available, either because simply the observations have not been attempted or because these quantities are in principle unobservable. Such unobservable variables are called *hidden variables*. To get an impression of the nature and virtues of hidden variables, consider the BN in Figure 61.

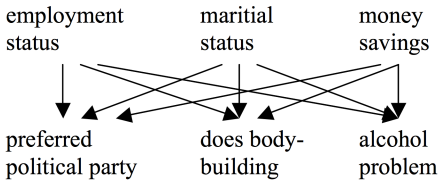

Figure 61: A BN for use by a social worker (apologies to professionals in the field)

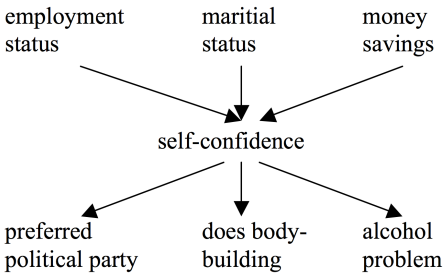

Figure 62: A BN for use by a psychologically and statistically enlightened social worker

Maritial status is hardly causal for political preferences. According to some (folk) psychology, the BN shown in Figure 62 would more appropriately capture the causal logics connecting the variables from the model in Figure 61.

However, nobody has yet found a convincing way to directly measure self-confidence — it is an *explanatory* concept, and becomes a hidden variable in a statistical model. While all other variables in this BN can be readily measured, self-confidence can't. Yet the augmented BN is, in an intuitive sense, more valuable than the first one, because it tries to reveal a causal mechanism whereas the former one only superficially connects variables by arrows that can hardly be understood.

Besides being intellectually more pleasing, the second BN offers substantial computational savings: its join tree (construct it!) is much more lightweight than the first BN's, so statistical inference algorithms will run much faster.

Generalizing from this simplistic example, it should be clear that hidden variables are a great asset in modeling reality. But — they are hidden, which means that the requisite probability tables cannot be directly estimated from empirical data.

When there are hidden variables in a BN for whose conditional distribution either no data are available one uses EM algorithms to estimate their probability tables. The basic version of EM for BNs which seems standard today has been introduced in a paper by Lauritzen 1995. The algorithm is also described in a number of online tutorials and open access papers, for instance Mouafo et al. 2016. The algorithm is complex. In the E-step it uses inference in join trees as a subroutine.

10.2 Undirected graphical models

Undirected graphical models (UGMs) play a much larger role than just helping out as intermediate representations on the way from a BN to a join tree. UGMs have been (re-)discovered independently in different fields and under different names, for instance as

Markov random fields, a quite generic concept/word used in statistics but also in a more special sense in image processing;

Ising models, a class of models of 2D or 3D magnetic / spintronic / quantum-dynamical materials explored in statistical physics,

Boltzmann machines, a kind of stochastic, recurrent neural networks which give a wonderfully elegant and powerful model of a universal learning system, — unfortunately, computationally intractable,

restricted Boltzmann machines, a stripped-down version of the former, computationally tractable, and instrumental in kicking off the deep learning revolution (Hinton and Salakuthdinov 2006).

I originally planned to have a section on these models, exploring their deep connection to physics and giving a demo in an image denoising task. But the BN part of this section has grown sooooo long that I think it would be too much

for one session of this course. If you are interested — the online course notes of Stefano Ermon (Ermon 2019) include an easy-reading fast introduction to Markov random fields in the chapter with the same name, and my legacy lecture notes on "Statistical and Algorithmical Modeling" (`https://www.ai.rug.nl/minds/uploads/LN_AlgMod.pdf`) have a Section 6.3 on UGMs which is somewhat more substantial.

10.3 Hidden Markov models

I also planned to introduce *hidden Markov models* (HMMs) in this session. HMMs are models of stochastic processes with memory — *the* standard model of such processes. A modern view of HMMs is to see them as graphical models, and since they are designed around hidden RVs (hence their name!), they are trained with a dedicated and efficient version of EM. All of this would be very "nice to have" but Christmas is approaching and we should better be starting to think about stopping to think about machine learning for a while. If you are very motivated — the classical tutorial text on HMMs is Rabiner 1990.

HMMs are models of stochastic *processes* — they describe how observations made in the *past* change conditional probabilities of things that may be observed in the *future*. HMMs use DAGs, like Bayesian networks, but with HMMs, there are causal arrows that mean *causation in time*: the causing RV X_n is *earlier* than the influenced RV X_{n+1}. This leads to potentially infinite DAGs (if time just runs on), and connects graphical models to the theory of stochastic processes. In recent years, directed graphical models which contain arrows that mean timesteps and which are more complex than HMMs have become studied. A pioneer is Kevin Murphy who more or less established this field with his PhD thesis (K. P. Murphy 2002) — another case of starting a stellar career by tying together all sorts of existing loose ends in one unifying, tutorial work.

11 Online adaptive modeling

Often an end-user of a machine learning model finds himself/herself in a situation where the distribution of the input data needed by the model change over time. The learnt model will then become inaccurate because it was trained with training data that had another distribution of the input data. It would be desirable if the learnt model could *adapt* itself to the new situation. Two examples:

- A speech recognition system is used in a situation where background noise obscures the speech input — and the background noise is of a sort that was not contained in the training data.
- A credit risk prediction system is used month after month — but when an economical crisis changes the loantakers' payback morale, the system should change its prediction biases.

Never-ending adaptation of machine learning systems has always been an issue for machine learning. Currently this theme is receiving renewed attention in deep learning in a special, somewhat restricted version, where it is discussed under the headline of *continual learning* (or *continuous learning*). Here one seeks solutions to the problem that, if an already trained neural network is subsequently trained even more on new incoming training data, the previously learnt competences will be destructively over-written by the process of continuing learning on new data. This phenomenon is known since long as *catastrophic forgetting*. Methods for counter-acting catastrophic forgetting are developing fast. I upload a snapshot summary of the continual learning scene on Nestor's "Contents" page (file *Brief Overview of Continual Learning Approaches*, written by Xu He, a PhD student in my group).

In this section I will however not deal with continual (deep) learning, for two reasons: (i) this material is advanced and requires substantial knowledge of deep learning methods, (ii) the currently available methods still fall short of the desired goal to enable ongoing, "life-long" learning.

Instead, I will present methods which have since long been explored and successfully used in the field of signal processing and control. This material is not normally treated in machine learning courses — I dare say, mostly because machine learners are mostly just not aware of this body of knowledge, and maybe also if they are, they find these methods too "linear" (no neural networks involved!). But I find this material most valuable to know,

- because these techniques are broadly applicable, especially in application contexts that involve signal processing and control — like robotics, industrial engineering applications, and modeling biological systems;
- because these techniques are mathematically elementary and transparent and give you a good understanding of conditions when gradient descent

optimization of loss functions becomes challenged — you will understand better why deep learning algorithms sometimes become veeeeery slow or numerically instable;

- and finally, because I think that machine learning is an interdisciplinary enterprise and I believe that these signal processing flavored methods will become important in a young and fast-growing field of research called *neuromorphic computing* which has a large overlap with machine learning — my own field since a few years.

Throughout this section, I am guided by the textbook *Adaptive Filters: Theory and Applications* (Farhang-Boroujeny 1998).

11.1 The adaptive linear combiner

In this subsection I introduce basic terminology and notation and the fundamental system model used throughout, the *adaptive linear combiner*.

I start with a refresher on systems and signals terminology. A discrete-time, real-valued *signal* is a left-right infinite, real-valued sequence $\mathbf{x} = (x(n))_{n\in\mathbb{Z}} \in \mathbb{R}^{\mathbb{Z}}$ (we will only consider discrete- time, real-valued signals). Note that in this section, $\mathbf{x}$ refers to a complete sequence of values; if we want to single out a particular signal value at time n, we write $x(n)$. I will often use the shorthand $(x(n))$ for $(x(n))_{n\in\mathbb{Z}}$.

A *filter* (or *system* — this word is a synonym for "filter" in the world of signal processing) H is a mapping from signals to signals, written $\mathbf{y} = H(\mathbf{x})$. The signal processing folks like to put this in a diagram where the filter is a box, see Figure 63.

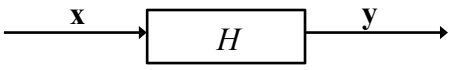

Figure 63: Diagram representation of a filter (or system) H.

The signal $\mathbf{x}$ is the *input* signal and $\mathbf{y}$ is the *output* signal of H.

There are arbitrarily complex filters — only think of a filter where the input signals are (sampled versions of) microphone recordings of an English speaker and the output is synthesized speech of an online Dutch translation of the input signal. In this section we will restrict ourselves to a particularly simple, yet immensely useful, class of filters called *transversal filters*. A transversal filter generates the output by a linear transform of the L preceding input values, where L is the *length* of the transversal filter:

Definition 11.1 *Let $L \geq 1$ be an integer, and let $\mathbf{w} \in \mathbb{R}^L$ be a vector of* filter weights. *The* transversal filter $H_{\mathbf{w}}$ *is the filter which transforms an input signal $\mathbf{x} = (x(n))$ into the output $\mathbf{y} = H_{\mathbf{w}}(\mathbf{x})$ defined by*

$$y(n) = \mathbf{w}' \ (x(n), x(n-1), \ldots, x(n-L+1))' \,. \tag{125}$$

Note that here we consider the vector $\mathbf{w}$ as a column vector (often in the literature, this specific weight vector is understood as row vector — as we did in our earlier treatment of linear regression). Transversal filters are linear filters. A filter H is called *linear* if for all $a, b \in \mathbb{R}$ and signals $\mathbf{x}_1, \mathbf{x}_2$

$$H(a\,\mathbf{x}_1 + b\,\mathbf{x}_2) = a\,H(\mathbf{x}_1) + b\,H(\mathbf{x}_2). \tag{126}$$

The proof that transversal filters are linear is an easy exercise.

I remark in passing that the theory of signals and systems works with complex numbers throughout both for signals and filter parameters; for us it is however good enough if we only use real-valued signals and model parameters.

The *unit impulse* $\delta = (\delta(n))$ is the signal that is zero everywhere except for $n = 0$, where $\delta(0) = 1$. The *unit impulse response* of a filter H is the signal $H(\delta)$. For a transversal filter $H_{\mathbf{w}}$, the unit impulse response is the signal which repeats $\mathbf{w} = (w_1, \ldots, w_L)'$ at times $n = 0, 1, \ldots, L-1$:

$$(H_{\mathbf{w}}(\delta))(n) = \begin{cases} w_i & \text{if } n = i-1 \quad (i = 1, \ldots, L), \\ 0 & \text{else.} \end{cases} \tag{127}$$

Figure 64 shows the structure of a transversal filter in the graphical notation used in signal processing.

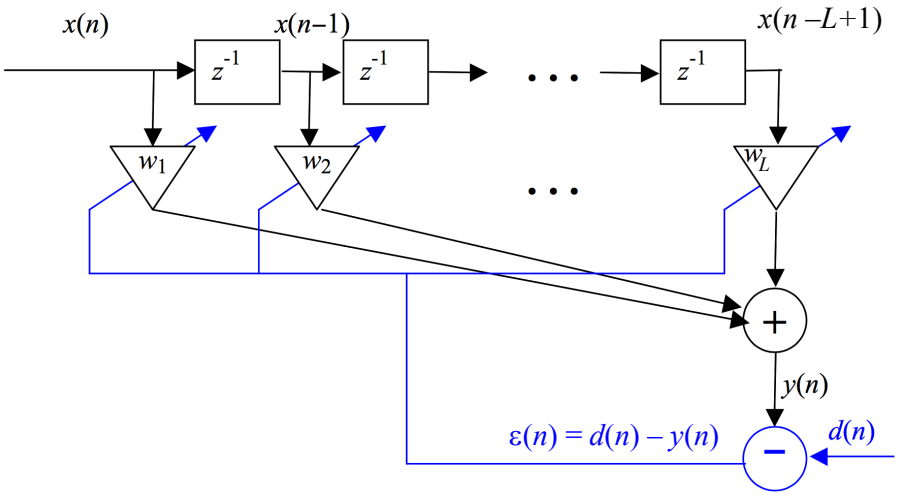

Figure 64: A transversal filter (black parts) and an adaptive linear combiner (blue parts). Boxes labeled z^{-1} are what signal processing people call "unit delays" — elementary filters which delay an input signal by one timestep. The triangular boxes mean "multiply with".

The theme of this section is online adaptive modeling. In the context of filters, this means that the filter changes over time in order to continue complying with new situational conditions. Concretely, we consider scenarios of supervised

training adaptation, where a teacher output signal is available. We denote this "desirable" filter output signal by $(d(n))$. The objective of *online adaptive filtering* is to continually adapt the filter weights w_i such that the filter output $y(n) = \mathbf{w}'\,(x(n), \ldots, x(n-L+1))'$ stays close to the desired output $d(n)$.

The situational conditions may change both with respect to the input signal $x(n)$, which might change its statistical properties, and/or with respect to the teacher $d(n)$, which might also change. For getting continual optimal performance this implies that the filter weights must change as well: the filter weight vector $\mathbf{w}$ becomes a temporal variable $\mathbf{w}(n)$. Using the shorthand $\mathbf{x}(n) = (x(n), \ldots, x(n-L+1))'$ for the last L inputs up to the current $x(n)$, this leads to the following online adaptation task:

Given at time n: the filter weight $\mathbf{w}(n-1)$ calculated at the end of the previous timestep; new data $x(n), d(n)$.

Compute error at time n: $\varepsilon(n) = d(n) - \mathbf{w}'(n-1)\,\mathbf{x}(n)$.

Adaptation goal: Compute new filter weights

$$\mathbf{w}(n) = \mathbf{w}(n-1) + \Delta_{\mathbf{w}}(n)$$

such that the squared error

$$\varepsilon^2(n+1) = (d(n+1) - \mathbf{w}'(n)\,\mathbf{x}(n+1))^2$$

at the *next* timestep can be predicted to be small. Notes:

- At the time of computing $\mathbf{w}(n)$, the next input/target pair $x(n+1), d(n+1)$ is not yet known. The filter weights $\mathbf{w}(n)$ can only be optimized with regards to the *expected* next input/target pair $x(n+1), d(n+1)$.
- Because the future signals x and d at time $n+1$ and later are not yet known, the best one can do is to assume that the x and d signals in the next timesteps will follow the same rules as during the known past $x(n), d(n), x(n-1), d(n-1), \ldots$ up to the present moment. The filter weights $\mathbf{w}(n)$ will (have to) be adapted such that the known squared errors that would be obtained *in the past*, namely $\varepsilon^2(n-l) = (d(n-l) - \mathbf{w}'(n)\,\mathbf{x}(n-l))^2$ (where $l = 0, 1, 2, \ldots$), are minimized on average. Since the input-output rule may be changing with time, only a limited-horizon past can be used to minimize the average past error. We will later see that the best option is to use a discounted past: the filter weights $\mathbf{w}(n)$ will be optimized to minimize more recent squared errors more strongly than squared errors that lie further in the past. This will automatically happen if the modification $\Delta_{\mathbf{w}}(n)$ is based only on the current error $\varepsilon(n) = d(n) - \mathbf{w}'(n-1)\,\mathbf{x}(n)$. Information from

earlier errors will already be incorporated in $\mathbf{w}(n-1)$. This leads to an error feedback based weight adaptation which is schematically shown in the blue parts of Figure 64. A diagonal arrow through a box is the way how parameter adaptation is depicted in such signal processing diagrams. Such continually adapted transversal filters are called *adaptive linear combiners* in the Farhang/Boroujeny textbook.

- The error signal $\varepsilon^2(n)$ which the adaptive filter tries to keep low need not always be obtained by comparing the current model output $\mathbf{w}(n-1)'\mathbf{x}(n)$ with a teacher $d(n)$. Often the "error" signal is obtained in other ways than by comparison with a "teacher". In any case, the objective for the adaptation algorithm is to keep the "error" amplitude at low levels. The error signal itself is the only source of information to steer the adaptation (compare Figure 64). Several examples in the next subsection will feature "error" signals which are not computed by comparison with a teacher signal.

11.2 Basic applications of adaptive linear combiners

Before explaining concrete algorithms for weight adaptation I want to highlight the importance and versatility of adaptive linear combiners with a choice of application examples, mostly taken from the Farhang/Boroujeny textbook.

11.2.1 System identification

This is the most basic task: reconstruct from $\mathbf{x}$ and teacher $\mathbf{d}$ a filter ("model system", "system model", "identification model") whose output $\mathbf{y}$ approximates $\mathbf{d}$. This kind of task is called *system identification*. A schematic block diagram for this kind of application is shown in Figure 65.

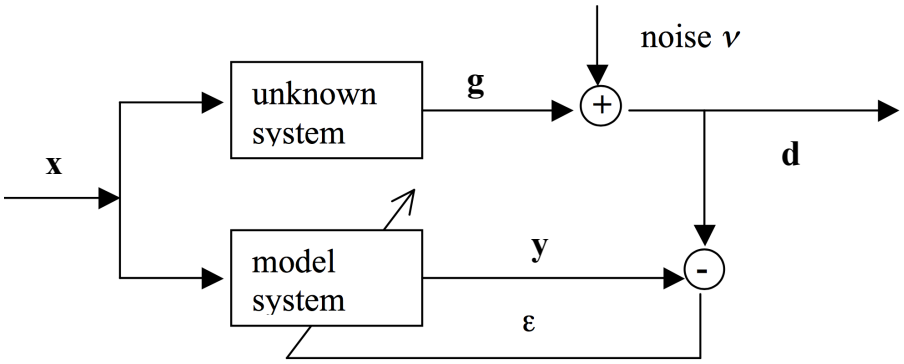

Figure 65: Schema of the system identification task.

The following game is played here. Some target system is monitored while it receives an input signal $\mathbf{x}$ and generates an output $\mathbf{g}$ which is (with added

observation noise ν) observed; this observed signal output becomes the teacher **d**. The model system is a transversal filter $H_{\mathbf{w}}$ whose weights are adapted such that the model system's output **y** stays close to the observed output **d** of the target system.

Obtaining and maintaining a model system $H_{\mathbf{w}}$ is a task which occurs ubiquitously in system engineering tasks. The model system can be used for manifold purposes because it allows to simulate the target system. Such simulation models are needed, for instance, for making predictions about the future behavior of the original system, or for assessing whether the target system might be running into malfunction modes. Almost every *control* or *predictive maintenance* task in electric or mechanical engineering requires system models. I proceed to illustrate the use of system models with two concrete examples taken from the Farhang/Boroujeny book.

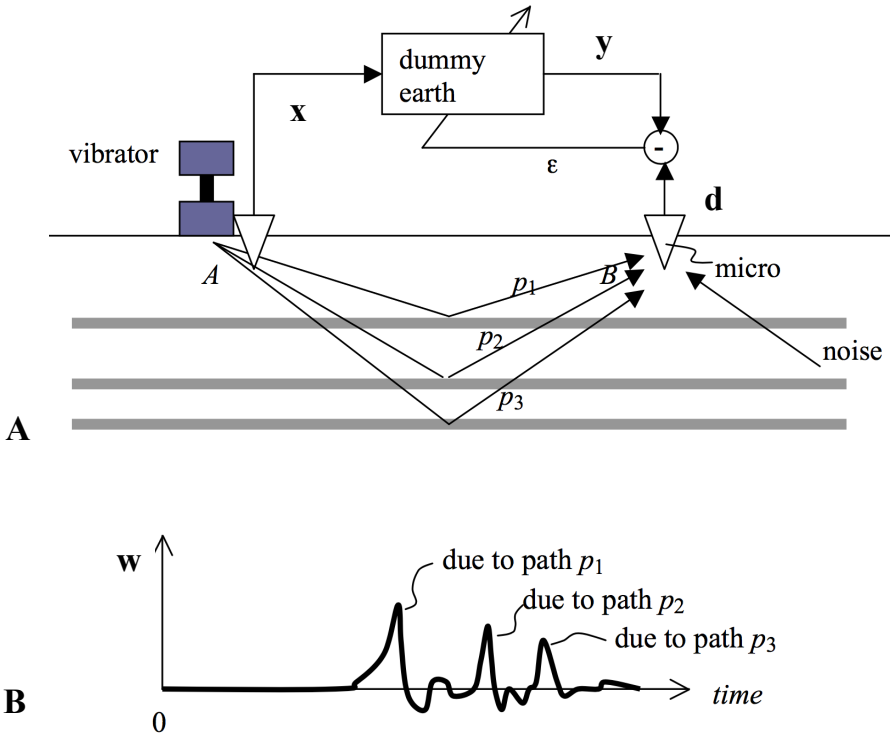

Figure 66: Geological exploration via impulse response of learnt earth model. **A**. Physical setup. **B**. Analysis of impulse response.

Geological exploration. In geological prospecting, before one digs expensive holes, one wishes to obtain an idea of what's what underground. Figure 66 shows the basic principle of exploring the structure of the ground under the earth surface. At some point A, the earth surface is excited by a strong acoustic signal (explosion or large vibrating mass). An earth microphone is placed at a distant point B,

picking up a signal $\mathbf{d}$. A model $H_{\mathbf{w}}$ (a "dummy earth") is learnt. After $H_{\mathbf{w}}$ is obtained, one analyses the impulse response $\mathbf{w}$ of this model. The peaks of $\mathbf{w}$ give indications about reflecting layers in the earth crust between A and B, which correspond to different delayed responses p_j of the input impulse.

Adaptive open-loop control. In general terms, an *open-loop* (or *direct* or *inverse* or *feedforward*) controller is a filter that generates an input signal $\mathbf{u}$ into a system (called "plant" in control engineering) such that the system output $\mathbf{y}$ follows a reference (or target) trajectory $\mathbf{r}$ as closely as possible. For example, when the plant is an electric motor which one desires to deliver a rotation speed ($r(n)$), generate a voltage signal ($u(n)$) such that the motor's actual speed ($y(n)$) comes close to the target ($r(n)$). Since electric motors are nonlinear and have inertia effects which delay the speed response to input voltage changes, this is not necessarily a simple task.

One way to achieve this objective is to maintain a transversal filter model $\hat{H} = H_{\mathbf{w}}(n)$ of the plant H by online weight adaptation and analytically compute an *inverse filter* $H_{\mathbf{w}}^{-1}(n)$ for $H_{\mathbf{w}}(n)$. The inverse G^{-1} of a filter G is a filter which cancels the effects of G, that is, for any input signal $\mathbf{x}$, one has $G^{-1}(G(\mathbf{x})) = \mathbf{x}$. Figure 67 shows the idea.

Note that the inverse of a transversal filter $H_{\mathbf{w}}$ is not itself a transversal filter — it will be a filter that needs its own output fed back as additional input.

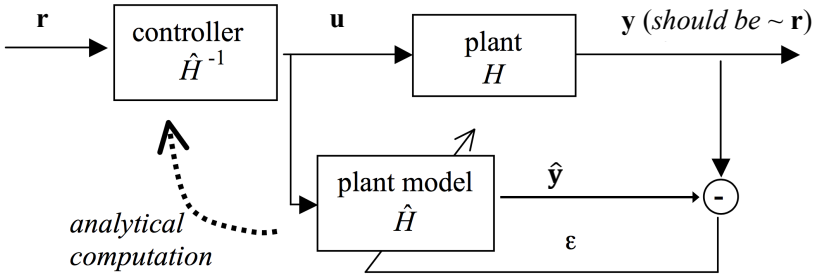

Figure 67: Schema of online adaptive direct control.

11.2.2 Inverse system identification

This is the second most basic task: given an unknown system H which on input $\mathbf{d}$ produces output $\mathbf{x}$, learn an inverse system that on input $\mathbf{x}$ produces output $\mathbf{d}$ (note the reversal of variable roles and names). A typical setup is shown in Figure 68.

This is an alternative to the analytical inversion of an estimated system model.

Introducing the delay $z^{-\Delta}$ is not always necessary but typically improves stability of the learnt system.

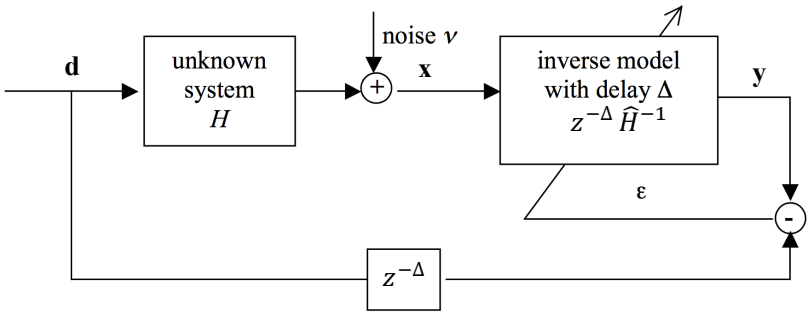

Figure 68: Schema of inverse system identification.

Equalization of a communication channel. A prime application of inverse system modeling is in digital telecommunication, where a binary signal $\mathbf{s}$ (a bit sequence) is distorted when it is passed through a noisy channel H, and should be un-distorted ("equalized") by passing it through an equalizing filter H^{-1} (for short, called an *equalizer*). In order to train the equalizer, the correct signal $\mathbf{s}$ must be known by the receiver when the equalizer is trained. But of course, if $\mathbf{s}$ would be already known, one would not need the communication in the first place. This hen-and-egg problem is often solved by using a predetermined, fixed training sequence $\mathbf{s} = \mathbf{d}$. From time to time (especially at the initialization of a transmission), the sender transmits $\mathbf{s} = \mathbf{d}$, which is known by the receiver and enables it to estimate an inverse channel model. But also while useful communication is taking place, the receiver can continue to train its equalizer, as long as the receiver is successful in restoring the binary signal $\mathbf{s}$: in that case, the correctly restored signal $\mathbf{s}$ can be used for continued training. The overall setup is sketched in Figure 69.

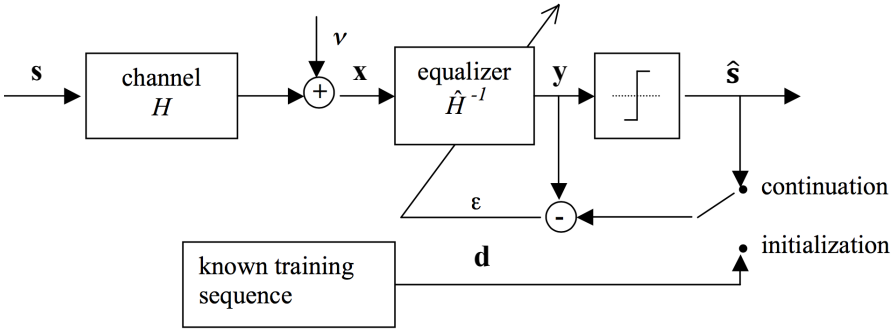

Figure 69: Schema of adaptive online channel equalization. Delays (which one would insert for stability) are omitted.

Feedback error learning for a composite direct / feedback controller. Pure open-loop control cannot cope with external disturbances to the plant. For example, if an electric motor has to cope with varying external loads, the resulting

breaking effects would remain invisible to the kind of open-loop controller shown in Figure 70. One needs to establish some sort of *feedback control*, where the observed mismatch between the reference signal **r** and the plant output **y** is used to insert corrective input to the plant. There are many ways to design feedback controllers. The "feedback controller" box in Figure 70 contains one of them without further specification.

The scheme shown in the figure (proposed in Jordan and Wolpert 1999 in a nonlinear control context, using neural networks) trains an open-loop inverse controller in conjunction with the operation of a fixed feedback controller.

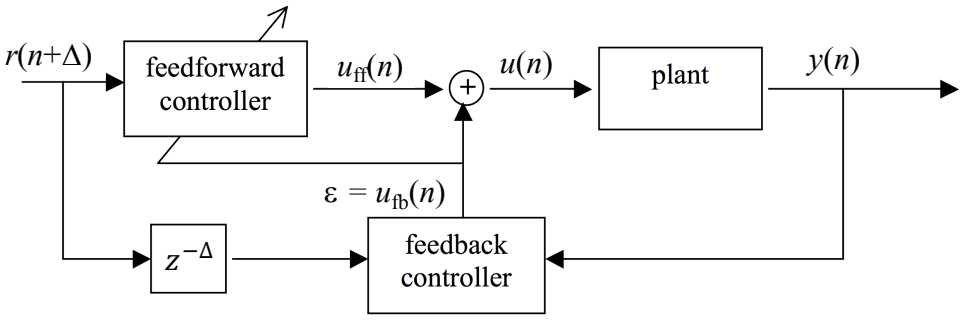

Figure 70: Schema of feedback error learning for a composite control system.

Some explanations for this ingenious architecture:

- The control input $u(n)$ is the sum of the outputs $u_{\text{fb}}(n)$ of the feedback controller and $u_{\text{ff}}(n)$ of the feedforward controller.
- There is no teacher signal **d** in this architecture. The feedforward controller is trained on an "error" signal which is defined differently than as a difference between a teacher and a system output. That is as well; the adaptation of the feedforward controller just attempts to minimize the squared "error" signal.
- If the feedforward controller works perfectly, the feedback controller detects no discrepancy between the reference $r(n)$ and the plant output $y(n)$ and therefore produces a zero output $u_{\text{fb}}(n)$ — that is, the feedforward controller sees zero error ε and does not change.
- When the feedback controller does not work perfectly, its output $u_{\text{fb}}(n)$ acts as an error signal for further adaptation of the feedforward controller. The feedforward controller tries to minimize this error — that is, it changes its way to generate output $u_{\text{ff}}(n)$ such that the feedback controller's output is minimized, that is, such that $(r(n) - y(n))^2$ is minimized, that is, such that the control improves (an admittedly superficial explanation).

- When the plant characteristics change, or when external disturbances set in, the feedback controller jumps to action, inducing further adaptation of the feedforward controller.

11.2.3 Interference cancelling, "denoising"

Assume that there is a signal $\mathbf{s}+\nu_0$ that is an additive mixture of a useful signal $\mathbf{s}$ and a noise component ν_0. You want to cancel the interfering component ν_0 from this mixture. Assume further that you also have another signal source ν_1 that is mainly generated by the same noise source as ν_0, but contains only weak traces of $\mathbf{s}$. In this situation you may use the denoising scheme shown in Figure 71.

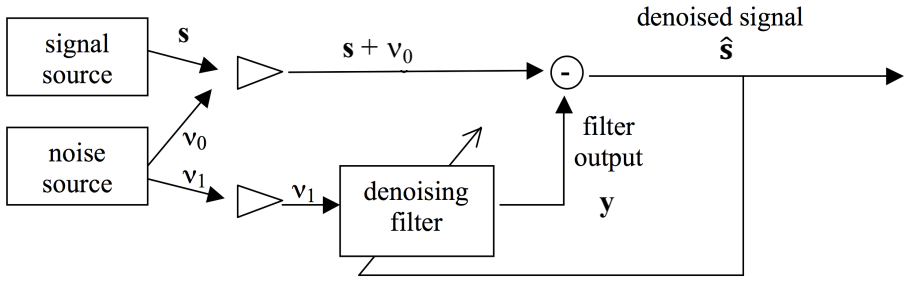

Figure 71: Schema of denoising filter.

Denoising has many applications, for instance in airplane cockpit crew communication (cancelling the acoustic airplane noises from pilot intercom speech), postprocessing of live concert recordings, or (like in one of the four suggested semester projects) cancelling the mother's ECG signal from the unborn child's in prenatal diagnostics. In the Powerpoint file *denoisingDemo.pptx* which you find on Nestor together with the lecture notes, you can find an acoustic demo that I once produced.

Explanations:

- The "error" which the adaptive denoising filter tries to minimize is $\mathbf{s}+\nu_0-\mathbf{y}$, where $\mathbf{y}$ is the filter output.

- The only information that the filter has to achieve this error minimization is its input ν_1. Because this input is (ideally) independent of $\mathbf{s}$, but related to ν_0 via some noise-to-noise filter, all that the filter can do is to subtract from $\mathbf{s}+\nu_0$ whatever it finds correlates in $\mathbf{s}+\nu_0$ with ν_1. Ideally, this is ν_0. Then, the residual "error" would be just $\mathbf{s}$.

- This scheme is interesting (not just a trivial subtraction of ν_1 from $\mathbf{s}+\nu_0$) because the mutual relationship between ν_1 and ν_0 may be complex, involving for instance a superposition of delayed versions of ν_0.

More sophisticated methods for denoising are known today, often based on mathematical principles from *independent component analysis* (ICA). You find an acoustic demo on `https://cnl.salk.edu/~tony/ica.html` (the author of this page, Anthony J. Bell, is an ICA pioneer).

11.3 Iterative learning algorithms by gradient descent on performance surfaces

So far in this course, we haven't encountered iterative learning algorithms for supervised learning tasks (the EM algorithms which we already saw are iterative, but were used for the estimation of distribution models, which is an unsupervised task). The online adaptive model estimation algorithms studied in the present section, and the "backpropagation" algorithm for training neural networks presented in the next section, are the first (and only) iterative supervised learning algorithms treated in this course. Both work by gradient descent on performance surfaces. In this subsection I give a general explanation of what that means.

11.3.1 Iterative supervised learning algorithms

A typical iterative supervised learning algorithm unfolds as follows:

Given: Training data $(\mathbf{x}_i, \mathbf{y}_i)_{i=1,\ldots,N}$ where $\mathbf{y}_i \in S_Y$; a parametric family of candidate models h_θ where each parameter vector $\theta \in \mathcal{H}$ defines a possible model ("decision function"); and a loss function $L : S_Y \times S_Y \to \mathbb{R}^{\geq 0}$.

Wanted: An optimal model

$$(\star) \qquad \theta_{\mathsf{opt}} = \operatorname*{argmin}_{\theta \in \mathcal{H}} R^{\mathsf{emp}}(\theta) = \operatorname*{argmin}_{\theta \in \mathcal{H}} \frac{1}{N} \sum_{i=1,\ldots,N} L(h_\theta(\mathbf{x}_i), \mathbf{y}_i).$$

But reality strikes: The optimization problem $(\star)$ often cannot be directly solved, for instance because it is analytically intractable (the case for neural network training) or because the training data come in as a time series and their statistical properties change with time (as in adaptive online modeling).

Second best approach: Design an iterative algorithm which produces a sequence of models (= parameter vectors) $\theta^{(0)}, \theta^{(1)}, \theta^{(2)}, \ldots$ with decreasing empirical risk $R^{\mathsf{emp}}(\theta^{(0)}) > R^{\mathsf{emp}}(\theta^{(1)}) > \ldots$. The model $\theta^{(n+1)}$ is typically computed by an incremental modification of the previous model $\theta^{(n)}$. The first model $\theta^{(0)}$ is a "guess" provided by the experimenter.

In neural network training, the hope is that this series converges to a model $\theta^{(\infty)} = \lim_{n\to\infty} \theta^{(n)}$ whose empirical risk is close to the minimal possible empirical risk. In online adaptive modeling, the hope is that if one incessantly-iteratively tries to minimize the empirical risk, one stays close to the moving target of the current best model (we'll see how that works).

This scheme only treats the approach where one tries to minimize the training loss. We know that in standard supervised learning settings this invites overfitting and that one should better employ a regularized loss function together with some cross-validation procedure, a complication that we ignore here. In online adaptive modeling, the empirical risk $R^{\mathsf{emp}}(\theta)$ is time-varying, another complication that for the time being we will ignore. Regardless of such complications, the general rationale of iterative supervised learning algorithms is to compute a sequence of models with decreasing empirical risk.

In standard (not online adaptive) settings, such iterative algorithms, if they converge, can find only locally optimal models. A model $\theta^{(\infty)}$ is locally optimal if every slight modification of it will lead to a higher empirical risk. The final converged model $\lim_{n\to\infty}\theta^{(n)}$ will depend on the initial guess $\theta^{(0)}$ — coming up with a method for good initial guesses was the crucial innovation that started the deep learning revolution (Hinton and Salakuthdinov 2006).

11.3.2 Performance surfaces

First a quick recap: the graph of a function. Recall that the graph of a function $f : A \to B$ is the set $\{(a, f(a)) \in A \times B \mid a \in A\}$ of all argument-value pairs of the function. For instance, the graph of the square function $f : \mathbb{R} \to \mathbb{R},\ x \mapsto x^2$ is the familiar parabola curve in $\mathbb{R}^2$.

A performance surface is the graph of a risk function. Depending on the specific situation, the risk function may be the empirical risk, the risk, a risk defined at a particular time (in online adaptive scenarios), or some other "cost". I will use the symbol $\mathcal{R}$ to denote a generic risk function of whatever kind.

Performance surfaces are typically discussed with parametric model families where a candidate set of models $\mathcal{H} = \{h_\theta \,|\, \theta \in \mathcal{H} \subseteq \mathbb{R}^k\}$ is given, in which an optimal (= minimal risk $\mathcal{R}$) model $h_{\mathsf{opt}} \in \mathcal{H}$ is sought by a learning algorithm. In such parametric model families, models h_θ are usually and conveniently identified with their corresponding parameter vectors θ. The performance surface then becomes the graph of the function $\mathcal{R} : \mathcal{H} \to \mathbb{R}^{\geq 0}$.

Specifically, if we have k-dimensional parameter vectors (that is, $\mathcal{H} \subseteq \mathbb{R}^k$), the performance surface is a k-dimensional hypersurface in $\mathbb{R}^{k+1}$.

Other terms are variously used for performance surfaces, for instance *performance landscape* or *error landscape* or *error surface* or *cost landscape* or similar wordings.

Performance surfaces can be objects of stunning complexity. In neural network training (next section), they are *tremendously* complex. Figure 72 shows a neural network error landscape randomly picked from the web.

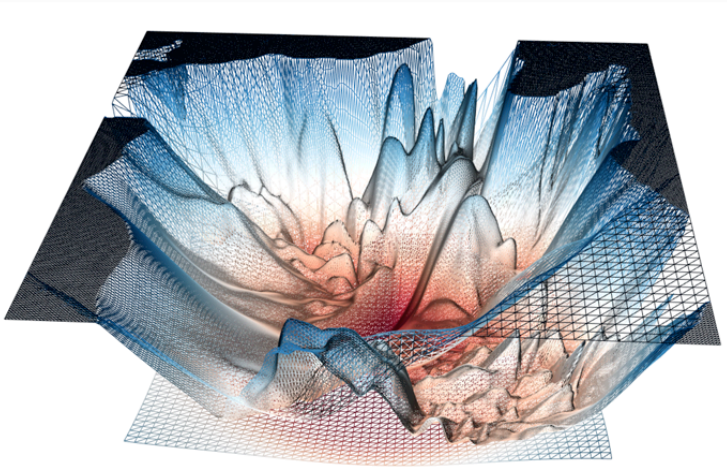

Figure 72: A (2-dimensional cross-section of) a performance surface for a neural network. The performance landscape shows the variation of the loss when (merely) 2 weights in the network are varied. Source: `http://www.telesens.co/2019/01/16/neural-network-loss-visualization/`

11.3.3 Iterative model learning by gradient descent on a performance surface

Often a risk function $\mathcal{R} : \mathcal{H} \to \mathbb{R}^{\geq 0}$ is differentiable. Then, for every $\theta \in \mathcal{H}$ the *gradient* of $\mathcal{R}$ with respect to $\theta = (\theta_1, \ldots, \theta_k)'$ is defined:

$$\nabla\mathcal{R}(\theta) = \left(\frac{\partial\mathcal{R}}{\partial\theta_1}(\theta), \cdots, \frac{\partial\mathcal{R}}{\partial\theta_k}(\theta)\right)'. \tag{128}$$

The gradient $\nabla\mathcal{R}(\theta)$ is the vector which points from θ in the direction of the steepest ascent ("uphill") of the performance surface. The negative gradient $-\nabla\mathcal{R}(\theta)$ is the direction of the steepest descent (Figure 73).

The idea of model optimization by gradient descent is to iteratively move toward a minimal-risk solution $\theta^{(\infty)} = \lim_{n\to\infty} \theta^{(n)}$ by always "sliding downhill" in the direction of steepest descent, starting from an initial model $\theta^{(0)}$. This idea is as natural and compelling as can be. Figure 74 shows one such itinerary.

The general recipe for iterative gradient descent learning goes like this:

Given: A differentiable risk function $\mathcal{R} : \mathcal{H} \to \mathbb{R}^{\geq 0}$.

Wanted: A minimal-risk model θ_{opt}.

Start: Guess an initial model $\theta^{(0)}$.

Iterate until convergence: Compute models

$$\theta^{(n)} = \theta^{(n-1)} - \mu\,\nabla\mathcal{R}(\theta^{(n-1)}). \tag{129}$$

The *adaptation rate* (or *learning rate*) μ is set to a small positive value.

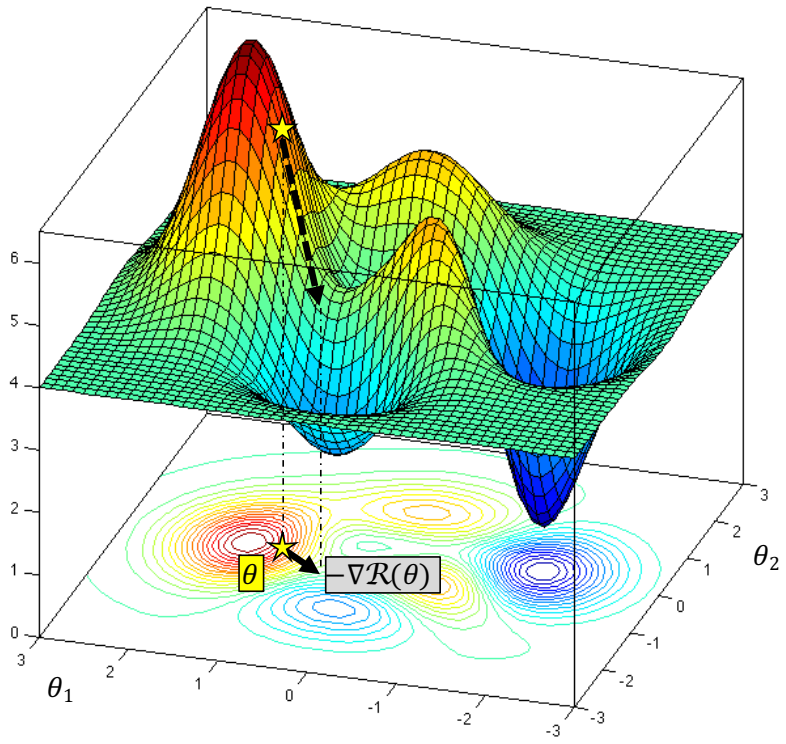

Figure 73: A performance surface for a 2-dimensional model family with parameters θ_1, θ_2, with its contour plot at the bottom. For a model θ (yellow star in contour plot) the negative gradient is shown as black solid arrow. It marks the direction of steepest descent (broken black arrow) on the performance surface.

An obvious weakness of this elegant and natural approach is that the final model $\theta^{(\infty)}$ depends on the choice of the initial model $\theta^{(0)}$. In complex risk landscapes (as the one shown in Figure 72) there is no hope of guessing an initial model which guarantees to end in the global minimum. This circumstance is generally perceived and accepted. There is a substantial mathematical literature that amounts to "if the initial model is chosen with a good heuristic, the local minimum that will be reached will be a rather good one with high probability".

We will see that the real headaches with gradient descent optimization are of a different nature — specifically, there is a inherently difficult tradeoff between speed of convergence (one does not want to invest millions or even billions of iterations) and stability (the iterations must not lead to erratic large-sized jumps that lead away from the downhill direction). The adaptation rate μ plays a key role in this difficult tradeoff. For good performance (stability plus satisfactory speed of convergence), it must be adapted online while the iterations proceed. And doing that sagaciously is not trivial. The situation shown in Figure 74 is deceptively

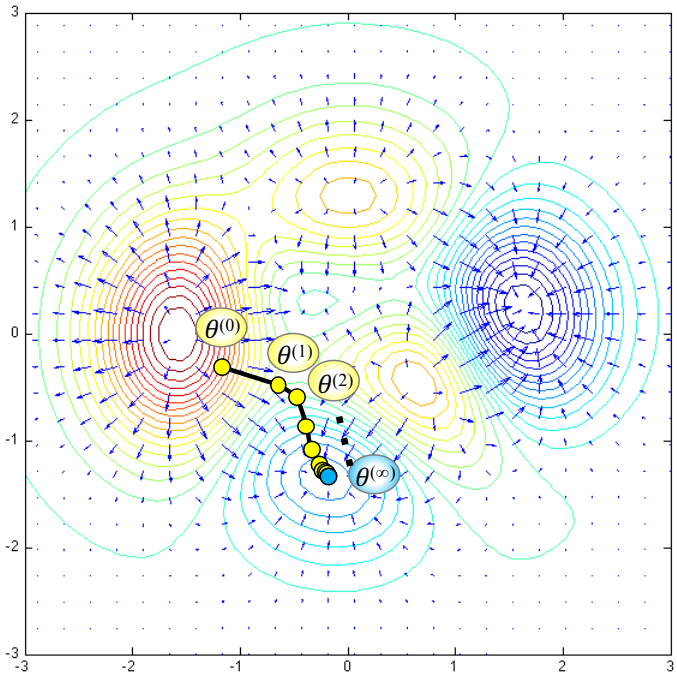

Figure 74: A gradient descent itinerary, re-using the contour map from Figure 73 and starting from the initial point shown in that figure. Notice the variable jump length and the sad fact that from this initial model $\theta^{(0)}$ the global minimum is missed. Instead, the itinerary slides toward a local minimum at $\theta^{(\infty)}$. The blue arrows show the negative gradient at raster points. They are perpendicular to the contour lines and their size is inversely proportional to the spacing between the contour lines.

simplistic; don't think that gradient descent works as smoothly as that in real-life applications.

These difficulties raise their ugly head already in the simplest possible risk surfaces, namely the ones that arise with iterative solutions to linear regression problems. Making you aware of these difficulties in an analytically tractable, transparent setting is one of the two main reasons why I believe a machine learning student should know about adaptive online learning of transversal filters. You will learn a lot about the challenges in neural network training as a side effect. The other main reason is that adaptive online learning of transversal filters is really, really useful in many practical tasks.

11.3.4 The performance surface of a stationary online learning task for transversal filters

We will now return to the specific scenario of online adaptive filtering. Recall that we are facing a left-right infinite signal of real-valued input data $(x(n))_{n\in\mathbb{Z}} \in \mathbb{R}^{\mathbb{Z}}$ paired with a desired output signal $(d(n))_{n\in\mathbb{Z}} \in \mathbb{R}^{\mathbb{Z}}$. Our goal is to compute, at every time n and on the basis of the input and teacher signals up to time n, an L-dimensional weight vector $\mathbf{w}(n)$ which we want to minimize the squared error $\varepsilon^2_{\mathbf{w}(n)}(n+1) = (d(n+1) - \mathbf{w}'(n)\,\mathbf{x}(n+1))^2$ at the next timestep.

For starters we will work under the assumption that the input and teacher statistics does not change with time. In mathematical terms, this means that the signals $\mathbf{x}$ and $\mathbf{d}$ are generated by a *stationary* stochastic process. That is, these signals come from random variables $(X_n)_{n\in\mathbb{Z}}$ and $(D_n)_{n\in\mathbb{Z}}$. Each time that we would "run" this process, we would get another pair of signals $\mathbf{x}, \mathbf{d}$. To define what "stationary" means in our context, let

$$[X^L D]_n := X_n \otimes X_{n-1} \otimes \cdots \otimes X_{n-L+1} \otimes D_n \tag{130}$$

be the combined RV which picks, at time n, the previous L inputs up to and including time n and the teacher at time n. We now say that the process is *stationary* with respect to these RVs $[X^L D]_n$, if $[X^L D]_k$ and $[X^L D]_m$ have the same distribution for all times k and m. Intuitively speaking, this means that if we look at signal sniplets $\mathbf{x}(k), d(k)$ and $\mathbf{x}(m), d(m)$ at different times m and k, the distribution of these sniplets across different runs of the stochastic process will be the same at both times. The process does not change its statistical properties over time. If this condition is met, the expectations

$$\mathbf{p} := E[\mathbf{x}(n)\, d(n)] = (E[x(n)d(n)], \ldots, E[x(n-L+1)d(n)])' \tag{131}$$

$$\mathbf{R} := E[\mathbf{x}(n)\, \mathbf{x}'(n)] \tag{132}$$

are well-defined and independent of n. $\mathbf{R}$ is called (in the field of signal processing) the *correlation matrix* of the input process; it has size $L \times L$. $\mathbf{p}$ is an L-dimensional vector.

In a stationary process there is no need to have different filter weights at different times. We can thus, for now, drop the time dependence from $\mathbf{w}(n)$ and consider unchanging weights $\mathbf{w}$. For any such weight vector $\mathbf{w}$ we consider the expected squared error

$$\begin{aligned} R(\mathbf{w}) &= E[\varepsilon^2_{\mathbf{w}}(n)] \\ &= E[((d(n) - \mathbf{w}'\,\mathbf{x}(n))\,((d(n) - \mathbf{w}'\,\mathbf{x}(n))] \\ &= E[(d(n))^2] - 2\,\mathbf{w}'\,E[\mathbf{x}(n)\,d(n)] + \mathbf{w}'\,E[\mathbf{x}(n)\,\mathbf{x}'(n)]\,\mathbf{w} \\ &= E[(d(n))^2] - 2\,\mathbf{w}'\,\mathbf{p} + \mathbf{w}'\,\mathbf{R}\,\mathbf{w}. \end{aligned} \tag{133}$$

This expected squared error for a filter $H_{\mathbf{w}}$ is the risk that we want to minimize. We now take a close look at the performance surface, that is the graph of the risk function $R : \mathbb{R}^L \to \mathbb{R}$. Its geometrical properties will turn out key for mastering the adaptive filtering task. Figure 75 gives a visual impression of the performance surface for the case of $L = 2$ dimensional weight vectors $\mathbf{w} = (w_1, w_2)'$.

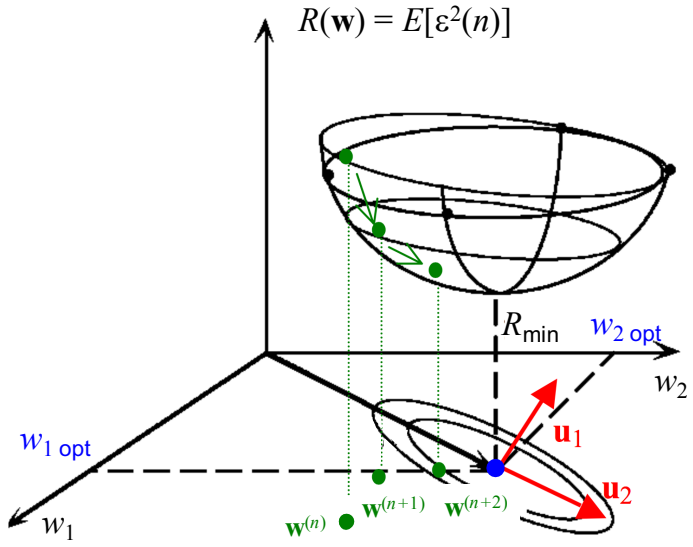

Figure 75: The performance surface, case of two-dimensional weight vectors (black parts of this drawing taken from `drip.colorado.edu/~kelvin/links/Sarto_Chapter2.ps` many years ago, page no longer online). An iterative algorithm for weight determination would try to determine a sequence of weights $\ldots, \mathbf{w}^{(n)}, \mathbf{w}^{(n+1)}, \mathbf{w}^{(n+2)}, \ldots$ (green) that moves toward $\mathbf{w}_{\text{opt}}$ (blue). The eigenvectors $\mathbf{u}_j$ of the correlation matrix $\mathbf{R}$ lie on the central axes of the hyperellipsiods given by the level curves of the performance surface (red).

I mention without proof some basic geometric properties of the performance surface. The function (133) is a (multidimensional) *quadratic function* of $\mathbf{w}$. The general form of a multidimensional quadratic function $F : \mathbb{R}^k \to \mathbb{R}$ for k-dimensional vectors $\mathbf{x}$ is $F(\mathbf{x}) = a + \mathbf{x}'\mathbf{b} + \mathbf{x}'\mathbf{C}\mathbf{x}$, where $a \in \mathbb{R}$ is a constant

offset, $\mathbf{x}'\mathbf{b}$ is the linear term, and $\mathbf{x}'\mathbf{C}\mathbf{x}$ is the quadratic term. $\mathbf{C}$ must be a positive definite matrix or negative definite matrix. The graph of a multidimensional quadratic function shares many properties with the graph of the one-dimensional quadratic function $f(x) = a + bx + cx^2$. The one-dimensional quadratic function graph has the familiar shape of a parabola, which depending on the sign of c is opened upwards or downwards. Similarly, the graph of k-dimensional quadratic function has the shape of a k-dimensional *paraboloid*, which is opened upwards if $\mathbf{C}$ is positive definite and opened downwards if $\mathbf{C}$ is negative definite. A k-dimensional paraboloid is a "bowl" whose vertical cross-sections are parabolas. The contour curves of a k-dimensional paraboloid (the horizontal cross-sections) are k-dimensional ellipsoids whose main axes lie in the directions of the k orthogonal eigenvectors $\mathbf{u}_1, \ldots, \mathbf{u}_k$ of $\mathbf{C}$.

In the 2-dimensional case of a performance surface shown in Figure 75, the paraboloid must open upwards because the risk R is an expected squared error and hence cannot be negative; in fact, the entire surface must be nonnegative. The figure also shows a projection of the ellipsoid contour curves of the paraboloid on the w_1-w_2 plane, together with the eigenvectors of $\mathbf{R}$.

Importantly, such quadratic performance surfaces have a single minimum (provided that $\mathbf{R}$ has full rank, which we tacitly take for granted). This minimum marks the position of the optimal (minimal risk) weight vector $\mathbf{w}_{\mathsf{opt}} = \operatorname{argmin}_{\mathbf{w}\in\mathbb{R}^L} R(\mathbf{w})$. An iterative learning algorithm would generate a sequence $\ldots, \mathbf{w}^{(n)}, \mathbf{w}^{(n+1)}, \mathbf{w}^{(n+2)}, \ldots$ of weight vectors where each new $\mathbf{w}^{(n)}$ would be positioned at a place where the performance surface is deeper than at the previous weight vector $\mathbf{w}^{(n-1)}$ (green dots in the figure).

The optimal weight vector $\mathbf{w}_{\mathsf{opt}}$ can be calculated analytically, if one exploits the fact that the partial derivatives $\partial R/\partial w_i$ are all zero (only) for $\mathbf{w}_{\mathsf{opt}}$. The gradient ∇R is given by

$$\nabla R = \left(\frac{\partial R}{\partial w_1}, \cdots, \frac{\partial R}{\partial w_L}\right)' = 2\,\mathbf{R}\mathbf{w} - 2\,\mathbf{p}$$

which follows from (133) (exercise). Setting this to zero gives the *Wiener-Hopf equation*

$$\mathbf{R}\mathbf{w}_{\mathsf{opt}} = \mathbf{p}, \tag{134}$$

which yields the optimal weights as

$$\mathbf{w}_{\mathsf{opt}} = \mathbf{R}^{-1}\,\mathbf{p}. \tag{135}$$

If you consider the definitions of $\mathbf{R}$ and $\mathbf{p}$ (Equations 132 and 131), you will find that this solution for $\mathbf{w}_{\mathsf{opt}}$ is the risk version of the linear regression solution (19) for the minimal empirical risk from a quadratic error loss.

In order to appreciate the challenges inherent in iterative gradient descent on quadratic performance surfaces we have to take a closer look at the shape of the hyperparaboloid.

First we use (133) and the Wiener-Hopf equation to express in the expected residual error R_{min} (see Figure 75) that we are left with when we have found $\mathbf{w}_{\mathsf{opt}}$:

$$\begin{aligned} R_{\mathsf{min}} &= E[(d(n))^2] - 2\,\mathbf{w}'_{\mathsf{opt}}\,\mathbf{p} + \mathbf{w}'_{\mathsf{opt}}\,\mathbf{R}\,\mathbf{w}_{\mathsf{opt}} \\ &= E[(d(n))^2] - \mathbf{w}'_{\mathsf{opt}}\,\mathbf{p} \\ &= E[(d(n))^2] - \mathbf{w}'_{\mathsf{opt}}\,\mathbf{R}\,\mathbf{w}_{\mathsf{opt}} \\ &= E[(d(n))^2] - \mathbf{p}'\,\mathbf{R}^{-1}\,\mathbf{p}. \end{aligned} \tag{136}$$

For a more convenient analysis we rewrite the error function R in new coordinates such that it becomes centered at the origin. Observing that the paraboloid is centered on $\mathbf{w}_{\mathsf{opt}}$, that it has "elevation" R_{min} over the weight space, and that the shape of the paraboloid itself is determined by $\mathbf{w}'_{\mathsf{opt}}\,\mathbf{R}\,\mathbf{w}_{\mathsf{opt}}$, we find that we can rewrite (133) as

$$R(\mathbf{v}) = R_{\mathsf{min}} + \mathbf{v}'\,\mathbf{R}\,\mathbf{v}, \tag{137}$$

where we introduced shifted (and transposed) weight coordinates $\mathbf{v} = (\mathbf{w} - \mathbf{w}_{\mathsf{opt}})$. Differentiating (137) with respect to $\mathbf{v}$ yields

$$\frac{\partial R}{\partial \mathbf{v}} = \left(\frac{\partial R}{\partial v_1}, \ldots, \frac{\partial R}{\partial v_L}\right)' = 2\,\mathbf{R}\,\mathbf{v}. \tag{138}$$

Since $\mathbf{R}$ is positive semi-definite, its svd factorization is $\mathbf{R} = \mathbf{U}\mathbf{D}\mathbf{U}' = \mathbf{U}\mathbf{D}\mathbf{U}^{-1}$, where the columns of $\mathbf{U}$ are made from L orthonormal eigenvectors of $\mathbf{R}$ and $\mathbf{D}$ is a diagonal matrix containinge the corresponding eigenvalues (which are real and non-negative) on its diagonal. Note that the eigenvectors $\mathbf{u}_j$ of $\mathbf{R}$ lie on the main axes of the hyperellipsoid formed by the contour lines of the performance surface (see Figure 75, red arrows).

By left-multiplication of the shifted coordinates $\mathbf{v} = (\mathbf{w} - \mathbf{w}_{\mathsf{opt}})$ with $\mathbf{U}'$ we finally get *normal* coordinates $\tilde{\mathbf{v}} = \mathbf{U}'\mathbf{v}$. The coordinate axes of the $\tilde{\mathbf{v}}$ system are in the direction of the eigenvectors of $\mathbf{R}$, and (138) becomes

$$\frac{\partial R}{\partial \tilde{\mathbf{v}}} = 2\,\mathbf{D}\,\tilde{\mathbf{v}} = 2\,(\lambda_1 \tilde{v}_1, \ldots, \lambda_L \tilde{v}_L)', \tag{139}$$

from which we get the second derivatives

$$\frac{\partial^2 R}{\partial \tilde{\mathbf{v}}^2} = 2\,(\lambda_1, \ldots, \lambda_L)', \tag{140}$$

that is, the eigenvalues of $\mathbf{R}$ are (up to a factor of 2) the curvatures of the performance surface in the direction of the central axes of the hyperparabeloid. We will shortly see that the computational efficiency of gradient descent on the performance surface depends critically on these curvatures.

11.3.5 Gradient descent on a quadratic performance surface

Now let us do an iterative gradient descent on the performane surface, using the normal coordinates $\tilde{\mathbf{v}}$. The generic gradient descent rule (129) here is $\tilde{\mathbf{v}}^{(n+1)} = \tilde{\mathbf{v}}^{(n)} - \mu \nabla R(\tilde{\mathbf{v}}^{(n)})$, which spells out (observing (139)) to

$$\tilde{\mathbf{v}}^{(n+1)} = (\mathbf{I} - 2\mu\mathbf{D})\, \tilde{\mathbf{v}}^{(n)}. \tag{141}$$

Because $\mathbf{I} - 2\mu\mathbf{D}$ is a diagonal matrix, this gradient descent operates on the L coordinates of $\tilde{\mathbf{v}}$ without mutual coupling, yielding for every individual coordinate a separate update rule

$$\tilde{v}_j^{(n+1)} = (1 - 2\mu\lambda_j)\, \tilde{v}_j^{(n)}. \tag{142}$$

This is a geometric sequence. If started in $\tilde{v}_j^{(0)}$, one obtains

$$\tilde{v}_j^{(n)} = (1 - 2\mu\lambda_j)^n\, \tilde{v}_j^{(0)}. \tag{143}$$

If we would define and carry out gradient descent in the original weight coordinates $\mathbf{w}^{(n)}$ via $\mathbf{w}^{(n+1)} = \mathbf{w}^{(n)} - \mu \nabla R(\mathbf{w}^{(n)})$, we would get the same model sequence (up to the coordinate change $\mathbf{w} \leftrightarrow \tilde{\mathbf{v}}$) as given by Equations 141, 142 and 143. The sequence $\mathbf{w}^{(n)}$ converges to $\mathbf{w}_{\mathsf{opt}}$ if and only if $\tilde{v}_j^{(n)}$ converges for all $1 \leq j \leq L$. Equation 141 implies that this happens if and only if $|1 - 2\mu\lambda_j| < 1$ for all j. These inequalities can be re-written equivalently as

$$0 < \mu < 1/\lambda_j \quad \text{for all } j. \tag{144}$$

Specifically, we must make sure that $0 < \mu < 1/\lambda_{\mathsf{max}}$, where λ_{max} is the largest eigenvalue of R. Depending on the size of μ, the convergence behavior of (141) can be grouped in four classes which may be referred to as *overdamped*, *underdamped*, and two types of *unstable*. Figure 76 illustrates how $\tilde{v}_j(n)$ evolves in these four classes.

We can find an explicit representation of $\mathbf{w}^{(n)}$ if we observe that

$$\mathbf{w}^{(n)} = \mathbf{w}_{\mathsf{opt}} + \mathbf{v}^{(n)} = \mathbf{w}_{\mathsf{opt}} + \sum_j \mathbf{u}_j\, \tilde{v}_j^{(n)},$$

where the $\mathbf{u}_j$ are again the orthonormal eigenvectors of $\mathbf{R}$. Inserting (143) gives us

$$\mathbf{w}^{(n)} = \mathbf{w}_{\mathsf{opt}} + \sum_{j=1,\ldots,L} \tilde{v}_j^{(0)}\, \mathbf{u}_j\, (1 - 2\mu\lambda_j)^n. \tag{145}$$

This representation reveals that the convergence of $\mathbf{w}^{(n)}$ toward $\mathbf{w}_{\mathsf{opt}}$ is governed by an additive overlay of L exponential terms, each of which describes convergence in the direction of the eigenvectors $\mathbf{u}_j$ and is determined in its convergence speed by λ_j and the stepsize parameter μ. One speaks of the L *modes of convergence* with geometric ratio factors $(1 - 2\mu\lambda_j)$. If all eigenvalues are roughly

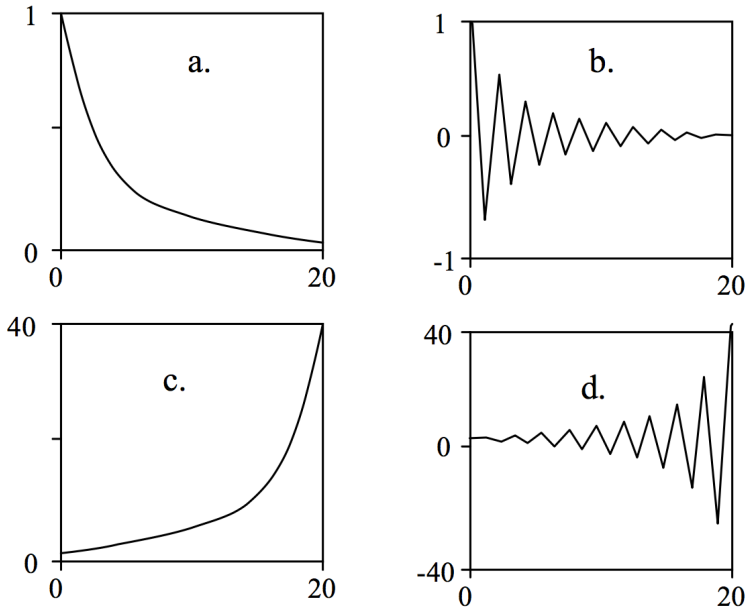

Figure 76: The development of $\tilde{v}_j^{(n)}$ [plotted in the y-axis] versus n [x-axis]. The qualitative behaviour depends on the stepsize parameter μ. **a**. Overdamped case: $0 < \mu < 1/(2\lambda_j)$. **b**. Underdamped case: $1/(2\lambda_j) < \mu < 1/\lambda_j$. **c**. Unstable with $\mu < 0$ and **d**. unstable with $1/\lambda_j < \mu$. All plots start with $\tilde{v}_j^{(0)} = 1$.

equal, convergence rates are roughly identical in the L directions. If however two eigenvalues are very different, say $\lambda_1 \ll \lambda_2$, and μ is small compared to the eigenvalues, then convergence in the direction of $\mathbf{u}_1$ will be much slower than in the direction of $\mathbf{u}_2$ (see Figure 77).

Next we turn to the question how the error R evolves over time. Recall from (137) that $R(\mathbf{v}) = R_{\mathsf{min}} + \mathbf{v}' \mathbf{R} \mathbf{v}$, which can be re-written as $R(\mathbf{v}) = R_{\mathsf{min}} + \tilde{\mathbf{v}}' \mathbf{D} \tilde{\mathbf{v}}$. Thus the error in the n-th iteration is

$$R^{(n)} = R_{\mathsf{min}} + \tilde{\mathbf{v}}'^{(n)} \mathbf{D} \tilde{\mathbf{v}}^{(n)} = R_{\mathsf{min}} + \sum_j \lambda_j (1 - 2\mu\lambda_j)^{2n} \tilde{v}_j^{(0)}. \qquad (146)$$

For suitable μ (considering (144)), $R^{(n)}$ converges to R_{min}. Plotting $R^{(n)}$ yields a graph known as *learning curve*. Equation 146 reveals that the learning curve is the sum of L decreasing exponentials (plus R_{min}).

How this learning curve looks like depends on the size of μ relative to the eigenvalues λ_j. If $2\mu\lambda_j$ is close to zero for all j, the learning curve separates into sections that each are determined by the convergence of one of the j components. Figure 78 shows a three-mode learning curve for the case of small μ, rendered in linear and logarithmic scale.

This separation of the learning curve into approximately linear sections (in logarithmic rendering) can be mathematically explained as follows. Each of the

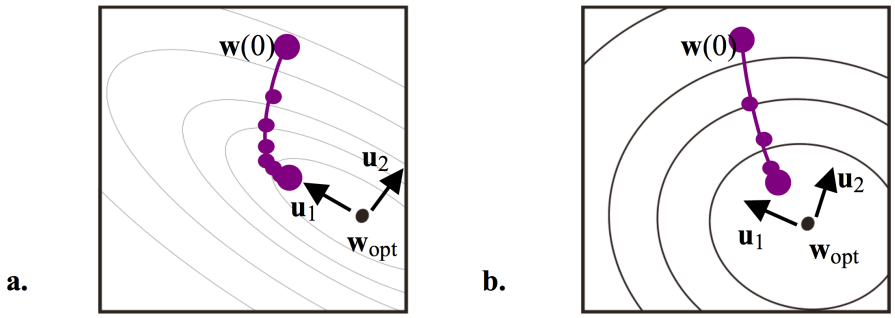

Figure 77: Two quite different modes of convergence (panel **a**.) versus rather similar modes of convergence (panel **b**.). Plots shows contour lines of performance surface for two-dimensional weights $\mathbf{w} = (w_1, w_2)$. Violet dotted lines indicate some initial steps of weight evolution.

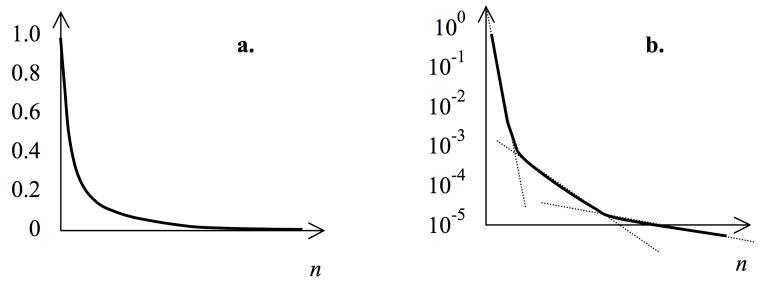

Figure 78: A learning curve with three modes of convergence, in linear (**a**.) and logarithmic (**b**.) scaling. This plot shows the qualitative behavior of modes of convergence when μ is small. R_{min} is assumed zero in these plots.

terms $(1 - 2\mu\lambda_j)^{2n}$ is characterized by a time constant τ_j according to

$$(1 - 2\mu\lambda_j)^{2n} = \exp(-n/\tau_j). \tag{147}$$

If $2\mu\lambda$ is close to zero, $\exp(2\mu\lambda)$ is close to $1+2\mu\lambda$ and thus $\log(1-2\mu\lambda) \approx 2\mu\lambda$. Using this approximation, solving (147) for τ_j yields for the j-th mode a time constant of

$$\tau_J \approx \frac{1}{4\mu\lambda_j}.$$

That is, the convergence rate (i.e. the inverse of the time constant) of the j-th mode is proportional to λ_j (for small μ).

However, this analysis is meaningless for larger μ. If we want to maximize the speed of convergence, we should use significantly larger μ, as we will presently see. The final rate of convergence is dominated by the slowest mode of convergence, which is characterized by the geometrical sequence factor

$$\max\{|1 - 2\mu\lambda_j| \;\big|\; j = 1, \ldots, L\} = \max\{|1 - 2\mu\lambda_{\mathsf{max}}|, |1 - 2\mu\lambda_{\mathsf{min}}|\}. \tag{148}$$

In order to maximize convergence speed, the learning rate μ should be chosen such that (148) is minimized. Elementary considerations reveal that this minimum is attained for $|1 - 2\mu\lambda_{\mathsf{max}}| = |1 - 2\mu\lambda_{\mathsf{min}}|$, which is equivalent to

$$\mu_{\mathsf{opt}} = \frac{1}{\lambda_{\mathsf{max}} + \lambda_{\mathsf{min}}}. \tag{149}$$

For this optimal learning rate, $1-2\mu_{\mathsf{opt}}\lambda_{\mathsf{min}}$ is positive and $1-2\mu_{\mathsf{opt}}\lambda_{\mathsf{max}}$ is negative, corresponding to the overdamped and underdamped cases shown in Figure 76. However, the two modes converge at the same speed (and all other modes are faster). Concretely, the optimal speed of convergence is given by the geometric factor

$$\beta = 1 - 2\mu_{\mathsf{opt}}\lambda_{\mathsf{min}} = \frac{\lambda_{\mathsf{max}}/\lambda_{\mathsf{min}} - 1}{\lambda_{\mathsf{max}}/\lambda_{\mathsf{min}} + 1},$$

which can be derived by substituting (149) for μ_{opt}. β has a value between 0 and 1. There are two extreme cases: if $\lambda_{\mathsf{max}} = \lambda_{\mathsf{min}}$, then $\beta = 0$ and we have convergence in a single step. As the ratio $\lambda_{\mathsf{max}}/\lambda_{\mathsf{min}}$ increases, β approaches 1 and the convergence slows down toward stillstand. The ratio $\lambda_{\mathsf{max}}/\lambda_{\mathsf{min}}$ thus plays a fundamental role in limiting the convergence speed of steepest descent algorithms. It is called the *eigenvalue spread*.

All of the derivations in this subsection were done in the context of quadratic performance surfaces. This may seem a rather limited class of performance landscapes. However, it is a mathematical fact that in most (the mathematically correct term for "most" is "generic", which is a deep probability-theory concept) differentiable performance surfaces, the shape of the surface in the vicinity of a local minimum can be approximated arbitrarily well a by a quadradic surface. The stability conditions and the speed of convergence toward local minima in generic gradient descent situations therefore is subject to the same conditions that we saw in this subsection.

Specifically, the eigenvalue spread (of the quadratic approximation) around a local minimum sets stability limits to the achieveable rate of convergence. It is a sad fact that this eigenvalue spread is typically large in neural networks with many layers — today famously known as deep networks. For almost twenty years (roughly, from 1985 when gradient descent training for neural networks became widely adopted, to 2006 when deep learning started) no general, good ways were known to achieve neural network training that was simultaneously stable and exhibited a fast enough speed of convergence. Only shallow neural networks (typically with a single hidden layer) could be effectively trained, limiting the applications of neural network modeling to not too nonlinear tasks. The deep learning revolution is based, among other factors, on an assortment of "tricks of the trade" to overcome the limitations of large eigenvalue spreads by clever modifications of gradient descent, which cannot work in its pure form. If you are interested — Section 8 in the deep learning "bible" (I. Goodfellow, Bengio, and Courville 2016) is all about these refinements and modifications of, and alternatives to, pure gradient descent.

11.4 Stochastic gradient descent with the LMS algorithm

The update formula $\mathbf{w}^{(n)}$ via $\mathbf{w}^{(n+1)} = \mathbf{w}^{(n)} - \mu \nabla R(\mathbf{w}^{(n)})$ for steepest gradient descent is not applicable in practice because the gradient ∇R of the expected squared error $R(\mathbf{w}^{(n)}) = E[\varepsilon^2_{\mathbf{w}^{(n)}}]$ is not known. Given filter weights $\mathbf{w}^{(n)}$, we need to *estimate* $E[\varepsilon^2_{\mathbf{w}^{(n)}}]$. At first sight, one would need to estimate an expected squared error by collecting information over time — namely, to observe the ongoing filtering with weights $\mathbf{w}^{(n)}$ for some time and then approximate $E[\varepsilon^2_{\mathbf{w}^{(n)}}]$ by averaging over the errors seen in this observation interval. But we don't have this time — because we want to be efficient and update $\mathbf{w}$ at every time step; and furthermore, in online model estimation scenarios the error statistics may change over time.

One ruthless way out of this impasse is to just use the *momentary* squared error as an approximation to its *expected* value, that is, use the brutal approximation

$$R^{(n)} \approx \varepsilon^2_{\mathbf{w}^{(n)}}(n) := (d(n) - \mathbf{w}'^{(n)}\,\mathbf{x}(n))^2. \tag{150}$$

The gradient descent update formula $\mathbf{w}^{(n+1)} = \mathbf{w}^{(n)} - \mu \nabla R(\mathbf{w}^{(n)})$ then becomes

$$\mathbf{w}^{(n+1)} = \mathbf{w}^{(n)} - \mu \nabla \varepsilon^2_{\mathbf{w}^{(n)}}(n), \tag{151}$$

where we can calculate $\nabla \varepsilon^2_{\mathbf{w}^{(n)}}(n)$ as follows:

$$\begin{aligned}
\nabla \varepsilon^2_{\mathbf{w}^{(n)}}(n) &= 2\,\varepsilon_{\mathbf{w}^{(n)}}(n)\ \nabla \varepsilon_{\mathbf{w}^{(n)}}(n) \\
&= 2\,\varepsilon_{\mathbf{w}^{(n)}}(n)\ \left(\frac{\partial \varepsilon_{\mathbf{w}^{(n)}}(n)}{\partial w_1}, \ldots, \frac{\partial \varepsilon_{\mathbf{w}^{(n)}}(n)}{\partial w_L}\right) \\
&= -2\,\varepsilon_{\mathbf{w}^{(n)}}(n)\ \left(\frac{\partial \mathbf{w}'^{(n)}\,\mathbf{x}(n)}{\partial w_1}, \ldots, \frac{\partial \mathbf{w}'^{(n)}\,\mathbf{x}(n)}{\partial w_L}\right) \\
&\qquad [\text{use } \varepsilon_{\mathbf{w}^{(n)}}(n) = d(n) - \mathbf{w}'^{(n)}\,\mathbf{x}(n)] \\
&= -2\,\varepsilon_{\mathbf{w}^{(n)}}(n)\ (x(n), \ldots, x(n-L+1)) \\
&= -2\,\varepsilon(n)\ \mathbf{x}(n),
\end{aligned} \tag{152}$$

where in the last step we simplified the notation $\varepsilon_{\mathbf{w}^{(n)}}(n)$ to $\varepsilon(n)$. Inserting this into (151) gives

$$\boxed{\mathbf{w}^{(n+1)} = \mathbf{w}^{(n)} + 2\,\mu\,\varepsilon(n)\ \mathbf{x}(n),} \tag{153}$$

which is the weight update formula of one of the most compact, cheap powerful and widely used algorithms I know of. It is called the *least means squares* (LMS) algorithm in signal processing, or *Widrow-Hoff* learning rule in neuroscience where the same weight adaptation rule has been (re-)discovered independently from the signal processing tradition. In fact, this online weight adaptation algorithm for linear regression has been independently discovered and re-discovered many times in many fields.

For completeness, here are all the computations needed to carry out one full step of online filtering and weight adaptation with the LMS algorithm:

1.	read in input and compute output:	$y(n) = \mathbf{w}'^{(n)}\,\mathbf{x}(n)$,
2.	compute current error:	$\varepsilon(n) = d(n) - y(n)$,
3.	compute weight update:	$\mathbf{w}^{(n)} + 2\,\mu\,\varepsilon(n)\,\mathbf{x}(n)$.

One fact about the LMS algorithm should always be kept in mind: being a stochastic version of steepest gradient descent, the LMS algorithm inherits the problems connected with the eigenvalue spread of the input process X_n. If its eigenvalue spread is very large, the LMS algorithm will not work satisfactorily.

As an aside, in my working with recurrent neural networks, I once tried out learning algorithms related to LMS. But the input signal to this learning algorithm had an eigenvalue spread of 10^{14} to 10^{16}, so the beautiful LMS algorithm was entirely inapplicable.

Because of its eminent usefulness (if the input vector correlation matrix has a reasonably small eigenvalue spread), the LMS algorithm has been analysed in minute detail. I conclude this section by reporting the most important insights without mathematical derivations. At the same time I introduce some of the standard vocabulary used in the field of adaptive signal processing.

For starters, we again assume that $[X^L D]$ is a stationary processes (recall (130)). The evolution $\mathbf{w}^{(n)}$ of weights is now also a stochastic process, because the LMS weight update depends on the stochastic vectors $\mathbf{x}(n)$. One interesting question is how fast the LMS algorithm converges in comparison with the ideal steepest gradient descent algorithm $\tilde{\mathbf{v}}^{(n+1)} = (\mathbf{I} - 2\mu\mathbf{D})\,\tilde{\mathbf{v}}^{(n)}$ from (141). Because we now have a stochastic update, the vectors $\tilde{\mathbf{v}}^{(n)}$ become random variables and one can only speak about their *expected* value $E[\tilde{\mathbf{v}}^{(n)}]$ at time n. (Intuitive explanation: this value would be obtained if many (infinitely many in the limit) training runs of the adaptive filter would be carried out and in each of these runs, the value of $\tilde{\mathbf{v}}^{(n)}$ at time n would be taken, and an average would be formed over all these $\tilde{\mathbf{v}}^{(n)}$). The following can be shown (using some additional assumptions, namely, that μ is small and that the signal $(x(n))$ has no substantial autocorrelation for time spans larger than L):

$$E[\tilde{\mathbf{v}}^{(n+1)}] = (I - 2\mu\mathbf{D})\,E[\tilde{\mathbf{v}}^{(n)}]. \tag{154}$$

Rather to our surprise, if the LMS algorithm is used, the weights converge — on average across different trials — as fast to the optimal weights as when the ideal algorithm (141) is employed. Figure 79 shows an overlay of the deterministic development of weights according to (141) with one run of the stochastic gradient descent using to the LMS algorithm.

The fact that on average the weights converge to the optimal weights by no means implies that $R^{(n)}$ converges to R_{min}. To see why, assume that at some time n, the LMS algorithm actually would have found the correct optimal weights, that is, $\mathbf{w}^{(n)} = \mathbf{w}_{\mathsf{opt}}$. What would happen next? Well, due to the random weight adjustment, these optimal weights would become misadjusted again in the next time step! So the best one can hope for asymptotically is that the LMS algorithms lets

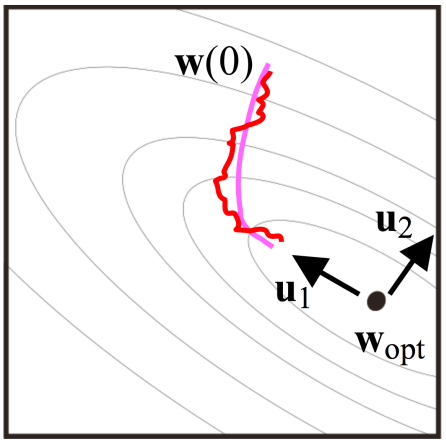

Figure 79: Illustrating the similar performance of deterministic (pink) and stochastic (red) gradient descent.

the weights $\mathbf{w}^{(n)}$ jitter randomly in the vicinity of $\mathbf{w}_{\mathsf{opt}}$. But this means that the effective best error that can be achieved by the LMS algorithm in the asymptotic average is not R_{min} but $R_{\mathsf{min}} + R_{\mathsf{excess}}$, where R_{excess} comes from the random scintillations of the weight update. It is intuitively clear that R_{excess} depends on the stepsize μ. The larger μ, the larger R_{excess}. The absolute size of the excess error is not so interesting as is the ratio $\mathcal{M} = R_{\mathsf{excess}}/R_{\mathsf{min}}$, that is the relative size of the excess error compared to the minimal error. The quantity $\mathcal{M}$ is called the *misadjustment* and describes what fraction of the *residual error* $R_{\mathsf{min}} + R_{\mathsf{excess}}$ can be attributed to the random oscillations effected by the stochastic weight update [i.e., R_{excess}], and what fraction is inevitably due to inherent limitations of the filter itself [i.e., R_{min}]. Notice that R_{excess} can in principle be brought to zero by tuning down μ toward zero — however, that would be at odds with the objective of fast convergence.

Under some assumptions (notably, small $\mathcal{M}$) and using some approximations (cf. Farhang-Boroujeny, Section 6.3), the misadjustment can be approximated by

$$\mathcal{M} \approx \mu \, \mathrm{trace}(\mathbf{R}), \tag{155}$$

where the *trace* of a square matrix is the sum of its diagonal elements. The misadjustment is thus proportional to the stepsize and can be steered by setting the latter, if $\mathrm{trace}(\mathbf{R})$ is known. Fortunately, $\mathrm{trace}(\mathbf{R})$ can be estimated online from the sequence $(x(n))$ simply and robustly [how? — easy exercise].

Another issue that one has always to be concerned about in online adaptive signal processing is stability. We have seen in the treatment of the ideal case that the adaptation rate μ must not exceed $1/\lambda_{\mathsf{max}}$ in order to guarantee convergence. But this result does not directly carry over to the stochastic version of gradient descent, because it does not take into account the stochastic jitter of the gradient descent, which is intuitively likely to be harmful for convergence. Furthermore, the value of λ_{max} cannot be estimated robustly from few data points in a practical

situation. Using again middle-league maths and several approximations, in the book of Farhang-Boroujeny the following upper bound for μ is derived:

$$\mu \leq \frac{1}{3\,\mathrm{trace}(\mathbf{R})}. \tag{156}$$

If this bound is respected, the LMS algorithm converges stably.

In practical applications, one often wishes to achieve an initial convergence that is as fast as possible: this can be done by using μ close to the stability boundary (156). After some time, when a reasonable degree of convergence has been attained, one wishes to control the misadjustment $\mathcal{M}$; then one switches into a control mode where μ is adapted dynamically according to $\mu = \mathcal{M}/\mathrm{trace}(\mathbf{R})$, which follows from (155).

Up to here we have been analyzing LMS under the assumption of a stationary process. But the real working arena for LMS are nonstationary processes, where the objective is to *track* the changing statistics of the $[X^L D]_n$ process by continually adapting the model $\mathbf{w}^{(n)}$. In this situation one still uses the same LMS rule (153). However, roughly speaking, the modeling error $R^{(n)}$ is now a sum of three components: $R^{(n)} = R_{\mathsf{min}}(n) + R_{\mathsf{excess}}(n) + R_{\mathsf{lag}}(n)$, all of which are temporally changing. The new component $R_{\mathsf{lag}}(n)$ reflects the fact that iterative model adaptation always needs time to converge to a certain error level — when the signal statistics change with time, the model adaptation always lags behind the changing statistics. A rigorous analysis of this situation is beyond the scope of this course. In practice one must tune μ online such that a good compromise is maintained between, on the one hand, making $R_{\mathsf{lag}}(n)$ small (which means speeding up convergence by increasing μ, in order to not lag behind the changing input statistics too much), and on the other hand, minimizing $R_{\mathsf{excess}}(n)$ (which means small μ); all this while watching out for staying stable.

The LMS algorithm has been since 50 years or so the workhorse of adaptive signal processing and numerous refinements and variants have been developed. Here are some:

1. An even simpler stochastic gradient descent algorithm than LMS uses only the sign of the error in the update: $\mathbf{w}^{(n+1)} = \mathbf{w}^{(n)} + 2\,\mu\,\mathrm{sign}(\varepsilon(n))\mathbf{x}(n)$. If μ is a power of 2, this algorithm does not need a multiplication (a shift does it then) and is suitable for very high throughput hardware implementations which are often needed in communication technology. There exist yet other "sign-simplified" versions of LMS [cf. Farhang-Boroujeny p. 169].

2. Online stepsize adaptation: at every update use a locally adapted stepsize $\mu(n) \sim 1/\|\mathbf{x}\|^2$. This is called *normalized LMS* (NLMS). In practice this pure NLMS is apt to run into stability problems; a safer version is $\mu(n) \sim \mu_0/(\|\mathbf{x}\|^2 + \psi)$, where μ_0 and ψ are hand-tuned constants [Farhang-B. p. 172]. In my own experience, normalized LMS sometimes works wonders in comparison with vanilla LMS.

3. Include a *whitening* mechanism into the update equation: $\mathbf{w}^{(n+1)} = \mathbf{w}^{(n)} + 2\mu\,\varepsilon(n)\,\mathbf{R}^{-1}\,\mathbf{x}(n)$. This *Newton-LMS* algorithm has a single mode of convergence, but a problem is to obtain a robust (noise-insensitive) approximation to $\mathbf{R}^{-1}$, and to get that cheaply enough [Farhang-B. p. 210].

4. Block implementations: for very long filters (say, $L > 10,000$) and high update rates, even LMS may become too slow. Various computationally efficient *block LMS* algorithms have been designed in which the input stream is partitioned into blocks, which are processed in the frequency domain and yield weight updates after every block only [Farhang-B. p. 247ff].

To conclude this section, it should be said that besides LMS algorithms there is another major class of online adaptive algorithms for transversal filters, namely *recursive least squares* (RLS) adaptation algorithms. RLS algorithms are not steepest gradient-descent algorithms. The background metaphor of RLS is not to minimize $R_{\mathbf{w}}$ but to minimize the accumulated squared error up to the current time, $\zeta(n) = \sum_{i=1,\ldots,n}(d(i)-y(i))^2$, so the performance surface we know from LMS plays no role for RLS. The main advantages and disadvantages of LMS vs. RLS are:

1. LMS has computational cost $O(L)$ per update step, where L is filter length; RLS has cost $O(L^2)$. Also the space complexity of RLS is an issue for long filters because it is $O(L^2)$.

2. LMS is numerically robust when set up diligently. RLS is plagued by numerical instability problems that are not easy to master.

3. RLS has a single mode of convergence and converges faster than LMS, *very much* faster when the input signal has a high eigenvalue spread.

4. RLS is more complicated than LMS and more difficult to implement in robust, stable ways.

5. In applications where fast tracking of highly nonstationary systems is required, LMS may have better tracking performance than RLS (says Farhang-Boroujeny).

The use of RLS in signal processing has been boosted by the development of *fast RLS algorithms* which reach a linear time complexity in the order of $O(20\,L)$ [Farhang-B. Section 13].

Both LMS and RLS algorithms play a role in a field of recurrent neural networks called *reservoir computing* (Jaeger 2007), which happens to be one of my personal professional playgrounds. In reservoir computing, the training of neural networks is reduced to computing a linear regression. Reservoir computing has recently become particularly relevant for low-power microchip hardware implementations of neural networks. If time permits I will give an introduction to this emerging field in a tutorial or extra session.

12 Feedforward neural networks: the Multilayer Perceptron

Artificial neural networks (ANNs) have been investigated for more than half a century in two scientific domains:

In computational neuroscience, ANNs are investigated as mathematical abstractions and computer simulation models of biological neural systems. These models aim at biological plausibility and serve as a research vehicle to better understand information processing in real brains.

In machine learning, ANNs are used for creating complex information processing architectures whose function can be shaped by training from training sample data. The goal here is to solve complex learning tasks in a data engineering spirit, aiming at models that combine good generalization with highly nonlinear data transformations.

Historically these two branches of ANN research had been united. The ancestor of all ANNs, the *perceptron* of Rosenblatt 1958, was a computational model of optical character recognition (as we would say today) which was explicitly inspired by design motifs imported from the human visual system (check out Wikipedia on "perceptron"). In later decades the two branches diverged further and further from each other, despite repeated and persistent attempts to re-unite them. Today most ANN research in machine learning has more or less lost its connections to biological origins. In this course we only consider ANNs in machine learning.

Even if we only look at machine learning, ANNs come in many kinds and variations. The common denominator for most (but not all) ANNs in ML can be summarized as follows.

- An ANN is composed of a (possibly large) number of interconnected processing units. These processing units are called "neurons" or just "units". Each such unit typically can perform only a very limited computational operation, for instance applying a fixed nonlinear function to the sum of its inputs.

- The units of an ANN are connected to each other by links called "synaptic connections" (an echo of the historical past) or just "connections" or "links".

- Each of the links is weighted with a parameter called "synaptic weight", "connection weight", or just "weight" of the link. Thus, in total an ANN can be represented as a labelled graph whose nodes are the neurons and whose vertices are the links, labelled with their weights. The structure of an ANN with L units can thus be represented by its $L \times L$ sized *connection weight matrix* $\mathbf{W}$, where the entry $\mathbf{W}(i, j) = w_{ij}$ is the weight on the link leading from unit j to unit i. When $w_{ij} = 0$, then unit j has no connection

to unit i. The nonzero elements in $\mathbf{W}$ therefore determine the network's connection topology. Often it is more convenient to split the global weight matrix in submatrices, one for each "layer" of weights. In what follows I will use the generic symbol θ as the vector of all weights in an ANN.

- Computing with an ANN means to compute a real-valued *activation* x_i for each unit i ($i = 1, \ldots, L$). In an ANN with L units, all of these activations together are combined into an *state vector* $\mathbf{x} \in \mathbb{R}^L$.
- The calculation of the state vector in a feedforward ANN depends on the input and connection weights, so we may write $\mathbf{x} = f(\mathbf{u}, \theta)$.
- The state calculation function f is almost always *local*: the activation x_i of unit i depends only on the activations x_j of units j that "feed into" i, that is where $w_{ij} \neq 0$.
- The external functionality of an ANN results from the combined local interactions between interconnected units. Very complex functionalities may thus arise from the structured local interaction between large numbers of simple processing units. This is, in a way, analog to Boolean circuits – and indeed some ANNs can be mapped on Boolean circuits. In fact, the famous paper which can be regarded as the starting shot for computational neuroscience, *A logical calculus of the ideas immanent in nervous activity* (McCulloch and Pitts 1943), compared biological brains directly to Boolean circuits.
- The global functionality of an ANN is determined by the connection weights θ. Absolutely drastic changes in functionality can be achieved by changing the entries in θ. For instance, an ANN with a given topology can serve as a recognizer of handwritten digits with some θ, and can serve as a recognizer of facial expressions with another θ' wherein only a fraction of the weights have been replaced.
- The hallmark of ANNs is that its functionality is *learnt* from training data. Most learning procedures that are in use today rely on some sort of iterative model estimation with a flavor of gradient descent.

This basic scenario allows for an immense spectrum of different ANNs, which can be set up for tasks as diverse as dimension reduction and data compression, approximate solving of NP-hard optimization problems, time series prediction, nonlinear control, game playing, dynamical pattern generation and many more.

In this course I give an introduction to a particular kind of ANNs called *feedfoward neural networks*, or often also – for historical reasons – *multilayer perceptrons* (MLPs).

MLPs are used for the supervised learning of vectorial input-output tasks. In such tasks the training sample is of the kind $(\mathbf{u}_i, \mathbf{y}_i)_{i=1,\ldots,N}$, where $\mathbf{u} \in \mathbb{R}^n, \mathbf{y} \in \mathbb{R}^k$ are drawn from a joint distribution $P_{U,Y}$.

Note that in this section my notation departs from the one used in earlier sections: I now use u instead of $\mathbf{x}$ to denote input patterns, in order to avoid confusion with the network states $\mathbf{x}$.

The MLP is trained to produce outputs $\mathbf{y} \in \mathbb{R}^k$ upon inputs $\mathbf{u} \in \mathbb{R}^n$ in a way that this input-output mapping is similar to the relationships $\mathbf{u}_i \mapsto \mathbf{y}_i$ found in the training data. Similarity is measured by a suitable loss function.

Supervised learning tasks of this kind – which we have already studied in previous sections – are generally called *function approximation* tasks or *regression* tasks. It is fair to say that today MLPs and their variations are the most widely used workhorse tool in machine learning when it comes to learning nonlinear function approximation models.

An MLP is a neural network structured equipped with n *input units* and k *output units*. An n-dimensional input pattern $\mathbf{u}$ can be sent to the input units, then the MLP does some interesting internal processing, at the end of which the k-dimensional result vector of the computation can be read from the k output units. An MLP $\mathcal{N}$ with n input units and k output units thus instantiates a function $\mathcal{N} : \mathbb{R}^n \to \mathbb{R}^k$. Since this function is shaped by the synaptic connection weights θ, one could also write $\mathcal{N}_\theta : \mathbb{R}^n \to \mathbb{R}^k$ if one wishes to emphasize the dependance of $\mathcal{N}$'s functionality on its weights.

The learning task is defined by a loss function $L : \mathbb{R}^k \times \mathbb{R}^k \to \mathbb{R}^{\geq 0}$. As we have seen before, a convenient and sometimes adequate choice for L is the quadratic loss $L(\mathcal{N}(\mathbf{u}), \mathbf{y}) = \|\mathcal{N}(\mathbf{u}) - \mathbf{y}\|^2$, but other loss functions are also widely used. Chapter 6.2 in the deep learning bible I. Goodfellow, Bengio, and Courville 2016 gives an introduction to the theory of which loss functions should be used in which task settings.

Given the loss function, the goal of training an MLP is to find a weight vector θ_{opt} which minimizes the empirical loss, that is

$$\theta_{\text{opt}} = \underset{\theta \in \mathcal{H}}{\operatorname{argmin}} \frac{1}{N} \sum_{i=1}^{N} L(\mathcal{N}_\theta(\mathbf{u}_i), \mathbf{y}_i), \tag{157}$$

where $\mathcal{H}$ is a set of candidate weight vectors. We have seen variants of this formula many times by now in these lecture notes!

"Function approximation" sounds dry and technical, but many kinds of learning problems can be framed as function approximation learning. Here are some examples:

Pattern recognition: inputs $\mathbf{u}$ are vectorized representations of any kind of "patterns", for example images, soundfiles, stock market time series. Outputs $\mathbf{y}$ are hypothesis vectors of the classes that are to be recognized.

Time series prediction: inputs are vector encodings of a past history of a temporal process, outputs are vector encodings of future observations of the process.

Denoising, restoration and pattern completion: inputs are patterns that are corrupted by noise or other distortions, outputs are cleaned-up or repaired or completed versions of the same patterns.

Data compression: Inputs are high-dimensional patterns, outputs are low-dimensional encodings which can be restored to the original patterns using a decoding MLP. The encoding and decoding MLPs are trained together.

Process control: In control tasks the objective is to send *control inputs* to a technological system (called "plant" in control engineering) such that the system performs in a desired way. The algorithm which computes the control inputs is called a "controller". Control tasks range in difficulty from almost trivial (like controlling a heater valve such that the room temperature is steered to a desired value) to almost impossible (like operating hundreds of valves and heaters and coolers and whatnots in a chemical factory such that the chemical production process is regulated to optimal quality and yield). The MLP instantiates the controller. Its inputs are settings for the desired plant behavior, plus optionally observation data from the current plant performance. The outputs are the control inputs which are sent to the plant.

This list should convince you that "function approximation" is a worthwhile topic indeed, and spending effort on learning how to properly handle MLPs is a good personal investment for any engineer or data analyst.

12.1 MLP structure

Figure 80 gives a schematic of the architecture of an MLP. It consists of several *layers* of units. Layers are numbered $0, \ldots, K$, where layer 0 is comprised of the input units and layer K of the output units. The number of units in layer m is L^m. The units of two successive layers are connected in an all-to-all fashion by synaptic links (arrows in Figure 80). The link from unit j in layer $m-1$ to unit i in layer m has a *weight* $w_{ij}^m \in \mathbb{R}$. The layer 0 is the *input layer* and the layer K is the *output layer*. The intermediate layers are called *hidden* layers. When an MLP is used for a computation, the i-th unit in layer m will have an *activation* $x_i^m \in \mathbb{R}$.

From a mathematical perspective, an MLP $\mathcal{N}$ implements a function $\mathcal{N} : \mathbb{R}^{L_0} \to \mathbb{R}^{L_K}$. Using the MLP and its layered structure, this function $\mathcal{N}(\mathbf{u})$ of an argument $\mathbf{u} \in \mathbb{R}^{L_0}$ is computed by a sequence of transformations as follows:

1. The activations x_j^0 of the input layer are set to the component values of the L_0-dimensional input vector $\mathbf{u}$.

2. For $m < K$, assume that the activations x_j^{m-1} of units in layer $m-1$ have already been computed (or have been externally set to the input values, in

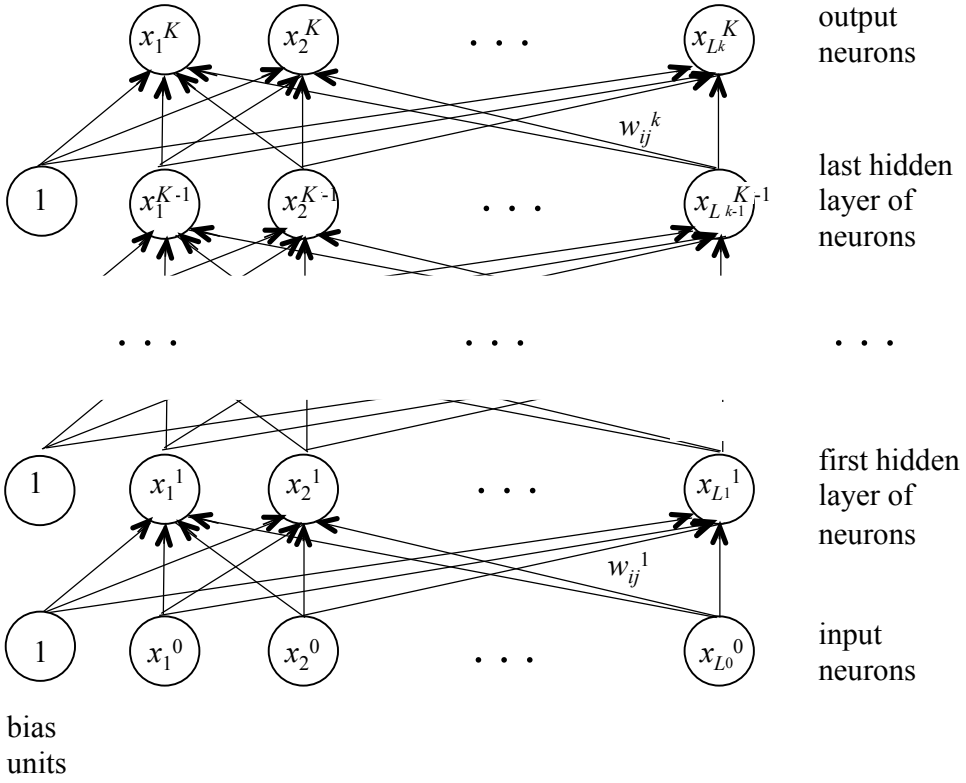

Figure 80: Schema of an MLP with $K-1$ hidden layers of neurons.

the case of $m-1=0$). Then the activation x_i^m is computed from the formula

$$x_i^m = \sigma\left(\sum_{j=1}^{L^{m-1}} w_{ij}^m\, x_j^{m-1} + w_{i0}^m\right). \tag{158}$$

That is, x_i^m is obtained from linearly combining the activations of the lower layer with combination weights w_{ij}^m, then adding the *bias* $w_{i0}^m \in \mathbb{R}$, then wrapping the obtained sum with the *activation function* σ. The activation function is a nonlinear, "S-shaped" function which I explain in more detail below. It is customary to interpret the bias w_{i0}^m as the weight of a synaptic link from a special *bias unit* in layer $m-1$ which always has a constant activation of 1 (as shown in Figure 80).

Equation 158 can be more conveniently written in matrix form. Let $\mathbf{x}^m = (x_1^m, \ldots, x_{L^m}^m)'$ be the activation vector in layer m, let $\mathbf{b}^m = (w_{10}^m, \ldots, w_{L^m 0}^m)'$ be the vector of bias weights, and let $\mathbf{W}^m = (w_{ij}^m)_{i=1,\ldots,L^m;\, j=1,\ldots,L^{m-1}}$ be the connection weight matrix for links between layers $m-1$ and m. Then (158) becomes

$$\mathbf{x}^m = \sigma\left(\mathbf{W}^m\, \mathbf{x}^{m-1} + \mathbf{b}^m\right), \tag{159}$$

where the activation function σ is applied component-wise to the activation vector.

3. The L^K-dimensional activation vector $\mathbf{y}$ of the output layer is computed from the activations of the pre-output layer $m = K-1$ in various ways, depending on the task setting (compare Chapter 6.2 in I. Goodfellow, Bengio, and Courville 2016). For simplicity we will consider the case of *linear* output units,

$$\mathbf{y} = \mathbf{x}^K = \mathbf{W}^K \, \mathbf{x}^{K-1} + \mathbf{b}^K, \tag{160}$$

that is, in the same way as it was done in the other layers except that no activation function is applied. The output activation vector $\mathbf{y}$ is the result $\mathbf{y} = \mathcal{N}(\mathbf{u})$.

The activation function σ is traditionally either the hyperbolic tangent (tanh) function or the *logistic sigmoid* given by $\sigma(a) = 1/(1 + \exp(-a))$. Figure 81 gives plots of these two S-shaped functions. Functions of such shape are often called *sigmoids*. There are two grand reasons for applying sigmoids:

- Historically, neural networks were conceived as abstractions of biological neural systems. The electrical activation of a biological neuron is bounded. Applying the tanh bounds the activations of MLP "neurons" to the interval $[-1, 1]$ and the logistic sigmoid to $[0, 1]$. This can be regarded as an abstract model of a biological property.

- Sigmoids introduce nonlinearity into the function $\mathcal{N}_\theta$. Without these sigmoids, $\mathcal{N}_\theta$ would boil down to a cascade of affine linear transformations, hence in total would be merely an affine linear function. No nonlinear function could be learnt by such a linear MLP.

In the area of deep learning a drastically simplified "sigmoid" is often used, the *rectifier* function defined by $r(a) = 0$ for $a < 0$ and $r(a) = a$ for $a \geq 0$. The rectifier has somewhat less pleasing mathematical properties compared to the classical sigmoids but can be computed much more cheaply. This is of great value in deep learning scenarios where the neural networks and the training samples both are often very large and the training process requires very many evaluations of the sigmoid.

In intuitive terms, the operation of an MLP can be summarized as follows. After an input vector $\mathbf{u}$ is written into the input units, a "wave of activation" sweeps forward through the layers of the network. The activation vector $\mathbf{x}^m$ in each layer m is directly triggered by the activations $\mathbf{x}^{m-1}$ according to (159). The data transformation from $\mathbf{x}^{m-1}$ to $\mathbf{x}^m$ is a relatively "mild" one: just an affine linear map $\mathbf{W}^m \, \mathbf{x}^{m-1} + \mathbf{b}^m$ followed by a wrapping with the gentle sigmoid σ. But when several such mild transformations are applied in sequence, very complex "foldings" of the input vector $\mathbf{u}$ can be effected. Figure 82 gives a visual impression of what a sequence of mild transformations can do. Also the term "feedforward

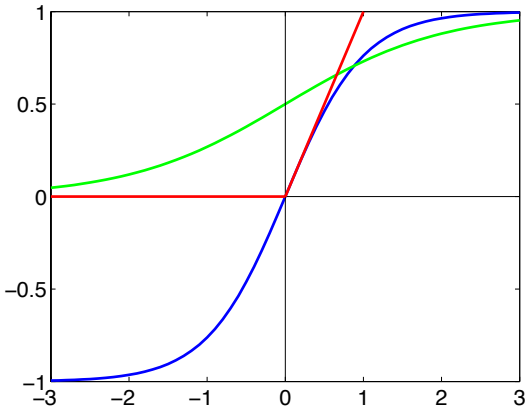

Figure 81: The tanh (blue), the logistic sigmoid (green), and the rectifier function (red).

neural network" becomes clear: the activation wave spreads in a single sweep unidirectionally from the input units to the output units.

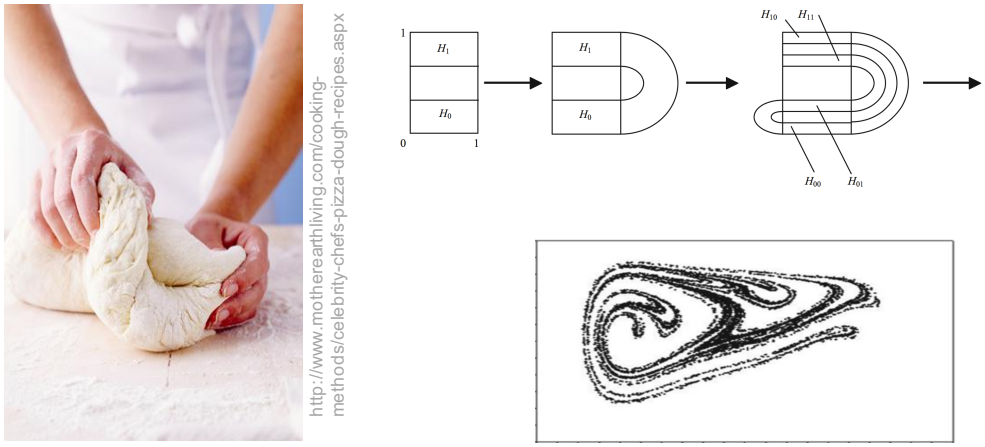

Figure 82: Illustrating the power of iterating a simple transformation. The *baker transformation* (also known as *horseshoe transformation*) takes a 2-dimensional rectangle, stretches it and folds it back onto itself. The bottom right diagram visualizes a set that is obtained after numerous baker transformations (plus some mild nonlinear distortion). — Diagrams on the right taken from Savi 2016.

12.2 Universal approximation and "deep" networks

One reason for the popularity of MLPs is that they can approximate arbitrary functions $f : \mathbb{R}^n \to \mathbb{R}^k$. Numerous results on the approximation qualities of MLPs have been published in the early 1990-ies. Such theorems have the following

general format:

Theorem (schematic). *Let $\mathcal{F}$ be a certain class of functions $f : \mathbb{R}^n \to \mathbb{R}^k$. Then for any $f \in \mathcal{F}$ and any $\varepsilon > 0$ there exists an multilayer perceptron $\mathcal{N}$ with one hidden layer such that $\|f - \mathcal{N}\| < \varepsilon$.*

Such theorems differ with respect to the classes $\mathcal{F}$ of functions that are approximated and with respect to the norms $\|\cdot\|$ that measure the mismatch between two functions. All practically relevant functions belong to classes that are covered by such approximation theorems. In a summary fashion it is claimed that MLPs are *universal function approximators*. Again, don't let yourself be misled by the dryness of the word "function approximator". Concretely the universal function approximation property of MLPs would spell out, for example, to the (proven) statement that any task of classifying pictures can be solved to any degree of perfection by a suitable MLP.

The proofs for such theorems are typically constructive: for some target function f and tolerance ε they explicitly construct an MLP $\mathcal{N}$ such that $\|f - \mathcal{N}\| < \varepsilon$. However, these constructions have little practical value because the constructed MLPs $\mathcal{N}$ are far too large for any practical implementation. You can find more details concerning such approximation theorems and related results in my legacy ML lecture notes `https://www.ai.rug.nl/minds/uploads/LN_ML_Fall11.pdf`, Section 8.1.

Even when the function f that one wants to train into an MLP is very complex (highly nonlinear and with many "folds"), it can be in principle approximated with 1-hidden-layer MLPs. However, when one employs MLPs that have *many* hidden layers, the required overall size of the MLP (quantified by total number of weights) is dramatically reduced (Bengio and LeCun 2007). Even for super-complex target functions f (like photographic image caption generation), MLPs of feasible size exist when enough layers are used (one of the subnetworks in the TICS system described in Section 1.2.1 used 17 hidden layers). This is the basic insight and motivation to consider *deep* networks, which is just another word for "many hidden layers". Unfortunately it is not at all easy to train deep networks. Traditional learning algorithms had made non-deep ("shallow") MLPs popular since the 1980-ies. But these shallow MLPs could only cope with relatively well-behaved and simple learning tasks. Attempts to scale up to larger numbers of hidden layers and more complex data sets largely failed, due to numerical instabilities, too slow convergence, or poor model quality. Since about 2006 an accumulation of clever "tricks of the trade" plus the availability of powerful (GPU-based) yet affordable computing hardware has overcome these hurdles. This area of training deep neural networks is now one of the most thriving fields of ML and has become widely known under the name *deep learning*.

12.3 Training an MLP with the backpropagation algorithm

In this section I give an overview of the main steps in training a non-deep MLP for a mildly nonlinear task — tasks that can be solved with one or two hidden layers. When it comes to unleash deep networks on gigantic training corpora for hypercomplex tasks, the basic recipes given in this section will not suffice. You would need to train yourself first in the art of deep learning, investing at least a full university course's effort (this is an advertisment of Marco Wiering's *Deep Learning* course in summer!). However, what you can learn in this section is necessary background for surviving in the wilderness of deep learning.

12.3.1 General outline of an MLP training project

Starting from a task specification and access to training data (given to you by your boss or a paying customer, with the task requirements likely spelled out in rather informal terms, like "please predict the load of our internet servers for the next 3 minutes"), a basic training procedure for a elementary MLP $\mathcal{N}$ goes like follows.

1. **Get a clear idea of the formal nature of your learning task.** Do you want a model output that is a probability vector? or a binary decision? or a maximally precise transformation of the input? how should "precision" best be measured? and so forth. Only proceed with using MLPs if they are really looking like a suitable model class for your problem.

2. **Decide on a loss function.** Go for a simple quadratic loss if you want a quick baseline solution but be prepared to invest into other loss functions if you have enough time and knowledge (read Chapter 6.2 in I. Goodfellow, Bengio, and Courville 2016).

3. **Decide on a regularization method.** For elementary MLP training, suitable candidates are adding an L_2 norm regularizer to your loss function; extending the size of the training data set by adding noisy / distorted exemplars; varying the network size; or early stopping (= stop gradient descent training a overfitting-enabled ANN when the validation error starts increasing — requires continual validation during gradient descent). Demyanov 2015 is a solid guide for ANN regularization.

4. **Think of a suitable vector encoding of the available training data,** including dimension reduction if that seems advisable (it *is* advisable in all situations where the ratio *raw data dimension / size of training data set* is high).

5. **Fix an MLP architecture.** Decide how many hidden layers the MLP shall have, how many units each layer shall have, what kind of sigmoid is used and what kind of output function and loss function. The structure should be

rich enough that data overfitting becomes possible and your regularization method can kick in.

6. **Set up a cross-validation scheme** in order to optimize the generalization performance of your MLPs. Recommended: implement a semi-automated k-fold cross-validation scheme which is built around two subroutines, (1) "train an MLP of certain structure for minimal training error on given training data", (2) "test MLP on validation data".

7. **Implement the training and testing subroutines.** The training will be done with a suitable version of the *error backpropagation* algorithm, which will require you to meddle with some global control parameters (like learning rate, stopping criterion, initialization scheme, and more).

8. **Do the job.** Enjoy the powers, and marvel at the wickedness, of ANNs.

You see that "neural network training" is a multi-faceted thing and requires you to consider all the issues that *always* jump at you in supervised machine learning tasks. It will *not* miraculously give good results just because it has "neural networks inside". The actual "learning" part, namely solving the optimization task (157), is only a subtask, albeit a conspicuous one because it is done with an algorithm that has risen to fame, namely the backpropagation algorithm.

12.3.2 The error backpropagation algorithm

ANNs are trained by an iterative optimization procedure. In the classical, elementary case, this is pure gradient descent. I repeat the setup:

Given: Labelled training data in vector/vector format (obtained possibly after preprocessing raw data) $(\mathbf{u}_i, \mathbf{y}_i)_{i=1,\dots,N}$, where $\mathbf{u} \in \mathbb{R}^n, \mathbf{y} \in \mathbb{R}^k$. Also given: a network architecture for models $\mathcal{N}_\theta$ that can be specified by l-dimensional weight vectors $\theta \in \mathcal{H}$. Also given: a loss function $L : \mathbb{R}^k \times \mathbb{R}^k \to \mathbb{R}^{\geq 0}$.

Initialization: Choose an initial model $\theta^{(0)}$. This needs an educated guess. A widely used strategy is to set all weight parameters $w_i^{(0)} \in \theta^{(0)}$ to small random values. *Remark:* For training deep neural networks this is not good enough — the deep learning field actually got kickstarted by a clever method for finding a good model initialization (Hinton and Salakuthdinov 2006).

Iterate: Compute a series $(\theta^{(n)})_{n=0,1,\dots}$ of models of decreasing empirical loss (aka training error) by gradient descent. Concretely, with

$$R^{\mathsf{emp}}(\mathcal{N}_{\theta^{(n)}}) = \frac{1}{N} \sum_{i=1,\dots,N} L(\mathcal{N}_{\theta^{(n)}}(\mathbf{u}_i), \mathbf{y}_i) \tag{161}$$

denoting the empirical risk of the model $\theta^{(n)}$, and with

$$\nabla R^{\mathsf{emp}}(\mathcal{N}_{\theta^{(n)}}) = \left(\frac{\partial R^{\mathsf{emp}}}{\partial w_i}(\theta^{(n)}), \ldots, \frac{\partial R^{\mathsf{emp}}}{\partial w_l}(\theta^{(n)}) \right)' \tag{162}$$

being the gradient of the empirical risk with respect to the parameter vector $\theta = (w_1, \ldots, w_l)'$ at point $\theta^{(n)}$, update $\theta^{(n)}$ by

$$\theta^{(n+1)} = \theta^{(n)} - \mu \, \nabla \, R^{\mathsf{emp}}(\mathcal{N}_{\theta^{(n)}}).$$

Stop when a stopping criterion chosen by you is met. This can be reaching a maximum number of iterations, or the empirical risk decrease falling under a predermined threshold, or some early stopping scheme.

Computing a gradient is a differentiation task, and differentiation is easy. With high-school maths you would be able to compute (162). However, the gradient formula that you get from textbook recipes would be too expensive to compute. The *error backpropagation* algorithm (or simply "backprop" for the initiated, or even just BP if you want to have a feeling of belonging to this select community) is a specific algorithmic scheme to compute this gradient in a computationally efficient way.

The backpropagation algorithm became widely known as late as 1986 (historical remarks further below). In historical perspective it was the one and only decisive breakthrough for making ANNs practically usable. Every student of machine learning *must* have understood it in detail at least once in his/her life, even if later it's just downloaded from a toolbox in some more sophisticated fashioning. Thus, brace yourself and follow along!

Let us take a closer look at the empirical risk (161). Its gradient can be written as a sum of gradients

$$\nabla R^{\mathrm{emp}}(\mathcal{N}_\theta) = \nabla \left(\frac{1}{N} \sum_{i=1,\ldots,N} L(\mathcal{N}_\theta(\mathbf{u}_i), \mathbf{y}_i) \right) = \frac{1}{N} \sum_{i=1,\ldots,N} \nabla L(\mathcal{N}_\theta(\mathbf{u}_i), \mathbf{y}_i),$$

and this is also how it is actually computed: the gradient $\nabla L(\mathcal{N}_\theta(\mathbf{u}_i), \mathbf{y}_i)$ is evaluated for each training data example $(\mathbf{u}_i, \mathbf{y}_i)$ and the obtained N gradients are averaged.

This means that at every gradient descent iteration $\theta^{(n)} \to \theta^{(n+1)}$, all training data points have to be visited individually. In MLP parlance, such a sweep through all data points is called an *epoch*. In the neural network literature one finds statements like "the training was done for 120 epochs", which means that 120 average gradients were computed, and for each of these computations, N gradients for individual training example points $(\mathbf{u}_i, \mathbf{y}_i)$ were computed.

When training samples are large — as they should be — one epoch can clearly be too expensive. Therefore one often takes resort to *minibatch* training, where for each gradient descent iteration only a subset of the total sample S is used.

The backpropagation algorithm is a subroutine in the gradient descent game. It is a particular algorithmic scheme for calculating the gradient $\nabla L(\mathcal{N}_\theta(\mathbf{u}_i), \mathbf{y}_i)$ for a single data point $(\mathbf{u}_i, \mathbf{y}_i)$. Naive highschool calculations of this quantity incur a cost of $O(l^2)$ (where l is the number of network weights). When l is not extremely small (it will almost never be extremely small — a few hundreds of weights will be needed for simple tasks, and easily a million for deep networks applied to serious real-life modeling problems), this cost $O(l^2)$ is too high for practical exploits (and it has to be paid N times in a single gradient descent step!). The backprop algorithm is a clever scheme for computing and storing certain auxiliary quantities which cuts down the cost from $O(l^2)$ to $O(l)$.

Here is how backprop works.

1. BP works in two stages. In the first stage, called the *forward pass*, the current network $\mathcal{N}_\theta$ is presented with the input $\mathbf{u}$ and the output $\hat{\mathbf{y}} = \mathcal{N}_\theta(\mathbf{u})$ is computed using the "forward" formulas (159) and (160). During this forward pass, for each unit x_i^m which is not a bias unit and not an input unit the quantity
$$a_i^m = \sum_{j=0,\ldots,L^{m-1}} w_{ij}^m \, x_j^{m-1} \tag{163}$$
is computed – this is sometimes referred to as the *potential* of unit x_i^m, that is its internal state before it is passed through the sigmoid.

2. *A little math in between.* Applying the chain rule of calculus we have
$$\frac{\partial L(\mathcal{N}_\theta(\mathbf{u}), \mathbf{y})}{\partial w_{ij}^m} = \frac{\partial L(\mathcal{N}_\theta(\mathbf{u}), \mathbf{y})}{\partial a_i^m} \, \frac{\partial a_i^m}{\partial w_{ij}^m}. \tag{164}$$
Define
$$\delta_i^m = \frac{\partial L(\mathcal{N}_\theta(\mathbf{u}), \mathbf{y})}{\partial a_i^m}. \tag{165}$$
Using (163) we find
$$\frac{\partial a_i^m}{\partial w_{ij}^m} = x_j^{m-1}. \tag{166}$$
Combining (165) with (166) we get
$$\frac{\partial L(\mathcal{N}_\theta(\mathbf{u}), \mathbf{y})}{\partial w_{ij}^m} = \delta_i^m \, x_j^{m-1}. \tag{167}$$
Thus, in order to calculate the desired derivatives (164), we only need to compute the values of δ_i^m for each hidden and output unit.

3. *Computing the δ's for output units.* Output units x_i^K are typically set up differently from hidden units, and their corresponding δ values must be computed in ways that depend on the special architecture. For concreteness here

I stick with the simple linear units introduced in (160). The potentials a_i^K are thus identical to the output values $\hat{y}_i$ and we obtain

$$\delta_i^K = \frac{\partial L(\mathcal{N}_\theta(\mathbf{u}), \mathbf{y})}{\partial \hat{y}_i}. \tag{168}$$

This quantity is thus just the partial derivative of the loss with respect to the i-th output, which is usually simple to compute. For the quadratic loss $L(\mathcal{N}_\theta(\mathbf{u}), \mathbf{y}) = \|\mathcal{N}_\theta(\mathbf{u}) - y\|^2$, for instance, we get

$$\delta_i^K = \frac{\partial \|\mathcal{N}_\theta(\mathbf{u}) - \mathbf{y}\|^2}{\partial \hat{y}_i} = \frac{\partial \|\hat{\mathbf{y}} - \mathbf{y}\|^2}{\partial \hat{y}_i} = \frac{\partial (\hat{y}_i - y_i)^2}{\partial \hat{y}_i} = 2\,(\hat{y}_i - y_i). \tag{169}$$

4. *Computing the δ's for hidden units.* In order to compute δ_i^m for $1 \leq m < K$ we again make use of the chain rule. We find

$$\delta_i^m = \frac{\partial L(\mathcal{N}_\theta(\mathbf{u}), \mathbf{y})}{\partial a_i^m} = \sum_{l=1,\ldots,L^{m+1}} \frac{\partial L(\mathcal{N}_\theta(\mathbf{u}), \mathbf{y})}{\partial a_l^{m+1}} \, \frac{\partial a_l^{m+1}}{\partial a_i^m}, \tag{170}$$

which is justified by the fact that the only path by which a_i^m can affect $L(\mathcal{N}_\theta(\mathbf{u}), \mathbf{y})$ is through the potentials a_l^{m+1} of the next higher layer. If we substitute (165) into (170) and observe (163) we get

$$\begin{aligned}
\delta_i^m &= \sum_{l=1,\ldots,L^{m+1}} \delta_l^{m+1} \, \frac{\partial a_l^{m+1}}{\partial a_i^m} \\
&= \sum_{l=1,\ldots,L^{m+1}} \delta_l^{m+1} \, \frac{\partial \sum_{j=0,\ldots,L^m} w_{lj}^{m+1}\, \sigma(a_j^m)}{\partial a_i^m} \\
&= \sum_{l=1,\ldots,L^{m+1}} \delta_l^{m+1} \, \frac{\partial\, w_{li}^{m+1}\, \sigma(a_i^m)}{\partial a_i^m} \\
&= \sigma'(a_i^m) \sum_{l=1,\ldots,L^{m+1}} \delta_l^{m+1}\, w_{li}^{m+1}.
\end{aligned} \tag{171}$$

This formula describes how the δ_i^m in a hidden layer can be computed by "back-propagating" the δ_l^{m+1} from the next higher layer. The formula can be used to compute all δ's, starting from the output layer (where (168) is used — in the special case of a quadratic loss, Equation 169), and then working backwards through the network in the *backward pass* of the algorithm.

When the logistic sigmoid $\sigma(a) = 1/(1+\exp(-a))$ is used, the computation of the derivative $\sigma'(a_i^m)$ takes a particularly simple form, observing that for this sigmoid it holds that $\sigma'(a) = \sigma(a)\,(1-\sigma(a))$, which leads to

$$\sigma'(a_i^m) = x_i^m\,(1 - x_i^m).$$

Although simple in principle, and readily implemented, using the backprop algorithm appropriately is something of an art, even in basic shallow MLP training. Here is only place to hint at some difficulties:

- The stepsize μ must be chosen sufficiently small in order to avoid instabilities. But it also should be set as large as possible to speed up the convergence. We have seen the inevitable conflict between these two requirements in Section 11. In neural networks it is however not possible to provide an analytical treatment of how to set the stepsize optimally. Generally one uses adaptation schemes that modulate the learning rate as the gradient descent proceeds, using larger stepsizes in early epochs. Novel, clever methods for online adjustment of stepsize have been one of the enabling factors for deep learning. For shallow MLPs typical stepsizes that can be fixed without much thinking are in the order from 0.001 to 0.01.

- Gradient descent on nonlinear performance landscapes may sometimes be crippling slow in "plateau" areas still far away from the next local minimum where the gradient is small in all directions, for other reasons than what we have seen in quadratic performance surfaces.

- Gradient-descent techniques on performance landscapes can only find a local minimum of the risk function. This problem can be addressed by various measures, all of which are computationally expensive. Some authors claim that the local minimum problem is overrated.

The error backpropagation "trick" to speed up gradient calculations in layered systems has been independently discovered several times and in a diversity of contexts, not only in neural network or machine learning research. Schmidhuber 2015, Section 5.5, provides a historical overview. In its specific versions for neural networks, backpropagation apparently was first described by Paul Werbos in his 1974 PhD thesis, but remained unappreciated until it was re-described in a widely read collection volume on neural networks (Rumelhart, Hinton, and Williams 1986). From that point onwards, backpropagation in MLPs developed into what today is likely the most widely used computational technique in machine learning.

A truly beautiful visualization of MLP training has been pointed out to me by Rubin Dellialisi: `playground.tensorflow.org/`.

Simple gradient descent, as described above, is cheaply computed but may take long to converge and/or run into stability issues. A large variety of refined iterative loss minimization methods have been developed in the deep learning field which in most cases (but none in all cases) combine an acceptable speed of convergence with stability. Some of them refine gradient descent, others use information from the local curvature (and are therefore called "second-order" methods) of the performance surface. The main alternatives are nicely sketched and compared at `https://www.neuraldesigner.com/blog/5_algorithms_to_train_a_`

`neural_network` (retrieved May 2017, local copy at `https://www.ai.rug.nl/minds/uploads/NNalgs.zip`).

That's it. I hope this course has helped you on your way into machine learning — that you have learnt a lot, that you enjoyed at least half of it, and that you will not forget the essential ten percent.

Appendix

A Elementary mathematical structure-forming operations

A.1 Pairs, tuples and indexed families

If two mathematical objects $\mathcal{O}_1, \mathcal{O}_2$ are given, they can be grouped together in a single new mathematical structure called the *ordered pair* (or just *pair*) of $\mathcal{O}_1, \mathcal{O}_2$. It is written as

$$(\mathcal{O}_1, \mathcal{O}_2).$$

In many cases, $\mathcal{O}_1, \mathcal{O}_2$ will be of the same kind, for instance both are integers. But the two objects need not be of the same kind. For instance, it is perfectly possible to group integer $\mathcal{O}_1 = 3$ together with a random variable (a function!) $\mathcal{O}_2 = X_7$ in a pair, getting $(3, X_7)$.

The crucial property of a pair $(\mathcal{O}_1, \mathcal{O}_2)$ which distinguishes it from the *set* $\{\mathcal{O}_1, \mathcal{O}_2\}$ is that the two members of a pair are *ordered*, that is, it makes sense to speak of the "first" and the "second" member of a pair. In contrast, it makes not sense to speak of the "first" or "second" element of the set $\{\mathcal{O}_1, \mathcal{O}_2\}$. Related to this is the fact that the two members of a pair can be the same, for instance $(2, 2)$ is a valid pair. In contrast, $\{2, 2\}$ makes no sense.

A generalization of pairs is *N-tuples*. For an integer $N > 0$, an N-tuple of N objects $\mathcal{O}_1, \mathcal{O}_2, \ldots, \mathcal{O}_N$ is written as

$$(\mathcal{O}_1, \mathcal{O}_2, \ldots, \mathcal{O}_N).$$

1-tuples are just individual objects; 2-tuples are pairs, and for $N > 2$, N-tuples are also called *lists* (by computer scientists that is; mathematicians rather don't use that term). Again, the crucial property of N-tuples is that one can identify its i-th member by its position in the tuple, or in more technical terminology, by its *index*. That is, in an N-tuple, every index $1 \leq i \leq N$ "picks" one member from the tuple.

The infinite generalization of N-tuples is provided by *indexed families*. For any nonempty set I, called an *index set* in this context,

$$(\mathcal{O}_i)_{i \in I}$$

denotes a compound object assembled from as many mathematical objects as there are index elements $i \in I$, and within this compound object, every individual member $\mathcal{O}_i$ can be "addressed" by its index i. One simply writes

$$\mathcal{O}_i$$

to denote the ith "component" of $(\mathcal{O}_i)_{i \in I}$. Writing $\mathcal{O}_i$ is a shorthand for applying the ith projection function on $(\mathcal{O}_i)_{i \in I}$, that is, $\mathcal{O}_i = \pi_i((\mathcal{O}_i)_{i \in I})$.

A.2 Products of sets

We first treat the case of products of a finite number of sets. Let $S_1, \ldots, S_N$ be (any) sets. Then the product $S_1 \times \ldots \times S_N$ is the set of all N-tuples of elements from the corresponding sets, that is,

$$S_1 \times \ldots \times S_N = \{(s_1, \ldots, s_N) \mid s_i \in S_i\}.$$

This generalizes to infinite products as follows. Let I be any set — we call it an *index* set in this context. For every $i \in I$, let S_i be some set. Then the *product set indexed by* I is the set of functions

$$\prod_{i \in I} S_i = \{\varphi : I \to \bigcup_{i \in I} S_i \mid \forall i \in I : \varphi(i) \in S_i\}.$$

Using the notation of indexed families, this could equivalently be written as

$$\prod_{i \in I} S_i = \{(s_i)_{i \in I} \mid \forall i \in I : s_i \in S_i\}.$$

If all the sets S_i are the same, say S, then the product $\prod_{i \in I} S_i = \prod_{i \in I} S$ is also written as S^I.

An important special case of infinite products is obtained when $I = \mathbb{N}$. This situation occurs universally in modeling stochastic processes with discrete time. The elements $n \in \mathbb{N}$ are the points in time when the amplitude of some signal is measured. The amplitude is a real number, so at any time $n \in \mathbb{N}$, one records an amplitude value $a_n \in S_n = \mathbb{R}$. The product set

$$\prod_{n \in \mathbb{N}} S_n = \{\varphi : \mathbb{N} \to \bigcup_{n \in \mathbb{N}} S_n \mid \forall n \in I : \varphi(n) \in S_n\} = \{\varphi : \mathbb{N} \to \mathbb{R}\}$$

is the set of all right-infinite real-valued timeseries (with discrete time points starting at time $n = 0$).

A.3 Products of functions

First, again, the case of finite products: let $f_1, \ldots, f_N$ be functions, all sharing the same domain D, with image sets S_i. Then the product $f_1 \otimes \ldots \otimes f_N$ of these functions is the function with domain D and image set $S_1 \times \ldots \times S_N$ given by

$$\begin{aligned} f_1 \otimes \ldots \otimes f_N : D &\to S_1 \times \ldots \times S_N \\ d &\mapsto (f_1(d), \ldots, f_N(d)). \end{aligned}$$

Again this generalizes to arbitrary products. Let $(f_i : D \to S_i)_{i \in I}$ be an indexed family of functions, all of them sharing the same domain D, and where the image set of f_i is S_i. The product $\bigotimes_{i \in I} f_i$ of this set of functions is defined by

$$\begin{aligned} \bigotimes_{i \in I} f_i : D &\to \prod_{i \in I} S_i \\ d &\mapsto \varphi : I \to \bigcup_{i \in I} S_i \quad \text{given by } \varphi(i) = f_i(d). \end{aligned}$$

B Joint, conditional and marginal probabilities

Note. This little section is only a quick memory refresher of some of the most basic concepts of probability. It does not replace a textbook chapter!

We first consider the case of two observations of some part of reality that have discrete values. For instance, an online shop creating customer profiles may record from their customers their age and gender (among many other items). The marketing optimizers of that shop are not interested in the exact age but only in age brackets, say $a_1 = \mathsf{at\ most\ 10\ years\ old}$, $a_2 = 11-20$ years, $a_3 = 21-30$ years, $a_4 = \mathsf{older\ than\ 30}$. Gender is roughly categorized into the possibilities $g_1 = \mathsf{f}, g_2 = \mathsf{m}, g_3 = \mathsf{o}$. From their customer data the marketing guys estimate the following probability table:

$P(X = g_i, Y = a_j)$	a_1	a_2	a_3	a_4
g_1	0.005	0.3	0.2	0.04
g_2	0.005	0.15	0.15	0.04
g_3	0.0	0.05	0.05	0.01

(172)

The cell (i, j) in this 3×4 table contains the probability that a customer with gender g_i falls into the age bracket a_j. This is the *joint probability* of the two observation values g_i and a_j. Notice that all the numbers in the table sum to 1.

The mathematical tool to formally describe a category of an observable value is a *random variable* (RV). We typically use symbols $X, Y, Z, \ldots$ for RVs in abstract mathematical formulas. When we deal with concrete applications, we may also use "telling names" for RVs. For instance, in Table (172), instead of $P(X = g_i, Y = a_j)$ we could have written $P(\mathsf{Gender} = g_i, \mathsf{Age} = a_j)$. Here we have two such observation categories: gender and age bracket, and hence we use two RVs X and Y for gender and age, respectively. In order to specify, for example, that female customers in the age bracket 11-20 occur with a probability of 0.3 in the shop's customer reservoir (the second entry in the top line of the table), we write $P(X = g_1, Y = a_2) = 0.3$.

Some more info bits of concepts and terminology connected with RVs. You should consider a RV as the mathematical counterpart of a procedure or apparatus to make observations or measurements. For instance, the real-world counterpart of the Gender RV could be an electronic questionnaire posted by the online shop, or more precisely, the "what is your age?" box on that questionnaire, plus the whole internet infrastructure needed to send the information entered by the customer back to the company's webserver. Or in a very different example (measuring the speed of a car and showing it to the driver on the speedometer) the real-world counterpart of a RV Speed would be the total on-board circuitry in a car, comprising the wheel rotation sensor, the processing DSP microchip, and the display at the dashboard.

A RV *always* comes with a set of possible outcomes. This set is called the *sample space* of the RV, and I usually denote it with the symbol S. Mathematically,

a sample space is a set. The sample space for the Gender RV would be the set $S = \{\mathsf{m}, \mathsf{f}, \mathsf{o}\}$. The sample space for Age that we used in the table above was $S = \{\{0, 1, \ldots, 10\}, \{11, \ldots, 20\}, \{21, \ldots, 30\}, \{31, 32, \ldots\}\}$. For car speed measuring we might opt for $S = \mathbb{R}^{\geq 0}$, the set of non-negative reals. A sample space can be larger than the set of measurement values that are realistically possible, but it must contain *at least* all the possible values.

Back to our table and the information it contains. If we are interested only in the age distribution of customers, ignoring the gender aspects, we sum the entries in each age column and get the *marginal probabilities* of the RV Y. Formally, we compute

$$P(Y = a_j) = \sum_{i=1,2,3} P(X = g_i, Y = a_j).$$

Similarly, we get the marginal distribution of the gender variable by summing along the rows. The two resulting marginal distributions are indicated in the table (173).

	a_1	a_2	a_3	a_4	
g_1	0.005	0.3	0.2	0.04	**0.545**
g_2	0.005	0.15	0.15	0.04	**0.345**
g_3	0.0	0.05	0.05	0.01	**0.110**
	0.01	**0.5**	**0.4**	**0.09**	

(173)

Notice that the marginal probabilities of age $0.01, 0.5, 0.4, 0.09$ sum to 1, as do the gender marginal probabilities.

Finally, the *conditional probability* $P(X = g_i \,|\, Y = a_j)$ that a customer has gender g_i given that the age bracket is a_j is computed through dividing the joint probabilities in column j by the sum of all values in this column:

$$P(X = g_i \,|\, Y = a_j) = \frac{P(X = g_i, Y = a_j)}{P(Y = a_j)}. \tag{174}$$

There are two equivalent versions of this formula:

$$P(X = g_i, Y = a_j) = P(X = g_i \,|\, Y = a_j) P(Y = a_j) \tag{175}$$

where the righthand side is called a *factorization* of the joint distribution on the lefthand side, and

$$P(Y = a_j) = \frac{P(X = g_i, Y = a_j)}{P(X = g_i \,|\, Y = a_j)}, \tag{176}$$

demonstrating that each of the three quantities (joint, conditional, marginal probability) can be expressed by the respective two others. If you memorize one of these formulas – I recommend the second one – you have memorized the very

key to master "probability arithmetics" and will never get lost when manipulating probability formulas.

The factorization (175) can be done in two ways: $P(Y = a_j \,|\, X = g_i)P(X = g_i) = P(X = g_i \,|\, Y = a_j)P(Y = a_j)$, which gives rise to *Bayes' formula*

$$P(Y = a_j \,|\, X = g_i) = \frac{P(X = g_i \,|\, Y = a_j)P(Y = a_j)}{P(X = g_i)}, \tag{177}$$

which has many uses in statistical modeling because it shows how one can revert the conditioning direction.

Joint, conditional, and marginal probabilities are also defined when there are more than two categories of observations. For instance, the online shop marketing people also record how much a customer spends on average, and formalize this by a third random variable, say Z. The values that Z can take are spending brackets, say $s_1 =$ less than 5 Euros to $s_{20} =$ more than 5000 Euros. The joint probability values $P(X = g_i, Y = a_j, Z = s_k)$ would be arranged in a 3-dimensional array sized $3 \times 4 \times 20$, and again all values in this array together sum to 1. Now there are different arrangements for conditional and marginal probabilities, for instance $P(Z = s_k \,|\, X = g_i, Y = a_j)$ is the probability that among the group of customers with gender g_i and age a_j, a person spends an amount in the range s_k. Or $P(Z = s_k, Y = a_j \,|\, X = g_i)$ is the probability that in the gender group g_i a person is aged a_j and spends s_k. As a last example, the probabilities $P(X = g_i, Z = s_j)$ are the marginal probabilities obtained by *summing away* the Y variable:

$$P(X = g_i, Z = s_j) = \sum_{k=1,2,3,4} P(X = g_i, Y = a_k, Z = s_j) \tag{178}$$

So far I have described cases where all kinds of observations were *discrete*, that is, they (i.e. all RVs) yield values from a finite set – for instance the three gender values or the four age brackets. Equally often one faces *continuous* random values which arise from observations that yield real numbers – for instance, measuring the body height or the weight of a person. Since each such RV can give infinitely many different observation outcomes, their probabilities cannot be represented in a table or array. Instead, one uses *probability density functions* (pdf's) to write down and compute probability values.

Let's start with a single RV, say $H =$ Body Height. Since body heights are non-negative and, say, never larger than 3 m, the distribution of body heights within some reference population can be represented by a pdf $f : [0, 3] \to \mathbb{R}^{\geq 0}$ which maps the interval $[0, 3]$ of possible values to the nonnegative reals (Figure 83). We will be using subscripts to make it clear which RV a pdf refers to, so the pdf describing the distribution of body height will be written f_H.

A pdf for the distribution of a continuous RV X can be used to calculate the probability that this RV takes values within a particular interval, by integrating the pdf over that interval. For instance, the probability that a measurement of

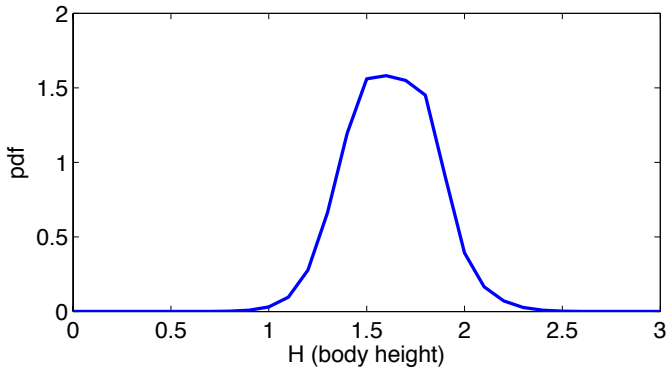

Figure 83: A hypothetical distribution of human body sizes in some reference population, represented by a pdf.

body height comes out between 1.5 and 2.0 meters is obtained by

$$P(H \in [1.5, 2.0]) = \int_{1.5}^{2.0} f_H(x)dx, \tag{179}$$

see the shaded area in Figure 83. Some comments:

- A probability density function is actually *defined* to be a function which allows one to compute probabilities of value intervals as in Equation 179. For a given continuous RV X over the reals there is exactly one function f_X which has this property, *the* pdf for X. (This is not quite true. There exist also continuous-valued RVs whose distribution is so complex that it cannot be captured by a pdf, but we will not meet with such phenomena in this lecture. Furthermore, a given pdf can be altered on isolated points – which come from what is called a *null set* in probability theory – and still be a pdf for the same distribution. But again, we will not be concerned with such subtelties in this lecture.)

- As a consequence, any pdf $f : \mathbb{R} \to \mathbb{R}^{\geq 0}$ has the property that it integrates to 1, that is, $\int_{-\infty}^{\infty} f(x)dx = 1$.

- Be aware that the values $f(x)$ of a pdf are not probabilities! Pdf's turn into probabilities only through integration over intervals.

- Values $f(x)$ can be greater than 1 (as in Figure 83), again indicating that they cannot be taken as probabilities.

Joint distributions of two continuous RVs X, Y can be captured by a pdf $f_{X,Y} : \mathbb{R}^2 \to \mathbb{R}^{\geq 0}$. Figure 84 shows an example. Again, the pdf $f_{X,Y}$ of a bivariate continuous distribution must integrate to 1 and be non-negative; and conversely, every such function is the pdf of a continuous distribution of two RV's.

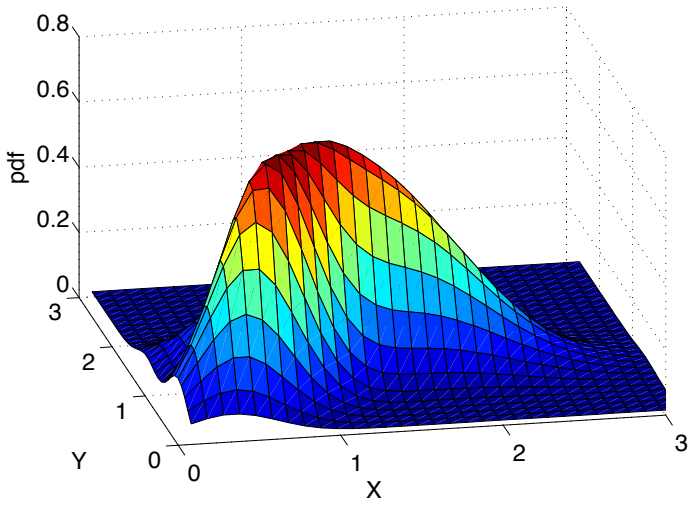

Figure 84: An exemplary joint distribution of two continuous-valued RVs X, Y, represented by its pdf.

Continuing on this track, the joint distribution of k continuous-valued RVs $X_1, \ldots, X_k$, where the possible values of each X_i are bounded to lie between a_i and b_i can be described by a unique pdf function $f_{X_1,\ldots,X_k} : \mathbb{R}^k \to \mathbb{R}^{\geq 0}$ which integrates to 1, i.e.

$$\int_{a_1}^{b_1} \ldots \int_{a_k}^{b_k} f(x_1, \ldots, x_k)\, dx_k \ldots dx_1,$$

where also the cases $a_i = -\infty$ and $b_i = \infty$ are possible. A more compact notation for the same integral is

$$\int_D f(\mathbf{x})\, d\mathbf{x},$$

where D denotes the k-dimensional box $[a_1, b_1] \times \ldots \times [a_k, b_k]$ and $\mathbf{x}$ denotes vectors in $\mathbb{R}^k$. Mathematicians speak of k-dimensional *intervals* instead of "boxes". The set of points $S = \{\mathbf{x} \in \mathbb{R}^k \mid f_{X_1,\ldots,X_k} > 0\}$ is called the *support* of the distribution. Obviously $S \subseteq D$.

In analogy to the 1-dim case from Figure 83, probabilities are obtained from a k-dimensional pdf $f_{X_1,\ldots,X_k}$ by integrating over sub-intervals. For such a k-dimensional subinterval $[r_1, s_1] \times \ldots \times [r_k, s_k] \subseteq [a_1, b_1] \times \ldots \times [a_k, b_k]$, we get its probability by

$$P(X_1 \in [r_1, s_1], \ldots, X_k \in [r_k, s_k]) = \int_{r_1}^{s_1} \ldots \int_{r_k}^{s_k} f(x_1, \ldots, x_k)\, dx_k \ldots dx_1. \quad (180)$$

In essentially the same way as we did for discrete distributions, the pdf's of marginal distributions are obtained by *integrating away* the RV's that one wishes

to expel. In analogy to (178), for instance, one would get

$$f_{X_1,X_3}(x_1,x_3) = \int_{a_2}^{b_2} f_{X_1,X_2,X_3}(x_1,x_2,x_3)\; dx_2. \tag{181}$$

And finally, pdf's of conditional distributions are obtained through dividing joint pdfs by marginal pdfs. Such conditional pdfs are used to calculate that some RVs fall into a certain multidimensional interval given that some other RVs take specific values. We only inspect a simple case analog to (174) where we want to calculate the probability that X falls into a range $[a,b]$ given that Y is known to be c, that is, we want to evaluate the probability $P(X \in [a,b] \,|\, Y = c)$, using pdfs. We can obtain this probability from the joint pdf $f_{X,Y}$ and the marginal pdf f_Y by

$$P(X \in [a,b] \,|\, Y = c) = \frac{\int_a^b f_{X,Y}(x,c)\; dx}{f_Y(c)}. \tag{182}$$

The r.h.s. expression $\int_a^b f_{X,Y}(x,c)\; dx \;/\; f_Y(c)$ is a function of x, parametrized by c. This function is a pdf, denoted by $f_{X\,|\,Y=c}$, and defined by

$$f_{X\,|\,Y=c}(x) = \frac{f_{X,Y}(x,c)}{f_Y(c)}. \tag{183}$$

Let me illustrate this with a concrete example. An electronics engineer is testing a device which transforms voltages V into currents I. In order to empirically measure the behavior of this device (an electronics engineer would say, in order to "characterize" the device), the engineer carries out a sequence of measurement trials where he first sets the input voltage V to a specific value, say $V = 0.0$. Then he (or she) measures the resulting current many times, in order to get an idea of the stochastic spread of the current. In mathematical terms, the engineer wants to get an idea of the pdf $f_{I\,|\,V=0.0}$. The engineer then carries on, setting the voltage to other values $c_1, c_2, ...$, measuring resulting currents in each case, and getting ideas of the conditional pdfs $f_{I\,|\,V=c_i}$. For understanding the characteristics of this device, the engineer needs to know all of these pdfs.

Conditional distributions arise whenever cause-effect relationships are being modeled. The conditioning variables are causes, the conditioned variables describe effects. In experimental and empirical research, the causes are under the control of an experimenter and can (and have to) be set to specific values in order to assess the statistics of the effects – which are not under the control of the experimenter. In ML pattern classification scenarios, the "causes" are the input patterns and the "effects" are the (stochastically distributed) class label assignments. Since research in the natural sciences is very much focussed on determining Nature's cause-effect workings, and 90% of the applications in machine learning concern pattern classification (my estimate), it is obvious that conditional distributions lie at the very heart of scientific (and engineering) modeling and data analysis.

In this appendix (and in the lecture) I consider only two ways of representing probability distributions: discrete ones by finite probability tables or probability tables; continuous ones by pdfs. These are the most elementary formats of representing probability distributions. There are many others which ML experts readily command on. This large and varied universe of concrete *representations* of probability distributions is tied together by an abstract mathematical theory of the probability distributions themselves, independent of particular representations. This theory is called *probability theory*. It is not an easy theory and we don't attempt an introduction to it. If you are mathematically minded, then you can get an introduction to probability theory in my graduate lecture notes "Principles of Statistical Modeling" (`https://www.ai.rug.nl/minds/uploads/LN_PSM.pdf`). At this point I only highlight two core facts from probability theory:

- A main object of study in probability theory are distributions. They are abstractly and axiomatically defined and analyzed, without reference to particular representations (such as tables or pdfs).
- A probability distribution *always* comes together with random variables. We write P_X for the distribution of a RV X, $P_{X,Y}$ for the joint distribution of two RVs X, Y, and $P_{X\,|\,Y}$ for the conditional distribution (a truly involved concept since it is actually a family of distributions) of X given Y.

C The argmax operator

Let $\varphi : D \to \mathbb{R}$ be some function from some domain D to the reals. Then

$$\operatorname*{argmax}_a \varphi(a)$$

is that $d \in D$ for which $\varphi(d)$ is maximal among all values of φ on D. If there are several arguments a for which φ gives the same maximal value, – that is, φ does not have a unique maximum –, or if φ has no maximum at all, then the argmax is undefined.

D Expectation, variance, covariance, and correlation of numerical random variables

Recall that a random variable is the mathematical model of an observation / measurement / recording procedure by which one can "sample" observations from that piece of reality that one wishes to model. We usually denote RVs by capital roman letters like X, Y or the like. For example, a data engineer of an internet shop who wants to get a statistical model of its (potential) customers might record the gender and age and spending of shop visitors – this would be formally captured

by three random variables G, A, S. A random variable always comes together with a *sample space*. This is the set of values that might be delivered by the random variable. For instance, the sample space of the gender RV G could be cast as $\{\mathrm{m}, \mathrm{f}, \mathrm{o}\}$ – a symbolic (and finite) set. A reasonable sample space for the age random variable A would be the set of integers between 0 and 200 – assuming that no customer will be older than 200 years and that age is measured in integers (years). Finally, a reasonable sample space for the spending RV S could be just the real numbers $\mathbb{R}$.

Note that in the A and S examples, the sample spaces that I proposed look very generous. We would not really expect that some customer is 200 years old, nor would we think that ever a customer spends 10^{1000} Euros – although both values are included in the respective sample space. The important thing about a sample space is that it must contain all the values that might be returned by the RV; but it may also contain values that will never be observed in practice.

Every mathematical set can serve as a sample space. We just saw symbolic, integer, and real sample spaces. Real sample spaces are used whenever one is dealing with an observation procedure that returns numerical values. Real-valued RVs are of great practical importance, and they allow many insightful statistical analyses that are not defined for non-numerical RVs. The most important analytical characteristics of real RVs are expectation, variance, and covariance, which I will now present in turn.

For the remainder of this appendix section we will be considering random variables X whose sample space is $\mathbb{R}^n$ — that is, observation procedures which return scalars (case $n = 1$) or vectors. We will furthermore assume that the distributions of all RVs X under consideration will be represented by pdf's $f_X : \mathbb{R}^n \to \mathbb{R}^{\geq 0}$. (In mathematical probability theory, more general numerical sample spaces are considered, as well as distributions that have no pdf — but we will focus on this basic scenario of real-valued RVs with pdfs).

The *expectation* of a RV X with sample space $\mathbb{R}^n$ and pdf f_X is defined as

$$E[X] = \int_{\mathbb{R}^n} x \, f_X(x) \, dx, \tag{184}$$

where the integral is written in a common shorthand for

$$\int_{x_1=-\infty}^{\infty} \dots \int_{x_n=-\infty}^{\infty} (x_1, \dots, x_n)' \, f_X((x_1, \dots, x_n)) \, dx_n \dots dx_1.$$

The expectation of a RV X can be intuitively understood as the "average" value that is delivered when the observation procedure X would be carried out infinitely often. The crucial thing to understand about the expectation is that it does not depend on a sample, – it does not depend on specific data.

In contrast, whenever in machine learning we base some learning algorithm on a (numerical) training sample $(x_i, y_i)_{i=1,\dots,N}$ drawn from the joint distribution

$P_{X,Y}$ of two RVs X, Y, we may compute the average value of the x_i by

$$\text{mean}(\{x_1, \ldots, x_N\}) = 1/N \sum_{i=1}^{N} x_i,$$

but this *sample mean* is NOT the expectation of X. If we would have used another random sample, we would most likely have obtained another sample mean. In contrast, the expectation $E[X]$ of X is defined not on the basis of a finite, random sample of X, but it is defined by averaging over the true underlying distribution.

Since in practice we will not have access to the true pdf f_X, the expectation of a RV X cannot usually be determined in full precision. The best one can do is to *estimate* it from observed sample data. The sample mean is an *estimator* for the expectation of a numerical RV X. Marking estimated quantities by a "hat" accent, we may write

$$\hat{E}[X] = 1/N \sum_{i=1}^{N} x_i.$$

A random variable X is *centered* if its expectation is zero. By subtracting the expectation one gets a centered RV. In these lecture notes I use the bar notation to mark centered RVs:

$$\bar{X} := X - E[X].$$

The *variance* of a scalar RV with sample space $\mathbb{R}$ is the expected squared deviation from the expectation

$$\sigma^2(X) = E[\bar{X}^2], \tag{185}$$

which in terms of the pdf $f_{\bar{X}}$ of $\bar{X}$ can be written as

$$\sigma^2(X) = \int_{\mathbb{R}} x^2 \, f_{\bar{X}}(x) \, dx.$$

Like the expectation, the variance is an intrinsic property of an observation procedure X and the part of the real world where the measurements may be taken from — it is independent of a concrete sample. A natural way to estimate the variance of X from a sample $(x_i)_{i=1,\ldots,N}$ is

$$\hat{\sigma}^2(\{x_1, \ldots, x_N\}) = 1/N \sum_{i=1}^{N} \left(x_i - 1/N \sum_{j=1}^{N} x_j \right)^2,$$

but in fact this estimator is not the best possible – on average (across different samples) it underestimates the true variance. If one wishes to have an estimator that is *unbiased*, that is, which on average across different samples gives the correct variance, one must use

$$\hat{\sigma}^2(\{x_1, \ldots, x_N\}) = 1/(N-1) \sum_{i=1}^{N} \left(x_i - 1/N \sum_{j=1}^{N} x_j \right)^2$$

instead. The Wikipedia article on "Variance", section "Population variance and sample variance" points out a number of other pitfalls and corrections that one should consider when one estimates variance from samples.

The square root of the variance of X, $\sigma(X) = \sqrt{\sigma^2(X)}$, is called the *standard deviation* of X.

The *covariance* between two real-valued scalar random variables X, Y is defined as

$$\mathrm{Cov}(X, Y) = E[\bar{X}\,\bar{Y}], \tag{186}$$

which in terms of a pdf $f_{\bar{X}\,\bar{Y}}$ for the joint distribution for the centered RVs spells out to

$$\mathrm{Cov}(X, Y) = \int_{\mathbb{R}\times\mathbb{R}} x\,y\,f_{\bar{X}\,\bar{Y}}((x, y)')\,dx\,dy.$$

An unbiased estimate of the covariance, based on a sample $(x_i, y_i)_{i=1,\ldots,N}$ is given by

$$\widehat{\mathrm{Cov}}((x_i, y_i)_{i=1,\ldots,N}) = 1/(N-1)\,\left(x_i - 1/N\,\sum_i x_i\right)\left(y_i - 1/N\,\sum_i y_i\right).$$

Finally, let us inspect the *correlation* of two scalar RVs X, Y. Here we have to be careful because this term is used differently in different fields. In statistics, the correlation is defined as

$$\mathrm{Corr}(X, Y) = \frac{\mathrm{Cov}(X, Y)}{\sigma(X)\,\sigma(Y)}. \tag{187}$$

It is easy to show that $-1 \leq \mathrm{Corr}(X, Y) \leq 1$. The correlation in the understanding of statistics can be regarded as a normalized covariance. It has a value of 1 if X and Y are identical up to some positive scaling factor, it has a value of -1 if X and Y are identical up to some negative scaling factor. When $\mathrm{Corr}(X, Y) = 0$, X and Y are said to be *uncorrelated*.

The quantity $\mathrm{Corr}(X, Y)$ is also referred to as *(population) Pearson's correlation coefficient*, and is often denoted by the greek letter $\varrho(X, Y) = \mathrm{Corr}(X, Y)$.

In the signal processing literature (for instance in my favorite textbook Farhang-Boroujeny 1998), the term "correlation" is sometimes used in quite a different way, denoting the quantity

$$E[X\,Y],$$

that is, simply the expectation of the product of the uncentered RVs X and Y. Just be careful when you read terms like "correlation" or "cross-correlation" or "cross-correlation matrix" and make sure that your understanding of the term is the same as the respective author's.

There are some basic rules for doing calculations with expectations and covariance which one should know:

1. Expectation is a linear operator:

$$E[\alpha\, X + \beta\, Y] = \alpha\, E[X] + \beta\, E[Y],$$

where $\alpha\, X$ is the RV obtained from X by scaling observations with a factor α.

2. Expectation is idempotent:

$$E[E[X]] = E[X].$$

3.

$$\mathrm{Cov}(X, Y) = E[X\, Y] - E[X]\, E[Y].$$

E Derivation of Equation 31

$$\begin{aligned}
1/N\ \sum_i \|x_i - \mathbf{d} \circ \mathbf{f}(x_i)\|^2 = \\
&= 1/N\ \sum_i \|\bar{x}_i - \sum_{k=1}^{m} (\bar{x}_i'\, u_k)\, u_k\|^2 \\
&= 1/N\ \sum_i \|\sum_{k=1}^{n} (\bar{x}_i'\, u_k)\, u_k - \sum_{k=1}^{m} (\bar{x}_i'\, u_k)\, u_k\|^2 \\
&= 1/N\ \sum_i \|\sum_{k=m+1}^{n} (\bar{x}_i'\, u_k)\, u_k\|^2 \\
&= 1/N\ \sum_i \sum_{k=m+1}^{n} (\bar{x}_i'\, u_k)^2 \quad = \quad \sum_{k=m+1}^{n} 1/N\ \sum_i (\bar{x}_i'\, u_k)^2 \\
&= \sum_{k=m+1}^{n} \sigma_k^2.
\end{aligned}$$

References

[1] D. H. Ackley, G. E. Hinton, and T. J. Sejnowski. "A Learning Algorithm for Boltzmann Machines". In: *Cognitive Science* 9 (1985), pp. 147–169.

[2] A. C. Antoulas and D. C. Sorensen. "Approximation of large-scale dynamical systems: an overview". In: *Int. J. Appl. Math. Comput. Sci.* 11.5 (2001), pp. 1093–1121.

[3] D. Bahdanau, K. Cho, and Y. Bengio. "Neural Machine Translation by Jointly Learning to Align and Translate". In: *International Conference on Learning Representations (ICLR)*. 2015. URL: `http://arxiv.org/abs/1409.0473v6`.

[4] J. A. Bednar and S. P. Wilson. "Cortical maps." In: *The Neuroscientist* 22.6 (2016), pp. 604–617.

[5] Y. Bengio and Y. LeCun. "Scaling Learning Algorithms towards AI". In: *Large-Scale Kernel Machines*. Ed. by Bottou L. et al. MIT Press, 2007.

[6] L. Breiman. "Random forests". In: *Machine Learning* 45 (2001), pp. 5–32.

[7] A. Clark. "Whatever Next? Predictive Brains, Situated Agents, and the Future of Cognitive Science." In: *Behavioural and Brain Sciences* 36.3 (2013), pp. 1–86.

[8] G. E. Crooks. *Field Guide to Continuous Probability Distributions, v 0.11 beta*. online manuscript, retrieved April 2017, extended version also available in print since 2019. 2017. URL: `http://threeplusone.com/fieldguide`.

[9] A. Deisenroth, A. Faisal, and C. S. Ong. *Mathematics for Machine Learning*. Free online copy at `https://mml-book.github.io/`. Cambridge University Press, 2019.

[10] A.P. Dempster, N.M. Laird, and D.B. Rubin. "Maximum likelihood from incomplete data via the EM-algorithm". In: *Journal of the Royal Statistical Society* 39 (1977), pp. 1–38.

[11] S. Demyanov. "Regularization Methods for Neural Networks and Related Models". PhD thesis. Dept of Computing and Information Systems, Univ. of Melbourne, 2015.

[12] R. O. Duda, P. E. Hart, and D. G. Stork. *Pattern Classification (second edition)*. Wiley Interscience, 2001.

[13] R. Durbin et al. *Biological Sequence Analysis: Probabilistic Models of Proteins and Nucleic Acids*. Cambridge University Press, 2000.

[14] D. Durstewitz, J. K. Seamans, and T. J. Sejnowski. "Neurocomputational models of working memory". In: *Nature Neuroscience* 3 (2000), pp. 1184–91.

[15] S. Edelman. “The minority report: some common assumptions to reconsider in the modelling of the brain and behaviour”. In: *J of Experimental and Theoretical Artificial Intelligence* (2015). URL: http://www.tandfonline.com/action/showCitFormats?doi=10.1080/0952813X.2015.1042534.

[16] S. Ermon. *Probabilistic Graphical Models*. Online lecture notes of a graduate course at Stanford University. 2019. URL: https://ermongroup.github.io/cs228-notes/.

[17] B. Farhang-Boroujeny. *Adaptive Filters: Theory and Applications*. Wiley, 1998.

[18] K. Friston. “A theory of cortical response”. In: *Phil. Trans. R. Soc. B* 360 (2005), pp. 815–836.

[19] K. Friston. “Learning and Inference in the Brain”. In: *Neural Networks* 16 (2003), pp. 1325–1352.

[20] S. Fusi and X.-J. Wang. “Short-term, long-term, and working memory”. In: *From Neuron to Cognition via Computational Neuroscience*. Ed. by M. Arbib and J. Bonaiuto. MIT Press, 2016, pp. 319–344.

[21] I. J. Goodfellow, J. Shlens, and C. Szegedy. “Explaining and Harnessing Adversarial Examples”. In: *Proc. ICLR 2015*. arXiv:1412.6572v3. 2014.

[22] I. Goodfellow, Y. Bengio, and A. Courville. *Deep Learning*. Open access version at http://www.deeplearningbook.org. MIT Press, 2016.

[23] A. N. Gorban et al. *Principal Manifolds for Data Visualization and Dimension Reduction*. Springer, 2008.

[24] A. Graves et al. “Hybrid computing using a neural network with dynamic external memory”. In: *Nature* 7626 (2016), pp. 471–476.

[25] M. Hasegawa, H. Kishino, and T. Yano. “Dating the human-ape splitting by a molecular clock of mitochondrial DNA”. In: *J. of Molecular Evolution* 22 (1985), pp. 160–174.

[26] G. E. Hinton and R. R. Salakuthdinov. “Reducing the Dimensionality of Data with Neural Networks”. In: *Science* 313.July 28 (2006), pp. 504–507.

[27] E. Horvitz and M. Barry. “Display of information for time-critical decision making”. In: *Proc. 11th Conf. on Uncertainty in Artificial Intelligence*. Morgan Kaufmann Publishers Inc., 1995, pp. 296–305.

[28] C. Huang and A. Darwiche. “Inference in Belief Networks: A Procedural Guide”. In: *Int. J. of Approximate Reasoning* 11.1 (1994), p. 158.

[29] J. P. Huelsenbeck and F. Ronquist. “MRBAYES: Bayesian inference of phylogenetic trees”. In: *Bioinformatics* 17.8 (2001), pp. 754–755.

[30] L. Hyafil and R. L. Rivest. “Computing optimal binary decision trees is NP-complete”. In: *Information Processing Letters* 5.1 (1976), pp. 15–17.

[31] G. Indiveri. *Rounding Methods for Neural Networks with Low Resolution Synaptic Weights*. arXiv preprint. Institute of Neuroinformatics, Univ. Zurich, 2015. URL: http://arxiv.org/abs/1504.05767.

[32] H. Jaeger. "Echo State Network". In: *Scholarpedia*. Vol. 2. 2007, p. 2330. URL: http://www.scholarpedia.org/article/Echo_State_Network.

[33] E. T. Jaynes. *Probability Theory: the Logic of Science*. First partial online editions in the late 1990ies. First three chapters online at http://bayes.wustl.edu/etj/prob/book.pdf. Cambridge University Press, 2003.

[34] D. Jones. *Good Practice in (Pseudo) Random Number Generation for Bioinformatics Applications*. technical report, published online. UCL Bioinformatics, 2010. URL: http://www.cs.ucl.ac.uk/staff/d.jones/GoodPracticeRNG.pdf.

[35] M. I. Jordan, Z. Ghahramani, et al. "An introduction to variational methods for graphical models". In: *Machine Learning* 37.2 (1999), pp. 183–233.

[36] M. I. Jordan and D. M. Wolpert. "Computational motor control". In: *The Cognitive Neurosciences, 2nd edition*. Ed. by M. Gazzaniga. MIT Press, 1999.

[37] S. Kirkpatrick, C. D. Gelatt, and M. P. Vecchi. "Optimization by Simulated Annealing". In: *Science* 220.4598 (1983), pp. 671–680.

[38] R. Kiros, R. Salakhutdinov, and R. S. Zemel. "Unifying Visual-Semantic Embeddings with Multimodal Neural Language Models". http://arxiv.org/abs/1411.2539 Presented at NIPS 2014 Deep Learning Workshop. 2014.

[39] J. Kittler et al. "On Combining Classifiers". In: *IEEE Transactions on Pattern Analysis and Machine Intelligence* 20.3 (1998), pp. 226–239.

[40] S.L. Lauritzen. "The EM algorithm for graphical association models with missing data". In: *Computational Statistics & Data Analysis* 19.2 (1995), pp. 191–201.

[41] D. Luchinsky and et al. "Overheating Anomalies during Flight Test due to the Base Bleeding". In: *Proc. 7th Int. Conf. on Computational Fluid Dynamics, Hawaii July 2012*. 2012.

[42] B. Mau, M.A. Newton, and B. Larget. "Bayesian phylogenetic inference via Markov chain Monte Carlo methods". In: *Biometrics* 55 (1999), pp. 1–12. URL: http://citeseerx.ist.psu.edu/viewdoc/download?doi=10.1.1.33.8433&rep=rep1&type=pdf.

[43] W. S. McCulloch and W. Pitts. "A logical calculus of the ideas immanent in nervous activity". In: *Bull. of Mathematical Biophysics* 5 (1943), pp. 115–133.

[44] N. Metropolis et al. "Equation of state calculations by fast computing machines". In: *The Journal of Chemical Physics* 21.6 (1953), pp. 1087–1092.

[45] T. Mikolov et al. “Distributed Representations of Words and Phrases and their Compositionality”. In: *Advances in Neural Information Processing Systems 26*. Ed. by C. J. C. Burges et al. 2013, pp. 3111–3119. URL: http://papers.nips.cc/paper/5021-distributed-representations-of-words-and-phrases-and-their-compositionality.pdf.

[46] A. Minnaar. *Wor2Vec tutorial part I: the Skip-Gram model*. Online tutorial. 2015. URL: http://mccormickml.com/2016/04/27/word2vec-resources/%5C#efficient-estimation-of-word-representations-in-vector-space.

[47] T. M. Mitchell. *Machine Learning*. McGraw-Hill, 1997.

[48] S. R. T. Mouafo et al. “A tutorial on the EM algorithm for Bayesian networks: application to self-diagnosis of GPON-FTTH networks”. In: *Proc. 12th International Wireless Communications & Mobile Computing Conference (IWCMC 2016)*. 2016, pp. 369–376. URL: https://hal.archives-ouvertes.fr/hal-01394337.

[49] K. Murphy. *An introduction to graphical models*. Technical Report. http://www.cs.ubc.ca/∼
Intel, 2001.

[50] K. P. Murphy. “Dynamic Bayesian Networks: Representation, Inference and Learning”. Univ. of California, Berkeley, 2002.

[51] R. M. Neal. *Probabilistic Inference Using Markov Chain Monte Carlo Methods*. Technical Report CRG-TR-93-1. Dpt. of Computer Science, University of Toronto, 1993.

[52] R. M. Neal. *Using Deterministic Maps when Sampling from Complex Distributions*. Presentation given at the Evolution of Deep Learning Symposium in honor of Geoffrey Hinton. 2019. URL: http://www.cs.utoronto.ca/~radford/ftp/geoff-sym-talk.pdf.

[53] O. M. Parkhi, A. Vedaldi, and A. Zisserman. “Deep Face Recognition”. In: *Proc. of BMVC*. 2015. URL: http://www.robots.ox.ac.uk:5000/~vgg/publications/2015/Parkhi15/parkhi15.pdf.

[54] R. Pascanu and H. Jaeger. “A Neurodynamical Model for Working Memory”. In: *Neural Networks* 24.2 (2011). DOI: 10.1016/j.neunet.2010.10.003, pp. 199–207.

[55] J. Pearl and S. Russell. “Bayesian Networks”. In: *Handbook of Brain Theory and Neural Networks, 2nd Ed.* Ed. by M.A. Arbib. MIT Press, 2003, pp. 157–160. URL: https://escholarship.org/uc/item/53n4f34m.

[56] S. E. Peters et al. “A Machine Reading System for Assembling Synthetic Paleontological Databases”. In: *PLOS-ONE* 9.12 (2014), e113523. URL: http://journals.plos.org/plosone/article?id=10.1371/journal.pone.0113523.

[57] L.R. Rabiner. “A tutorial on Hidden Markov Models and Selected Applications in Speech Recognition”. In: *Readings in Speech Recognition*. Ed. by A. Waibel and K.-F. Lee. Reprinted from Proceedings of the IEEE 77 (2), 257-286 (1989). Morgan Kaufmann, San Mateo, 1990, pp. 267–296.

[58] F. Rosenblatt. “The Perceptron: a probabilistic model for information storage and organization in the brain”. In: *Psychological Review* 65.6 (1958), pp. 386–408.

[59] S. Roweis and Z. Ghahramani. “A unifying review of linear Gaussian models”. In: *Neural Computation* 11.2 (1999), pp. 305–345.

[60] D. E. Rumelhart, G. E. Hinton, and R. J. Williams. “Learning Internal Representations by Error Propagation”. In: *Parallel Distributed Processing Vol. 1*. Ed. by D. E. Rumelhart and J. L. McClelland. Also as Technical Report, La Jolla Inst. for Cognitive Science, 1985. MIT Press, 1986, pp. 318–362.

[61] M. A. Savi. “Nonlinear Dynamics and Chaos”. In: *Dynamics of Smart Systems and Structures*. Ed. by V. Lopes Junior and et al. Springer International Publishing Switzerland, 2016, pp. 93–117.

[62] J. Schmidhuber. “Deep Learning in Neural Networks: An Overview”. In: *Neural Networks* 61 (2015). Preprint: arXiv:1404.7828, pp. 85–117.

[63] D. Silver et al. “Mastering the game of Go with deep neural networks and tree search”. In: *Nature* 529 (2016), pp. 484–489.

[64] P. Smyth. “Belief Networks, Hidden Markov Models, and Markov Random Fields: a Unifying View”. In: *Pattern Recognition Letters* 18.11-13 (1997), pp. 1261–1268.

[65] F. Suchanek et al. “Advances in automated knowledge base construction”. In: *SIGMOD Records Journal* March (2013). URL: `http://suchanek.name/work/publications/sigmodrec2013akbc.pdf`.

[66] N. V. Swindale and H.-U. Bauer. “Application of Kohonen’s self-organizing feature map algorithm to cortical maps of orientation and direction preference”. In: *Proc. R. Soc. Lond. B* 265 (1998), pp. 827–838.

[67] F. Takens. “Detecting strange attractors in turbulence”. In: *Dynamical Systems and Turbulence*. Ed. by D.A. Rand and L.-S. Young. Lecture Notes in Mathematics 898. Springer-Verlag, 1981, pp. 366–381.

[68] J. Tenenbaum, T. L. Griffiths, and C. Kemp. “Theory-based Bayesian models of inductive learning and reasoning”. In: *Trends in Cognitive Science* 10.7 (2006), pp. 309–318.

[69] M. Weliky, W. H. Bosking, and D. Fitzpatrick. “A systematic map of direction preference in primary visual cortex”. In: *Nature* 379 (1996), pp. 725–728.

[70] H. Yin. “Learning nonlinear principal manifolds by self-organising maps”. In: *Principal Manifolds for Data Visualization and Dimension Reduction*. Ed. by A. N. Gorban et al. Vol. 58. Lecture Notes in Computer Science and Engineering. Springer, 2008, pp. 68–95.

[71] P. Young et al. “From image descriptions to visual denotations: New similarity metrics for semantic inference over event descriptions.” In: *Transactions of the Association for Computational Linguistics* 2 (2014), pp. 67–78.